



*Pf*CLK3 as a Therapeutic Antimalarial Drug Target

Thesis Submitted for the Degree of Doctor of Philosophy at
the University of Leicester

By Omar Janha

College of Medicine, Biological Sciences, and
Psychology

University of Leicester

2019

Abstract

***Pf*CLK3 as a Therapeutic Antimalarial Drug Target**

Artemisinin resistance, the current frontline antimalarial, is threatening to significantly increase the global incidence of malaria. Hence, novel targets for development of next generation antimalarials is urgently required. Here I focus on the essential malaria protein kinase *Pf*CLK3, involved in RNA processing, to investigate if it is a suitable pharmacological target for malaria treatment. The molecule TCMDC-135051, identified from a screen at GlaxoSmithKline, was used as a probe inhibitor of *Pf*CLK3. The evidence presented here shows that TCMDC-135051 had parasitocidal activity at multiple stages of *P. falciparum* growth at low nanomolar potency, with an IC₅₀ of 180 nM in asexual ring stage parasites. TCMDC-135051 is also potent against asexual *P. knowlesi* and *P. berghei* parasites, meeting cross species requirements for new antimalarial agents. Against recombinant CLK3 kinases, TCMDC-135051 demonstrated a high potency, with an IC₅₀ value of ~40 nM towards *Pf*CLK3, *Pv*CLK3 and *Pb*CLK3 kinases. Additionally, a mode of action behaviour suggestive of non-ATP competitive inhibition was observed.

For target validation, a mutant *Pf*CLK3 parasite line (*Pf*CLK3_G449P) reduced TCMDC-135051 potency by ~1.5 fold log units compared to wild type. Long-term exposure of Dd2 parasites to TCMDC-135051 showed two single point mutations on the *Pf*CLK3 gene, indicating TCMDC-135051 selectivity towards *Pf*CLK3. Using the parasite reduction rate to investigate the speed of action, TCMDC-135051 demonstrate activity levels similar to dihydroartemisinin, a standard antimalarial. Furthermore, inhibition of *Pf*CLK3 resulted in impaired splicing in wild type 3D7 parasites compared to mutant *Pf*CLK3_G449P, demonstrating the role of *Pf*CLK3 in regulating RNA splicing.

In conclusion, inhibition of *Pf*CLK3 activity results in rapid killing of asexual *P. falciparum* parasites and other *Plasmodium* species at multiple stages through inhibition of RNA splicing. Therefore, the data presented here revealed *Pf*CLK3 as a suitable target for treatment of symptomatic malaria and a potential transmission-blocking target.

Publications

Papers

*Alam, M., *Sanchez-Azqueta, A., *Janha, O., Flannery, E., Mahindra, A., Mapesa, K., Brancucci, N., Antonova-Koch, Y., Crouch, K., Simwela, N. V., Akinwale, J., Mitcheson, D., Solyakov, L., Dudek, K., Jones, C., Zapatero, C., Doerig, C., Nwakanma, D. C., Vazquez, M.-J., Colmenarejo, G., Lafuente, M.-J., Leon, M. L., Waters, A. P., Jamieson, A. G., Alvaro, L. E. F., Marti, M., Winzeler, E. A., Gamo, F. J. & Tobin, A. 2018. Validation of the protein kinase PfCLK3 as a multi-stage cross species malarial drug target. *bioRxiv*. *Joint first Author. 'Under Review'.

Abstracts

Janha, O., Sanchez-Azqueta, A., Alam, M., Bojang, F., Nwakanma, D., and Tobin, A. Targeting *Plasmodium falciparum* cyclin-dependent kinase like kinases (*PfCLKs*) for antimalarial drug development. Malaria Gordon Research Seminar and Conference, Les Diablerets Conference Center, Switzerland, July 1-7, 2017.

Janha, O., A., Alam, M., Sanchez-Azqueta, Nwakanma, D., and Tobin, A. Targeting the Protein kinase PfCLK3 in malaria. 1st World Malaria Congress. Melbourne, Australia. July 1-5, 2018

Acknowledgement

Firstly, a huge thank you to my supervisor Professor Andrew Tobin for your support and encouragement throughout my PhD. Without you the project would never have taken off and I am so grateful for your confidence and trust in my abilities and the continued support. Thanks to my second supervisor from Medical Research Council the Gambia at LSHTM, Dr. Davis Nwankama for your interest and contributions towards this project. Your advice and scientific guidance have been helpful throughout the duration of this PhD. Also, thanks to Dr Mahmood Alam for your help and support at different stages of my PhD, your help is appreciated. You have taught me a lot both in Science and life in general. I would also like to acknowledge my committee members for their valuable contributions and feedback. Prof Andrew Smith and Amanda Harris of MRC Toxicology Unit at Cambridge University (formerly University of Leicester), thank you for all your support. I am incredibly grateful to Dr Alfred Amambua-Ngwa, you have made a huge impact in my life and career, am grateful for all the trust and confidence you have in me. This PhD was jointly funded by the MRC the Gambia Unit, at LSHTM, and MRC Toxicology Unit at Cambridge (formerly Leicester). Thank you for supporting my career.

Special thanks go to all of my friends in the Tobin lab, past (from Leicester) and present. I would especially like to thank Ana Sanchez for your patience teaching me the TR-FRET assay and Sophie Bradley for helpful discussions about science, careers and many other subjects! Also thanks to Louis for your help and advice, but also for the political discussions we always had which was useful to reducing the stressful moments. To Mario, Natasha and Miriam, thanks for making coffee available all the time especially during the stressful writing period. Thank you Rudi for helping me out so much during the first 2 years of my PhD, I really appreciate it. To the rest of the Tobin group, Karen, Paulina, Colin

and Lisa, you all made me looking forward to come in every morning knowing how caring you are. Thank you Sarah Hess for all the printing, I know it was a burden but you always smiled and say, “yes I can print it”. To Peter Bowman, thank you for keeping the “focus” with me all the time in preparation to “change the world”. To the rest of the members of lab-241 and office 205, thank you all for your support in many different ways.

Finally, I would like to say thank you to all of my family and friends. Thank you to Dr Saikou Y. Bah and Dr Fatoumatta Darboe for your advice and support, I probably wouldn't have gotten this far if you hadn't encouraged me to take on this challenge in the first place. Abdoulie Kanteh, thank for always being there, no amount of words can describe what you mean to me. To my siblings, you have made me the Omar you're all proud of; thank you for supporting me from the very beginning. You all sacrificed a lot for, especially Alhagie, my life would have been different if not for your immense sacrifice towards my personal development.

Last but not the least, a very big thank you to my wife Yassin Lowe for abandoning everything to make sure I come to the end of this PhD successfully. To my adorable daughters Zainabou and Phatoumatta Janha, this thesis is dedicated to you.

Table of Contents

ABSTRACT	I
PUBLICATIONS	III
PAPERS	III
ABSTRACTS	III
ACKNOWLEDGEMENT	IV
ABBREVIATIONS	IX
CHAPTER 1	1
1.1 INTRODUCTION	1
1.1.1 <i>Malaria Transmission</i>	6
1.1.2 <i>Malaria Life Cycle</i>	7
1.1.3 <i>Malaria control strategies and treatment</i>	22
1.2 PROTEIN KINASES AND PHOSPHORYLATION	37
1.2.1 <i>The Plasmodium Kinome</i>	43
1.2.2 <i>Structure of Protein Kinases</i>	49
1.2.3 <i>Function of Protein Kinases</i>	57
1.2.4 <i>mRNA splicing</i>	60
1.3 KINASE INHIBITORS	65
1.3.1 <i>Type I inhibitors</i>	65
1.3.2 <i>Type II inhibitors</i>	67
1.3.3 <i>Type III Inhibitors</i>	68
1.4 THESIS AIMS	70
CHAPTER 2 MATERIALS AND METHODS	74
2.1 MATERIALS	74
2.1.1 <i>Standard Reagents, Chemicals and Consumables</i>	74
2.1.2 <i>Specific Reagents and assay kits</i>	74
2.1.3 <i>Bioinformatics tools and online applications</i>	75
2.1.4 <i>Primers</i>	75
2.1.5 <i>Bacterial Strains</i>	76
2.1.6 <i>DNA and plasmid constructs</i>	76
2.1.7 <i>Specialised Equipment</i>	76
2.2 METHODS	80
2.2.1 <i>Bacterial Growth</i>	80
2.2.2 <i>Bacterial Transformation</i>	80
2.2.3 <i>Preparation of plasmid DNA</i>	81
2.2.4 <i>Plasmid DNA and nucleic Quantification – NanoDrop</i>	83
2.2.5 <i>Polymerase Chain Reaction (PCR)</i>	83
2.2.6 <i>Site directed Mutagenesis PCR</i>	84
2.2.7 <i>Protein Expression and Purification</i>	85
2.2.8 <i>Western Blot analysis</i>	86
2.2.9 <i>In vitro Kinase activities and inhibition assay</i>	87
2.2.10 <i>Plasmodium falciparum culture</i>	89
2.2.11 <i>RNA Isolation (Qiagen Kit)</i>	95
2.2.12 <i>Complementary DNA (cDNA) synthesis</i>	96
CHAPTER 3 CHARACTERIZATION OF AN INHIBITOR TOOL COMPOUND FOR PFCLK3	97
3.1 INTRODUCTION	97

3.2	RESULTS	99
3.2.1	<i>Protein Expression</i>	99
3.2.2	<i>Expression of PfCLK1 Kinase domain</i>	99
3.2.3	<i>Kinase Activity and Inhibition Assays</i>	105
3.3	DISCUSSIONS	118
CHAPTER 4	DETERMINING THE MECHANISM OF ACTION OF TCMDC-135051	120
4.1	INTRODUCTION	120
4.2	RESULTS	122
4.2.1	<i>High ATP concentration affects the inhibition potency of TCMDC-135051 and TCMDC-138736 differently</i>	122
4.2.2	<i>Determining the mechanism of action of TCMDC-138736 and TCMDC-135051</i>	125
4.3	DISCUSSION.....	128
CHAPTER 5	TARGET VALIDATION.....	131
5.1	INTRODUCTION	131
5.2	RESULTS	136
5.2.1	<i>Generation of PfCLK3 variant gene resistant to TCMDC-135051</i>	136
5.2.2	<i>Continuous parasite exposure to TCMDC-135051 results in PfCLK3 gene mutations causing resistance</i>	147
5.2.3	<i>ATP-competitive mechanism of inhibition of PfCLK3_KD recombinant kinase by TCMDC-135051</i>	161
5.3	DISCUSSION.....	165
CHAPTER 6	INHIBITION OF OTHER <i>PLASMODIUM</i> SPECIES BY TCMDC-135051	168
6.1	INTRODUCTION	168
6.2	RESULTS	170
6.2.1	<i>Expression of full length <i>P. vivax</i> CLK3 (PvCLK3) and PbCLK3, and kinase domain of PvCLK1 and PbCLK1</i>	170
6.2.2	<i>TCMDC-138736 and TCMDC-135051 inhibits kinase mediated MBP phosphorylation in all Plasmodium CLK3 kinases</i>	173
6.2.3	<i>TCMDC-138736 and TCMDC-135051 have no effect on Plasmodium CLK1s kinase mediated substrate phosphorylation</i>	175
6.2.4	<i>Time course for optimum TR-FRET assay conditions for <i>P. vivax</i> and <i>P. berghei</i> kinases</i>	177
6.2.5	<i>The Michaelis-Menten constant (Km for ATP) for <i>P. vivax</i> and <i>P. berghei</i> CLKs were determined using TR-FRET</i>	179
6.2.6	<i>TCMDC-135051 is a potent inhibitor against PvCLK3 and PbCLK3</i> 181	
6.2.7	<i>The effect of PvCLK3_H273P and PbCLK3_H276P on kinase activity and potency of TCMDC-135051</i>	183
6.2.8	<i>The effects of PvCLK3_H273P and PbCLK3_H276P to the inhibitory activity of TCMDC-135051</i>	185
6.2.9	<i>TCMDC-135051 potently inhibits <i>P. knowlesi</i> at low nanomolar concentration in vitro</i>	188
6.3	DISCUSSION.....	190
CHAPTER 7	TCMDC-135051 IS POTENT AGAINST CLINICAL <i>P. FALCIPARUM</i> MALARIA	192
7.1	INTRODUCTION:	192
7.2	RESULTS:	195

7.2.1	<i>Determining the EC₅₀ of laboratory Isolates</i>	195
7.2.2	<i>Assay Dynamic Range</i>	197
7.2.3	<i>Data analysis and validation</i>	197
7.2.4	<i>The parasite reduction rate (PRR)</i>	199
7.3	DISCUSSION.....	207
CHAPTER 8 INHIBITION OF PFCLK3 SHOWS DIRECT EFFECT ON SPLICING		
209		
8.1	INTRODUCTION	209
8.2	EXPERIMENTAL PROCEDURE	211
8.3	RESULTS:	214
8.4	DISCUSSION.....	217
CHAPTER 9 DISCUSSION		220
9.1	GENERAL DISCUSSION	220
9.2	FUTURE WORK	227
9.2.1	<i>Conditional knockout</i>	227
9.2.2	<i>Inhibition of asexual parasites in animal malaria challenge</i>	227
9.2.3	<i>Transmission blocking</i>	228
9.2.4	<i>Bigger Clinical study</i>	228
9.2.5	<i>Crystal Structure</i>	229
REFERENCE:		230

Abbreviations

ACT	Artemisinin combination therapy
AMA1	Apical membrane antigen 1
ANOVA	Analysis of variance
ARVs	Androgen receptor variants
AS	Alternative splicing
ATP	Adenosine Triphosphate
BSA	Bovine serum albumin
BTO	Benzothiazinone
BPS	Branch point sequence
CDK	Cylin-dependent protein kinase
CDPK1	Calcium dependent protein kinase 1
cDNA	Complementary DNA
CK1	Casein Kinase 1
CLK	Cyclin dependent kinase like kinases
<i>CpCDPK1</i>	<i>Cryptosporidium parvum</i> CDPK1
CO ₂	Carbon dioxide
CSA	Chondroitin-4- sulphate
CSP	Circumsporozoite protein
DHFR	Dihydrofolate reductase
DHPS	Dihydropteroate synthetase
DMSO	Dimethyl sulfoxide
DNA	Deoxyribonucleic acid
dNTPs	deoxyribonucleotide triphosphates
DTT	1,4-dithiothreitol
DV	Digestive vacoule
DYRK	Dual-specificity tyrosine-regulated kinase
EBL	Erythrocyte binding like
ECL	Enhanced chemiluminescence
EC ₅₀	Concentration of drug that gives half maximal response
EDTA	Ethylenediaminetetraacetic acid

EGTA	Ethylene glycol-bis(β -aminoethyl ether)- N,N,N',N'-tetraacetic acid tetrasodium salt
EMP1	Erythrocyte membrane protein 1
ePK	eukaryotic protein kinase
ER	Endoplasmic reticulum
FITC	Fluorescein isothiocyanate
FPIX	Ferriprotoporphyrin IX
GEXP5	Gametocyte export protein 5
GSK3	Glycogen synthase kinase 3
G6PD	Glucose 6 dehydrogenase
HEPES	4-(2-hydroxyethyl)-1-piperazineethanesulfonic acid)
H ₂ O ₂	Hydrogen peroxide
ICAM1	Intracellular adhesion molecule 1
IC ₅₀	Concentration of an inhibitor where the response is reduce by half (50% inhibition)
IFA	Immunofluorescence assay
IPT	Intermittent preventative treatment
IPTG	Isopropyl β -D-1-thiogalactopyranoside
IP3	Inositol 1,4,5-trisphosphate
Kb	kilobase
K _m ATP	Michelis menton constant for ATP
KCl	Potassium Chloride
LB	Lauria Broth
LysoPC	Lysophosphatidicholine
MAPK	Mitogen activated protein kinase
MBP	Myelin Basic Protein
MgCl ₂	Magnesium Chloride
MgSO ₄	Magnesium Sulphate
MLCK	myosin light chain kinases
NaCl	Sodium Chloride
NBT	4-Nitroblue-tetrazolium-chloride solution
NMD	Nonsense mediate decay
OAT	ornithine aminotransferase

PBS	Phosphate Buffered Saline
PCR	Polymerase Chain Reaction
<i>Pf</i> CDPK1	<i>Plasmodium falciparum</i> Calcium dependent protein kinase 1
<i>Pb</i> CLK3	<i>Plasmodium berghei</i> cyclin dependent kinase like kinase 3
<i>Pf</i> CLK3	<i>Plasmodium falciparum</i> cyclin dependent kinase like kinase 3
<i>Pf</i> PKG	<i>Plasmodium falciparum</i> Protein Kinase G
PI(4,5)P2	Phosphatidylinositol (4,5)-biphosphate
PK	Protein kinase
PKA	Protein kinase A
PKC	Protein kinase C
PKG	Protein kinase G
<i>Pv</i> CLK3	<i>Plasmodium vivax</i> cyclin dependent kinase like kinase 3
PVM	Parasitophorous vacuole membrane
PYT	Polypyrimidine tract
RH	Reticulocyte-binding homologue
RNA	Ribonucleic acid
ROS	Reactive Oxygen Species
RPM	Rotation per minute
RRM	RNA recognition motif
RSA	Ring Survival Assay
RT	Room temperature
SBF-SEM	Serial block-free scanning electron microscope
SDS	Sodium dodecyl sulphate
SDS-PAGE	Sodium dodecyl sulfate polyacrylamide gel electrophoresis
S.E.M	Standard error of the mean
SEA	South East Asia
SERA1	Serine-rich antigen 1
SF1	Splicing factor 1

SMC	Seasonal malaria chemoprevention
snRNP	small nuclear ribonucleoprotein particles
SOAP	Secreted ookinete adhesion protein
SRPK	Serine Arginine Protein Kinases
SR-B1	Scavenger receptor type B class I
SS	Splice site
SSA	Sub-Saharan Africa
SUB1	Subtilisin like protease 1
TAE	Tris acetate-EDTA
TE	Tris EDTA
TEMED	N,N,N',N'-Tetramethylethylenediamine (1,2-Bis(dimethylamino) ethane
TBS	Tris buffered saline
TBST	Tris buffered saline/Tween 20
TGS	Tris glycine saline
<i>Tg</i> CDPK1	<i>Toxoplasma gondii</i> CDPK1
TLK	Tyrosine like kinase
TR-FRET	Time-resolved fluorescence energy transfer
U2AF	U2 auxiliary factor
<i>ULight</i> -MBP	<i>ULight</i> -Myelin Basic Protein
VCAM1	Vascular cell adhesion molecule 1
VRK	vaccinia-related kinase
VSA	Variant surface antigen
WHO	World Health Organisation
WT	Wild type
WWARN	Worldwide anti-malarial Resistance Network
XA	xanthurenic acid

Chapter 1

1.1 Introduction

Malaria is caused by an obligate unicellular eukaryotic parasite belonging to the *Plasmodium* genus. It is a multi-organ life-threatening disease caused by blood stage infections with the asexual forms of the parasite, which have a complex life cycle involving a vertebrate host and a mosquito vector (Bijker *et al.*, 2015, Talevich *et al.*, 2012). Interacting with humans for millions of years, these vector-borne parasites have caused multiple signatures of natural selection in the human genome (Shaw and Catteruccia, 2018). Four main species affect humans: *Plasmodium falciparum* (*P. falciparum*), *P. malariae*, *P. ovale*, and *P. vivax*. Recently, *P. knowlesi* malaria is reportedly infecting humans in the Malaysian Borneo region and spreading across Southeast Asia (SEA) (Ahmed and Cox-Singh, 2015). In 2016, 216 million cases and 445,000 malaria deaths were registered, 90% of which occurred in sub-Saharan Africa (SSA) (WHO, 2017b). Almost all the malaria cases (99%) reported in sub-Saharan Africa (SSA) were due to infection with *P. falciparum*. In contrast, *P. vivax* causes most of the malaria reported outside Africa with prevalence of 64, 30 and 40% of malaria cases in the World Health Organisation (WHO) region of the Americas, SEA and the East Mediterranean regions respectively (WHO, 2017b). Malaria transmission is reasonably seasonal in most malaria endemic areas. Although sub-Saharan Africa has a suitable temperature for malaria transmission across the year, seasonal changes in rainfall influenced the malaria transmission dynamics (Greenwood *et al.*, 2017). The current global malaria distribution of 2016 as reported in the WHO Malaria Report (WHO, 2017b) is shown in the map in Figure 1.1.

Significant gains in the reduction of the global malaria burden have been reported. The United Nations millennium development goal and the roll back malaria initiatives resulted in a decrease of 40% in the prevalence of malaria, a credit to good vector control strategies (wide spread use of long lasting insecticide treated bed nets (LLINs) and indoor residual spraying), and proper case management (prompt treatment of cases with artemisinin-based combination therapy (ACT)) (Bhatt *et al.*, 2015). The WHO certified two countries (Kyrgyzstan and Sri Lanka) malaria free, 21 counties identified with potential to eliminate malaria by 2020 and 44 countries with less than 10,000 cases (WHO, 2017b).

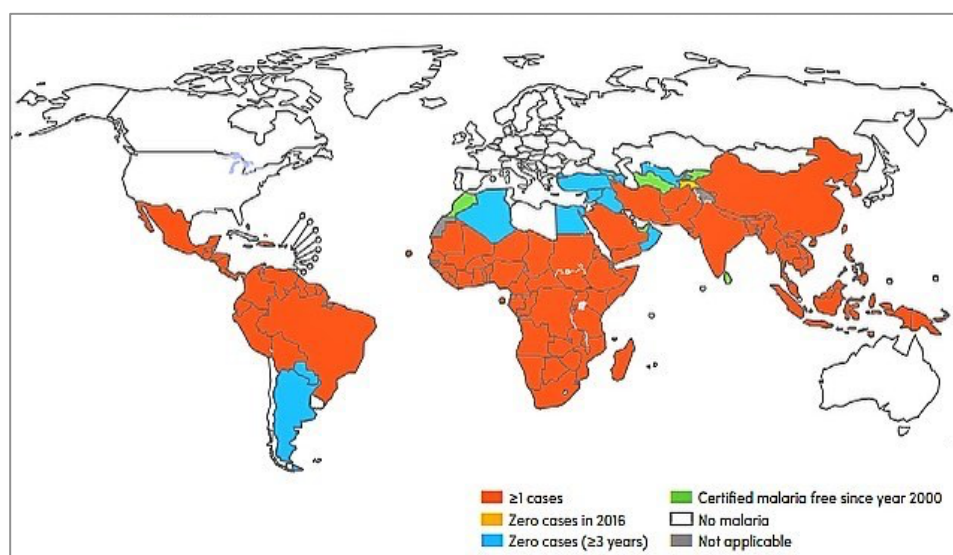


Figure 1.1: Countries and territories with indigenous malaria cases in 2016 (WHO, 2017b).

P. vivax is one of four species of malaria that infect humans and causes most of the malaria cases outside Africa (Baird, 2004). It is estimated that *P. vivax malaria*, previously called benign tertian malaria, caused 13.8 million cases in 2015 with 1400-14900 deaths globally (Singh *et al.*, 2011, Nyunt *et al.*, 2017). However, this malaria species is no longer referred to benign malaria due to the reported deadly disease caused by this *Plasmodium* species (Kano *et al.*, 2018). The symptoms associated with *P. vivax*

malaria are anaemia, intrauterine growth retardation, miscarriage, severe malaria and in some cases fatality (Price *et al.*, 2014). Additionally, infection with *P. vivax* malaria reportedly induces greater inflammation of the lungs than observed with *P. falciparum* infections plus other heterogeneous clinical manifestations (Mercereau-Puijalon and Ménard, 2010). Globally, *P. vivax* malaria is the most widely distributed parasite in malaria endemic areas and up to 100 countries and territories have been identified as endemic countries (Guerra *et al.*, 2010, Lu *et al.*, 2011). These populations are identified to have high prevalence of Duffy antigens on the surface of their reticulocytes which are needed for interaction with the parasite and to establish a successful *P. vivax* infection (Kano *et al.*, 2018). Interestingly, Duffy positive phenotypes have been reported in Sudan, Somalia and Ethiopia and these populations are reportedly infected with *P. vivax*, confirming the significance of the Duffy antigens for vivax infection (Mercereau-Puijalon and Ménard, 2010). Due to the high prevalence of the Duffy negative phenotype, *P. vivax* infections are rare in Africa (Gething *et al.*, 2012), except a few infections reported in Duffy negative individuals in Kenya, Mali and Cameroon (Gunalan *et al.*, 2018).

One of the prominent features that distinguishes *P. vivax* from *P. falciparum* is its ability to develop into dormant liver stage forms called hypnozoites, plus its ability to develop at lower temperatures in the mosquito vector (Mikolajczak *et al.*, 2015). Hypnozoites are important transmission drivers and their reactivation (relapse) is sporadic, and is a major cause of malaria particularly in young children (Markus, 2015, White and Imwong, 2012). The factors that drive hypnozoite formation and relapse are not fully understood (Gural *et al.*, 2018). However, relapse is seemingly influenced by the infecting parasite strain, sporozoite inoculum, immunity against the infecting genotype, and drug treatment (White and Imwong, 2012). Noteworthy, occurrence of

relapse varies from 50-80% in equatorial regions and 5-10% in temperate areas (Price *et al.*, 2014).

P. ovale is a distinct malaria species causing benign tertian malaria (Miller *et al.*, 2015), and infected erythrocytes have a characteristic morphological oval shape and fimbriated edges (Zaw and Lin, 2017). *P. ovale* reportedly has diverged into two species: *P. ovale curtisi* (classic-type), and *P. ovale wallikeri* (variant-type) both occurring sympatrically in Africa and Asia and co-infecting patients (Fuehrer and Noedl, 2014, Sutherland *et al.*, 2010, Zaw and Lin, 2017). *P. ovale* is distributed in most countries where malaria is endemic including southern Asia, SEA and SSA, as well as in the Americas (Fuehrer and Noedl, 2014, Williams *et al.*, 2016, Zaw and Lin, 2017). Infections with *P. ovale* rarely cause significant clinical disease (Miller *et al.*, 2015, Roucher *et al.*, 2014, Zaw and Lin, 2017). However, like *P. vivax*, *P. ovale* produces hypnozoites, which can relapse, and non-immune travellers to malaria endemic countries have reported disease manifestation several months after their return (de Laval *et al.*, 2014, Zaw and Lin, 2017, Singh *et al.*, 2013). Prevalence of hypnozoites in *P. vivax* and *P. ovale* make treatment of these *Plasmodium* species difficult because they are dormant and refractory to most antimalarial drugs. Primaquine, an 8-aminoquinoline is the only drug effective against these forms of malaria and can completely eliminate hypnozoites, however, the high prevalence of glucose-6-phosphate dehydrogenase (G6PD) deficiency limits its use due to high toxicity to these individuals (Flannery *et al.*, 2013).

P. malariae, like *P. ovale* is also widely distributed in Africa and other major malaria-endemic areas of the world with a prevalence range of 15-40%, largely co-existing with *P. falciparum* (Dinko *et al.*, 2013, Miller *et al.*, 2015). Prevalence in west and central African forest and the Sahel is between 10 and 40% (Roucher *et*

al., 2014). Although *P. falciparum* causes most of the malaria in Africa, incidences of *P. malariae* infections have been detected in Africa and fever episodes in patients with high *P. malariae* parasitaemia have been reported in Liberian and Gambian children (Roucher *et al.*, 2014). *P. knowlesi* malaria is now regarded as the fifth human malaria species that has spread significantly across all SEA countries (Singh and Daneshvar, 2013). In Sabah, Malaysia, incidences of reported *P. falciparum* and *vivax* malaria are declining but *P. knowlesi* malaria cases are rising causing up to 62% of malaria cases (William *et al.*, 2014). It is currently the most common cause of malaria in Malaysians (Fornace *et al.*, 2018), with mortality rates of up to ~10% (Millar and Cox-Singh, 2015). Furthermore, there are several reports of *P. knowlesi* infections in Europeans and other travellers returning from *P. knowlesi* transmission zones, demonstrating sustained transmission in humans (Millar and Cox-Singh, 2015).

Clinical malaria infections are mostly detected in children under 5 years, pregnant women and non-immune travelers, while adults living in endemic areas show reduced prevalence of symptomatic infection, parasitaemia, and clinical episode (Moncunill *et al.*, 2013). However, infection dynamics might be shifting to older children in many endemic countries, mainly due to increased availability, distribution and used of malaria interventions, protecting younger children. As demonstrated by a series of cross sectional surveys carried out in the Gambia (Ceasay *et al.*, 2008, Satoguina *et al.*, 2009, Takem *et al.*, 2013), it has been shown that malaria incidence has increased in school aged children (older than 5 years), and early adulthood. A study in Gabon also showed significantly higher malaria prevalence in children older than 60 months compared to younger children (Maghendji-Nzondo *et al.*, 2016). This is strengthened by a review showing similar findings from different studies across Africa including countries from as far apart as Kenya and Mozambique with estimated malaria

prevalence in school children of about 25% generally (Nankabirwa *et al.*, 2014). This change in malaria burden is thought to be due to the reduced exposure to malaria in children under 5 years due to interventions like LLINs, therefore reducing malaria immunity in early childhood thus shifting the disease burden towards adulthood (Doolan *et al.*, 2009).

1.1.1 Malaria Transmission

Malaria is transmitted by the *Anopheles gambiae sensu lato (s.l.)* complex (*An. Sensu stricto (s.s)*, *An. Clouzzii*, and *An arabiensis*) and *An. funestus* mosquito vectors (Emami *et al.*, 2017). Principally, female *Anopheles gambiae (A. gambiae)* complex is a highly customized and proficient vector that transmits malaria from person to person in Africa because it exclusively feeds on humans (Crompton *et al.*, 2014), while *An. arabiensis* prefers cattle over human blood (Emami *et al.*, 2017). Earlier investigations reported other *Anopheles* species as important malaria vectors in SSA - *A. funestus* has been transmitting malaria in some regions of Senegal and various other regions in SSA (Kelly-Hope and McKenzie, 2009). The feeding preference of *An. gambiae s.s.* and *An. coluzzii* on humans and the feeding of *An. arabiensis* on cattle is regarded as the general mosquito behaviour, however, there are instances of vectors feeding on different mammalian species mostly influenced by geographic variations (Emami *et al.*, 2017). Mosquitoes use olfactory and other sensory cues (such as CO₂ and heat) to target a host for blood meal during which its takes along the malaria parasites from an infected person, after a few days, the mosquito needs to bite again to transmit the infection to another person – indicating a vector must bite twice for a successful transmission (Shaw and Catteruccia, 2018). Additionally, the vector must survive long enough for the pathogen to develop through the required stages within the host to be transmitted successfully.

Different mosquito species are reported as efficient vectors of malaria responsible for disease transmission from one infected person to another. In India, the mosquito species transmitting malaria are widespread and different geographic areas have different vector species: in rural and pre-urban India, *An. culicifacies*; north southern, *An. fluviatilis* (*Species S*); north eastern region, *An. minimus* (*Sub-species A*); North east region (forested and forest-fringe areas), *An. dirus* (*Sub-species An. baimaii*); in the coastal region, *An. sundaicus*; and in the urban region *An. stephensi* (Bharati and Ganguly, 2013). Several other mosquito species are reported in other parts of SEA including Sri Lanka, Malaysia, and Indonesia (Bharati and Ganguly, 2013). In China the most widely distributed mosquitoes species are *An. sinensis* (feeds on animals) and *An. anthropophagus*, (belonging to the *An. hyrcanus* species group) and feed on humans, transmitting *P. vivax* and *P. falciparum* malaria respectively (Zhu *et al.*, 2013). In southern China, malaria is mainly transmitted by *An. minimus* and *An. dirus* (Zhu *et al.*, 2013).

1.1.2 Malaria Life Cycle

The malaria parasite has an intricate life cycle shared between a vertebrate host and an insect vector as shown in Figure 1.2 (Bousema and Drakeley, 2011). Gametocytes ingested by mosquitoes during a blood meal need up to 15 days to fully develop to mature infective *sporozoites* which would be transmitted during the next blood meal in mosquitoes that survive long enough for the parasite to complete its life-cycle within the vector (Costa *et al.*, 2018). The Malaria life cycle involves exo-erythrocytic and intra-erythrocytic schizogony in the human, plus sporozoite maturation in the mosquito.

1.1.2.1 Exo-erythrocytic schizogony

Introduction of the unicellular protozoan *Plasmodium sporozoite* to the vertebrate host during a blood meal by the female *Anopheles* mosquito starts malarial infection and the replication cycle (Karunamoorthi, 2014). Within minutes of being released into the blood stream, using specific and efficient targeting mechanisms through interactions between parasite-encoded surface proteins and host molecules (Prudencio *et al.*, 2006), the *sporozoites* reach the mammalian liver, invade hepatocytes and either remain dormant (form hypnozoites) or develop over several days, ultimately forming *schizonts*, the prelude to a blood stage infection (Delves *et al.*, 2012).

Successful invasion of hepatocytes depends on host factors such as CD81 receptor, scavenger receptor type B class I (SR-BI), and the surface protein EphA2 amongst other factors (Posfai *et al.*, 2018). Hepatocyte invasion by merozoites causes host cell membrane invagination forming the parasitophorous vacuole membrane (PVM) around the parasite where it undergoes morphological changes dividing into tens of thousands merozoites within a single hepatocyte (Posfai *et al.*, 2018). The factors attracting sporozoites to the liver are not fully understood but the liver is rich in the nutrients required for the development of the sporozoites (Vaughan *et al.*, 2008). Additionally, aquaporin-3 (AQP3), an aquaglycoprotein that transports water and glycerol in mammalian cells was found in the PVM as an essential protein for parasite development (Posfai *et al.*, 2018). The *sporozoites* develop into trophozoites within 16 hours post infection (hpi) and later into schizonts, which undergo growth and nuclear replication lasting about 30 hours (Prado *et al.*, 2015). At the schizont stage, organelles critical for erythrocyte invasion are produced and the plasma membrane of the schizonts invaginates, forming the plasma membrane of thousands of merozoites (50–55 hpi) to end

the exo-erythrocytic schizogony (Jayabalasingham *et al.*, 2010, Prado *et al.*, 2015).

By action of parasite proteases, the PVM is ruptured and the merozoites, packed into vesicles (merosomes) are released into the host cytoplasm (Jayabalasingham *et al.*, 2010), where they accumulate calcium (Ca^{2+}) from host cell stores and avoid exposure to phosphatidylserine residues (Prado *et al.*, 2015). The merozoite-carrying merosomes are transported through the blood vessels into the lung capillaries where they are released to initiate infection of erythrocytes (erythrocytic schizogony), starting the pathogenic phase of malaria infection (Prado *et al.*, 2015, Talevich *et al.*, 2012). In this usually asymptomatic phase, called the first round of schizogonic replication, the mature schizonts produce up to 40,000 invasive blood stage parasites called merozoites, in *P. falciparum*, the most virulent malaria species (Talevich *et al.*, 2012). Noteworthy, *P. vivax* and *P. ovale* give rise to the metabolically dormant forms of the parasite that instead of developing to the usual *schizont*, form *hypnozoites* that can persist for many years and be reactivated into *schizogony* (Doerig *et al.*, 2015).

1.1.2.2 Erythrocytic Schizogony

Immediately after egress, merozoite invasion of erythrocytes starting the blood-stage (erythrocytic schizogony) infection becomes a necessity. Merozoite invasion of erythrocytes is divided into three important steps: pre-invasion characterised by deformation of target erythrocyte; followed by internalisation, the phase the newly infected erythrocyte takes a stellate appearance and finally echinocytosis (Weiss *et al.*, 2015). This complex multistep process facilitated by multiple interactions between parasite ligands and erythrocyte receptors involving proteins localised in apical organelles referred to as micronemes and

rhoptries, are secreted timely for successful invasion (Bansal *et al.*, 2013).

The interaction of erythrocytes with the parasite in what is called host-parasite interactions, involves at least two protein families, the reticulocyte-binding protein homologue (RH) and the erythrocyte binding like (EBL) proteins, which coordinate initial contact, apical reorientation, junction formation and active invagination (Wright *et al.*, 2014). Members of these proteins, which bind specific receptors on erythrocyte surfaces and play a role in invasion are: EBL (EBA-175, EBA-181 and EBA-140) and *PfRh* (*PfRh1*, *PfRh2a*, *PfRh2b*, *PfRh4* and *PfRh5*) (Tham *et al.*, 2012). Among these merozoite proteins, only the *PfRh5* demonstrate essentiality for erythrocyte invasion because it is a non-redundant protein (Crosnier *et al.*, 2011, Wright *et al.*, 2014). The BASIGIN (BSG), member of the immunoglobulin superfamily (IgSF) existing in two splice forms (basigin-short and basigin-long) was identified as the erythrocyte receptor for *PfRh5* (Crosnier *et al.*, 2011). Egressed merozoites are exposed to low-potassium ion concentrations in blood plasma, raise cytosolic calcium levels through phospholipase C-mediated pathway (Cowman *et al.*, 2016). This triggers secretion of microneme proteins such as EBA-175 and apical membrane antigen-1 (AMA-1) to the merozoite surface and finally the binding of EBA-175 to its receptor glycophorin A (glyA) on erythrocytes restoring basal cytosolic calcium levels and release of rhoptry proteins (Singh *et al.*, 2010). Other glycoproteins interacting with parasite proteins are glyB, which interact with EBL1 and glycoprotein C interacts with EBA 140; importantly, all glycoprotein-EBL interactions are dependent on sialic acid moieties present on erythrocyte surfaces (Singh *et al.*, 2010).

Following binding to erythrocytes, the merozoites' apical end is reoriented to the surface of the erythrocyte forming a connective

ring called the tight junction or moving junction through which the merozoite pass and enter the erythrocyte, a process powered by the parasite's actin-myosin motor (Weiss *et al.*, 2015). The moving junction is a complex of AMA1 and RON2, the receptor for AMA-1 displayed on parasite cell surface, which internalises the parasite in the parasitophorous vacuole from the anterior to the posterior of the parasite (Tonkin *et al.*, 2011, Weiss *et al.*, 2015). The AMA1-RON interactions have been shown to be crucial for invasion of host cells both in *P. falciparum* and *T. gondii*, yet these proteins have diverged between these two apicomplexans (Lamarque *et al.*, 2011). A protein kinase identified to be essential in merozoites invasion of erythrocyte is *Pf*PKG. Using a mutant parasite resistant to *Pf*PKG inhibitor compound 2, free merozoites of wild type (WT) and mutant parasites were compared for invasion after treatment, no invasion was observed in the WT treated parasite compared to >90% of successful invasion by the mutant merozoites (Alam *et al.*, 2015). Within the erythrocytes, *merozoites*, now known as a rings begin to progress into a *trophozoite*, undergoes three to four rounds of DNA synthesis, mitosis and nuclear division to produce a *schizont* with 16 to 22 nuclei forming new daughter *merozoites* (Gerald *et al.*, 2011). These newly formed merozoites egress the erythrocyte and infect new RBCs, a process that is continued until halted by the immune system or a drug treatment. This continued rounds of parasite maturation and RBC destruction, results in the pathology associated with malaria - either mild or severe malaria. The WHO defines severe malaria as the occurrence of one or more complications including impaired consciousness, prostration, multiple convulsions, acidosis, hypoglycaemia, severe malarial anaemia, renal impairment, pulmonary oedema, jaundice and cerebral malaria (CM) amongst others in the presence of *P. falciparum* asexual parasitaemia (WHO, 2015a).

Ring-stage parasitized erythrocytes remain in peripheral circulation, whereas the more mature trophozoite- and schizont-

infected erythrocytes displaying parasite-encoded adhesins at their surface mediate binding to endothelial cell surface ligands and sequester in the microvasculature (Blasco *et al.*, 2017). Electron dense knobs develop at from erythrocyte membrane of newly invaded erythrocytes, on which parasite variant surface antigens (VSA) (known as antigenic variation) anchor, bind endothelial cells, avoid splenic passage and evade host immune response and destruction to establish chronic infection (Bachmann *et al.*, 2012). The erythrocyte membrane protein 1 (*PfEMP1*) is one such protein with about 60 *var* gene variants that mediate adhesion of infected erythrocytes to endothelial receptors such as CD36, intercellular adhesion molecule 1 (ICAM-1), vascular cell adhesion molecule 1 (VCAM-1), chondroitin-4-sulfate A (CSA) and P- and E-selectin (Bachmann *et al.*, 2012). Mature *P. falciparum* parasites adhere to endothelial cells of the microvasculature in several organs including the brain and placenta where they sequester and cause cerebral malaria (CM) or placental malaria in pregnancy respectively (Siciliano and Alano, 2015). The ability to bind to endothelium and sequester in organs including the brain is a distinguished characteristic of *P. falciparum* used to differentiate it from other *Plasmodium* species (Greenwood *et al.*, 2008). CM affects children under 5 years and pregnant women and is generally defined as the presence of diffuse encephalopathy with coma associated with seizures not attributable to other causes of unconsciousness in the presence of asexual parasites (Claser *et al.*, 2011). The factors responsible for CM are still not fully deciphered, but the sequestration of parasites and the downstream pathological processes are key initiation factors (Claser *et al.*, 2011, Howland *et al.*, 2015). But Claser *et al.* identified CD8⁺ T-cells and interferon gamma (IFN- γ) as attractants of infected RBCs (iRBC) to accumulate in the brain and other organs only during experimental CM in mice (Claser *et al.*, 2011). This suggests that accumulation of iRBC in the brain is a result of CM and not the cause of CM. Additionally, IFN- γ has

been reported recently to mediate the development of CM in mouse because IFN- γ deficient mice were reported to be resistant to CM while the WT mice develop CM within 7 days of infection (Villegas-Mendez *et al.*, 2017).

The infective *merozoites* rupture the PVM from the mature schizonts and exit the enclosing erythrocytes in a process called egress and are ready to engage in a further round of erythrocytes invasion and expansion (Margos *et al.*, 2004). Schizont rupture and merozoite release involve a number of *Plasmodium* cysteine proteases (falcipain-2, SERA protein, dipeptidyl aminopeptidase 3 (DPAP 3)), aspartic protease (plasmepsin II) and serine protease (subtilisin-like protease 1 (SUB1)) (Iyer *et al.*, 2018). Among these proteases, the serine-rich antigen (SERA) family with 9 members, SERA1-9, have gained a significant focus (Yeoh *et al.*, 2007). Found in the PV of infected erythrocytes, blood stage SERA proteins are 100-130 kDa precursors, and only SERA5 and SERA6 are known to be essential for erythrocytic parasite viability (Hodder *et al.*, 2009), they are non-redundant and resistant to deletion (Iyer *et al.*, 2018). For efficient egress, activated *Pf*PKG triggers the release of *Pf*SUB1 from merozoite secretory organelles called exonemes which cleave merozoite surface and PV proteins including SERA5 and SERA6, and within 10 minutes the PV swells, iRBC transforms to a rounded-up structure, breaking PVM into vesicles, permeabilising the RBC membrane which rupture within seconds to release the merozoites (Collins *et al.*, 2017, Thomas *et al.*, 2018). Inhibition of *Pf*SUB1 and DPAP-3 has been shown to inhibit parasite egress and SERA maturation (Hodder *et al.*, 2009), indicating that SUB1 activates SERA enzymes and trigger egress (Koussis *et al.*, 2009). *Pf*SUB1 also target the multi-protein merozoite surface protein complex MSP1/6/7, processing of which is important for escape of merozoites (Hale *et al.*, 2017). Further investigations showed that *Pf*CDPK1 phosphorylates SERA5 and modulate its protease

activity; the importance of SERA5 activity in egress was confirmed by inhibiting *Pf*CDPK1 phosphorylation, which directly blocked merozoite egress (Iyer *et al.*, 2018). Therefore, protein kinases are important egress facilitators because they phosphorylate egress-associated proteins such as: *Pf*SUB1, DPAP-3, SERA5 and SERA6 and potentially other proteins not mentioned.

This sequence of uncontrolled *merozoites* invasion and expansion of new erythrocytes continuous nonstop in non-immune individuals until they are restricted by innate and adaptive immune responses or an antimalarial chemotherapy (Gerald *et al.*, 2011). This repeated invasion and destruction of erythrocytes by merozoites and subsequent development to trophozoites and schizonts releasing daughter merozoites after each cycle is known as the asexual developmental phase. In a process called gametocytogenesis, a fraction of the asexual parasites in the erythrocytic phase commit and develop into male and female gametocytes, the form transmittable to the mosquito vector from the host for further differentiation (Doerig *et al.*, 2015).

1.1.2.3 Gametocytogenesis

Factors determining sexual commitment are not fully understood but is female biased, with a ratio of one male to about five female gametocytes depending on parasite clone (Kuehn and Pradel, 2010). Down regulation of the histone deacetylase gene *PfHda2*, heterochromatin protein *PfHP1* and the ABC transporter-encoding gene *gabcg2* are factors related to increased gametocyte numbers in blood stage infections (Sinden, 2015). Each step of RBC infection in the asexual life cycle, commitment to asexual replication and continuation of the current infection or differentiation into non-dividing male and female gametocytes occurs (Kafsack *et al.*, 2014). This commitment occurs before egress and once committed, merozoites develop into male or female gametocytes (Miao *et al.*, 2017). Host environmental cues

such as release of malarial haemozoin, induced host immunity, and haematological response from erythrocyte destruction such as anaemia, increased production of erythropoietin and reticulocytes influence the gametocytogenesis trigger (Liu *et al.*, 2011). Several studies evaluated the commitment to gametocytogenesis, and the AP2-G gene has been identified as an essential activator of gametocyte transcription gene and a regulator of gametocyte formation in *P. falciparum* and *P. berghei* (Kafsack *et al.*, 2014, Sinha *et al.*, 2014). This conserved DNA binding protein, PfAP2-G (PF3D7_1222600), belongs to the apicomplexan AP2 (ApiAP2) family (Kafsack *et al.*, 2014). Maturation of gametocytes to stage V takes about 30 hours in all *Plasmodium* species and morphologically resemble late trophozoites except in *P. falciparum* where development and maturation takes 10-12 days progressing through five morphologically distinct stages (I-V) as shown in Figure 1.2B (Miao *et al.*, 2017, Nixon, 2016). The morphological difference and time to maturation suggest species divergence in the regulation of gametocytogenesis (Josling and Llinás, 2015). In contrast to genes enhancing commitment to gametocytogenesis, a recent study identified lysophosphatidylcholine (LysoPC) as a suppressor of sexual commitment and differentiation (Brancucci *et al.*, 2017), which is important for malaria transmission.

Stage I gametocytes (up to 40 hours post invasion (hpi)) of sexually committed merozoites are difficult to distinguish from young trophozoites using Giemsa stained blood films except for the presence of roundish and pointed end with distinctive pigment pattern (Baker, 2010). Membrane protein *Pfs16*, an early gametocyte marker, can be detected using immunofluorescence-based assay as well as *Pfg27* expressed in gametocyte cytoplasm and nucleus (Baker, 2010, Nixon, 2016, Tiburcio *et al.*, 2015). The *Pfs16* protein is located in the PVM, and in membranous clefts in the erythrocyte cytoplasm (Baker, 2010). Another protein associated with stage I gametocyte development and detected

within few hours post infection is gametocyte export protein 5 (GEXP5, PF3D7_0936600). This protein is detected in significant amounts 6 hpi with levels peaking to 55 fold increase at 12 hpi remaining high up to 24 hpi compared to schizonts (Farid *et al.*, 2017). This protein is an early gametocyte marker expressed and exported once parasites commit to sexual development, maintained until stage IV and declines in stage V (Tiburcio *et al.*, 2015). A study to identify genes regulating gametocytogenesis initiation, comparing gametocyte-over producing and gametocyte-deficient 3D7 parasite lines, 3D7.G⁺ and 3D7.G_{def} respectively using stage I gametocytes, detected 11 genes named *P. falciparum* gametocytogenesis early (*Pfge*) 1-11 (*Pfg27*, *Pfs16*, *Pfg14.744*, *Pfg14.748*, *Pfs47*, *Pfmdv1*, PF11_0038, PF14_0290, PF14_0588, PF14_0708 and PF14_0735) showing ≥ 5 fold increase expression in 3D7.G⁺ compared to 3D7.G_{def} (Eksi *et al.*, 2012). Other characteristics of early stage gametocytes (stage Ib and II), such as assembly of a bilamellar membrane structure enclosed by a network of subpellicular microtubules will begin to manifest at about 48 hpi (Tiburcio *et al.*, 2015). Late stage I gametocytes show pellicular complex consisting of an inner pellicular membrane vacuole and microtubules underneath the gametocyte plasma membrane, starting the formation of the crescent shape (Figure 1.2B) (Liu *et al.*, 2011).

Stage II-IV gametocytes sequester in the bone marrow to evade clearance by the host immune system. In stage II gametocytes, mitochondria appear as branching structures clustered around the small apicoplast and remain present throughout the gametocyte development (Liu *et al.*, 2011, Schneider *et al.*, 2017). Sequestration of maturing gametocytes involves host receptors and parasite ligands: stage I-IIA use CD36 for adherence whereas stages III-IV uses ICAM-1, CD49C, CD166, and CD164, intriguingly parasite ligands binding these receptors remained poorly defined (Wang *et al.*, 2010a). Stage III/IV gametocyte

morphologies show even distribution of mitochondrion and digestive vacuole complex and central nuclei with no apical complex observed using scanning electron microscopy (Schneider *et al.*, 2017). Host cytoplasm of stage IV and V gametocytes have a thin layer around the parasite, and they continuously express *PfGEXP5* protein (Tiburcio *et al.*, 2015). Serial block-face scanning electron microscopy (SBF-SEM), which generates high-resolution 3D images, was used by Schneider *et al.* to obtain a detailed view of membrane organisation and organelle placement across gametocyte development. From the SBF-SEM analysis of stage IV and V gametocytes, osmophillic bodies were observed within the parasites and mitochondrial elongating (length to width ratio) to a maximum value of 4.6 and 3.5 at stage IV, reduced to 3.3 and 1.2 at stage V respectively (Schneider *et al.*, 2017). Fully differentiated mature stage V gametocytes (Figure 1.2B), are released into peripheral blood where they remain for two to three days before they are readily infective to mosquitoes (Kuehn and Pradel, 2010).

1.1.2.4 Gametogenesis

Ingestion of gametocytes by a mosquito during a blood meal from an infective vertebrate host begins the parasite life cycle in the mosquito vector, activating the formation of gametes (gametogenesis) in the mosquito mid-gut lumen. Gametocyte activation is initiated by temperature shift and pH change alongside molecular events that trigger male gametogenesis within a few minutes of ingestion (Aly *et al.*, 2009, Orfano *et al.*, 2016). An approximate 5⁰C drop in temperature, increase in pH from 7.2 to about 8 together with exposure to gametocyte-activating mosquito derived factor, xanthurenic acid (XA), are signals that trigger activation (Carter *et al.*, 2016, Kuehn and Pradel, 2010). The activation of gametocytes is routinely measured by quantifying the exflagellation centers, which occurs shortly after activation. Exflagellation is the formation of motile male microgametes from

male microgametocytes, which detach and free themselves from erythrocytes to locate and fertilize a female macrogamete (Kuehn and Pradel, 2010, Bousema and Drakeley, 2011). During exflagellation, the male microgametocyte rapidly undergoes DNA replication (within 10 minutes) to produce 8N, forming the highly motile flagellated microgametes that fertilize the immotile female macrogametes (McRobert *et al.*, 2008b, Prado *et al.*, 2015). First, within 15 seconds of XA induction, eight basal bodies are assembled from a single microtubule organizing centre and first genome replication and spindle formation of mitosis I completed within 1 minute and the formed basal bodies each nucleates an axonemes. At the of end mitosis III, about 6 minutes post activation, chromatin condensation occurs in parallel with gametocyte exflagellation from host cells following release of membranolytic proteins from vesicles with release of residual axonemes (Fang *et al.*, 2017).

Additionally, exflagellation involves an increase in intracellular calcium and cGMP (3'-5'-cyclic guanosine monophosphate); increased cGMP activates PKG independent of calcium increase, a cGMP dependent protein kinase which, when activated leads to rounding up of gametocytes (Kuehn and Pradel, 2010). XA activated gametocytes also rapidly hydrolyse phosphatidylinositol (4,5)-biphosphate (PI(4,5)P₂) generating inositol (1,4,5)-triphosphate (IP3), thus indicating the importance of PI-PLC pathway (Brochet and Billker, 2016). PKG controls the synthesis of phosphoinositide and production of PI(4,5)P₂, the precursor for IP3 and diacylglycerol (DAG): IP3 triggers mobilisation and release of intracellular Ca²⁺ and DAG activates protein kinase C (PKC) (Brochet *et al.*, 2014a, Raabe *et al.*, 2011). Furthermore, activated microgametocytes require the calcium dependent protein kinase 4 (CDPK4) to initiate first round of DNA replication, assembly of first mitotic spindle and initiation of axoneme motility (Fang *et al.*, 2017, Invergo *et al.*, 2017). These were confirmed to be dependent on

CDPK4 because inhibition of the activity of this kinase abolished these activities either completely or by greater than 90%. CDPK1 has also been identified as important contributor to exflagellation; while both wild type CDPK1 and CDPK1 knock-out (CDPK1-KO) produce mature male and female gametocytes, WT gametocytes round up after induction, with >95% of male gametes exflagellated whereas $\leq 1\%$ exflagellation in the CDPK1-KO males was reportedly observed (Bansal *et al.*, 2018).

Activated male gametocytes produce up to 8 microgametes each, resulting to 1:1 ratio of microgamete and macrogamete; one microgamete can fertilize one female macrogamete which are each derived from a single female gametocyte (Bousema and Drakeley, 2011, Kuehn and Pradel, 2010). Fertilization forms a diploid zygote that undergoes a round of DNA replication to form a tetraploid, which differentiate into motile ookinetes within 24 hours and migrate rapidly through the blood meal to invade and traverse the mosquito monolayer mid-gut epithelium (Brochet *et al.*, 2014a, Smith *et al.*, 2014). Ookinete motility and gliding is also dependent on PKG (Brochet *et al.*, 2014a, Invergo *et al.*, 2017). Migrating ookinetes travel through mid-gut epithelial cells in a toxic intracellular environment with high concentration of reactive oxygen and nitrogen species due to cellular damage they cause resulting in the activation of nitration responses and apoptosis of invaded epithelial cells (Smith and Barillas-Mury, 2016). The nitration 'mark' the ookinete surfaces for immune recognition by the mosquito complement-like system resulting in a significant loss in ookinete numbers destroying about 80% of the invading ookinetes (Smith and Barillas-Mury, 2016). The differentiation of ookinetes to oocysts is initiated when ookinetes contact basal lamina (collagen and laminin); and laminin interacts with ookinete surface proteins P25/28, circumsporozoite- and TRAP-related protein (CTRP), and secreted ookinete adhesive protein (SOAP) (Smith and Barillas-Mury, 2016). Finally, a few ookinetes that

escape immune destruction settle in the basal site of the mid-gut epithelium and convert to sessile oocysts (Bennink *et al.*, 2016). Between 1-2 weeks the immotile oocysts undergo growth and cell division in a process known as sporogony producing up to 40,000 sporozoites from a single oocyst through a dynamic developmental process with mature stages much larger than early stages (Smith and Barillas-Mury, 2016, Doerig *et al.*, 2015). Mature oocyst release sporozoites into the haemolymph where they circulate and invade salivary gland lumen and when this infective mosquito feeds on the next human host (Figure 1.2A), the sporozoites through the saliva are deposited in the skin completing the transmission cycle (Smith *et al.*, 2014).

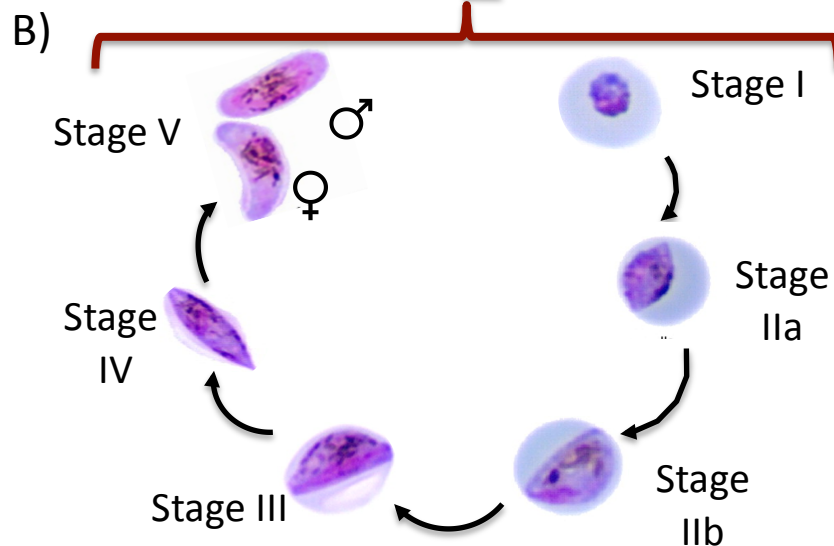
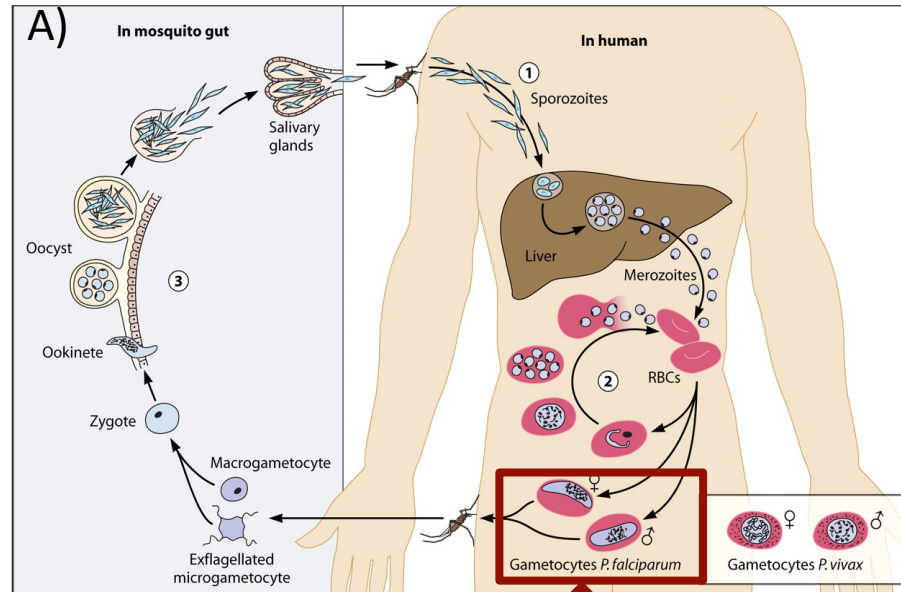


Figure 1.2: Lifecycle of *Plasmodium falciparum*. a) Malaria parasites enter the human bloodstream when an infected female *Anopheles* mosquito taking a blood meal injects sporozoites. The sporozoites migrate to the liver, invade hepatocytes and multiply. Merozoites are formed that are released into the bloodstream, where they invade red blood cells, initiating the asexual multiplication cycle. A fraction of the released merozoites form gametocytes, the transmissible parasite form. b) The development of gametocytes from stage I to stage IIa and IIb then to stage III and stage IV and finally to mature stage V male and female gametocytes in the human host before they are ingested by a susceptible mosquito [Source modified: (Bousema and Drakeley, 2011)].

1.1.3 Malaria control strategies and treatment

1.1.3.1 Malaria vector control strategies

The WHO malaria control strategy is the introduction and use of vector control (i.e, preventing humans from mosquito bites) or chemoprevention (drugs to suppress infection) targeting specific groups and for specific context (for example elimination) (WHO, 2017b). Malaria vector control includes the use of long-lasting insecticide treated bed nets (LLINs), indoor residual spraying (IRS) and recently improvement of housing structures (Tusting *et al.*, 2015, WHO, 2015c). The WHO further reports significant reduction in malaria incidence (up to 50%) in different settings in pregnant women using LLINs, these women had reduced maternal anaemia, placental infection and low birth weight (WHO, 2015c). Furthermore, elimination of mosquitoes by IRS to reduce the infective bites have been reported to have a significant impact on the reduction of malaria prevalence and disease incidence (Coleman *et al.*, 2017). LLINs and IRS together have contributed up to 75% of the averted malaria deaths since the beginning of this century, and it is estimated that vector control is the single intervention capable of reducing malaria transmission from very high levels to close to zero (Shaw and Catteruccia, 2018). Addition to LLINs and IRS, improved housing with close eaves to reduce malaria vectors access to the human host have shown a reduction in prevalence and incidence of malaria (Tusting *et al.*, 2015). Unfortunately, in addition to emergence of insecticide resistant mosquitoes, none of the described tools are useful in controlling outdoor biting and feeding mosquitoes because LLIN and IRS strategies only target *Anopheles* species that feed and rest indoors (Shaw and Catteruccia, 2018).

1.1.3.2 Chemoprevention

The use of intermittent preventive treatment in pregnancy (IPTp) using sulfadoxine-pyrimethamine (SP) as recommended by WHO was reported to reduce maternal anaemia, low birth weight, and perinatal mortality (WHO, 2015c). However, the use of IPTp was reported to be less beneficial in Ugandan women due to the high prevalence of SP resistant parasites (Braun *et al.*, 2015). Seasonal Malaria Chemoprevention (SMC) with amodiaquine (AQ) and SP has reduced clinical and severe malaria incidence by about 75% in children under 5 years, hypothetically averting millions of clinical cases and thousands of deaths in vulnerable communities (WHO, 2017b).

1.1.3.3 Malaria vaccine

1.1.3.3.1 Pre-erythrocytic vaccine

Despite increased malaria research funding (\$2.5 billion in 2015), a significant amount of morbidity and mortality are still due to malaria, hence a highly effective, protective, well tolerated, and safe vaccine to ensure compliance is needed for used in mass campaigns to control and eradicate malaria (Sissoko *et al.*, 2017). Repeated infections with high parasite densities gives immunity against severe clinical disease in malaria endemic areas, suggesting vaccines targeting blood-stage parasites to be protective of severe disease and parasite life cycle progression (Nahrendorf *et al.*, 2015). Unfortunately, naturally acquired malaria immunity develops very slowly, does not give complete protection, and has a limited durability (Partey *et al.*, 2018). Notwithstanding, a successful malaria vaccine would be a high-impact, low-cost public intervention strategy that would control disease progression and malaria transmission (Giersing *et al.*, 2016). Several stages of parasite development have been identified as suitable vaccine targets, and the sporozoite stage is one such attractive vaccine target (Richie *et al.*, 2015). This pre-erythrocytic vaccine concept

delivers attenuated sporozoites to induce anti-sporozoite and anti-liver stage immune response that would kill sporozoites as they try to reach or establish a liver infection, subsequently averting blood stage infection and production of gametocytes (Bijker *et al.*, 2015, Richie *et al.*, 2015). Sporozoite vaccines have been delivered as *Pf*SPZ vaccine (radiated-attenuated cryopreserved *Pf*SPZ), *Pf*SPZ Challenge, delivered by controlled human malaria infection (CHMI), and finally as *Pf*SPZ-CVaz (CVac is Chemoprophylaxis vaccine, sporozoite given along chloroquine for prophylaxis) with both test demonstrating levels of immunogenicity and protection (Richie *et al.*, 2015). *Pf*SPZ vaccine induces a breadth of responses such as CD4, CD8, and gamma delta T cells as well as antibody responses with a breadth induction of antigenicity (Coelho *et al.*, 2017). In a clinical trial in Mali, *Pf*SPZ vaccine gave a protective efficacy against naturally acquired malaria infection to the vaccinated group compared to the 93% infection rate during follow-up in the placebo group, demonstrating vaccine efficacy (Sissoko *et al.*, 2017).

The most successful malaria vaccine developed so far, RTS,S/A01, targets *P. falciparum* circumsporozoite protein (CSP), (CSP is a protein secreted of the sporozoite stage of the malaria parasite and is the antigenic of RTS,S) (Ouattara *et al.*, 2015). A randomised phase 3 clinical study with children (5-17 months) and infants (6-12 weeks) showed a high efficacy by preventing clinical malaria by 55.8% and 31.3% respectively 18 months after 3 monthly doses (RTS, 2015). This showed that repeated dosing with RTS,S is protective against malaria infection and suggest this vaccine to be the first to be deployed against malaria for clinical use (Kaslow and Biernaux, 2015).

1.1.3.3.2 Blood stage vaccine

Repeated blood-stage infection exposes the immune system to parasite diversity and cause generation of a broad antibody

repertoire against merozoites and infected erythrocytes with a complex interplay of inflammatory and immune-regulatory cellular responses, making this phase attractive for vaccine development (Draper *et al.*, 2018). Several blood-stage parasite proteins have been targeted for vaccine development but 10 have been listed in a study: the leading vaccine candidates merozoite surface protein 1 (*PfMSP1*) and apical membrane protein 1 (*PfAMA1*); rhoptry-associated protein 3 (*PfRAP3*); *PfRAP2*; *PfMSP9*; *Pf38* and 5 members of the erythrocyte binding-like (EBL) and reticulocyte binding-like (RBL or *P. falciparum* reticulocyte-binding homologue (*PfRH*) proteins (Douglas *et al.*, 2011). This study reported anti-*PfRH5FL* IgG as an attractive candidate for blood-stage vaccine with higher efficacy compared to *PfAMA1* and *PfMSP1* when tested against vaccine-homologous of 3D7 parasites (Douglas *et al.*, 2011). Fortunately, this protein is highly conserved and indispensable for invasion (Partey *et al.*, 2018). Blood-stage vaccines are needed in concentrations and functional quality to be efficacious to induced pAb because merozoite invasion of erythrocytes is a very rapid process and associated antigens released are exposed for even a much shorter time (Draper *et al.*, 2018), thus a major bottle-neck.

The Malaria Vaccine Technology roadmap launched in 2006 set the ambitious goal of having a licensed first generation malaria vaccine by 2015 with greater than 50% protective efficacy against severe disease and death, effective for at least for year (Kaslow and Biernaux, 2015). This ambition is not yet met even though significant progress has been made unfortunately though; there is no approved malaria vaccine either to block transmission or disease progression. These are attributed to the complex parasite life-cycle between two host, antigenic variation, sophisticated immune evasion ability and genome complexity (Sack *et al.*, 2017).

1.1.3.4 Malaria Treatment

Efforts to prevent malaria transmission and infection using control mechanisms are widely available and used. However, once an infection occurs, treatment needs to be initiated promptly because malaria can be severe and potentially fatal. Several drugs including chloroquine, sulphadoxine-pyrimethamine, quinine, as well as primaquine have been used to treat clinical malaria and recently artemisinin-based combination therapies are the front-line anti-malarial drugs.

1.1.3.4.1 Chloroquine

Chloroquine (CQ), the most widely used antimalarial drug is a 4-aminoquinoline derivative of quinine and has been used for treatment of non-severe and uncomplicated malaria as well as for chemoprophylaxis (Awasthi and Das, 2013, Wellems and Plowe, 2001). CQ has been used widely for malaria treatment to reduce disease prevalence, incidence, mortality, and transmission due to its good efficacy, low toxicity, and affordability (Boudhar *et al.*, 2016).

Malaria parasites ingest host haemoglobin and digest it within the lysosome-like organelle, the digestive vacuole (DV), to generate amino acids to synthesise its protein requirements releasing ferriprotoporphyrin IX (FPIX) in the process which subsequently produce toxic radicals (Ecker *et al.*, 2012). These permeabilise parasite membranes, leading to cell lysis and eventually parasite death (Reiling *et al.*, 2018). Parasites engage the parasitic enzyme haem polymerase to convert the toxic FPIX and crystallise it into the non-toxic haemozoin (5-haematin, Hz) (Awasthi and Das, 2013), in a pH dependent environment accelerated by lipids (Roepe, 2009).

CQ treatment of malaria involves the inhibition of FPIX detoxification and Hz crystallisation. To exert its parasite killing

ability, the mainly alkaline CQ in its neutral state diffuses through the parasite membrane and accumulates within the acidic digestive vacuole of the parasite (Ecker *et al.*, 2012, Reiling *et al.*, 2018), and raises its pH (Awasthi and Das, 2013). Because a greater percentage of CQ in is found in the DV in high concentrations in parasite-infected erythrocytes where FPIX is generated, CQ easily access and bind the FPIX forming the CQ-FPIX aggregates inhibiting haem polymerase and the detoxification of haem resulting in the poisoning of the parasites with their own waste products (Awasthi and Das, 2013, Ecker *et al.*, 2012). CQ-FPIX in addition to causing membrane alteration preventing the proper settlement of mature haemoglobin-laden endocytic vesicles to the DV membrane, also cause DV membrane permeabilisation, and release of DV contents into the cytosol resulting in irreversible parasite damage (Reiling *et al.*, 2018).

The continued use of CQ over long period of time as monotherapy and the of course misuse of the drug led to the selection of resistant parasite strains resulting in the spread and re-introduction of malaria in areas previously identified as malaria free (Reiling *et al.*, 2018). CQ resistance emerged in SEA (Thailand-Cambodia border) and spread to SSA, where it caused a huge increase in morbidity and mortality, thwarting global malaria control efforts (Mwanza *et al.*, 2016, Awasthi and Das, 2013). The CQ resistance transporter (*PfCRT*) gene with the K76T mutation, transporting CQ out of the DV from its active site to limit vacuolar concentrations that enhance CQ-FPIX complex formation is attributed to CQ resistance (Reiling *et al.*, 2018). The mechanism leading the flush of CQ out of the DV is that the un-protonated CQ that crossed the membrane and became protonated to mono-protonated (CQ⁺) and/or di-protonated (CQ⁺⁺) forms bind the *PfCRT* K76T mutant which makes CQ membrane permeable and exit the DV reducing the net CQ

concentration within the DV of CQ resistant (CQR) parasites (Chinappi *et al.*, 2010). Parasites with CQR phenotype have been found to carry two other allelic variants of K76, K76N and K76I; however, a single amino acid change, S163R, restores the CQ sensitivity of CQR parasites (Chinappi *et al.*, 2010). The wild type *PfCRT* CVMNK haplotype at codons 72 to 76 is the main region to monitor CQ resistance in the field and the non-synonymous mutations observed to replace the wild type *PfCRT* haplotypes are SVMNT or CVIET and their prevalence from a study of clinical samples in Ethiopia were very low, 4.1% and undetected levels respectively (Mekonnen *et al.*, 2014). A similar study to monitor resistance levels in India reported different combination of mutations of the *PfCRT* gene in malaria samples, 27% were shown to carry the double mutant haplotype SVMNT and 7% had the triple mutant CVIET genotype (Patel *et al.*, 2017). The CVIET haplotype originated from the Thailand-Cambodia border, and several other haplotypes have been reported since, with SEA having: CVIEA, CVIDT, CVTNT, CVMNT, and CVMHT haplotypes (Awasthi and Das, 2013). Although *PfCRT* haplotypes are the main factors for CQ resistance in *Plasmodium* parasites, the *PfMDR1* (*P. falciparum* multidrug resistant gene 1) gene with mutant haplotypes S1034C, N1042D, and D1246Y have been identified to intensify CQR (Ecker *et al.*, 2012). *PfCRT* mutations causing CQR affects parasite sensitivity to several antimalarial especially the quinolone scaffolds such as quinine, amodiaquine and mefloquine, others that have moieties present in quinolone drugs such as lumefantrine and halofantrine and several other antimalarial scaffolds (Bellanca *et al.*, 2014). The *PfMDR1* gene mutations affect the parasite's ability to transport and accumulate CQ in the parasite's food vacuole leading to reduced CQ sensitivity (Mekonnen *et al.*, 2014). Although *P. falciparum* parasites resistant to CQ are widespread, resistant *P. vivax* parasites are yet to be widespread and therefore CQ is still recommended to treat *P. vivax* infections (Flannery *et al.*, 2013).

The widespread prevalence of CQR parasites led to the withdrawal of CQ as first line antimalarial in many endemic countries (Lu *et al.*, 2017). This reduces the selection pressure of CQR *P. falciparum* isolates, and reverted resistant haplotypes to CQ sensitive haplotypes in samples from areas where CQR was previously prevalent (Lu *et al.*, 2017). A Kenyan study also showed that long-term withdrawal of CQ result in reduced prevalence of *PfCRT* resistant marker K76T by about 60% (Kiarie *et al.*, 2015). In Malawi, the prevalence of CQR parasites has been shown to be less than 0.5% of all cases of malaria tested nationwide, due to early withdrawal of CQ as first-line antimalarial drug (Frosch *et al.*, 2014). The revert to CQ sensitivity may have occurred due to spread of a highly fit susceptible isolate; reverse mutation of *PfCRT* K76T to restore chloroquine sensitivity; or expansion of a chloroquine sensitive parasite that survived chloroquine pressure (Takala-Harrison and Laufer, 2015). Clearly the withdrawal of CQ pressure resulted in emergence of CQ sensitive parasites and indicates that this useful antimalarial could be re-introduced for malaria treatment (Frosch *et al.*, 2014).

Primaquine, an 8-aminoquinoline is an effective drug to clear the dormant hypnozoites of *P. vivax* and *P. ovale* infections that are refractory to most anti-malarial drugs (Flannery *et al.*, 2013). However, because primaquine is toxic to individuals with glucose-6-phosphate dehydrogenase deficiency (G6PD) and its efficacy requires repeated dosing, the use of primaquine is limited because G6PD is prevalent in malaria endemic regions (Flannery *et al.*, 2013).

1.1.3.4.2 Sulfadoxine and Pyrimethamine

Several malaria endemic countries introduced sulfadoxine-pyrimethamine (SP) as first-line antimalarial drug for uncomplicated malaria following the widespread appearance of

CQR (Matondo *et al.*, 2014, Tahita *et al.*, 2015, Bareng *et al.*, 2018). Sulfadoxine interrupts the folate pathway by inhibiting the enzyme dihydropterate synthase (DHPS) domain and prevents the catalysis of *p*-aminobenzoic acid (PABA) to folic acid and, pyrimethamine inhibits the activity of dihydrofolate reductase-thymidylate synthase (DHFR-TS) activity, which reduces dTMP (thymidine monophosphate) levels and arrest DNA synthesis (Bareng *et al.*, 2018, Tahita *et al.*, 2015). In combination they act synergistically, and inhibit the folate biosynthesis pathway and were introduced as first-line antimalarial after the uncontrolled global spread of CQR (Bareng *et al.*, 2018). The complete synthesis of folate is important because folate derivatives are essential for DNA replication, protein synthesis and cell survival, and malaria parasites unlike humans can synthesise folate *de novo* with the *Pf*DHPS enzyme, which is mimicked by its structural analog sulfadoxine (Heinberg and Kirkman, 2015). Furthermore, *Pf*DHFR with two other enzymes; serine hydroxymethyltransferase (SHMT) and thymidylate synthase (TS), convert dihydrofolate to folate, and in addition to its *de novo* function, *Pf*DHFR also help to salvage folate from its environment making it a great antimalarial target (Heinberg and Kirkman, 2015).

Malaria in pregnancy is a major public health problem causing maternal anaemia, low birth weight due to intrauterine growth retardation, and premature delivery with specific complications to the pregnant woman including acute lung injury, severe hypoglycaemia and coma (Desai *et al.*, 2018). The WHO recommended pregnant women to be given monthly SP for IPTp starting in the second trimester for at least three doses during each pregnancy as a chemoprevention for malaria (WHO, 2017b). Accurate administration IPTp has been reported to reduce the prevalence of placental malaria, maternal and foetal anaemia, improved birth weight, and reduced neonatal mortality (Owusu-Boateng and Anto, 2017, Tahita *et al.*, 2015). Where this fails,

prompt treatment is initiated with a safe antimalarial to protect both the mother and the foetus and be efficacious to clear parasites within the shortest possible time (D'Alessandro *et al.*, 2018). Pregnant women with malaria in the second or third trimester are treated with ACTs as normal un-pregnant adults because they clear parasites efficiently; however, there are currently no guidelines for treatment in the first trimester and a clever treatment choice with little potential for complications needs to be chosen (D'Alessandro *et al.*, 2018).

The use of SP for treatment and IPT to prevent malaria in pregnancy and infants was threatened by the emergence of mutations within the target genes. Five *PfDHFR* mutant alleles (A16V, N51I, C59R, S108N/T and I164L) are associated with *in vitro* and *in vivo* resistance to pyrimethamine while 5 other point mutations ((S436A/F, A437G, K540E, A581G and A613S/T) in *PfDHPS* are associated with *in vitro* resistance to sulfadoxine. The combined *PfDHFR* triple mutation (51I-59R-108N) with *PfDHPS* double mutant (437G-540E), generating the *dhfr/dhps* quintuple mutation are generally associated with treatment failure (Tahita *et al.*, 2015). These quintuple mutations associate with mutations recently detected in Africa in *PfDHFR* (I164L) and *PfDHPS* (A581G, A613S/T) to confer higher resistance and, appearance of the sextuple A581G mutation results in clinical failure (Nkoli Mandoko *et al.*, 2018).

Like CQR, resistance to SP emerged from the Thailand-Cambodia border in SEA and spread across Asia before finally reaching Africa; the triple *PfDHFR* mutant alleles (51I, 59R, 108N) in Africa share the same ancestral genes as those in SEA as shown by microsatellite analysis (Vinayak *et al.*, 2010). Interestingly, analysis of samples from SEA, South America, and Africa shows that *PfDHPS* mutant alleles are evolutionary distinct, indicating resistance to sulfadoxine has independent global origins (Zhang *et*

al., 2014b, Vinayak *et al.*, 2010). *PfDHPS* mutation only appear following established *DHFR* mutations, hence the emergence of *PfDHPS* mutant alleles was delayed compared to the emergence to pyrimethamine resistant alleles (Zhang *et al.*, 2014b).

1.1.3.4.3 Artemisinin

Chinese scientists discovered Artemisinin (qinghaosu) in 1970 in a screen that identified several plants with good antimalarial activity including *Artemisia annua* from which artemisinin, effective against rodent malaria was extracted (Cui and Su, 2009). Artemisinin (ART) has a 1,2,4-trioxane core incorporating an endoperoxide bridge essential for its activity and are activated by a ring opening generating radical intermediates that react with susceptible parasite targets (Klonis *et al.*, 2011). The endoperoxide bridge is important for ART to exert its effect and this has been proven comparing the action of deoxyartemisinin and ART for the inhibition of malaria growth and yeast and only ART was able to inhibit parasite growth (Wang *et al.*, 2010b). Because ART is insoluble in water and oil, its carbonyl group was reduced to produce dihydroartemisinin (DHA), its water soluble derivative artesunate, and oil-soluble artemether and arteether (Cui and Su, 2009). These are referred to as first generation ART derivatives synthesised and use for malaria treatment (Wang *et al.*, 2010b). The endoperoxide bridge is the key functional part of this class of antimalarial and their backbones can be varied without loss of functional efficacy (Wang *et al.*, 2010b).

Though ARTs have a short half-life (about 1 hour), it is the fastest antimalarial, potent against all erythrocytic stages and results in rapid clinical responses (Cui and Su, 2009), reducing parasite burden by about 10,000 fold every 48 hours of treatment, and fatality from severe malaria (Tilley *et al.*, 2016). The short half-life prevents the development of resistant parasites by residual

concentration of drugs after treatment (Cui and Su, 2009). ART are active against gametocytes making them important antimalarial agents for transmission blocking in low transmission settings (O'Neill *et al.*, 2010). However, they are less active against the quiescent mature stage V gametocytes and liver stage parasites where no haemoglobin digestion occurs (Tilley *et al.*, 2016, Andrews *et al.*, 2018). The long treatment course of ACTs given over 3 days with multiple daily doses reducing compliance and result in treatment failure and drug resistance (Andrews *et al.*, 2018).

ARTs are activated by iron-catalysed reductive scission of its endoperoxide bond to produce carbon-centred radicals that react with susceptible groups of parasite proteins and other biomolecules; *Plasmodial* protease-mediated digestion of imported haemoglobin is the main source of iron in parasites (Tilley *et al.*, 2016). Haemoglobin digestion generates redox by-products including haem and superoxide radicals, which are rapidly converted to hydrogen peroxide (H₂O₂), resulting to oxidative stress to the parasite. The parasites detoxify this cytotoxic environment by engaging antioxidant enzymes such as glutathione and thioredoxin-dependent proteins such as ornithine aminotransferase (OAT) which are essential in the parasite redox pathway (Ismail *et al.*, 2016). The haemoglobin degradation products, haem or ferrous iron is needed for the potent antimalarial activity of ART because once activated, ART reacts with haem to cause oxidative stress through oxidative insult in the parasite cytoplasm (Klonis *et al.*, 2011). Additionally, ART and free Fe⁺² generate ROS (reactive oxygen species) in the parasite through endoperoxide bridge activation and by Fenton process respectively (Ismail *et al.*, 2016). Evidence confirm the activation and generation of ROS, and the ART-activated ROS overwhelms the parasite antioxidant defence systems which finally lead to parasite death (Ismail *et al.*, 2016). Interestingly, the iron

dependent bioactivation of the endoperoxide bridge drives the selectivity of ART to parasite-infected erythrocytes over normal erythrocytes (O'Neill *et al.*, 2010).

Although the exact ART targets remained undetermined, an earlier study suggested target was parasite mitochondria as demonstrated by comparing ART with deoxyartemisinin on the inhibition potential of malaria parasite, yeast and mammalian mitochondria where yeast and malaria mitochondria were inhibited by ART only (Wang *et al.*, 2010b). However, a recent study suggest that ART target two important sources of carbon/energy and amino acid supply in blood stage infections but other important metabolic pathways including DNA, protein, and lipid synthesis pathways were implicated as ART targets (Ismail *et al.*, 2016). *Pf*ATP6ase has also been identified as target dependent on iron, and the potency of ART was compared with deoxyartemisinin which showed no inhibitory effect to this protein (O'Neill *et al.*, 2010) similar to inhibition of the sarco/endoplasmic reticulum Ca^{2+} -ATPase by thapsigargin (Klonis *et al.*, 2011). Phosphatidylinositol-3-kinase (*Pf*PI3K), a protein important for export of *P. falciparum* proteins from the endoplasmic reticulum (ER) to the erythrocyte, is another protein kinase identified as DHA target because immuno-purified *Pf*PI3K was inhibited by DHA at low nanomolar concentration (4 nM) and not by deoxyartemisinin and other inhibitors (Mbengue *et al.*, 2015). Several sites, proteins, and lipids have been suggested as targets for ART, however, the accumulation of damage to a level that overwhelms parasite protein repair system, together with inactivation of multiple proteins with important housekeeping functions, parasite death is the eventual outcome following exposure to ART (Tilley *et al.*, 2016).

In an effort to reduce the early emergence of resistance, WHO in 2005 recommended the use of ART in artemisinin-based

combination therapies (ACT) with a longer lasting partner drug as first-line antimalarial drug in all malaria endemic countries (Ashley *et al.*, 2014). This gives the short half-lived and fast acting ART the opportunity to kill most of the parasites whereas the longer lasting partner drug clears the residual parasites (Winzeler and Manary, 2014). For ACT, derivatives of ART are used in the following combinations: artemether and lumefantrine; artesunate and amodiaquine; artesunate and mefloquine; and dihydroartemisinin and sulfadoxine-pyrimethamine for the treatment of uncomplicated malaria in children and adults for 3 days (WHO, 2015b). Recommended severe malaria treatment is intravenous or intramuscular artesunate for minimum of 24 hours until oral medication is tolerated before switching to ACTs (WHO, 2015b). To strengthen this recommendation, WHO only funds the use of ART in combination with other antimalarial ideally to delay the emergence of drug resistant parasites (Winzeler and Manary, 2014). The continued availability and use of ACT coupled with increased and improved vector control strategies, global morbidity, and mortality due to malaria declined sharply (Ashley *et al.*, 2014, Dondorp *et al.*, 2009). However, reports of reduced efficacy of ACT and artesunate monotherapy emerged in western Cambodia (Dondorp *et al.*, 2009), threatening the gains in reducing morbidity and mortality and prospects for global malaria elimination (Ashley *et al.*, 2014).

ART resistance is defined as delayed parasite clearance half-life ≥ 5 -hours following treatment with an artesunate monotherapy or with ACT in the presence of K13 mutations (WHO, 2017a). ART resistance in SEA is associated with mutations in the amino acid sequence of the propeller region of the *kelch* motif-containing gene on chromosome 13, *PfKelch13* (K13) and several mutations with statistical significance have been identified in this region (Tun *et al.*, 2015). However only a few these mutations are validated (C580Y, I543T, R539T, Y493H and N458Y) to be associated with

delayed parasite clearance phenotype after treatment with many others yet to be validated (WHO, 2017a). However, Tun and colleagues report that significant levels of K13 mutations are only present in regions with ART resistance, and suggest that surveillance of molecular markers of ART resistance will help the containment and elimination effort in real time (Tun *et al.*, 2015). Surprisingly however, previous antimalarial drug resistance emerged from this region and spread to Africa. Hence, the prevalence of K13 mutations either associated or confirmed alongside delayed parasite clearance was investigated in Africa from 12 malaria endemic countries using ACTs, but none of the K13 mutations reported in SEA were detected from >1200 samples analysed (Kamau *et al.*, 2015).

ART resistant *P. falciparum* parasites have spread rapidly within SEA following the detection of the first cases of resistance in western Cambodia and may spread to Africa if not contained (St. Laurent *et al.*, 2015). The rapid spreads of resistant parasite species is enhanced firstly because patients in areas with reduced parasite clearance rates carry more gametocytes and were more likely to develop gametocytes following treatment compared to other patients (Ashley *et al.*, 2014). Additionally, ART resistant parasite lines carrying different K13 alleles: R539T, Y493H and C580Y were infective to different mosquito species: *An. dirus* from Pursat Province, Western Cambodia, and *An. coluzzii* from Theirola, Mali; a long-term-adapted colony of *An. inimus* from western Thailand; and two long-term-adapted *Anopheles stephensi* Nijmegen and *An. gambiae* G3 lines (St. Laurent *et al.*, 2015). The high infectivity of ART resistant parasites to different mosquito species suggest increased transmission potential of these parasites (St. Laurent *et al.*, 2015). Hence, ART-resistant parasites could spread faster in SEA and stretch to Africa if not contained promptly and immediately eliminated, using strategies mapped out by the WHO (WHO, 2011).

1.2 Protein Kinases and Phosphorylation

Protein kinases (PK) phosphorylate other proteins by the addition of a phosphate group (PO_4) to the polar group of various amino acids modifying the protein from a hydrophobic apolar to hydrophilic polar therefore changing its conformation when it interacts with other molecules as shown in

Figure 1.3 (Ardito *et al.*, 2017). The presence of phosphorous, 5 outer electrons that can form a covalent bond, high water solubility, and the versatility to form mono, di and trialkyl and aryl esters with hydroxyl and anhydride makes phosphate groups highly interactive with other proteins to effect phosphorylation (Ardito *et al.*, 2017). Protein phosphorylation equilibrium is maintained through a constant balance interaction between protein kinases and phosphorylation phosphatases making phosphorylation and de-phosphorylation activity an overall reversible process (Ardito *et al.*, 2017, Roskoski, 2015). Once phosphorylated, proteins acquire a different reactivity, interaction specificity or cellular localization that allow them to carry out functions that the un-phosphorylated protein could normally not do and de-phosphorylated proteins through the action of phosphatase, regain their previous functionality (Smoly *et al.*, 2017). Although most eukaryotic genomes contained twice as much protein kinases as phosphatases, the phosphatase genes express higher-copy numbers of proteins to maintain a quantitative balance between kinases and phosphatases (Smoly *et al.*, 2017).

As a regulatory physiological mechanism affecting every basic cellular process, protein phosphorylation has been documented in protozoan parasites and all other eukaryotes for a number of years, and the invasion of erythrocytes by malaria parasites initiated by phosphorylation of important proteins is a good example (Doerig, 2004). An exemplar kinase, protein kinase G (*Pf*PKG), has been shown to be a significant kinase in egress

from, and invasion of erythrocytes by merozoites (Alam *et al.*, 2015). Protein phosphorylation therefore has several functions and participates in almost all regulatory mechanisms in living cells, such as controlling increasing or decreasing protein activity, altering biological activities such as transcription and translation, stabilize or destabilize a protein and control of cellular localization of other proteins (Roskoski, 2015). PK activity and phosphorylation can be quantified and several techniques have been developed, but the transfer of radioactive phosphate from [γ - ^{32}P]-ATP to a protein or peptide substrate remains the “gold standard” (Roskoski, 2015).

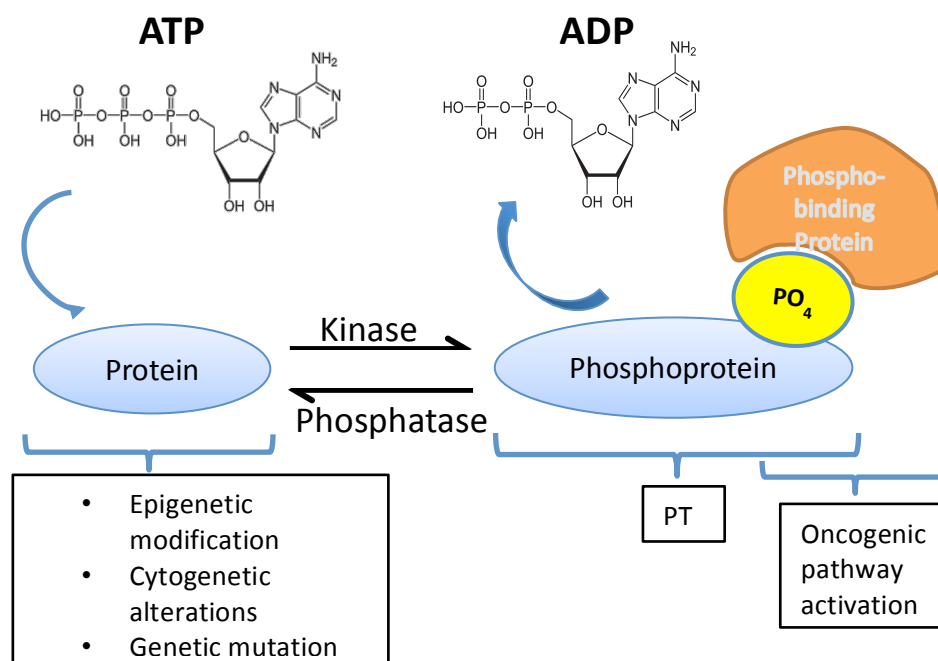


Figure 1.3: Phosphorylation and de-phosphorylation network. The mechanism of phosphorylation regulation consists of kinases, phosphatases and their substrates, phospho-binding proteins. For example, phosphorylation is activated by stimuli such as epigenetic modifications, cytogenetic alterations, genetic mutations, or tumour micro- environment. Consequently, the protein receives a phosphate group from adenosine triphosphate (ATP) hydrolysis due to enzymatic activity of the kinase. This is the mechanism for the basis of post-translational modification (PTM) formation. In addition, phosphorylation is a reversible process due to activity of phosphatase. Phosphorylation and de-phosphorylation are a molecular switch and, in particular, a PTM can cause oncogenic pathway activation by a phospho- binding protein that bind to the phosphate group of a phosphoprotein (figure modified) (Ardito *et al.*, 2017).

Eukaryotic PKs (ePKs) catalyse the transfer of the terminal phosphate group from Adenosine triphosphate (ATP) (γ -phosphate) to the hydroxyl group of a serine, threonine or tyrosine residues in protein substrates using the kinase catalytic core. Kinase catalytic core domain are about 250-300 amino acids residues that are greatly conserved and remarkably specific to substrate binding in signalling pathways (de Oliveira *et al.*, 2016, Oruganty and Kannan, 2012). These activities are highly complex and influence a lot of vital processes such as instigating a cascade of events critical for cell survival. Phosphorylation of a signaling cascade could result in amplification of several phosphorylation events, one PK catalyzing the phosphorylation of thousands of substrate molecules and if the substrate is a kinase another several phosphorylation events can be catalyzed leading to amplifications of greater than a million events (Roskoski, 2015). Uncontrolled catalytic kinase activity can lead to diseases such as cancer (de Oliveira *et al.*, 2016), but through several highly complex and greatly regulated mechanisms, kinases are maintained inactive, and only activated when necessary (Taylor and Kornev, 2011). These regulatory mechanisms are either kinase specific, where the substrate-binding site (SBS) is masked with a pseudo-substrate, or intra-molecular interactions that hide the kinase catalytic domain (de Oliveira *et al.*, 2016). Protein kinase C for example, is presented with a pseudo-substrate similar to its substrate except that alanine substitutes its phosphorylatable residues serine and threonine, and PKA pseudo-substrate regulatory domains are encoded in a different gene (de Oliveira *et al.*, 2016). These pseudo-substrates interact with the SBS, maintaining kinases in an inactive state. Failure of this control mechanism results in altered PK activity leading to a variety of diseases in humans including cancer, making kinases an attractive drug target, currently representing approximately 30% of drug development programs (Leroux *et al.*, 2018).

Crystal structure of ePKs as shown in **Error! Reference source not found.** discloses the conformational flexibility of the catalytic core and its function in regulating PK activity (Oruganty and Kannan, 2012). The phosphorylation of the activation loop through either auto- and/or heterophosphorylation, activates PKs and releases the activation loop from the active site to enable it bind substrates (de Oliveira *et al.*, 2016). Intracellular signals such as a hormone, neurotransmitter, nutrient deprivation, and/or some other kinds of stress initiate this process (Taylor and Kornev, 2011). For activation, the orientation of the α C-helix in the small lobe and the activation segment in the large lobe are changed and once activated, the active kinase toggles between open and closed conformations as it goes through the catalytic cycle (Kornev *et al.*, 2006). The activation loop has a DFG (DLG in *Plasmodium* species) motif at its N-terminus flipped out (referred as DFG out), and inward (referred as DFG-in) in the inactive and active kinase respectively, controlled by the gatekeeper residue, exposing a hydrophobic pocket suitable for drug binding (de Oliveira *et al.*, 2016). DFG out conformation partially occupy the active site and prevent ATP binding; the C-helix out state can bind ATP but activity would be lost because the catalytic machinery is disrupted (Xing *et al.*, 2015).

The high number of genes encoding PK present in eukaryotes has established the significance of protein phosphorylation. In the human genome, 518 genes were identified in the kinome with 478 as eukaryotic PK genes and 40 as atypical kinase genes (Manning *et al.*, 2002), representing about ~2% of the total number of genes in the human genome (Doerig *et al.*, 2008). This makes them the second largest enzyme family and the fifth largest gene family in humans (Roskoski, 2015). The malarial kinome encodes 91 protein kinase genes (Talevich *et al.*, 2011).

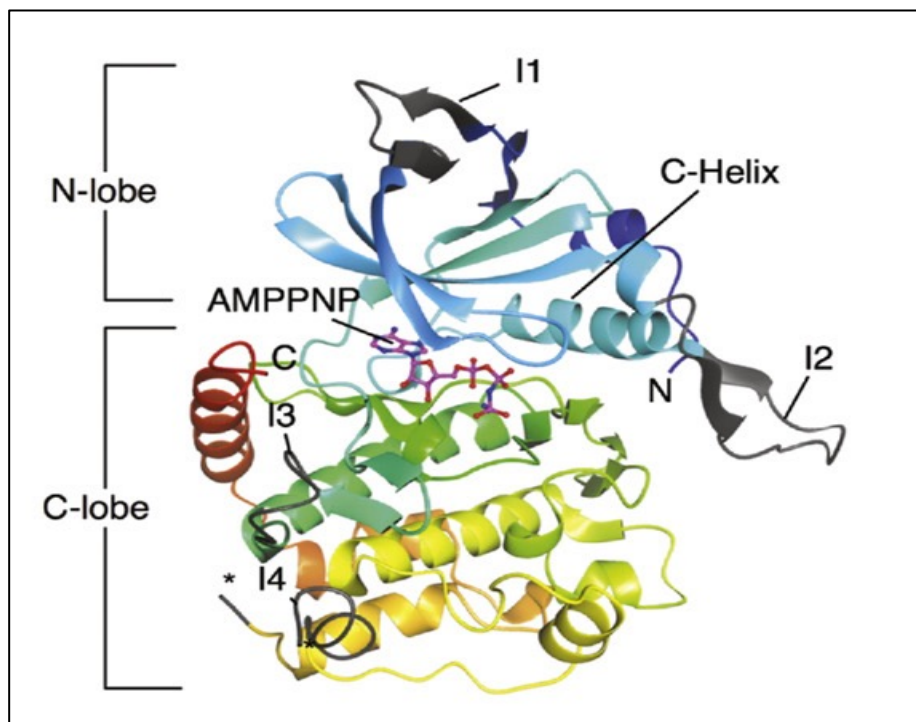


Figure 1.4: The three-dimensional structure of PfPK7 as an example of the ePK fold, presented in ribbon representation and colour ramped from blue at the N-terminus (N-lobe) through green to red at the C-terminus (C-lobe). A β -sheet-rich N-terminal lobe characterizes the bi-lobal ePK fold, and a largely α -helical C-terminal lobe, between which the catalytic cleft is located (shown with AMPPNP, an ATP analogue, in magenta; the so-called C helix, which forms the back of the ATP-binding cleft, is indicated) (Doerig *et al.*, 2008).

1.2.1 The *Plasmodium* Kinome

Based on the sequence similarity of their catalytic domains, presence of accessory domains and their modes of regulation, ePKs are classified into nine groups by phylogenetic analysis (Talevich *et al.*, 2012). Many of the sequences that constitute the *P. falciparum* kinome and kinomes of other organisms cluster within the familiar AGC, CMGC, cGMP, CK1, TKL and CaMK groups of the mammalian kinome (Manning *et al.*, 2002). However, a novel family of atypical protein kinase-like enzymes, the FIKKs, named after a conserved Phe-Ile-Lys-Lys motif, and a family of calcium dependent protein kinases (CDPKs) similar to calcium-regulated protein kinases found in plants but not in metazoans are absent in the established ePK groups of the human kinome whereas the kinases and the MAPKK family in the STE group are absent in malaria (Talevich *et al.*, 2012). These kinase groups are presented in a phylogenetic tree in Figure 1.5 and discussed in details below with examples of physiological functions in humans and implications of dysfunction in disease (Roskoski, 2015). The *Plasmodium* kinases have similar biochemical behaviour as their homologues in other organisms hence adapting the description of the human kinome (Talevich *et al.*, 2012).

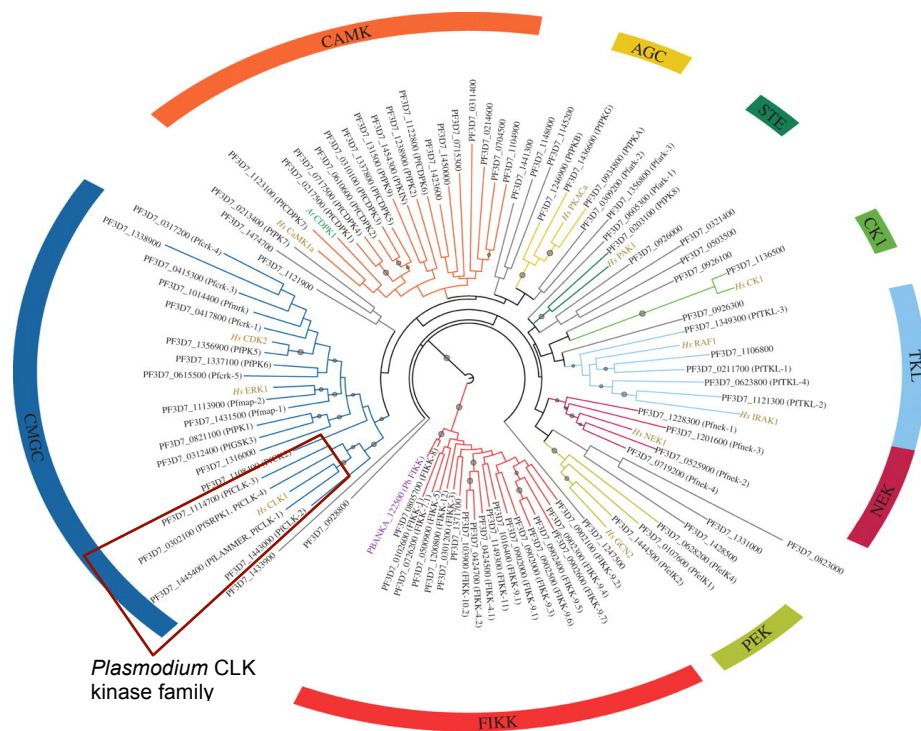


Figure 1.5: Phylogenetic tree of the *P. falciparum* kinome. Circular tree of all 91 ePKs in *P. falciparum* as defined (Talevich et al., 2011). Representative genes from human (Hs), *Arabidopsis thaliana* (At) and *P. berghei* are indicated with labels coloured gold, green and purple, respectively. Branch and arc colours indicate kinase classification by ePK major groups (Hanks, 2003, Hanks and Hunter, 1995) according to Talevich *et al* (2011) with minor modifications in group assignment according to the gene tree. The tree was constructed using conserved sequence regions of 91 protein kinases retrieved from GeneDB (<http://genedb.org>), *P. falciparum* 3D7 sequence v. 3 and u conserved sequence regions were removed. A gene tree was then inferred from the resulting 245-column alignment using RAxML with the rapid bootstrap analysis and maximum-likelihood tree search algorithm, LG amino acid substitution model, and gamma model of substitution rate heterogeneity. The tree was rendered with the Interactive Tree of Life server (iTOL) and edited in InScape (<http://inkscape.org>). A grey circle on a branch indicates bootstrap support greater than 50; larger circles indicate greater bootstrap values. The *Plasmodium* CLK kinase family, belonging to the CMGC subgroup is indicated with a brown rectangular box. Source modified, (Talevich *et al.*, 2012).

- (I) Cyclic-nucleotide and calcium/phospholipid dependent kinases (the AGC group): This group consists of 63 PKs in humans and contains 3 key families: cyclic adenosine monophosphate (cAMP)-dependent PK catalytic subunit alpha (containing PKA), cGMP-dependent PK 1 (PKG) and PK C, (PKC) families, along other families such as Akt1/2/3 (PKB1/2/3), Aur1/2/3 (Aurora kinase), PDK1 (phosphoinositide-dependent kinase), and RSK1/2/3/4 (ribosomal protein S6 kinase) (Roskoski, 2015). Twelve per cent of the human kinome is made of this kinase group which is highly conserved and widely represented across eukaryotes, has 2 pseudokinases, RSKL1 and RSKL2 (that lack the catalytic activity features) and 6 pseudogenes (MRCKps, GPRK6ps, PRKXps, PKCips, p70S6Kps1 and p70S6Kps2), coding for non-functional gene copies that are not expressed or are severely truncated (Arencibia *et al.*, 2013, Leroux *et al.*, 2018). Kinases in this group are involved in the regulation of cell proliferation, differentiation and survival through the phosphorylation of large substrates *in vivo* such as BCL2-antagonist to prevent activation of the apoptotic pathway, and transcription factor forkhead box-O to control gene regulation (Jester *et al.*, 2012). This kinase group plays several other physiological roles in human: the PKA family play a physiological role in glucose homeostasis and triglyceride storage while PKG is the main effector kinase of the NO/cGMP signalling cascade with a significant role in regulating cardiovascular and neurological functions (Arencibia *et al.*, 2013). PKC-iota, a highly expressed PKC, is present in different types of cancers and inhibition of this gene inhibits lung tumour growth whereas PKC-theta is involved in the activation of T cells; both are attractive pharmacological targets (Arencibia *et al.*, 2013).
- (II) The calmodulin-dependent kinases (the CAMK group): The CAMK group consists of 74 members and contains

calcium/calmodulin-dependent protein kinases including CaMK1/2/4, PhK γ 1/2 (phosphorylase kinase), MAPKAPK2/3/5 (mitogen-activated protein kinase activating protein kinases), Nek1–11 (Never in mitosis kinases), and MLCK (myosin light chain kinases). These kinases are activated by high intracellular calcium concentrations and once activated they phosphorylate several transcription factors through serine or threonine residues (Ardito *et al.*, 2017).

(III) CK group: The CK1 group consists of 12 members and contains the CK1 $\alpha/\gamma/\delta/\epsilon$ (casein kinase 1), TTBK1/2 (tau tubulin kinase), and the VRK1/2/3 (vaccinia-related kinase) families.

(IV) CMGC group: The CMGC group consists of 62 members and contains the CDK (Cyclin-dependent protein kinases, CDK1–11), MAPK (mitogen activated protein kinase) (ERK1–5), GSK3 (glycogen synthase kinase), and CDC like kinases (CLK) families (Roskoski, 2015, Varjosalo *et al.*, 2013) as shown in Figure 1.5. Ardito *et al.* described the functions of the individual members of this group and the residues they phosphorylate. The different phases of the cell cycle progression are regulated by action of the CDKs (Ardito *et al.*, 2017); the CMGC further control the activity of human tumour suppressors and are of prime interest in molecular cancer research (Varjosalo *et al.*, 2013). MAP kinases play key roles in regulating many cellular processes including proliferation, differentiation and cell death; and dysfunction of the MAP kinase cascade has a direct link to oncogenic transformation (Ardito *et al.*, 2017). A separate group of the CMGC kinase families are the dual-specificity tyrosine-regulated kinase (DYRK) and the serine-arginine protein kinases (SRPK) (Varjosalo *et al.*, 2013). SRPKs involved in pre-mRNA processing are phosphorylated and released into the nucleoplasm by CLK kinases which

potentially have a strong role in governing splice site selection (Ardito *et al.*, 2017). The CMGC kinases preferentially phosphorylate their substrates using the proline at position P+1 and their mechanisms are regulated by phosphorylated tyrosine in the activation loop, or pre-phosphorylated substrate residues and they interact with the CMGC insert in the C-lobe (Oruganty and Kannan, 2012). The arginine residue (R1192^{Erk2}) distinguished CMGC from other kinases, facilitate proline binding and substrate specificity of the P+1 pocket, and coordinate with the phosphorylatable tyrosine (Y1185) in the activation loop to regulate activity (Oruganty and Kannan, 2012).

(V) STE group: The STE group (related to yeast non-mating or sterile genes) contains 47 members and consists of MAPK cascade families (Ste7/MAP2K, Ste11/MAP3K, and Ste20/MAP4K). MEK1/2/5/7 of the Ste7 family are dual specificity protein kinases that catalyze the phosphorylation of tyrosine and then threonine residues of the target ERK/MAP kinases.

(VI) TK group: The TK (tyrosyl kinase) group consists of 90 members including 58 receptor (e.g., EGFR, FGFR, Flt, InsulinR, PDGFR) and 32 non-receptor tyrosine kinases (e.g., Abl, Eph, JAK, and Src). Tyrosine kinase group is absent in *Plasmodium* parasites but *Plasmodium* can still phosphorylate tyrosine residues and the two proteins that phosphorylate on tyrosine residues are *Pf*GSK3 which phosphorylate on Y229 analogous to Y279 and Y216 on mammalian GSK3 α/β , and *Pf*CLK3 kinase, a serine/threonine kinase related to the pre-mRNA processing kinase hPRP4: both *Pf*CLK3 and hPRP4 are dual-specificity tyrosine phosphorylated-regulated kinase (DYRK) and tyrosine phosphorylation in *Pf*CLK3 occurs on Y526 within the TSY (Talevich *et al.*, 2012).

- (VII) TKL group: The TKL (tyrosyl kinase-like) group is a diverse family that resembles both protein-tyrosine and protein-serine/threonine kinases; it contains 43 members and consists of MLK1–4 (mixed-lineage kinases), LISK (LIMK/TESK for LIM (Lin-11, Isl-1, Mec-3) kinase and testes expressing serine kinase), IRAK (interleukin-1 receptor-associated kinase), Raf, RIPK (receptor-interacting protein kinase, or RIP), and STRK (activin and transforming growth factor receptors). LIM kinase contains paired zinc fingers that participate in protein–protein interactions as opposed to DNA binding.
- (VIII) RCG group: The RCG (receptor guanylyl cyclase) group contains 5 members and is similar in domain sequences to protein-tyrosine kinases.
- (IX) OTHERs group: The final group, labelled OTHER, is diverse with 83 members.

Plasmodium kinases mostly distinguish themselves from their homologues in other eukaryotes by displaying complex extensions and insertions within their catalytic domains (Talevich *et al.*, 2012). Additionally, ePKs are further characterized centered on substrate specificity falling within one of two broad classes, serine/threonine-specific and tyrosine-specific kinases (Andrade *et al.*, 2011). The classifications based on the nature of the phosphorylated-OH group (alcohol or phenol), as protein-serine/threonine kinases that phosphorylate serine and threonine residues (385 members), protein-tyrosine kinases (90 members) phosphorylate tyrosine residues, and tyrosine-like kinases (90 members), because serine and threonine contain an alcoholic side chain while tyrosine contains a phenolic side chain (Ardito *et al.*, 2017, Roskoski, 2015). It is also important to note that there are dual specificity kinases (Hybrid), which can phosphorylate both serine/threonine and tyrosine residues (Andrade *et al.*, 2011, Ardito *et al.*, 2017).

1.2.2 Structure of Protein Kinases

PKs are categorized into two super families; one comprising the eukaryotic or conventional protein kinases (ePK) that share a conserved catalytic domain, and the other covering the atypical protein kinases (aPKs) (Andrade *et al.*, 2011). All ePKs are composed of the non-conserved regulatory domains and a catalytic core domain of ~250 amino acids conserved across all kinases which binds to and anchor substrates and catalyze their phosphorylation (de Oliveira *et al.*, 2016). The small, mostly β -sheet and one conserved alpha helix (C-helix) is the N-terminal subdomain and, the larger mostly helical C-terminal subdomain (**Error! Reference source not found.**) contains the activation segment phosphorylated in many kinases once the kinase is activated (Scheeff and Bourne, 2005, Xing *et al.*, 2015). The two lobes are connected with a hinge region and a folding cleft within which ATP binds forming conserved hydrogen bond interactions (Xing *et al.*, 2015). These lobes converge once the kinase is activated forming the deep cleft for binding of ATP adenine ring to position the γ -phosphate at the outer edge for phosphoryl group transferred at the same time burying the adenosine moiety in the hydrophobic region of the pocket (de Oliveira *et al.*, 2016). The substrate is anchored and correctly positioned within the SBS for positioning of the phosphorylatable residue (de Oliveira *et al.*, 2016). Several small molecule kinase inhibitor templates have been identified/developed targeting the ATP binding site in many drug discovery approaches (Xing *et al.*, 2015).

1.2.2.1 The N-Lobe

In the N-terminal lobe, there are three β strands ($\beta 1$, $\beta 2$ and $\beta 3$) trailed by α -helix (αC) and two additional β strands ($\beta 4$ and $\beta 5$) (Bullock *et al.*, 2009, Jain P. *et al.*, 2014). These beta sheets are anti-parallel and have an essential role in the ATP binding site (de Oliveira *et al.*, 2016). Within the first three beta strands are two important motifs, the Glycine-rich loop (GxGxxG) between $\beta 1$ and $\beta 2$ and the AxK motif in the $\beta 3$ strand which has a lysine that couples the phosphate of ATP to the C-helix, a unique and dynamic kinase regulatory molecule (Taylor and Kornev, 2011). The G-loop has dynamic conformation dependent on the presence of ligands and activation of the catalytic domain (Schwartz and Murray, 2011). In PKA, the Glycine-rich loop contains ⁵⁰GTGSFG⁵⁵ (conserved in *Plasmodium* CLK3 kinases as KGVVFS as shown in Figure 6.1, page 167), and the phenylalanine (F54) and the third glycine (G55) anchoring the beta phosphate of ATP whereas the γ -phosphate interacts with the –NH and the hydroxyl groups of Ser53 while the second (G52) and third (G55) glycine form hydrogen bonds. Additionally, the α - and β -phosphates are held in position by the Lys72 in $\beta 3$, which forms a salt bridge with Glu91 of αC -Helix stabilizing the phosphate interactions (Roskoski, 2015, Taylor and Kornev, 2011). The C-helix is strategically positioned between the two lobes connecting different parts of the kinase and serving as ‘Signal Integration Motif’ with its C-terminus anchored to the C-lobe by the αC - $\beta 4$ Loop and its N-terminus interfaces with the Activation Loop (Taylor and Kornev, 2011). Another important loop within this lobe is the P-loop, it binds ATP and position its γ -phosphate for transfer at the base of the active site cleft (Kornev and Taylor, 2015). This P loop also known as the Walker motif has a consensus sequence of GxxxxGK and the conserved Lys at the end of the loop (Arg56 in PKA), helps position the γ -phosphate of ATP and reaches outwards to couple the G-loop to other distal segments that contribute to closing of the G-loop (Kornev and Taylor, 2015).

1.2.2.2 The C-lobe

This lobe is mostly helical and contains the activation segment with residues phosphorylated once the kinase is activated by phosphorylation on the activation loop (Xing *et al.*, 2015). Several unique features are present in the C-terminal lobe. Part of the helix α G, situated at the bottom of the C-terminal lobe is the greatly conserved signature motif of this group (EHLAMMERILG, residues 386-396 and 381-391 in human CLK1 and CLK3 respectively), from which the name LAMMER kinases originated (Bullock *et al.*, 2009). The second helix in the CLK structures is replaced by a small two-strand β sheet (at residues 409-418 in CLK1 and 404-413 in CLK3); followed by helix α H unique to these CLK structures (residues 424-432 and 419-427 in CLK1 and CLK3 respectively). Forming an extended β -hairpin (β hp- β hp') is a second conserved unique insertion in this protein family present at residues 300-317 and 295-312 in CLK1 and CLK3 respectively at the top of the C-terminal lobe (Bullock *et al.*, 2009). Using the local spatial pattern alignment analysis to compare active and inactive kinases, a skeleton of highly conserved four non-consecutive hydrophobic residues that constitute a regulatory or R-spine and eight hydrophobic residues constituting the catalytic or C-spine were discovered through their three-dimensional location from X-ray data of their crystal structures (Roskoski, 2015).

1.2.2.3 Regulatory spine

In PKA, the four non-consecutive hydrophobic residues in the R-spine found only in active kinases are: two from the N-lobe - Leu106 from the β 4 strand and Leu91 from the C-helix; and two from the C-lobe: Phe185 from the Activation Loop and Tyr164 from the Catalytic Loop; these are the hydrophobic spine linking the two lobes (Taylor and Kornev, 2011). The regulatory spine directs the positioning of substrates for catalysis employing residues from the activation segment and the α C-helix, which are

necessary for defining active and inactive states of kinases (Roskoski, 2015). $\beta 5$ from the N-lobe, which carry the residues Met120 (known as the gatekeeper) and Met118 are part of the “shell” surrounding the R-spine and interact with RS3 residue which together are important for kinase activity regulation (Kornev and Taylor, 2015).

1.2.2.4 Catalytic spine

Formation of the C-spine depends on the presence of ATP, the adenine ring of which determines the integration of the small and large lobes in a way similar to the R-spine (Kornev *et al.*, 2008). The C-spine bears two residues from the F-helix: Leu227 and Met231; one residue from the D-helix, Met128; and the three hydrophobic residues, which comprise the $\beta 7$ -strand: Leu172, Leu173 and Ile174 (Kornev *et al.*, 2008). From the N-lobe are two residues in the C-spine, Val57 in $\beta 2$ and Ala70 from the “AxK” motif in $\beta 3$ which directly dock onto the adenine ring of ATP whereas in the C-lobe Leu173 lying in the middle of $\beta 7$ is flanked by two hydrophobic residues, Leu172 and Leu174 in PKA and dock onto the adenine directly (Taylor and Kornev, 2011). The D-helix hydrophobic residue Met238 that binds Leu227 and Met231 of the F-helix is the resting place for the residues Leu172 and Leu174 (Roskoski, 2015, Taylor and Kornev, 2011). Noteworthy, the C-spine is conserved in both serine/threonine and tyrosine kinases and is more sensitive to the nature of the substrate to be phosphorylated, the R-spine on the other hand is less conserved across different kinases (Kornev *et al.*, 2008).

1.2.2.5 Kinase subdomains

The conserved catalytic domain of protein kinases is subdivided into twelve subdomains containing characteristic patterns of conserved residues as regions never interrupted by large amino acid insertions (Hanks and Hunter, 1995). The amino-terminal

lobe, constituting subdomains I-IV, is largely involved in anchoring and orienting the nucleotide, and the larger carboxy-terminal lobe, containing subdomains VIA-XI, is responsible for binding peptide substrate and initiating phosphotransfer while subdomain V residue extent between these two loops (Hanks, 2003). A demonstration of this subdomain classification is shown in figure 1.5A.

Subdomain I contains the conserved GxGxxG motif (Glycine-rich-loop) and acts as a flexible clamp that covers and anchors the nontransferable α - and β - phosphates of ATP through ionic interactions (Schwartz and Murray, 2011) as shown both in the schematic and ribbon diagrams in Figure 1.6A and B. This domain contributes to the hydrophobic pocket that encloses the adenine ring of ATP. A highly conserved valine follows the Glycine-rich loop making a hydrophobic contact to the base of the ATP (Taylor and Kornev, 2011). The glycine-rich loop in subdomain I correlate with β 1 and β 2 (Figure 1.6B) whereas subdomain II associates with β 3 (Kornev and Taylor, 2015). Subdomain II contains the invariant Lysine (K) in the Ala-xxx-Lys in the active conformation (Roskoski, 2015), crucial for maximal enzyme activity and lies within β -strand of the small lobe and helps anchor and orient ATP by networking with its α - and β - phosphates (Ward *et al.*, 2004). Subdomain III, a large α -helix C with a conserved glutamate residue help stabilize the interactions between the lysine in Ala-xxx-Lys and the α - and β -phosphate of ATP (Ward *et al.*, 2004). Not directly involved in catalysis or substrate recognition, subdomain IV contains a variable sequence with a conserved hydrophobic residue (Leu, Ile, or Val) (Roskoski, 2015). Linking the small and large lobes of the catalytic subunit is subdomain V, which has three residues forming hydrogen bonds with either the adenine or the ribose ring and contributes to the hydrophobic pocket surrounding the adenine ring (Hanks and Hunter, 1995).

Subdomain VIa contains a small residue such as glycine, two spacers, and two hydrophobic residues such as tyrosine/leucine and act mainly as a support structure (Roskoski, 2015). Subdomain VIb includes the variant aspartate and asparagine amino acids within the DxKxxN (conserved as DLKPDN in *Plasmodium* species as shown in Figure 6.1, page 170) or corresponding motif, this lies between $\beta 6$ and $\beta 7$ (Asp164 in PKA is the catalytic base), and this segment contains many of the key residues that direct the γ -phosphate of ATP to the protein substrate (Taylor *et al.*, 2012). The catalytic loop is stabilized by the side chain asparagine through hydroxyl bonding which also chelates the magnesium ion (Mg^{2+}) that bridges the α - and γ -phosphates of ATP (Hanks and Hunter, 1995).

Subdomain VII anchors and orients ATP, and is the region spanning the conserved sequences containing residues DFG (DLG in *Plasmodium*, as shown in Figure 6.1, page 170) referred to as the activation segment (Hanks, 2003). The aspartate of the DFG binds Mg^{2+} , is implicated in catalysis and nucleotide exchange making it catalytically important and referred to as “Magnesium Positioning Loop” (Kornev and Taylor, 2015). Subdomain VIII, containing the highly conserved APE residues (Johnson *et al.*, 1998), also called the activation loop, contains activating phosphorylation sites in many serine/threonine and tyrosine kinases (Taylor *et al.*, 1995). The alanine and proline of the APE are anchored to a conserved tryptophan in the αF -helix (Trp222) (Kornev and Taylor, 2015). This subdomain folds into a loop, which faces the catalytic cleft and the nearly invariant glutamate (E) forms an ion pair with an arginine in subdomain XI, stabilizing the kinase domain lobe (Schenk and Snaar-Jagalska, 1999). The interaction of arginine and glutamate through a salt bridge play a significant role in the structure of PKA; mutation in this gene leads to destabilization of the kinase structure, decreased catalytic efficiency and disease (Kornev and Taylor,

2015).

Although highly conserved, protein kinases are exceedingly diverse in their ability to recognize unique substrates and other molecular peptides that serve as activators and inhibitors (Kung and Jura, 2016). This diversity in peptide binding capacity enable kinases to perform a diverse array of non-catalytic functions such as allosterically regulating other kinases and/or unrelated enzymes, coordinate interactions between different components of signaling pathways, interact with transcription factors to regulate transcription or directly bind to DNA (Kung and Jura, 2016).

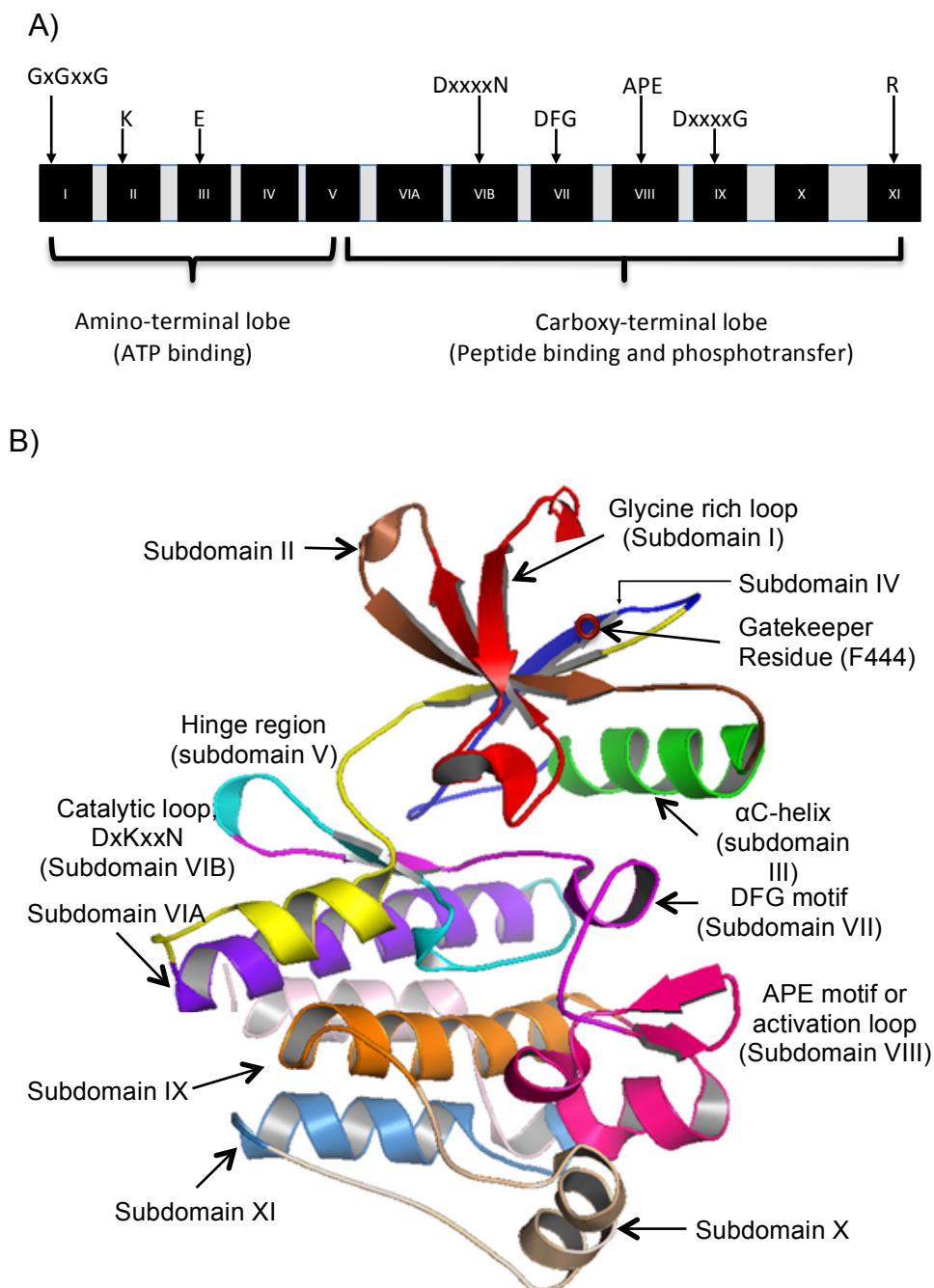


Figure 1.5: A) The ePK catalytic domain schematic diagram. The 12 conserved subdomains are indicated by Roman numerals. The positions of amino-acid residues and motifs highly conserved throughout the ePK superfamily are indicated above the subdomains, using the single-letter amino-acid code with x as any amino acid, modified figure (Hanks, 2003). B) Ribbon structure of a protein kinase showing location of functional subdomains of the kinase Catalytic core showing the glycine rich loop in subdomain I, the gatekeeper residue (Phenylalanine (F) at position 444 in *PfCLK3*), the catalytic loop in subdomain VI, the DFG motif in subdomain VII as DLG in *PfCLK3* at positions 511, 512, and 513; Figure modified (Dixit *et al.*, 2009).

1.2.3 Function of Protein Kinases

1.2.3.1 Function of CLKs

P. falciparum encodes four members of the CLK family in its genome and these *PfCLK1* (PF3D7_1445400), *PfCLK2* (PF3D7_1443000), *PfCLK3* (PF3D7_1114700), and *PfCLK4* (PF3D7_0302100) (Kern *et al.*, 2014, Agarwal *et al.*, 2011). The *PfCLKs* are located on different chromosomes within the parasite genome: *PfCLK1* and *PfCLK2* are located on chromosome 14, *PfCLK3* is located on chromosome 11, and *PfCLK4* is located on Chromosome 3. These kinases are reported to control gene expression and are perhaps important in malaria parasites because of the importance of post-transcriptional regulation of gene expression in these parasites (Agarwal *et al.*, 2011). *PfCLK1* is the homologue of the mammalian lammer kinase and phosphorylate serine/arginine-rich (SR-rich) proteins (Agarwal *et al.*, 2011). Schematic representation of the *PfCLK* kinases is shown in Figure 1.6.

The *PfCLKs* were localized using immuno-labelling and other techniques, *PfCLK1* clearly localises in the nucleus of trophozoites, and in the nucleus and cytoplasm of schizonts and gametocytes of *P. falciparum* parasites (Agarwal *et al.*, 2011, Kern *et al.*, 2014). Additionally, using real time RT-PCR, *PfCLK1* mRNA expression was confirmed present in the asexual blood stages and gametocytes (Agarwal *et al.*, 2011). Similarly, localization of *PfCLK3* in prepared IFA slides showed that *PfCLK3* is predominantly present in the nucleus of trophozoites, however, in schizonts and gametocytes the kinase is present primarily in the cytoplasm, as detected by anti-*PfCLK3* antibody (Kern *et al.*, 2014). To further confirm the presence of *PfCLK3* in the nucleus and cytoplasm of blood stage parasites, western blotting was employed using rat anti-*PfCLK3* antisera, and full length *PfCLK3*

was detected in the nuclear pellet and cytoplasmic fractions using blood stage parasite lysates (Kern *et al.*, 2014).

Investigating the role of *Pf*CLK kinases, it was discovered that parasite development to the next stage of the life cycle was severely impaired when the kinases (*Pf*CLKs) were inhibited; thus confirming that *Pf*CLKs play essential roles for erythrocytic schizogony, gametocyte differentiation, and gametogenesis (Kern *et al.*, 2014), demonstrating the significance of these kinases in parasite survival. Furthermore, it has been shown in humans that CLK1 plays an important role in neuronal differentiation while CLK3, expressed abundantly in mature spermatozoa plays a role in fertilization (Bullock *et al.*, 2009). Thus, *Pf*CLK1 and *Pf*CLK3 kinases expressed profusely in both asexual stages and in gametocytes are playing substantial roles for development and gametogenesis of *Plasmodium* parasites.

Kinases achieve their physiological roles by acting on suitable substrates and partners in a controlled mechanism. The expression of several protein isoforms is controlled through alternative splicing, which results in different and sometimes antagonistic functions (Fedorov *et al.*, 2011). Alternative splicing however, is further controlled by phosphorylation of SR-rich splicing factors, which have been recognized as CLK interaction associates and substrates (Bullock *et al.*, 2009). Present in these proteins are serine/arginine-rich sequences from which the group derived its name and are phosphorylated by serine/arginine-rich protein kinases (SRPKs) (Fedorov *et al.*, 2011). In *P. falciparum*, the three SR proteins previously identified are *Pf*SRSF12, *Pf*SFRS4, and *Pf*SF-1 (Eshar *et al.*, 2012). These SR proteins are phosphorylated by different *Pf*CLK protein kinases. In a kinase assay using immunoprecipitated kinases, it was revealed that *Pf*SFRS4 was phosphorylated by both anti-*Pf*CLK3 and anti-*Pf*CLK1, whereas *Pf*SRSF12 and *Pf*SF1 were phosphorylated by anti-*Pf*CLK3 and anti-*Pf*CLK1 respectively (Kern *et al.*, 2014).

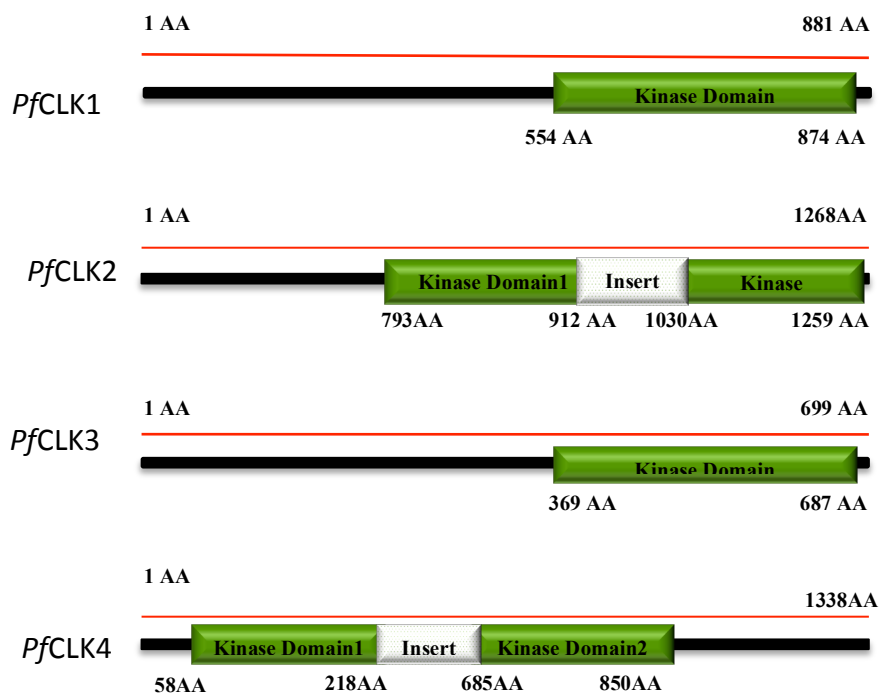


Figure 1.6: Schematic structure of *Plasmodium* CLK kinases. The kinase domains are depicted in green and the inserts in PfCLK2 and 4 are depicted as grey. The kinase domains of all the CLKs are in the C-terminal domain except for PfCLK4, which has its kinase domain starting from the N-terminus and span across the middle towards the C-terminus.

1.2.4 mRNA splicing

Proteome diversity in higher eukaryotes is a result of the splicing order of non-coding intron sequences that split the protein coding exon sequences of pre-mRNA replicated at the transcription level and accurately linking these exons in the correct reading frame (Ritchie *et al.*, 2009, Sahebi *et al.*, 2016). Different mRNA isoforms have distinct coding capabilities and stabilities; hence pre-mRNA splicing is an additional regulatory step in gene expression (Sahebi *et al.*, 2016). This is facilitated by chemical reactions of functional groups between the spliceosome and the regions of the pre-mRNA in a process described as alternative splicing (AS). AS produces multiple different mRNAs from individual genes expanding the information content and versatility of the transcriptome through production of variable segments within identical mRNAs (Wang and Cooper, 2007).

The spliceosome, a complex macromolecular machinery of the cell, made of five Uridine-rich (U-rich) small nuclear ribonucleoprotein particles (snRNP) (U1, U2, U4, U5 and U6) and, other proteins such as small nuclear ribonucleic proteins are tasked to remove introns from pre-mRNA following transcription in the nucleus (Papasaikas *et al.*, 2015, Wahl *et al.*, 2009, Sahebi *et al.*, 2016). The minor spliceosome present in some plants and metazoan species, made of functionally analogous U11/U12 and U4atac/U6atac snRNPs, share the U5 snRNP with the major spliceosome (Wahl *et al.*, 2009). These snRNPs contain an snRNA each, and a variable number of complex-specific proteins together with the seven Sm proteins contained by U1, U2, U4 and U5 snRNPs (Wahl *et al.*, 2009). The exact number of proteins forming the spliceosome is difficult to confirm, however proteome studies have identified about 80 and 170 in the spliceosome of *Saccharomyces cerevisiae* and humans respectively (Zhang *et al.*, 2013).

Introns generally contain conserved 5' splice site (5'ss), a branch point sequence (BPS), a polypyrimidine tract (PYT) and a 3' splice site (3'ss) removed by the spliceosome in two step transesterification reactions (Zhang *et al.*, 2013). Spliceosome assembly starts with the initial recognition of an intron and formation of complex E, with the 5'ss recognised by U1 snRNP through RNA-RNA interaction and a set of cofactors, the BPS recognised by splicing factor 1 (SF1), and the PYT by U2 auxiliary factor (U2AF) (Zhang *et al.*, 2013). The 5'ss and 3'ss of introns are recognised by the interaction of SF1/BBP 65 kDa subunit through its C-terminal RNA recognition motif (RRM) and the U2AF 35 kDa subunit tightly bound to U2AF65 and the U2AF heterodimer binds the AG dinucleotide of the 3'ss (Wahl *et al.*, 2009).

The first splicing step is the binding of the U1 snRNP to the 5'ss and the U2 snRNP to the BPS forming the spliceosomal A complex (Sahebi *et al.*, 2016). The binding of U2 snRNP involves U2 snRNA, and U2 proteins interacting with pre-mRNA sequences are preceded by the recognition and binding of U2AF (a heterodimer of 35 and 65 kDa subunits) to the 3' ends of introns (Papasaikas *et al.*, 2015). Complex A then associate with the pre-assembled tri-snRNP U4/U6-U5 forming the pre-catalytic B complex (Schneider *et al.*, 2010). This association involves the 5' and 3' exon nucleotides pairing with the U5, and the 3' end of the U6 base-pairing with the 5' end of U2; activation of U6 by base pairing with U2 coordinates the positioning of the catalytic metals required for splicing (Fica *et al.*, 2013). U6 snRNA comprises of essential components of the active site but, to avoid premature pre-mRNA cleavage it is delivered inactive, base paired to U4 (Wahl *et al.*, 2009). This complex is activated by conformational changes and destabilisation of U1 and U4 results in the formation of complex C (Ritchie *et al.*, 2009). The dissociation of U1 snRNP from the 5'ss before or during catalytic activation requires the action of PRP28 RNA helicase (Mathew *et al.*, 2008), which

facilitates ATP binding/hydrolysis (Boesler *et al.*, 2016). An ATP dependent generation of mature spliceosome from small subunits involves replacement of U1 snRNP at the 5' splice site by U6 snRNP and disruption of U4/U6 snRNA base pairing forming U2/U6 snRNA complex (Ritchie *et al.*, 2009). The U2/U6 complex forms the active site of the spliceosome where intron excision and exon joining catalytic trans-esterification reaction occurs (Lee and Rio, 2015). The conserved ACAGAG box of the U6 snRNA engages intron nucleotides at the 5' splice site (Wahl *et al.*, 2009). These ATP dependent conformational rearrangements (spliceosomal assembly, activation and disassembly) are facilitated by DExD/H-box RNA helicases, which are also important for splicing fidelity control (Zhang *et al.*, 2013).

Activated B complex starts splicing by cleaving the pre-mRNA's 5'ss and ligates the intron's 5' end to the branch site forming a lariat. The 3'ss cleavage and the ligation of the 5' and 3' ends of exons forming the mRNA catalysed by complex C is the second step of splicing (Schneider *et al.*, 2010). The chemical reaction occurring during splicing can be distinguished into two important steps. First, the 2'-hydroxyl of an adenosine of the BPS in the intron attacks the phosphodiester bond at the 5'ss creating a free 5' exon and an intron lariat-3' exon. Exon ligation and lariat intron excision follows as the 5'-exon's 3'-hydroxyl attacks the phosphodiester bond at the 3'ss of the lariat-3' exon (Ritchie *et al.*, 2009, Wahl *et al.*, 2009). Following the completion of splicing, post catalytic rearrangements ensue to dissociate the spliceosome liberating the mature mRNA for export, the lariat intron for degradation and the snRNPs for reuse (Zhang *et al.*, 2013).

Alternative splicing of pre-mRNA involves intricate and dynamic RNA-RNA, RNA-protein, and protein-protein interaction networks crucial for splice site selection and creation of the catalytic core of the spliceosome (Mathew *et al.*, 2008, Dixit *et al.*, 2010). Wahl and colleagues

explained that these functionally important RNA-RNA interactions formed within the spliceosome are generally weak and are stabilized by members of the SR protein family (Wahl *et al.*, 2009). SR proteins are required for splice site selection, playing important roles in RNA processing and gene expression (Anko, 2014). For efficient functioning and regulation of SR proteins, their RS domains are phosphorylated by several other kinases. SR proteins contain RNA recognition motif (RRM) and an Arginine/Serine-rich domain required for protein-protein interaction during splicing (Kern *et al.*, 2014). SR protein kinases (SRPKs), are a highly conserved kinase family that phosphorylate the repetitive RS domains with great specificity and efficiency (Dixit *et al.*, 2010). Additionally, CDC-like kinases (CLKs1-4) (Sako *et al.*, 2017), PRP4 (pre-mRNA processing 4) and dual-specificity tyrosine-regulated kinases have been reported to phosphorylate SR proteins (Ninomiya *et al.*, 2011). Majority of SR proteins have only a single RRM (SRSF2, SRSF3, SRSF7, SRSF8 and SRSF10-12) but a handful (SRSF1, SRSF4-6 and SRSF9) have a second RRM called pseudo-RRM. RNA-binding specificities are conferred by RRM; however, RS domains mediate protein-protein and protein-RNA interactions (Dominguez *et al.*, 2016). It is thought that independent RRM activity increases cell specific regulation; where both are involved in recognition and a perfect fit not necessary, a wider RNA association is possible with an increased specificity where a perfect fit is needed; or one has a non-RNA binding function (Anko, 2014). Being a general splicing factor required for core spliceosome assembly and catalysis, SR proteins have a decisive role in the regulation of AS (Mathew *et al.*, 2008). *PfSR1* has been shown to be involved in splice site (ss) selection similar to mammalian SRSF1 (Eshar *et al.*, 2012). This demonstrates the importance of AS as a mechanism used by *Plasmodium* parasites to expand its proteome from a limited gene numbers to have capacity to adapt its complex life cycle involving more than one host.

AS has been grouped into four types: exon skipping; intron retention/creation; 3' and 5' alternative splicing (coordinate changes to external exons) and 3' and 5' splicing which result in alternative start or stop codon (Otto *et al.*, 2010). Splicing is promoted or inhibited by *trans*-acting splicing factors recruited by AS regulators the *cis*-acting splicing regulatory elements (Dominguez *et al.*, 2016). This control by *cis*-acting elements help the spliceosome identify and distinguish exons from introns and direct it to the correct nucleotide for exon joining and intron removal, as well as finally bind auxiliary factors regulating AS and a called splicing codes (Wang and Cooper, 2007). Mis-regulation of this tightly controlled process is generally a common cause of human disease due to activation of cancer-specific splicing programs controlling cell cycle progression and migration, down regulation of oncogenes and tumour suppressors (Dominguez *et al.*, 2016).

1.3 Kinase Inhibitors

Deregulation of protein kinases leads to various diseases like cancer, immunological, neurological, and metabolic diseases and the search for treatment of these disorders led to the development of small molecule kinase inhibitors (Zhang *et al.*, 2009). However, designing selective kinase inhibitors that specifically inhibit only a single kinase without off-target effects is a difficult task (Huggins *et al.*, 2012). Notwithstanding, several kinase inhibitors specifically targeting the active or inactive conformations of enzymes directed towards the ATP-binding site, the substrate binding site or the allosteric sites have been identified (Smyth and Collins, 2009) and the modes of inhibition of these inhibitors are discussed below.

1.3.1 Type I inhibitors

This class of inhibitors, known as ATP-competitive inhibitors bind in the region occupied by the adenine ring of ATP targeting an active DFG-in conformation directly competing with ATP (Figure 1.6) (Hsu *et al.*, 2015, Liu and Gray, 2006). The DFG motif is a conserved sequence of three amino acids, aspartate (D), phenylalanine (F) and Glycine (G), forming part of the ATP binding site in the active kinase (Smyth and Collins, 2009). The interaction between type I inhibitors and the target protein is the formation of 1-3 hydrogen bonds in the kinase hinge region (Liu and Gray, 2006) that mimic the hydrogen bonds naturally formed through the adenine ring of ATP (Zhang *et al.*, 2009).

In addition to the ATP-binding site, structural studies showed extra binding sub-pockets (present in a number of kinases providing additional compartments for inhibitor binding) not occupied by ATP that large kinase inhibitors can span to increasing their binding affinity (Dar and Shokat, 2011). Type I inhibitor binding sites can be divided into sub-regions: hydrophobic regions I and II, the adenine region, the ribose region and the phosphate-binding region. Inhibitor selectivity of different kinases is influenced by their

ability to present diverse functionality to these regions except the adenine region which is generally occupied by all type I inhibitors (Liu and Gray, 2006). Using these structural features, inhibitors can distinguish target kinases from others irrespective of type, giving type I inhibitors some selectivity (Davis *et al.*, 2011). However, ATP-competitive inhibitors show poor selectivity because they lack contact with the 'DFG-out' conformation of the activation loop (Davis *et al.*, 2011), thus increasing their potential for off-target effects (Blanc *et al.*, 2013). Additionally, the conserved ATP-binding site of active kinases makes it more difficult for inhibitor specificity (Smyth and Collins, 2009).

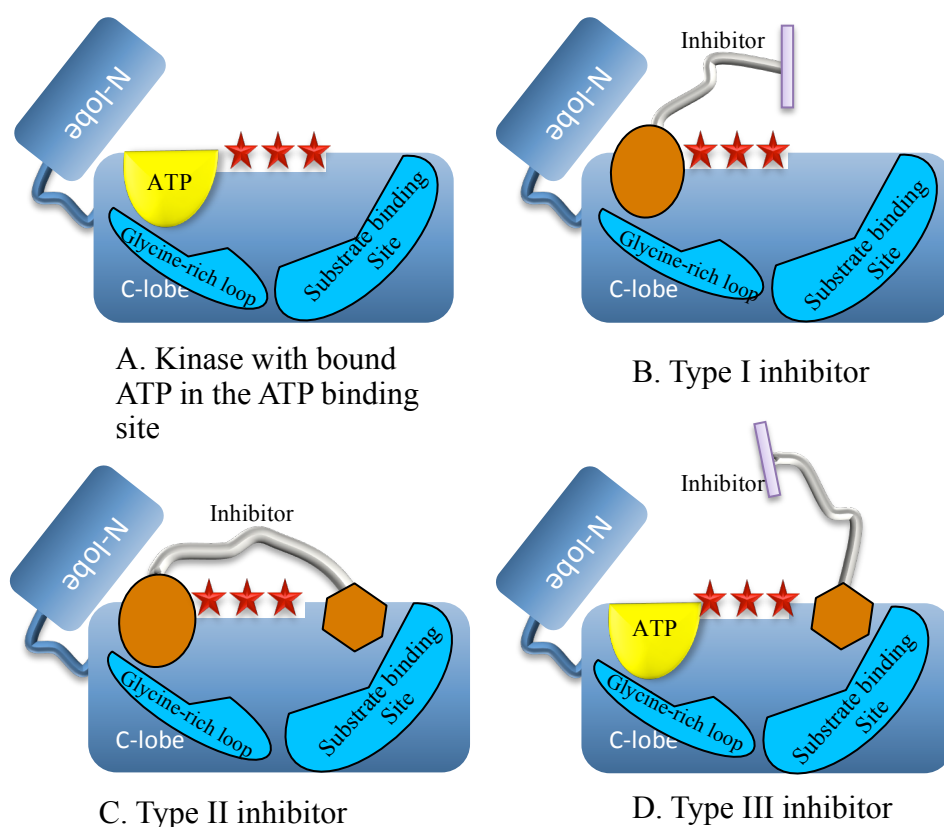


Figure 1.7: Schematic view of kinase inhibitors bound to a target kinase.

A) ATP bound to the ATP binding site of the kinase. B) Type I kinase inhibitor bound to the ATP binding site inhibiting the ATP access to its binding pocket. C) Type II inhibitor binding to both the ATP binding site and an allosteric site. D) Type III inhibitor bound to an allosteric site only.

1.3.2 Type II inhibitors

Type II inhibitors recognise the inactive conformation of the kinase referred to as the DFG-out, and the hydrophobic binding site directly adjacent to the ATP is exposed when the activation loop moves towards the DFG-out conformation (Zhang *et al.*, 2009), as shown in Figure 1.6. This class of inhibitors occupy this hydrophobic site but additional hydrophobic pockets adjacent to the ATP pocket referred to as 'allosteric site' are also created by the DFG-out conformation (Liu and Gray, 2006). The allosteric site offer type II inhibitors better selectivity since the amino acids surrounding this site are less conserved compared to those of the ATP binding site (Liu and Gray, 2006). Type II inhibitors have weaker antagonism for cellular ATP because the targeted DFG-out of the kinase has a higher ATP competition ($K_{M,ATP}$) value compared to the DFG-in active state given them increased *in vivo* activity (Zuccotto *et al.*, 2010).

A comparison analysis showed type II inhibitors been more selective than type I inhibitors, however, high selectivity is not guaranteed because of the inhibitor binding mode and the kinase confirmation used to discriminate between target kinase from other kinases (Davis *et al.*, 2011). Through reversible interactions with the kinase, these inhibitors form up to 3 hydrogen bonds with the protein in the hinge region (Blanc *et al.*, 2013). The hydrogen bonding characteristics of type II inhibitors are described by Liu and Gary as "they all possess a conserved hydrogen-bond pair between the ligand (using an amide or a urea) and the residues in the allosteric site: one hydrogen bond with the side chain of a conserved glutamic acid in the α C-helix and the other with the backbone amide of aspartic acid in the DFG motif" (Liu and Gray, 2006). Compared to type I inhibitors, type II inhibitors have a high kinase inhibition effect because of their lower dissociation rate and

prolonged residence time due to wider interaction and higher potency characteristics (Zuccotto *et al.*, 2010).

Type II inhibitors have major advantages compared to type I, however, they are characterised by two major disadvantages: First, their high molecular weight means they have a poor cellular penetration capacity resulting in lower ligand efficiency; and second, because a non-conserved region of the kinase is targeted, mutations in the kinase domain result in loss of function and resistance to type II compounds (Zuccotto *et al.*, 2010).

1.3.3 Type III Inhibitors

Targeting only specific binding sites and regulatory mechanisms, this group of inhibitors are generally considered as demonstrating the highest level of selectivity among kinase inhibitors (Zhang *et al.*, 2009). Allostery is the rearrangement of protein conformational structure resulting in dynamic and functional effects and designing this group of inhibitors is generally based on such variability in the DFG motif (Fasano *et al.*, 2014). Because they avoid the conserved ATP binding site (Figure 1.6D), allosteric kinase inhibitors create the prospect of extremely selective and single specific inhibition capacity. One such example is the highly selective and potent Akt inhibitors, which are not only selective for Akt over its homologous AGC enzyme group but can discriminate between its three isoforms by binding to the kinase allosteric site located between the kinase domain and the N-terminal regulatory pleckstrin homology domain of the kinase (Smyth and Collins, 2009).

Although a very good improvement for inhibitor development, the disadvantages with this class of inhibitors is their poor solubility and bioavailability in addition to low *in vivo* activity (Fasano *et al.*, 2014). These are significant disadvantages since the drugs only have limited time to reach their targets before they are eliminated from circulation or their half-lives are met. Another significant

problem of allosteric kinase inhibitor design is the fact that it is generally very difficult to predict the allosteric target site because these conformations are not well understood (Huggins *et al.*, 2012, Smyth and Collins, 2009).

1.4 Thesis aims

As discussed, there is enough evidence showing delayed parasite clearance rates in malaria-infected patients treated with the current front-line antimalarial drugs, ACT (Ashley *et al.*, 2014, Dondorp *et al.*, 2009, Wongsrichanalai C., 2008, WHO, 2017a). The first reports of resistance emerged from the epicentre for malaria drug resistance, SEA region of Thailand-Cambodia border where all previous antimalarial resistant parasites reportedly emerged before spreading to the rest of the malaria endemic regions of the world (Wongsrichanalai C., 2008). This threatens the gains made in the malaria control and elimination efforts; hence, several efforts to find a suitable antimalarial replacement before a global spread of artemisinin resistance parasites. The intended new antimalarial should be able to block all stages of the parasite life cycle, including transmissible gametocytes and liver stages, be potent to work in a single curative and prophylaxis treatment dose, and be cheap to manufacture and supply to poor malaria endemic populations (Flannery *et al.*, 2013).

The initial aims of this thesis were focused on the characterisation of the *Pf*CLK3 kinase as a suitable therapeutic antimalarial target of the kinase inhibitors TCMDC-135051 and TCMDC-138736 (Figure 1.8, A and B). These compounds were identified from a screen of 24,619 compounds, gathered from publicly available compound inhibitors (Dranchak *et al.*, 2013, Gamo *et al.*, 2010) and from the MRCT index library (<https://www.lifearc.org/mrc-technology-launches-small-molecule-compound-library-access-scheme/>) known to have anti-malarial potency. Initial screening of these compounds were at a single dose of 10 μ M using high throughput time-resolved Florescence energy transfer (TR-FRET) assay, and any compound with >40% inhibition and >3 standard deviations from the mean of the percentage inhibition distribution curve were selected as hits. Using this criteria, 2579 compounds

(MRCT=250, PKIS=4 and TCAMS=2325) plus 259 Medicine for Malaria Venture (MMV) compounds identified as kinase inhibitors (Spangenberg *et al.*, 2013) were identified and used to generate concentration inhibition curves (Alam *et al.*, 2018). A further selection criteria of >1.5 log fold difference in pIC₅₀, 13% of these were identified to specifically inhibit *Pf*CLK3 and among these TCMDC-135051 stand out showing the highest selectivity and efficacy.

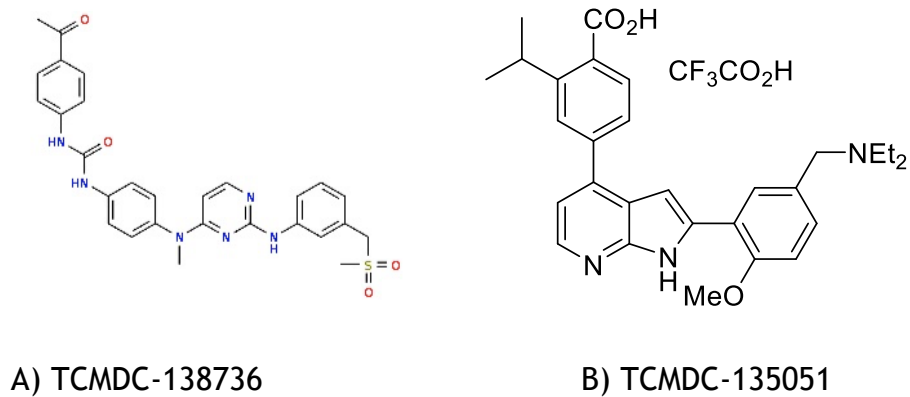


Figure 1.8: Structure of the kinase inhibitors. A) Structure of TCMDC-138736 with its Chemical formula: $C_{28}H_{28}N_6O_4S$, it has a molecular weight of 544.62472 and B) Structure of TCMDC-135051 and its Chemical formula: $C_{31}H_{34}F_3N_3O_5$ with a molecular mass of 585.2451.

Following the characterisation and determining the inhibition potency of these inhibitors to the *Pf*CLK kinase family, specifically *Pf*CLK3 kinase, experiments were designed to validate inhibitor target specificity and mode of action of the identified selective inhibitor. Furthermore, the inhibition of other *Plasmodium* recombinant CLK3 kinases (*Pv*CLK3 and *Pb*CLK) was assessed. *P. vivax* malaria has significant public health importance causing morbidity and mortality and is the most important human malaria after *P. falciparum* (Gething *et al.*, 2012). Additionally, clinical field isolates and *P. knowlesi* parasites were tested for growth inhibition by the inhibitor and the data shows a potent inhibitory action against these parasites.

Finally, in chapter 8, the direct involvement of *Pf*CLK3 in regulating the splicing machinery and its participation in pre-mRNA splicing is elucidated. The aims of these experiment were to confirm that *Pf*CLK3 is directly involved in splicing and also to establish that the action of the inhibitor TCMDC-135051 was specifically targeting *Pf*CLK3 by comparing treatment outcome between wild type and mutant parasites. Put together, the data presented here shows that *Pf*CLK3 is a therapeutic target for anti-malarial drug development. In addition, the inhibitor TCMDC-135051 although not fully optimised is selective towards *Plasmodium* CLK3 (especially *Pf*CLK3), has a multi-species and multistage activity against malaria parasites. Furthermore, its mode of inhibition (non-ATP competitive inhibition) increases its selectivity to this parasite kinase. The characteristic displayed by TCMDC-135051 makes it a good antimalarial tool compound.

Chapter 2 Materials and methods

2.1 Materials

2.1.1 Standard Reagents, Chemicals and Consumables

General laboratory consumables were purchased either from Sigma Aldrich (Poole, U.K), or Fisher Scientific (Loughborough, U.K). Ultra pure quality water used for preparation of reagents was obtained using water from ELGA Filtration system (ELGA Labwater, Marlow, UK). For bacterial cell culture and molecular biology, the water was filter sterilised and autoclaved at 121°C for 15 minutes.

2.1.2 Specific Reagents and assay kits

LANCE Ultra *ULight* myelin basic protein (MBP) (Sequence: CFFKNIVTPRTPPPSQGK-amide) peptide, LANCE *Ultra ULight*TM-Creptide peptide, LANCE anti-P-Creptide, LANCE anti-P-MBP, and LANCE detection buffer were supplied by Perkin Elmer (Perkin Elmer, USA). DNA (deoxyribonucleic acid) ladder (1 kb and 100 bp to 1 kb) and restriction enzymes were purchased from New England Biolabs (Hitchin, UK). Complete EDTA (ethylenediamine tetraacetic acid) free protease inhibitor cocktail tablets, T4 DNA ligase, Roche high pure plasmid isolation mini kit (Catalogue number: 11754777001) and polymerase chain reaction (PCR) product purification kits were supplied by Roche Applied Science (Burgess Hill, UK). Strategene (Cheshire UK) supplied the PfuUltra DNA polymerase and dNTPs for polymerase chain reaction (PCR). SDS-PAGE (sodium dodecyl sulfate-polyacrylamide gel electrophoresis) reagents (Resolving Gel Buffer, 1.5 M Tris-HCl pH 8.8; Stacking Gel Buffer for PAGE, 0.5 M Tris-HCl, pH 6.8; 30% Acrylamide; and pre-stained protein molecular size marker for immune blotting (10-250 kDa range)

were purchased from Bio-Rad (Hemel Hempstead, UK). TEMED (tetramethylethylenediamine) and SDS solutions were obtained from Sigma Aldrich (Poole, U.K). Bradford reagent for protein quantification was obtained from Bio-Rad (Hemel Hempstead, UK). CellTrace Far Red Cell Proliferation kit was purchase from Fisher Scientific (Loughborough, U.K.). Plastic tubes were supplied by: 15 ml tube (Corning, Catalogue number: 430790), 50 ml tube (Corning, Catalogue number: 430828), 1.5 ml tube and 0.2 ml tubes. Giemsa stain solution was purchased from Sigma Aldrich (Poole, U.K).

2.1.3 Bioinformatics tools and online applications

For *in silico* studies, a couple of programs and databases were used: *Plasmodb* database (<http://plasmodb.org/plasmo/>) was used to obtain and analyze the sequences and annotations of the *Plasmodium* CLK family of kinases and all other *Plasmodium* genes from different *Plasmodium* species. For multiple sequence alignment, Clustal Omega was used (<https://www.ebi.ac.uk/Tools/msa/clustalo/>). To determine the location of kinase domains and other protein features, *Pfam* 31.0v was used (<https://pfam.xfam.org>). All sequenced data were analyzed using Chromas software. NCBI database was used to blast for sequences. Vector NTI, primer 3 and Gensript softwares were used for designing primers.

2.1.4 Primers

Primers for PCR amplification, plasmid construct generation, and site-directed mutagenesis were designed using Vector-NTI primer design. Primers and probes for Real-time PCR (Taqman) were designed using the Genscript real-time PCR taqman primer design tool, software freely available online. Primers were purchased either from Eurogenetec (Southampton, U.K) or Sigma Aldrich.

2.1.5 Bacterial Strains

Commercially available chemically competent α -select cells, XL-1 Blue competent cells (Catalog number: 200249), supplied by Agilent Technologies (Edinburgh Park, 4-5 Lochside Ave, Edinburgh EH12 9DJ) were used for cloning. For all sub cloning BL-21 codon plus pLys competent cells also supplied by Agilent Technologies were used routinely transformations of DNA plasmids.

2.1.6 DNA and plasmid constructs

All *Plasmodium* CLK genes were cloned into pLEICS-05 vector employing the services of the PROTEX (Protein Expression Laboratory) department, University of Leicester, U.K. This Histidine (His6) tagged vector contains an ampicillin resistant gene for selection in *E. coli* competent cell lines. *P. falciparum* total RNA was extracted from schizont stage parasites and complementary DNA (cDNA) generated and used as template. The constructs of interest (*PfCLK1*, *PfCLK3* and *PfCLK4*) were amplified from this cDNA using gene specific primers. PCR products were separated on agarose gel and the product of the right size gel purified and supplied for cloning into the pLEICS-05 vectors. RNA for generation of the *P. berghei* CLK kinases was obtained as a kind gift from Dr Rita Tewari (Nottingham University, U.K). Complementary DNA (cDNA) was generated and subsequently the genes amplified and submitted for cloning as described for *P. falciparum*. Codon optimized sequence for *P. vivax* CLK3 and CLK1 were purchased and used as plasmids for cloning. The primers used are listed in Table 2-1.

2.1.7 Specialised Equipment

CLARIOstar microplate reader was obtained from BMG-Labtech (Aylesbury, U.K). PCR thermal cyclers, micro tube centrifuge

machines, and spectrophotometer were obtained from Eppendorf (Cambridge, UK). Beckman Coulter centrifuge from Beckman Coulter Inc (High Wycombe, UK). BD Biosciences (Le Pont de Claix, France) supplied the BD Accuri C6 flow cytometer.

Table 2-1: List of primers used for cloning of the CLK kinases

Primer Name	Sequence
PfCLK3_FL_Fwd	AGGAGATATACATATGTCCAAAGATAAGAGAAACTCG
PfCLK3_FL_Rev	GAAGTACAGGTTCTCTTCAATTTTGAGATTTGAAAATGAATAGATTCTCTTA
P196R_CLK3_Fwd	TCAATAACATCATTGTTGGCGTGGAAAAATGCAGGCC
P196R_CLK3_Rev	GGCCGTGCATTTTCGCACGCAACAATGATGTTATTGA
H259P_CLK3_Fwd	TATCATCCACATTTCAATTTTAATCTTTCAGGTAATTTCTTCTGTTTGATTATAAATGAC
H259P_CLK3_Rev	GTCATTTATAATCAAACAGAAAAGAAATTACCTGAAGAGATTAATAAATGAATGTGGATGATA
CLK3_L440M_Fwd	CATCATTTGTTTAAAGTAGTATAAAAATATAAAAAATCATATGTTAGTATTGAGTGGATGTGGG
CLK3_L440M_Rev	CCCACATCCACTCAAATACTAAACACATATGATTTTATATTTTATACTACTTAATAAACGAATGATG
CLK3_V443I_Fwd	AAGTAGTATAAAAATATAAAAATCATTTATGTTTAAATATTTGAGTGGATGGGGTAAC
CLK3_V443I_Rev	GTTACCCACACATCCACTCAAATATAAATAAACAATAAATGATTTTATATTTTATACTACTT
CLK3_G449P_Fwd	ATGTTTAGTATTTGAGTGGATGTGGCCTAACCTTAAGAAATAGCACGTGAAAAAG
CLK3_G449P_Rev	CTTTTTCAAGTCTATTCTTAAGTTAAGCCACATCCACTCAAATACTAAACAT
PfCLK3-His_353_Fwd	AGGAGATATACATATGGACTCAGAGGGATATTACAAGGCTATG
PfCLK3-His_353_Rev	GAAGTACAGGTTCTCTTCAATTTTGAGATTTTGAAAAATGAATAGATTCTCTTA
PvCLK3_CO_Famb_Fwd	AGGAGATATACATATGGCGAAAAGATAAACCGCGTCC
PvCLK3_CO_Famb_Rev	GAAGTACAGGTTCTCTTCAATTTTGAGATTTTGAAAAATGAAT
PvCLK3_P210R_Fwd	CCATCACCTCTTTAATTCGAGCAAAAGATGCAGGGCG
PvCLK3_P210R_Rev	CGCCCTGCATCTTTGCTCGGAATAAAGAGGTGATGG
PvCLK3_H273P_Fwd	GATGTTCAATTTGGTAGCGTTCCGGGACGTTCTTCTGTTTAATGAT
PvCLK3_H273P_Rev	ATCATTAAACAGAAAAGAACTGCCCGAACGTACCAAAATGAACATC
PbCLK3_FL_Famb_Fwd	AGGAGATATACATATGCCCTAAAGATAAACGGCGAAGAA
PbCLK3_FL_Famb_Rev	GAAGTACAGGTTCTCATCATTTGGCATTTTGAAGTAAATGATTTGA
PbCLK3_P213R_Fwd	CTTGCATAACTTCATTGTTGGCAGGCAAAATATACAAGCTGCT

PbCLK3_P213R_Rev	AGCAGCTTGTATATTTGGCTCGCAACAATGAAGTTATCGAAG
PbCLK3_H276P_Fwd	GAATTTTATAATTAAAGCAAAAGGAATTACCTGAAGAATAAATGAATGGTGATGATTCC
PbCLK3_H276P_Rev	GAATCATCACCATTTCATTTTATTTCTTTCAGGTAATTCCTTTGGCTTAATTAATAAAATTTTC
PbCLK3_FL_Famb_Fwd	AGGAGATATACATATGCCCTAAAGATAAACGCCGGAAGAA
PbCLK3_FL_Famb_Rev	GAAGTACAGGTTCTCATCATCTTGGCATTTTGGCAATTTTGAAGTAATGTATTGA
PvCLK1_KD_CO_Famb_Fwd	AGGAGATATACATATGGATGATGAGATCGTACACTTTTCCTGG
PvCLK1_KD_CO_Famb_Rev	GAAGTACAGGTTCTCCTGCAGAAAAGCCGGTGTTTAAGGAG
PbCLK1_KD_Famb_Fwd	AGGAGATATACATATGGATGATGAAAATTGTTCAATTTTCAGTTGG
PbCLK1_KD_Famb_Rev	GAAGTACAGGTTCTCATAAAAAATTCATGTTTCAATAAATCAACCG

2.2 Methods

2.2.1 Bacterial Growth

Transformed *Escherichia coli* (*E. coli*) cells were maintained at 37⁰C on Luria broth (LB) agar plates (1% w/v sodium chloride, 1% w/v tryptone, 0.5% yeast extract and 1.5% agar) containing the appropriate antibiotics concentrations overnight. After overnight incubation, presence of bacterial colonies indicates growth of the respective cells with the transformed plasmid. LB media (1% w/v sodium chloride, 1% w/v tryptone and 0.5% yeast extract) was used for expression of large volumes of bacteria shaking at 220-250 rotations per minute (rpm). The cells are initially grown at 37⁰C until an optical density (OD) of between 0.6-0.8 before they are induced with IPTG. For induction, cells were incubated with 100 μ M of IPTG either at 37⁰C for the CLK3 kinases and at 22⁰C for CLK1 4 hours or at 18⁰C overnight for expression of *PfCLK4*.

2.2.2 Bacterial Transformation

Plasmids of the target sequence were transformed into chemically competent BL21-CodonPlus (DE3)-RIPL cells (e.g. *E. coli*). These cells increase the supply of rare *E. coli* tRNA that corresponds to codons used more frequently by other organisms; they contain extra copies of the *argU*, *ileY*, and *leuW* as well as additional tRNA genes. For transformation, 0.5 - 1 μ g of plasmid DNA or 5 μ l of ligated PCR product were aliquotted into sterile 15 ml round-bottom polypropylene Falcon tubes (Catalogue number: 14-959-12A) on ice. To the plasmid DNA/ligate, 50 - 100 μ l of the competent cells previously thawed on ice (usually for 10 minutes) were added, mixed gently, and incubated on ice for 30 minutes. The mixture was heat-pulsed at 42⁰C for 20 seconds for BL21 Codon Plus cells or 45 seconds for XL1-Blue cells and immediately returned on ice for 2 minutes. Five hundred millilitres of Super Optimal broth with Catabolite repression (SOC) media

(0.5% w/v yeast extract, 2% w/v tryptone, 1 mM NaCl, 2.5 mM KCl, 10 mM MgCl₂, 10 mM MgSO₄, 20 mM glucose) was added to the mixture and incubated at 37°C shaking at 220 rpm for 1 hour. With NEB 5-alpha competent *E coli* (High efficiency) (catalogue # 29871), transformation was similar to BL21 and XL1 blue cells except that they were heat shock for 30 seconds and incubated on ice for 5 minutes instead of 2 minutes prior to addition of SOC media. Following incubation, 50 - 100 µl of the cell suspension was spread onto LB agar plates containing the appropriate antibiotics and incubated at 37°C overnight. Successfully transformed cells will grow as single colonies on the plates. The plates were sealed with Parafilm and stored at 4°C until needed.

2.2.3 Preparation of plasmid DNA

Following transformation, bacterial cells that have taken up the plasmid were enhanced to propagate by the antibiotic selection. Isolation of plasmid DNA was carried out using either mini prep plasmid isolation kit from Roche or maxi prep plasmid isolation kit (Qiagen, UK).

2.2.3.1 Miniprep plasmid preparation

For plasmid DNA isolation, the Roche high pure plasmid isolation kit was used. Three milliliters of an overnight bacterial culture was collected by centrifugation at 6000 xg for 5 minutes and the supernatant discarded. To the cell pellet, 250 µl of suspension buffer (50 mM Tris-HCl and 10 mM EDTA, pH 8.0) supplemented with RNase A was added. Cells were lysed by adding 250 µl of lysis buffer (0.2 M NaOH and 1% SDS) and incubated for 5 minutes at room temperature. After 5 minutes of cell lysis, 350 µl of pre-chilled binding buffer (4 M guanidine hydrochloride and 0.5 M potassium acetate, pH 4.2) was added and the mixture incubated on ice for another 5 minutes before a 10 minutes

centrifugation at maximum speed 13000 xg. The supernatant was then loaded to a high pure filter column with collection tube and centrifuged at maximum speed for 1 minute. The flow through was discarded and the column containing the bound DNA washed twice with wash buffer II (20 mM NaCl and 2 mM Tris-HCl, pH 7.5). The DNA was eluted into a new 1.5 ml centrifuge tube by adding 50 - 100 μ l of elution buffer (containing 10 mM Tris-HCl, pH 8.5) and centrifuged at maximum speed for 1 minute. The eluate was quantified by NanoDrop and stored at -20°C.

2.2.3.2 Maxipreps plasmid preparation

For generation of high quantity plasmid DNA, QIAGEN Plasmid Maxi kit (catalogue number: 12163) was used according to the manufacturer's instructions. A starter culture of 5 ml was set up from a single bacterial colony and incubated for about 8 hours shaking (220 rpm) at 37°C. Twenty-five ml culture was setup using the starter culture and grown overnight at 37°C shaking vigorously at 220 rpm. Cells were harvested the following day by centrifugation at 6000 xg for 15 minutes at 4°C. The bacterial pellet was re-suspended in 10 ml Buffer P1 (re-suspension buffer) (50 mM Tris-HCl, pH 8.0; 10 mM EDTA; 100 μ g/ml RNase A) and 10 ml Buffer P2 (lysis buffer) (200 mM NaOH; 1% SDS w/v) was added. This was mixed thoroughly by vigorously inverting the tube up to 6 times and incubated for 5 minutes at room temperature (RT). Ten ml of pre-chilled Buffer P3 (neutralization buffer) (3.0 M Potassium acetate, pH 5.5) was added, mixed thoroughly and incubated on ice for 20 minutes. After incubation, the mixture was centrifuged at 20,000 xg for 30 minutes at 4°C. The supernatant was collected and kept on ice. QIAGEN-tip column was equilibrated with 10 ml Buffer QBT (equilibration buffer) (750 mM NaCl; 50 mM MOPS, pH 7.0; 15% isopropanol, v/v; and 0.15% Triton X-100, v/v) and allowed to empty by gravity before the supernatant (kept on ice) was applied to the QIAGEN-tip and allowed to enter the resin by gravity flow. The QIAGEN-tip column

was washed twice with 30 ml Buffer QC (wash buffer) (1 M NaCl; 50 mM MOPS, pH 7.0; 15% isopropanol, v/v) after all the supernatant has flowed through the column. DNA was eluted with 15 ml Buffer QF (elution buffer) (1.25 M NaCl; 50 mM Tris-HCl, pH 8.5; 15% isopropanol, v/v) into a new 50 ml tube. To the eluate, 10.5 ml (0.7 volumes) of isopropanol at room temperature was added and mixed to precipitate the DNA and centrifuged at 15,000 xg for 30 minutes at 4⁰C. The supernatant was carefully decanted and DNA pellet washed with 5 ml of 70% ethanol at RT and centrifuged for 10 minutes at 15,000 xg. The supernatant was carefully decanted and pellet air-dried for 10 minutes. Finally, the DNA was re-dissolved in appropriate volume of TE buffer (10 mM Tris-HCl, pH 8.0) and quantified by NanoDrop.

2.2.4 Plasmid DNA and nucleic Quantification – NanoDrop

Concentrations of isolated plasmid DNA and nucleic acids were determined by measuring absorbance at 260 nm wavelength using NanoDrop Microvolume Spectrophotometer 3300 (NanoDrop). At this wavelength, an absorbance of 1 is equivalent to 50 µg DNA per ml. Highly concentrated samples were diluted 1:100 µl before quantification. Sample purity was determined by measuring absorbance at 280 nm and a ratio of A₂₆₀/A₂₈₀ of 1.8 - 2.0 indicates a pure sample.

2.2.5 Polymerase Chain Reaction (PCR)

All PCRs were performed in sterile environment using PCR tubes in reaction volumes of 50 µl. The reactions, in the appropriate volumes of water contain 1X of Pfu reaction buffer, 200 µM each dNTPs, 400 µM of forward and reverse (5' and 3' respectively) primers, magnesium chloride (MgCl₂) concentration between 1.5 - 2.5 mM, 0.5 µl of the thermostable DNA polymerase PfuUltra (2,00 unit/mls), and plasmid at 0.1 - 0.5 µg. The reactions were carried

out in eppendorf thermal cyclers using specified cycling conditions as in Table 2-2. After thermal cycling, the PCR products were separated on ethidium bromide stained agarose gel electrophoresis technique, and the target product visualised using Geldoc under UV light. For size determination, the PCR products were analysed in the presence of molecular weight markers with predetermined sizes and the amplified products are expected to be at the right molecular weight.

Table 2-2: Polymerase Chain Reaction (PCR) cycling conditions

Step	Number of Cycles	Temperature	Time
1	1	98 ⁰ C	30 Seconds
2	30	98 ⁰ C	30 Seconds
		55 ⁰ C	1 minute
		68 ⁰ C	1 minute/kb of plasmid length
3	1	72	5 minutes

2.2.6 Site directed Mutagenesis PCR

Site-directed mutagenesis PCR were performed in sterile PCR tubes in 50 µl reaction volumes containing the PCR components described in the previous section. However, in site directed mutagenesis, PCR primers were designed to introduce the desired site-specific mutations. The intended mutations could be deletion, insertion, and/or substitution. To introduce a mutation, mutagenic oligonucleotide primers are designed to harbour the desired mutation, at the middle of the primer allowing enough bases of the normal sequence on either side. After PCR amplification, the methylated non-mutated parental DNA was digested with DpnI restriction enzyme by adding the enzyme and incubating at 37⁰C for 1 hour. The mutated DNA samples remain unaffected by the activity of DpnI and are ready for transformation.

Table 2-3: Site directed mutagenesis PCR cycling conditions

Step	Number of Cycles	Temperature	Time
1	1	98 ⁰ C	30 Seconds
2	18	98 ⁰ C	30 Seconds
		55 ⁰ C	1 minute
		68 ⁰ C	1 minute/kb of plasmid length

2.2.7 Protein Expression and Purification

Plasmodium falciparum (*P. falciparum*) and *P. berghei* parasite total RNA were isolated from schizonts and cDNA was generated using Oligo (dT)s with the First Strand cDNA synthesis kit (Roche) according to the manufacturer's protocol. The full-length kinase and the kinase catalytic domains were amplified using primers for *PfCLK1*, *PfCLK3*, and *PfCLK4* and *PbCLK1* and *PbCLK3* (Table 2-1). *P. vivax* CLK1 (*PvCLK1*) and *PvCLK3* sequences were codon optimised (CO) and ordered for synthesised from Eurogentec and this was submitted for cloning. *PfCLK1* and *PfCLK4* kinase domain, and *PfCLK3* full-length plasmids were cloned into pLEICS-05 vectors incorporated with ampicillin resistance gene. All the cloning was done employing the services of the Protein Expression Laboratory (Protex) facility of the University of Leicester. The cloned plasmids were mainly C-terminal Histidine-tagged unless otherwise stated. The generated plasmids were chemically transformed into competent *Escherichia coli* BL21-CodonPlus (DE3)-RIPL cells (Stratagene cat No-230280) and grown on Luria Broth (LB) agar at 37⁰C overnight. A single colony was used to setup in 50 ml of overnight primary culture and 1-2% of the primary culture was inoculated in 500 ml secondary culture with 50 µg/ml of ampicillin and chloramphenicol as antibiotic. After the cells reached the mid-log phase of growth with optical density (OD₆₀₀) between 0.6 and 0.8, 100 µM IPTG (Isopropyl β-D-1-thiogalactopyranoside) was used to induce the

production of *PfCLK1* and *PfCLK4* at 22^oC, and *PfCLK3* at 37^oC shaking for 4 hours at 220 rpm. Cells were then harvested by centrifugation at 8000 xg for 15 minutes and lysed by sonication in lysis buffer containing 20 mM Tris, 150 mM NaCl and 20 mM Imidazole, pH-8.0. The lysate was purified using nickel-nitrilotriacetic acid (Ni-NTA) affinity chromatography and eluted in elution buffer containing 20 mM Tris, 150 mM NaCl and 350 mM Imidazole pH-7.4. The protein was dialyzed overnight in dialysis buffer containing 20 mM Tris and 150 mM NaCl pH-7.4 at 4^oC and finally stored at -80^oC in 10% glycerol. All the mutant forms of plasmids used in this project were generated by site directed mutagenesis PCR from these parent plasmids.

2.2.8 Western Blot analysis

Expressed *PfCLK* protein were re-suspended in lysis buffer (1 mM DTT and 1 mM EDTA in PBS) and sonicated for 10 cycles (5 seconds on, 10 seconds off at 10 Amplitude). 0.2 µg of protein lysate or PBS (negative control) was separated on 12% SDS-PAGE gel electrophoresis and transferred to a Hybond ECL nitrocellulose membrane (Amersham Biosciences). The membranes were blocked overnight with 5% (w/v) skimmed milk dissolved in Tris-buffered saline (TBS) containing 0.1% Tween 20 (TBST). Primary antibody, anti-*PfCLK3* antibody, a *PfCLK3* specific polyclonal antibody produced against a peptide corresponding to part of the *PfCLK3* C-terminus, was diluted in 5% milk (1:2500) and added to the membrane and incubated for 1 hour at RT. Alternatively, a primary antibody corresponding to the tags on the protein, either Histidine (6His or GST), were used. After four 15 minute washes with TBST, conjugated secondary antibody, diluted 1:2000 was then added, incubated for another hour, and washed 4 times with 15 minute intervals. Finally the blots were developed in a solution of nitroblue tetrazolium chloride (NBT) and 5-bromo-4-chloro-3-indoxyl phosphate (BCIP; Sigma-

Aldrich) for 5 minutes before exposed to radiography. The radiographs were developed and scanned blots processed using Adobe Photoshop software.

2.2.9 In vitro Kinase activities and inhibition assay

Kinase assays for *Pf*CLKs were carried in kinase buffer containing (20 mM Hepes, pH 7.4, 10 mM MgCl₂, 1 mM DTT, 50 μM adenosine triphosphate (ATP), 0.1 MBq γ-³²P-ATP) using 0.5 μg purified recombinant protein kinases. As exogenous substrate, kinases were incubated with 2 μg histone type IIA; 2 μg myelin basic protein (MBP); and 2 μg α-casein for 30 minutes at 37⁰C.

To examine the *in vitro* kinase activity for recombinant his-tagged *Pf*PKG, the kinase buffer was supplemented with 10 μM cGMP, this increases phosphotransferase activity by about 10 fold (Francis *et al.*, 2010) using Histone as substrate. For *Pf*CDPK1, the kinase buffer was supplemented with 1 mM CaCl₂ using MBP as substrate.

Kinase reactions were stopped by adding equal volume of 2X Laemmli sample buffer (12.5 mM Tris-base, pH 6.8, 4% SDS w/v, 20% glycerol, 50 mM DTT and 0.01% bromophenol blue) to give a final 1X concentration. Samples were incubated for 5 minutes at 60⁰C and centrifuged for 1 minute at 1200 rpm. 25 μl of each sample was separated on 12% SDS-PAGE ran at 180 V for at least 60 minutes. Gels were stained with Coomassie and dried by means of vacuum gel drying. Dried gels were exposed to X-ray film overnight at -20⁰C and autoradiography collected the phosphorylation signal.

For *in vitro* inhibition assays, TAMCD-138736 and TCMD-135051 were added to a final concentration of 2 μM. For control, a no inhibitor reaction tube was setup to exclude any other unknown inhibitory effect. All other reaction conditions remained the same.

Quantification of activity was carried out using ImageJ (1.49v).

2.2.9.1 Time Resolved Florescence Energy Transfer (TR-FRET)

Biochemical kinase assays were carried out using time-resolved florescence energy transfer (TR-FRET) to determine kinase activity, K_m for ATP and IC_{50} (concentration of inhibitor to reduce kinase activity by half) values for the respective enzymes. TR-FRET reactions were performed using the appropriate amount of kinase (5 nM for *Pf*CLK1 and 50 nM for *Pf*CLK3 wild type and mutant, G449P) in a kinase buffer (containing 50 mM HEPES, 10 mM $MgCl_2$, 2 mM DTT, 0.01% Tween 20, and 1 mM EGTA), *ULight*-labeled peptide substrate (MBP peptide (sequence: CFFKNIVTPRTPPPSQGK) and CREPtide (Sequence: CKRREILSRRPSYRK)) and the corresponding europium-labeled anti-phospho antibody in two steps. First, in a 10 μ L reaction volume, 5 μ l of twice the required enzyme concentration and 5 μ l of twice the required substrate concentration mix containing cold ATP were incubated in a black 384 plate well plate at 37⁰C for 1 hour. Following incubation, 30 mM EDTA in 1X Lance detection buffer containing 3 nM Europium-labeled anti-phospho specific antibody is added to the plate to stop the reaction and enhance detection. This mixture was incubated at RT for 1 hour and then the signal read using the ClarioStar.

Kinase substrate phosphorylation results in the Europium-labeled anti-phospho specific antibody recognizing the phosphorylated site on the substrate. The Europium donor fluorophore is excited at 320 or 340 nm and energy is transferred to the *ULight* acceptor dye on the substrate, which finally results in the emission of light at 665 nm. The level of *ULight* peptide phosphorylation correlates with the intensity of the emission.

To test for inhibition by small molecules such as TCMDC 135051, serial dilution of the inhibitor (made at four times the required

concentration) was made and added to the protein mixture before adding the substrate mix at four times the required concentration. For normalization, a no kinase and a no inhibitor reaction wells were included and all experiments conducted in triplicates.

2.2.10 *Plasmodium falciparum* culture

P. falciparum parasite culture was done in RPMI media supplemented with 100 μ M hypoxanthine, 25 mM Hepes, L-glutamine and 12.5 μ g/ml gentamicin as antibiotic and 0.5% (w/v) Albumax I. For continuous culture, the parasites were kept at 4% haematocrit in human erythrocytes from donors and between 0.5 - 3% parasitaemia incubated at 37⁰C in an incubator maintained at 5% carbon dioxide (CO₂), 5% oxygen (O₂) and 90% nitrogen (N₂) in a 37⁰C incubator. Cultures were only manipulated in laminar flow cabinets using standard aseptic techniques. Gloves and personal protective equipment were used at all times and all materials used were sterile. Incomplete RPMI medium was used for all washes. All mutant *P. falciparum* parasites (*Pf*CLK3_G449P and *Pf*CLK3_H259P) used in this work were a kind gift from Dr Mahmood Alam, who generated and genetically validated them.

2.2.10.1 Giemsa Staining and slide microscopy

To monitor parasites for continuous growth by microscopy, thin blood smears were prepared. To prepare a thin smear, about 5 μ l of blood was taken from the culture plate and a thin smear is made on a frosted slide using a cover slide. The smear was air-dried quickly with the aid of a hair-drier and fixed with absolute methanol in a Coplin jar by dipping the slide for about 20 seconds. The air-dried slide was stained with 10% Giemsa stain in buffered water pH 7.0-7.2 (1:10, v/v) for 15 minutes. Slides were washed under a running tap water, air-dried, and then observed with 100X eyepiece objective lens using a light microscope.

2.2.10.2 Synchronisation of cultures

Parasites were synchronised using one of two techniques or both: sorbitol – it is versatile and simple to perform and concentrate the young stages of the parasite whereas Percoll helps concentrate the older parasite stages mainly the mature schizonts (Roncalés *et al.*, 2015). For tighter synchronisation, two-step synchronisations were employed.

2.2.10.2.1 Sorbitol synchronisation

Sorbitol synchronisation is based on the differential permeability of parasitized erythrocyte membranes. Mature forms of the malaria parasites induce structural modifications to erythrocytes resulting in them being permeable to sorbitol to which they are naturally impermeable. With this property, erythrocytes containing the mature forms of the parasites are selectively killed due to the osmotic shock, and the uninfected and ring stage parasitized erythrocytes remain unaffected (Roncalés *et al.*, 2015).

For sorbitol synchronisation, cultures were spun down and the supernatant discarded. To the pellet, 9 volumes of pre-warmed 5% sorbitol (w/v) solution was added and mixed vigorously by vortexing for 30 seconds. Parasite-sorbitol mixtures were then incubated at 37⁰C for 10 minutes shaking at 240 rpm. The mixture was centrifuged at 250 xg for 5 minutes at 37⁰C and a red coloured supernatant was observed, indicating lysis of RBCs containing mature parasite forms. This was discarded and the remaining pellet washed twice with 10 ml of wash media. After washing, smears were prepared to assess ring enrichment and confirm the absence of mature parasite forms. Parasitaemia was confirmed at this stage before proceeding with any further experiments.

2.2.10.2.2 Percoll synchronisation

The 70% Percoll, the wash media and the complete media were warmed to 37⁰C before starting. Cultures were centrifuged at 250

xg for 5 minutes at 37⁰C and supernatant discarded saving the red cell pellets. For easy recovery of mature forms, as much of the supernatant as possible was removed to help get a thin upper layer of schizonts in the tubes after centrifugation for collection. To 15 ml tubes, 4 ml of 70% Percoll (v/v) was added. To the top of the Percoll, 0.5 - 1 ml of the pelleted infected erythrocytes were gently added by carefully pouring down the side of the tube with a pipette aid to avoid mixing the Percoll and the RBC. The Percoll-RBC tube was then centrifuged at 1200 xg for 10 minutes at 37⁰C without brakes. The top layer containing schizonts and late trophozoites parasitized erythrocytes were removed using sterile plastic Pasteur pipette and transferred to a fresh 15 ml tube. This was washed twice with wash media, a slide prepared and assessed before adding an appropriate volume of blood for continuous culture in 10 ml growth media.

2.2.10.3 Determining the 50% Inhibitory concentration (IC₅₀) of compound inhibitors and drugs

Reference or standard antimalarial drugs were a kind donation from Chris Lourens of Worldwide Antimalarial Resistance Network (WWARN), Thailand. Drugs were dissolved either in water or dimethyl sulfoxide (DMSO) as stock solutions and diluted to intermediate and working solutions in complete growth media. Starting concentrations in nanomolar and the dilution factors of individual drugs are as shown in the tables below. The dilutions, at twice the required final concentrations were made in 96 deep-well plates and stored in aliquots of 50 µl at -20⁰C in black assay plates. EC_{50s} were determined using cultures between 0.5- and 1% parasitaemia of young rings at 4% haematocrit maintained at 5% carbon dioxide (CO₂), 5% oxygen (O₂) and 90% nitrogen (N₂) in a 37⁰C incubator. Standard antimalarial drugs used were Dihydroartemisinin (DHA), Pyrimethmine (PYR) and mefloquine (MFQ), a fast acting, slow acting and moderate acting drugs respectively.

To set up the drug plates, parasites were prepared at 8% haematocrit (2X required) at the required parasitaemia and equal volume (50 µl) and added to the previously diluted drug plates and mixed by pipetting up and down several times. This gives a final culture volume of 100 µl at the required drug concentration and haematocrit. To the 'no drug' control, growth media was added, and the respective stock drug concentrations were added to the kill well (contains high concentration of chloroquine to kill all parasites) to confirm killing for each plate. The outer wells of the plates without cultures were filled with media to reduce evaporation from the experimental wells and the plates incubated. After about 48 hours (± 2 hours), the plates were monitored for growth by making a thin smear from the control wells to confirm developmental stage. Plates were only harvested for reading if the parasites grew to the next generation of rings otherwise they are allowed to grow until they re-invade. The plates were collected and frozen at least overnight to enhance lysis of the red blood cells for staining of parasite DNA.

For quantification, previously frozen plates were thawed at room temperature for at least 1 hour and 100 µl of lysis buffer (20 mM Tris-HCl; 5 mM EDTA; 0.004% saponin and triton X-100) in PBS containing Sybr Green I (1 µl in 5 ml) was added to each well and mixed by pipetting up and down several times. The plates were then incubated at RT for 1 hour shaking in the dark. Using a Fluroskan plate reader at excitation of 485 nm and emission of 538 nm, plate absorbances were acquired and percentage growth calculated using the formula below. Analysis and graphs were generated using Graph Pad Prism 7 and the EC₅₀ values were determined using the non-linear regression log (inhibitor) versus response (three parameter) curve.

Percentage grow

$$= 100 \times \left(\frac{(\text{Kinase activity} - \text{Blank})}{(\text{maximum kinase activity} - \text{blank})} \right)$$

2.2.10.4 DDAO-SE staining of erythrocytes

Erythrocytes used for the parasite reduction rate assay were stained with 10 μM DDAO-SE. To 3 ml of blood at 2% haematocrit in incomplete RPMI, (iRPMI), DDAO-SE was added to a final concentration of 10 μM and tubes incubated on a rotator at 37⁰C for 2 hours. Cell suspension centrifuged for 5 minutes at 1200 rpm on low brakes at RT. The supernatant was removed and cells washed twice with 10 ml of iRPMI. Cells were further incubated with 3 mls of iRPMI for an additional 30 minutes on the rotator to wash off excess stain. After 30 minutes incubation, the cells were washed twice and pellet re-suspended in 3 ml complete RPMI media and kept at 4⁰C ready to use.

2.2.10.5 Drug treatment and infection of labeled erythrocytes (parasite reduction rate)

The conditions for the parasite reduction rate assay were chosen to mimic those used for standard IC₅₀ determination (2% haematocrit, 0.5% parasitaemia with $\geq 80\%$ ring stages). Asynchronous cultures were incubated at 37⁰C for the required time. A culture volume of 50 μl per well with parasites at 4% haematocrit and 0.5% parasitaemia was dispensed into flat-bottom, 96 well plates containing 50 μl of previously diluted drugs prepared to give a final volume of 100 μl per well. Four drug concentrations were tested; 1, 5, 10 and 100X the respective EC₅₀ values earlier determined. Treated samples were exposed to drugs for 24, 48, and 72 hours at 37⁰C using standard incubation conditions. Drugs were replenished every 24 hours by replacing the old drug with fresh media containing drug at the required concentration. After each time point, drug pressure was removed by washing twice with complete media. For removal, 80 μl of media containing drug was removed and 100 μl media added to the remaining culture. The plates were then centrifuged at 1200 rpm for 10 minutes and 100 μl media removed again; the same is

repeated to ensure complete removal of the drugs. The washed parasitized cells were then re-suspended to 100 µl of growth media. Fifty microliters of this was added to a new plate containing 100 µl of DDAO-SE stained erythrocytes at 2% haematocrit making a ratio of 1:3. Plates were then incubated for 48 hours at 37°C to allow new infections to develop in labeled erythrocytes as a measure of the presence of viable parasites. Control wells containing no drug were setup and treated identical to the experimental wells. The outer wells of the plate were filled with incomplete media to avoid evaporation from the experimental wells.

2.2.10.6 Parasite labeling

After 48 hours of incubation post drug treatment, the plates were washed twice each with 100 µl of PBS. The cells were then stained with 75 µl of SYBR Green I (1:5000 dilution in PBS) for 20 minutes at RT with constant agitation. Following staining, the cells were washed twice with 100 µl of PBS each and then re-suspended in 200 µl PBS ready for flow cytometry analysis.

2.2.10.7 Flow cytometry

For flow cytometry, 50 µl of erythrocytes suspension in PBS was added to a new plate containing 150 µl PBS (1:4 dilution) and mixed by pipetting up and down several times. To acquire the samples, the cytometer was set to read the colours for DDAO-SE on the APC channel at emission of 656 nm and excitation at 648 nm whereas SYBR Green I was read on the FITC Channel with an emission and excitation of 538 and 488 nm respectively (shown in the table below). Using these settings, 100,000 events were acquired per sample and gatings set to capture at least 98% of the acquired cells.

Table 2-4: SYBR Green I and DDAO-SE flow cytometer detection channels

Stain	Emission (nm)	Excitation (nm)	Laser lines
SYBR Green I	538	488	FITC Channel
DDAO-SE far red dye	656	648	APC Channel

2.2.10.8 *P. falciparum* Stage of inhibition assay

To evaluate which parasite blood stages are most sensitive to TCMDC-135051, in vitro cultures of synchronised *P. falciparum* 3D7 parasites were set up and parasites treated with TCMDC-135051 at time point 0, 10, 20, 30, and 40 hours to a final concentration of 1 μ M and allowed to grow for 70 hours. Thin blood smears were collected every 10 hours from time point 0, 10, 20, 30, 40, 50 and 70 hours. The slides were stained with 10% Giemsa and parasite development stages determined by light microscopy and images were taken for all the time points at 100X magnification.

2.2.11 RNA Isolation (Qiagen Kit)

For total RNA, 200 μ l of infected erythrocytes were collected and 750 μ l of QIAzol lysis reagent was added and homogenised. To isolate RNA, 200 μ l of chloroform was added, shaken vigorously for 15 seconds, and incubated at room temperature for 5 minutes. Following incubation, the tube was centrifuged at 12,000 xg for 15 minutes at 4^oC and the upper aqueous phase was transferred to a new 1.5 ml eppendorf tube. Equal volumes of 70% ethanol was added to this phase and mixed thoroughly by vortexing. To RNeasy Mini spin column in a 2 ml collection tube, 700 μ l of the sample mixture was loaded and centrifuged at 8000 xg for 30 seconds. The flow through was discarded retaining the collection tube and any left over from the sample was reloaded and the spinning procedure repeated. To wash, 700 μ l of buffer RW1 was added to the column and centrifuged at 8000 xg for 15 seconds;

flow through discarded and collection tube re-used. Buffer RPE was added to the spin column (500 µl) and centrifuged at 8000 xg for 15 seconds and the flow through discarded. Another wash with buffer RPE was done, centrifuging for 2 minutes. To eliminate any possible carryover of buffer RPE or any residual flow-through on the outside of the RNeasy, the column was placed in a new collection tube and centrifuged for 1 minute. The clean spin column placed in a 1.5 ml Eppendorf tube and 50 µl of RNase free water added directly to the spin column membrane and centrifuged for 1 minute at 8000 xg. The eluate was re-loaded to the spin column and centrifuged again to increase RNA concentration. The RNA was immediately transferred on ice to prevent RNA degradation and quantified by nanodrop.

2.2.12 Complementary DNA (cDNA) synthesis

For cDNA synthesis, the QuantiTect Reverse Transcription kit (Catalogue number: 205311) was used starting with 50 ng total RNA. With this kit reverse transcription involves genomic DNA (gDNA) wipe-out followed by reverse transcription reaction. Genomic DNA wipe-out step was carried out in a 14 µl reaction volume containing gDNA wipe-out buffer at 1X final concentration, template RNA at 50 ng final concentration and variable amount of water. The mixture was incubated at 42⁰C for 2 minutes and immediately transferred on ice. To this, the reverse transcription master mix containing 1 µl of Quantiscript Reverse Transcriptase, 4 µl of Quantiscript RT buffer at 5X, and 1 µl of RT primer mix was added to give a final reaction volume of 20 µl. This was incubated for 15 minutes at 42⁰C followed by reverse transcriptase.

Chapter 3 Characterization of an inhibitor tool compound for *Pf*CLK3

3.1 Introduction

This chapter aimed to characterize members of the *Pf*CLK kinase family as a suitable therapeutic target in *P. falciparum* using tool compounds TCMDC-138736 and TCMDC-135051. These compounds were identified from a screen of 24,619 compounds, gathered from publicly available compound inhibitors (Dranchak *et al.*, 2013, Gamo *et al.*, 2010) and from the MRCT index library (<https://www.lifearc.org/mrc-technology-launches-small-molecule-compound-library-access-scheme/>) known to have anti-malarial potency. The screen was carried out using a high-throughput inhibition assay, the time-resolved fluorescence energy transfer (TR-FRET), optimized for use with 1536-well plate format with the substrates CREP-tide for *Pf*CLK1 and MBP-peptide for *Pf*CLK3. K_m for ATP of 10 μ M and 30 μ M were used for *Pf*CLK3 and *Pf*CLK1 kinases respectively, kinase activity linearly increased with respect to protein concentration with a stable activity signal over the assay period (generally 60 minutes). Using this assay, TCMDC-135051 was identified as 1 of 13% of the hits (2579) that specifically and selectively inhibited *Pf*CLK3 activity (Alam *et al.*, 2018). This inhibitor is a member of the TCAMS with a reported EC_{50} for anti-parasitocidal activity of 320 nM (Gamo *et al.*, 2010).

TCMDC-138736 and TCMDC-135051 have strong inhibitory activity against *Pf*CLK3, with IC_{50} values of 281.9 nM ($pIC_{50}=6.55\pm 0.11$) and 40.86 nM ($pIC_{50}=7.39\pm 0.071$) respectively, and less or no inhibitory activity against *Pf*CLK1 and *Pf*CLK4. This chapter describes the characterization of these inhibitors with high specificity and selectivity for *Pf*CLK3 over the other members of this kinase family. The selectivity was further confirmed by testing inhibition of other *Plasmodium* kinases (*Pf*CDPK1 and *Pf*PKG) in gel-based assays using 2 μ M TCMDC-135051 but no inhibition of

kinase activity was detectable. In *in vitro* parasite cultures, both inhibitors show potency inhibiting parasite growth with low nanomolar potencies. Additionally, synchronized 3D7 *P. falciparum* parasites challenged with TCMDC-135051 at different asexual stages (rings, trophozoites and schizonts), to evaluate the phenotypic response of PfCLK3 inhibition showed that in the presence of TCMDC-135051, parasites were arrested in rings and whereas later stages perished to the effects of the inhibitor without progressing to the next growth stage.

3.2 Results

3.2.1 Protein Expression

3.2.2 Expression of *Pf*CLK1 Kinase domain

The *Pf*CLK1 C-terminal kinase catalytic domain from phenylalanine-552 to leucine-874 was cloned into an IPTG-inducible bacterial expression vector (pLIECS-05) that placed a his-tag at the C-terminus.

As shown in Figure 3.1A, Coomassie stain of the bacterial lysate from induced and un-induced cultures showed a weak band at ~37kDa in both the soluble and insoluble fractions of induced bacteria that corresponds to the expected molecular weight of *Pf*CLK1-KD. Large-scale cultures were then used to express *Pf*CLK1-KD and purified using chromatography with Nickel NTA (Ni-NTA) resin. Aliquots of these were separated on SDS-PAGE gel and Coomassie stained. Although other bands were present at ~75 and ~25 kDa which are suggested to represent fragments of *Pf*CLK1 or unrelated proteins that cross react with Ni-NTA, the *Pf*CLK1 protein was detected at the expected molecular weight of about 37 kDa (figure 3.1A) Bradford quantification showed higher protein concentration with elutes 2, 3, 4, and 5 as observed in the coomassie-stained gel in Figure 3.1B. These fractions were pulled together and dialyse overnight to reduce imidazole concentration before it was stored in 10% glycerol at -80⁰C until use.

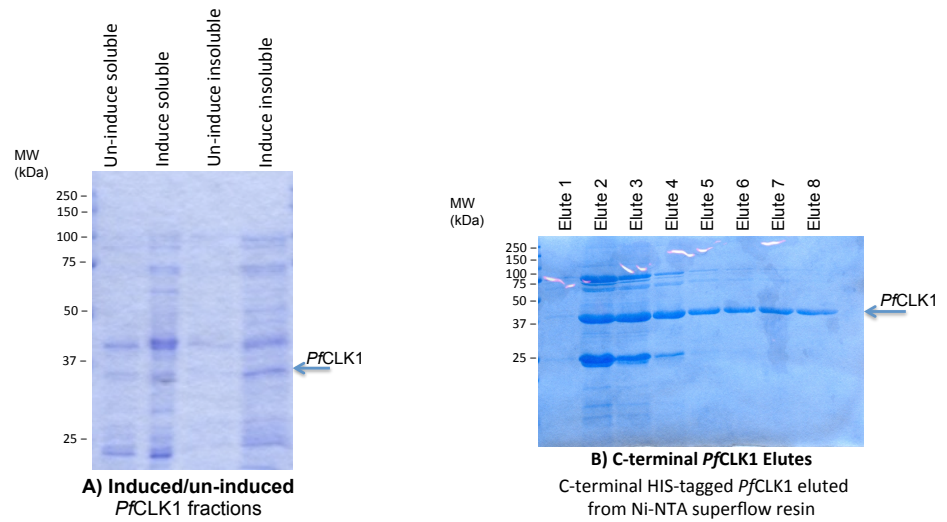


Figure 3.1: *PfCLK1* Expression in *E. coli* (BL-21 Codon Plus). A) Lysate of un-induced and induced bacterial samples showing the soluble and insoluble fractions. Compared to un-induced samples, the induced samples shows most of the protein is in the soluble fraction. B) Fractions of the purified protein eluate separated on SDS-PAGE gel at the expected molecular weight of ~37 kDa.

3.2.2.1 Expression of full length *PfCLK3*

The full length *PfCLK3* gene was amplified from cDNA and submitted to PROTEX for cloning into pLEICES-05 vector. This C-terminal His-tagged fusion *PfCLK3* was expressed in competent bacterial cells (*E. coli*) induced at 37⁰C for 4 hours and purified using Ni-NTA chromatography purification technique. Coomassie staining of the bacterial lysates from induced and un-induced cultures showed a very weak band at ~100 kDa, the molecular weight expected for full length *PfCLK3* (Figure 3.2A). To confirm the expression of *PfCLK3* protein, the lysate was probed in a western blot with anti-*PfCLK3* antibody. As seen in Figure 3.2B, a band was detected at ~100 kDa in the induced bacterial lysates that was the same molecular weight as that observed in fractions from the Ni-NTA chromatography purified sample (Figure 3.2B). However, in the bacterial lysate samples a further band at ~40 kDa was also detected which might represent a fragment of *PfCLK3* or an unrelated protein that cross-reacts with the antibody.

Large scale purification of *PfCLK3* from induced bacterial cultures was then performed. The purified protein fractions were quantified using standard Bradford reagent and separated on SDS-PAGE gel (Figure 3.2C). A band at ~100 kDa consistent with the molecular weight of *PfCLK3* was eluted in fractions 2-5. These fractions were pooled and dialysed overnight before protein was collected and stored at -80⁰C in 10% glycerol until use.

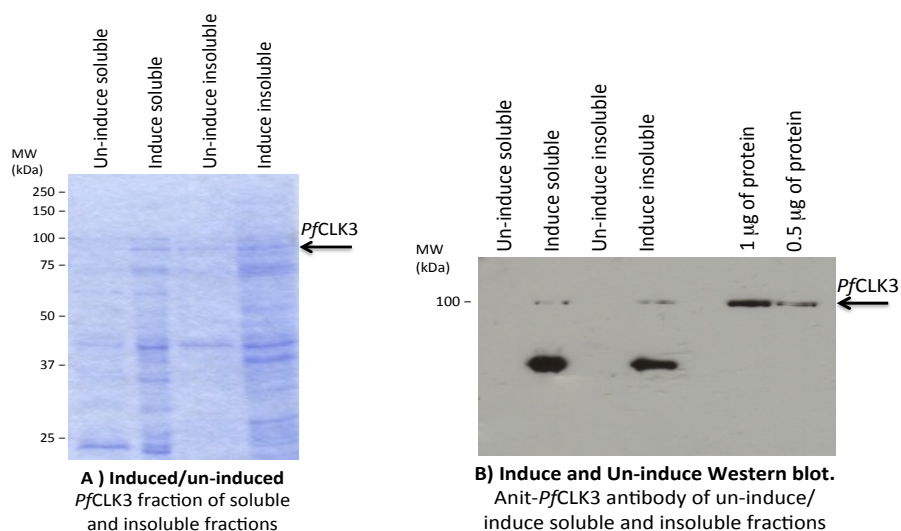
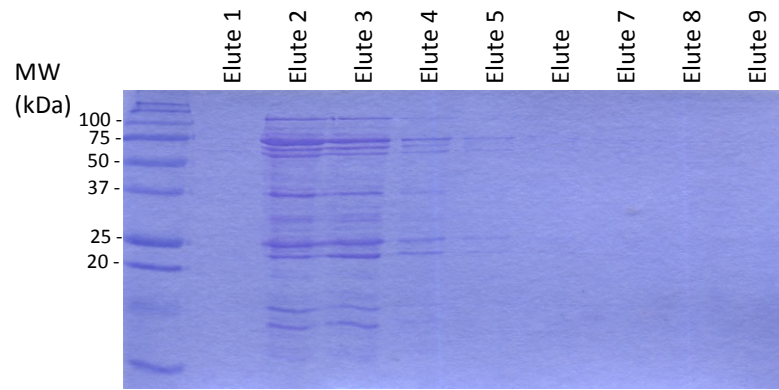


Figure 3.2: *PfCLK3* Expression in *E. coli* (BL-21 Codon Plus). A) Induce or un-induced fractions of bacterial lysate analysed for protein solubility on SDS-PAGE gel. B) Confirmation of the bacterial lysate and the purified protein fractions by western blot using anti-*PfCLK3* antibody. C) Fractions of the purified *PfCLK3* eluted protein, elutes 2, 3, 4 and 5 pooled together and dialyse for total protein stored at -80°C .

3.2.2.2 Expression of *Pf*CLK4 Kinase domain

The kinase catalytic domain of *Pf*CLK4 located at the N-terminus spanning towards the C-terminus was amplified from cDNA and submitted to PROTEX for cloning into pLIECS-05 as His-tagged fusion protein. The clones were transformed into competent *E. coli* (BL-21 Codon Plus) cells as described in the methods section. For large-scale purification of *Pf*CLK4-KD inducible bacterial cultures were setup with a single colony from an overnight agar plate. The protein was purified using Ni-NTA chromatography and the elutes were separated on SDS-PAGE gel. As shown in Figure 3.3, elutes 2, 3, and 4 are protein bands consistent with the expected molecular weight of *Pf*CLK4. These fractions were pooled and dialysed overnight before protein was collected and stored at -80°C in 10% glycerol until use.



C-terminal His-tag *PfCLK4* eluted from Ni-NTA purification

Figure 3.3: *PfCLK4* kinase domain expression in competent bacterial cells (*E. coli*). Elutes of purified protein.

3.2.3 Kinase Activity and Inhibition Assays

To characterise the effects of the inhibitors TCMDC-138736 and TCMDC-135051 to *Plasmodium* CLK kinases, suitable exogenous substrates to use were first investigated. Detailed γ -³²P-ATP kinase activity and inhibition assay is described in the methods section and in an earlier publication (Kern *et al.*, 2014).

3.2.3.1 Identification of suitable exogenous substrate for *Pf*CLK1, 3 and 4 employing radiolabelled γ -³²P-ATP kinase assay

Using γ -³²P-ATP to radiolabelled phosphorylated substrates in a kinase assay, the phosphorylation of the exogenous substrates: Histone, Myelin Basic Protein (MBP) and Casein, the most commonly used substrates (Haubrich and Swinney, 2016), by recombinant *Plasmodium* CLK family of kinases (*Pf*CLK1, 3 and 4) was investigated. The signals for substrate phosphorylation were detected by autoradiography and the Coomassie stained bottom panel is the loading control. Consistent with previous studies (Kern *et al.*, 2014), it is shown here that *Pf*CLK1 phosphorylated all three substrates, with histone phosphorylation detected at about 33 kDa, MBP phosphorylation at 18 kDa and casein at about 30 kDa (Figure 3.4A) *Pf*CLK4 demonstrated a similar phosphorylation pattern, showing stronger phosphorylation activity with MBP as shown in Figure 3.4C. *Pf*CLK3 however, only phosphorylated MBP but to a lower activity level compared to *Pf*CLK1 and *Pf*CLK4 (Figure 3.4B). This kinase showed a significant level of auto-phosphorylation as indicated by the band at ~100 kDa. This phosphorylation data shows MBP as a common substrate phosphorylated by all members of this kinase family. Therefore, MBP is used as exogenous substrate in all experiments to characterise these kinases and test the compound kinase inhibitors TCMDC-138736 and TCMDC-135051.

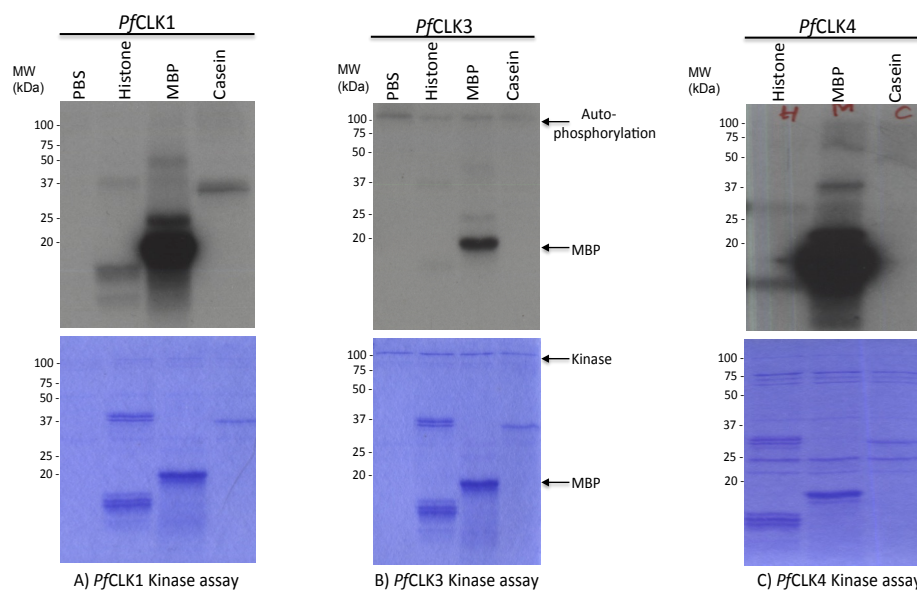


Figure 3.4: Kinase phosphorylation assay of exogenous substrate using γ - 32 P-ATP assay. Kinase activity assays were used to detect phosphorylation of the exogenous substrates histone H1, MBP and α/β casein with recombinant *PfCLK1*, *PfCLK3* and *PfCLK4*. SDS-PAGE gels stained blue with Coomassie (lower panel) are loading controls and PBS as negative controls.

3.2.3.2 Inhibition of Kinase mediated MBP phosphorylation using TCMDC-138736 and TCMDC-135051 inhibitors

Next I investigated the efficacy of TCMDC-138736 and TCMDC-135051 inhibition against the *PfCLK* kinase family. Kinase inhibition assays were setup as described in the methods section and the effect of the inhibitors on MBP phosphorylation determined by detecting phosphorylation signal of the substrate using autoradiography.

The results showed a significant inhibition of *PfCLK3* kinase phosphorylation activity when treated with both TCMDC-138736 and TCMDC-135051 (Figure 3.5A). TCMDC-135051 showed higher inhibition efficacy compared to TCMDC-138736. TCMDC-138736 inhibits *PfCLK3* phosphorylation activity by nearly 75% and TCMDC-135051 inhibits *PfCLK3* phosphorylation by greater than 95% (Figure 3.5B). Thus, both TCMDC-138736 and TCMDC-135051 are efficacious *PfCLK3* inhibitors.

In contrast, no inhibition of kinase activity is observed when *PfCLK1* and *PfCLK4* were tested for inhibition by both inhibitors (Figure 3.6A, B). This lack of inhibition of these 2 kinases demonstrates specificity of the inhibitors to inhibiting *PfCLK3* only and not other members of the same kinase family.

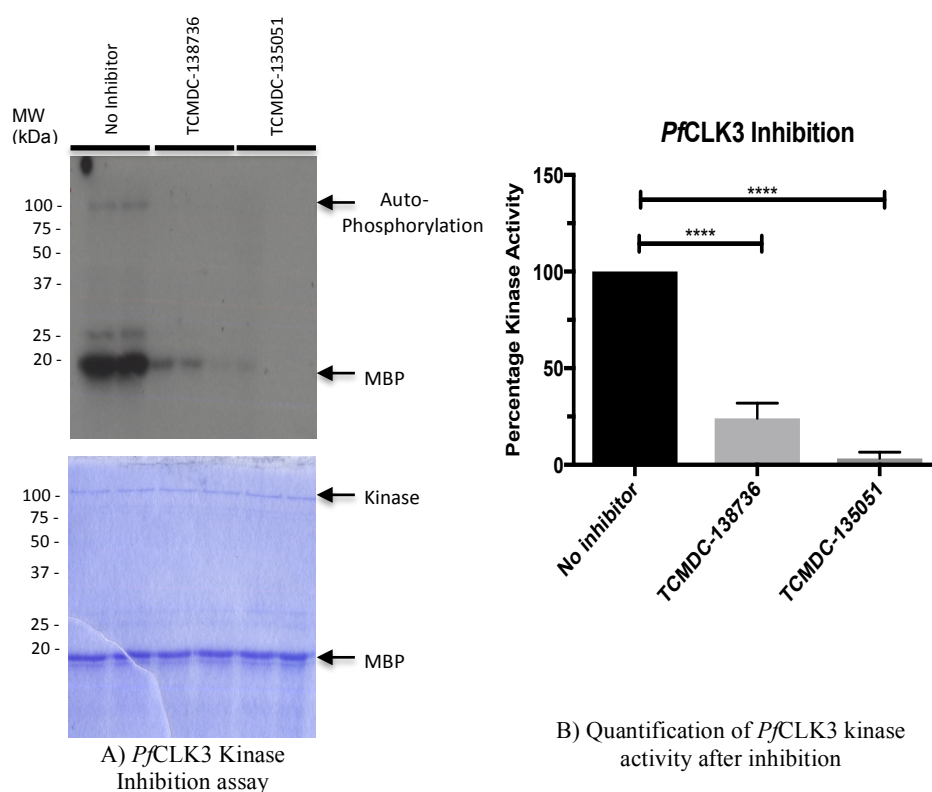


Figure 3.5: Effects of TCMDC-138736 and TCMDC-135051 on MBP-phosphorylation by *Pf*CLK3 using γ -³²P-ATP *in vitro* kinase assay. A) Activity of *Pf*CLK3-mediated MBP-phosphorylation is inhibited by TCMDC-138736 and TCMDC-135051 significantly in a kinase inhibition assay. B) Graphical representation of quantified phosphorylation inhibition levels of TCMDC-138736 and TCMDC-135051 on *Pf*CLK3-mediated phosphorylation of MBP showed significant inhibition of kinase activity by ~75 and ~95% respectively using ANOVA. The top panel is autoradiograph of the kinase inhibition readout and the lower panel is the Coomassie stained SDS-PAGE gel as loading control. The graph represents data from three independent experiments in duplicates with error bars as standard error of the mean (S.E.M).

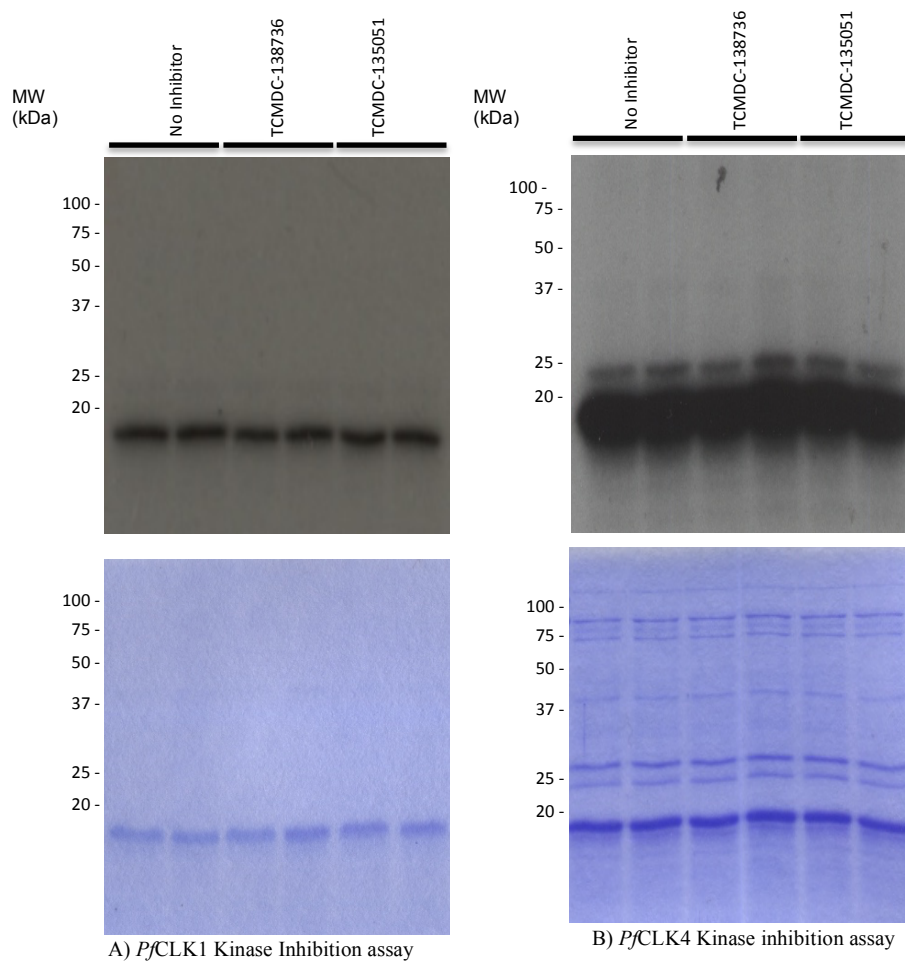


Figure 3.6: Effects of TCMDC-138736 and TCMDC-135051 on MBP-phosphorylation by *Pf*CLK1 and 4 using γ -³²P-ATP kinase assay. A) *Pf*CLK1-mediated MBP phosphorylation is not inhibited by the presence of either of the compound inhibitors (TCMDC-138736 and TCMDC-135051). B) *Pf*CLK4-mediated MBP phosphorylation activity like *Pf*CLK1 is not inhibited by either of the two inhibitors.

3.2.3.3 Inhibition of other *Plasmodium* protein kinases by TCMDC-135051

To confirm the specificity of TCMDC-135051 towards *PfCLK3*, the inhibition efficacy of TCMDC-135051 was investigated against two other kinases, *PfCDPK1* and *PfPKG* using γ -³²P-ATP kinase inhibition assay. *PfPKG* inhibition reactions were setup with 0.5 μ g protein supplemented with 10 μ M cGMP (cyclic GMP) using Histone as exogenous substrate in the presence of 2 μ M inhibitor with no a inhibitor control. Similarly, *PfCDPK1* reactions were setup with 0.5 μ g protein supplemented with 1 mM CaCl₂ using MBP as substrate in the presence of 2 μ M inhibitor with no a inhibitor control. In these experiments *PfCLK3* was used as a positive control and as expected, addition of TCMDC-135051 inhibited the phosphorylation of MBP by *PfCLK3* (Figure 3.7A). In contrast, TCMDC-135051 inhibited the phosphorylation activity of none of these kinases (Figure 3.7B, C) confirming the selectivity of TCMDC-135051 towards *PfCLK3*.

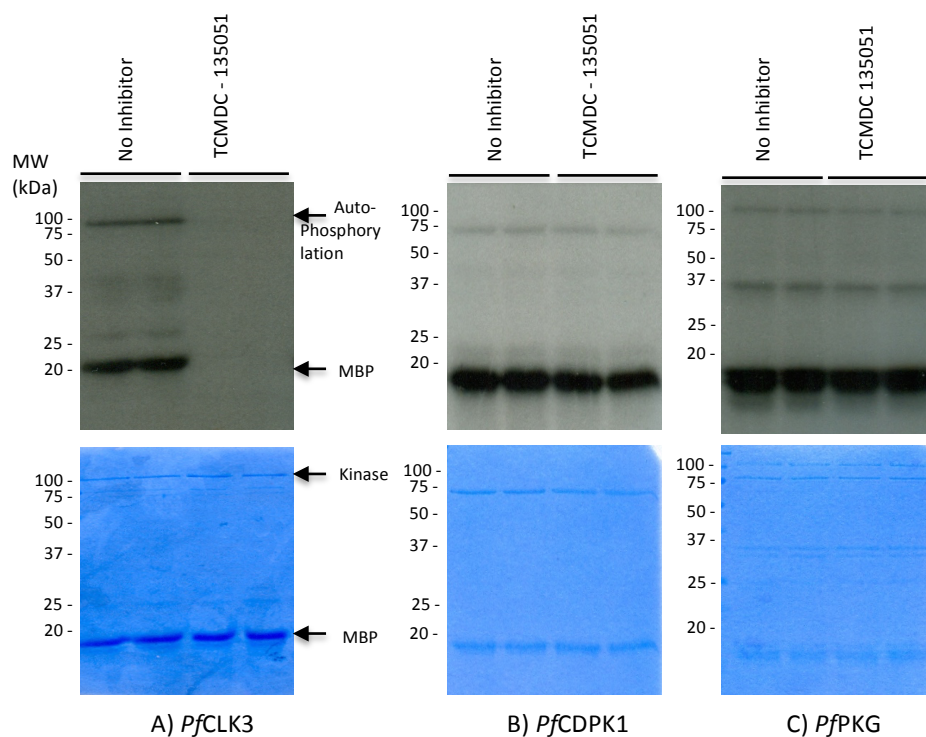


Figure 3.7: Inhibition of other *Plasmodium* protein kinases with TCMD-135051 using *PfCLK3* as control. The top panels are autoradiographs detecting phosphorylation and the bottom panels are coomassie blue stained loading control. A) *PfCLK3* kinase inhibition assay using 0.5 μ g protein and MBP as substrate with PBS as a no drug control and 2 μ M TCMD-135051. B) *PfCDPK1* kinase inhibition assay supplemented with 1 mM CaCl_2 and MBP as substrate in the presence of either PBS as control for inhibition and 2 μ M of TCMD-135051 as inhibitor. C) Kinase inhibition of *PfPKG* supplemented with 10 μ M cGMP using Histone as exogenous substrate in the presence of 2 μ M inhibitor.

3.2.3.4 Potency of TCMDC-138736 and TCMDC-135051 to inhibiting *Pf*CLK3 kinase – determining the IC₅₀

The inhibitors TCMDC-138736 and TCMDC-135051 were shown to efficaciously inhibit the activity of *Pf*CLK3 using γ -32P-APT kinase inhibition assay. Following this evidence, the potency of the inhibitors was investigated by determining their IC_{50s} (the concentration of drug at which 50% of target activity is inhibited) using the previously optimised LANCE *Ultra* time-resolved fluorescence energy transfer (TR-FRET) kinase assay from Perkin Elmer as described in methods section; lower IC₅₀ value of a drug indicates a better potency.

First, the Michaelis-Menten constant (*K_m* for ATP) for the kinase was investigated to establish the concentration of ATP needed to facilitate substrate phosphorylation, in this case Europium-anti-phospho-Myelin Basic Protein (MBP) was used. The data showed that the *K_m* for ATP was 6.27 μ M (\pm 0.68) in the presence of saturating concentrations of MBP substrate and enzyme (Figure 3.8A) however; 10 μ M was used in subsequent TR-FRET kinase assays. At this ATP concentration, using 50 nM protein and MBP substrate, the IC₅₀ values for TCMDC-138736 and TCMDC-135051 were determined using the formula below. The inhibition data show that, TCMDC-135051 has a greater potency compared to TCMDC-138736 with IC₅₀ values of 40.86 nM (pIC₅₀=7.4 \pm 0.07) and 281.9 nM (pIC₅₀=6.55 \pm 0.11), respectively (Figure 3.8B, C). However, IC₅₀ data must be interpreted with caution because measured IC₅₀ in a biochemical assay is proportional to the target protein concentration used in the assay (Strelow, 2017).

Percentage Kinase inhibition: 100

$$- \left(\frac{(\text{Kinase activity} - \text{Blank})}{(\text{maximum kinase activity} - \text{blank})} \right) * 100$$

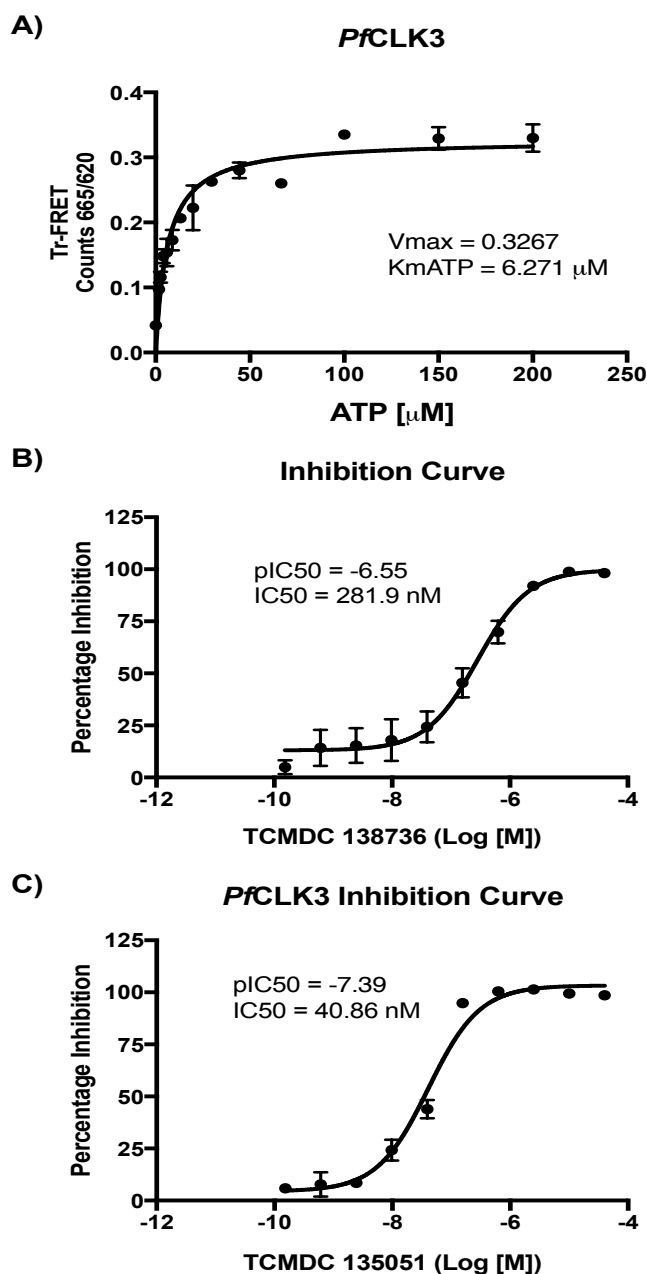


Figure 3.8: Time-resolved fluorescence energy transfer to determine K_m for ATP and IC_{50} for TCMDC-138736 and TCMDC-135051. A) Michaelis-Menten constant (K_m for ATP) curve determined using 50 nM protein (*Pf*CLK3) in the presence of 50 nM MBP with cold ATP at a top concentration of 200 μ M serially diluted. B) and C) Kinase inhibition curve of *Pf*CLK3 using the determined K_m for ATP (10 μ M) and 50 nM recombinant protein kinase in the presence of TCMDC 138736 and TCMDC 135051 inhibitors serially diluted with a dilution factor of 1 in 3 with a starting concentration of 100 μ M. All experiments were done in triplicates and the data presented is the S.E.M of three independent experiments run in triplicates and plotted using GraphPad prism software.

3.2.3.5 The inhibitors TCMDC-138736 and TCMDC-135051 both inhibit 3D7 parasite growth with a low EC₅₀ value – strong drug potency.

Following confirmation of inhibition property and specificity of the inhibitors towards *Pf*CLK3 kinase, the potency of the inhibitors against asexual *P. falciparum* parasites were determined using *in vivo* growth inhibition assays. This was carried out using synchronised asexual ring stage 3D7 laboratory isolates at about 0.5% parasitaemia and a drug concentration gradient. Parasites were cultured for at least 48 hours or until next generation of rings were detected.

Direct measurement of parasite growth inhibition using standard drug assays revealed low nanomolar potencies. Both inhibitors TCMDC-138736 and TCMDC-135051 showed potent inhibition of *P. falciparum* growth with EC₅₀ values of 1053 nM (pEC₅₀=5.978±0.015) and 180.8 nM (pEC₅₀=6.74±0.033) respectively as shown in Figure 3.9A and B.

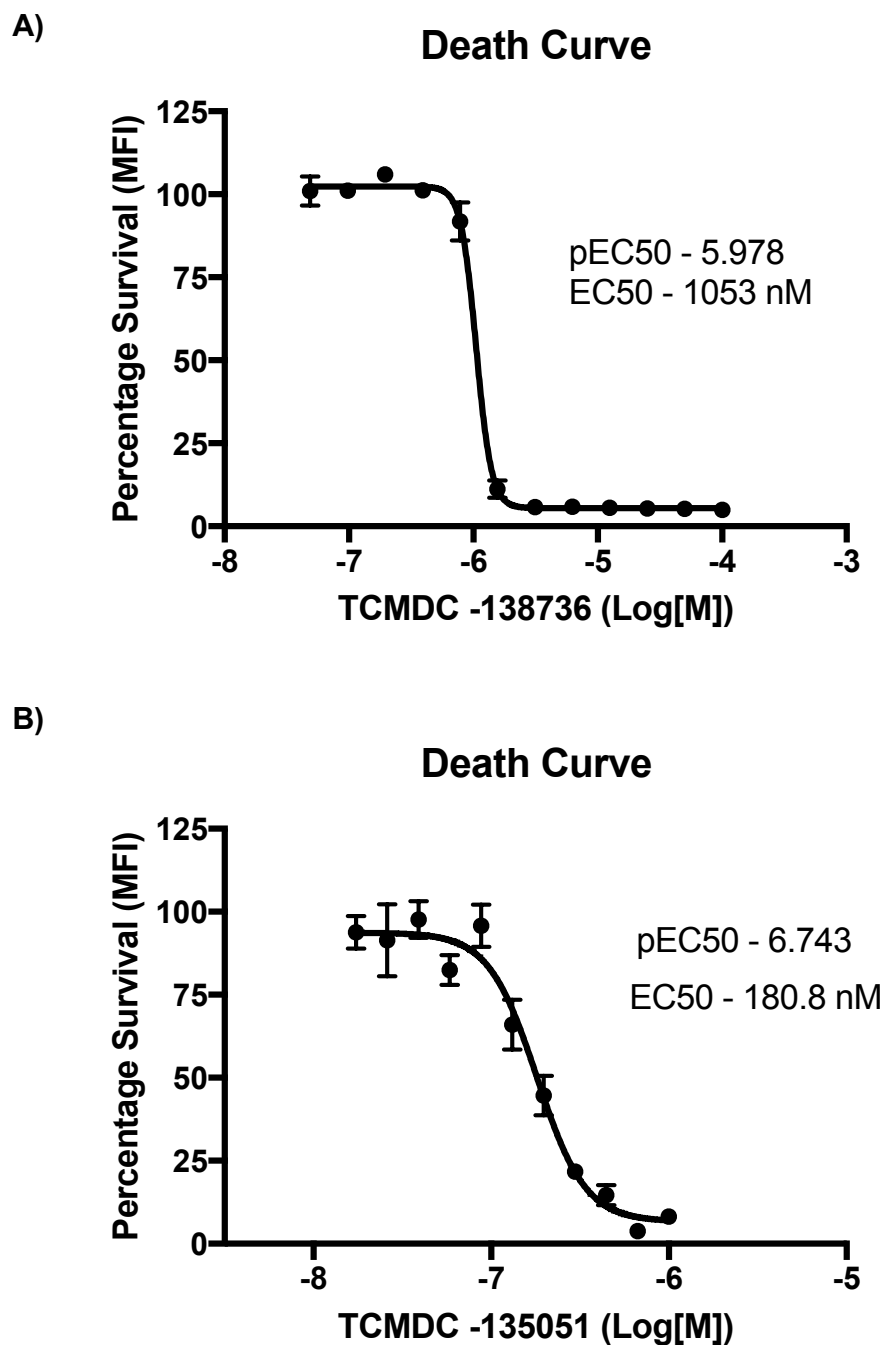


Figure 3.9: *P. falciparum* 3D7 parasite death curve with TCMDC-138736 and TCMDC-135051 inhibitors. A) Death curve of 3D7 parasites with TCMDC138736 with an EC50 of 1053 nM (pEC50=5.98±0.015). B) Death curve of 3D7 parasites with TCMDC135051 shows an EC50 of 180.8 nM (pEC50=6.74±0.033). The data presented here is the average of three independent experiments in triplicates plotted using Prism Graph Pad.

3.2.3.6 TCMDC-135051 interrupts asexual parasite growth and development

To evaluate the parasite blood stages most sensitive to TCMDC-135051, *in vitro* cultures of synchronised *P. falciparum* 3D7 parasites were set up and parasites treated with TCMDC-135051 at time point 0, 10, 20, 30, and 40 hours to a final inhibitor concentration of 1 μ M and allowed to grow for 70 hours. Thin blood smears were collected every 10 hours from time point 0 to 70 hours. The slides were Giemsa stained and parasite development stages determined by microscopy. The results showed that untreated controls (Figure 3.10) developed normally, mature into schizonts and invasive next generation rings were formed within the expected time limit. However, parasites challenged at time point 0 (0 - 3 hours old rings), were arrested, and did not progress further than early trophozoites, looked condensed and with pigmentation. To older rings (10 and 20 hours old rings), addition of the inhibitor also stalled parasite growth, demonstrated with the appearance of pycnotic nuclei and condensation of nuclear material. When the inhibitor was added to trophozoites (30 hours) and schizonts (40 hours), a similar growth arrest was observed (Figure 3.10). Allowing the parasites longer time did not give them any survival advantage and were all identified dead by the observed nuclear condensation and pigmentation of nuclear material, indicating that inhibition of *PfCLK3* directly inhibits parasite growth. The *in vitro* data presented here shows that TCMDC-135051 is potent against all the stages of intra-erythrocytic asexual life cycle of *P. falciparum*. This indicates that the target is present across all developmental stages, but the higher nuclear activity later in their life cycle might be responsible for the observed increased activity against late trophozoites and schizonts. The potency of TCMDC-135051 against other *Plasmodium* species and *P. falciparum* clinical isolates are described in subsequent chapters.

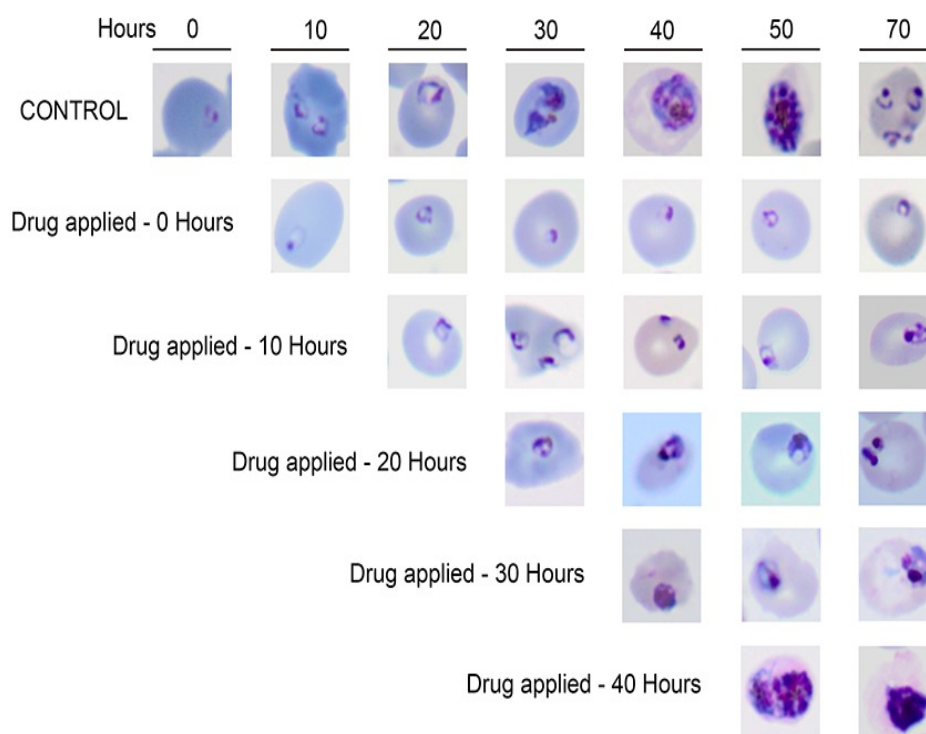


Figure 3.10: TCMDC-135051 inhibits parasite growth and development at all stages. Synchronised *P. falciparum* parasites were challenged with continuous drug exposure from time point zero hours to 40 hours with drug added every 10 hours. Samples were collected from 0, 10, 20, 30, 40, 50 and 70 hours and thin smear blood films were prepared, Giemsa stained and images of parasites captured using evos microscope with magnification of 100X. As shown, irrespective of the time the drug was added, parasite growth is stalled once the inhibitor was added resulting to parasite growth stagnation and eventual death. The untreated control however, grew to trophozoites and schizont and finally to the next generation of mature rings within 70 hours as expected. This demonstrates that TCMDC-135051 is potent against multiple stages of the parasite life cycle.

3.3 Discussions

Active recombinant *Plasmodium* CLK kinases can be expressed in bacterial cells using standard protein expression systems. All the *Pf*CLK kinases were successfully expressed as His-tagged protein kinases except *Pf*CLK2 after several attempts. The purified kinases were tested for phosphorylation of exogenous substrates and all 3 kinases phosphorylated MBP peptide, which was used as an exogenous substrate in all subsequent kinase assays.

To determine the therapeutic opportunities offered by the *Plasmodium* CLK kinases, members of splicing-regulated kinases (Araki *et al.*, 2015), the inhibitors TCMDC-138736 and TCMDC-135051 were used to characterize this kinase family. Inhibition assays using gel-based γ -³²P-ATP assay and TR-FRET assay showed that both inhibitors selectively inhibited *Pf*CLK3 with TCMDC-135051 demonstrating higher efficacy; *Pf*CLK1 and *Pf*CLK4 kinases were not inhibited. The lack of efficacy of the inhibitors against *Pf*CLK1 and *Pf*CLK4 demonstrates the selectivity of the inhibitors towards *Pf*CLK3 over these CLKs. To further confirm selectivity, *Pf*PKG and *Pf*CDPK1 were tested for inhibition and none of these were inhibited, further demonstrating selectivity towards *Pf*CLK3.

Although this is the first time that TCMDC-135051 and TCMDC-138736 have been reported to selectively inhibit *Pf*CLK3, an earlier study identified inhibitors of *Pf*CLK3 (Kern *et al.*, 2014). However, this study identified 5 oxo- β -carboline inhibitors for *Pf*CLK3 but they show low potency, IC₅₀ values ranges were 4-7 μ M, indicating that TCMDC-135051 is a more potent *Pf*CLK3 inhibitor. However, low nanomolar potency of splicing-related inhibitors has been reported earlier in independent experiments inhibiting human CLKs and SRPKs (Araki *et al.*, 2015, Fedorov *et al.*, 2011).

These inhibitors also inhibited asexual *P. falciparum* parasites at low nanomolar concentrations, and TCMDC-135051 demonstrated stronger potency compared to TCMDC-138736. Although small molecules with better potency acting at multiple life-cycle stages, DDD107489, targeting translation elongation factor 2 has an EC_{50} <10 nM (Baragaña *et al.*, 2015). However, the small molecules described here demonstrated better potencies compared to a set of MMV inhibitors with EC_{50} values in high micromolar concentration ranges (Hallyburton *et al.*, 2017a). The high specificity and low nanomolar potency of these inhibitors against *PfCLK3* is not surprising because kinase inhibitors with high selectivity for CLK1 and its closely related CLK4 have been reported in a study investigating inhibitors for human CLKs (Fedorov *et al.*, 2011).

ATP-competitive inhibitors are common because ATP-binding pockets are conserved among kinases resulting in lack of selectivity (Roskoski, 2015, Uitdehaag *et al.*, 2012) and reduced potency because of high cellular ATP and promiscuous binding (Rudolf *et al.*, 2014). A detailed analysis of the mechanism of action of these inhibitors and the effects of increased ATP concentration on inhibitor efficacy is evaluated in chapter 4.

The data presented here demonstrates that TCMDC-135051 has a higher potency both in *in vitro* kinase assays and cellular assays compared to TCMDC-138736. Furthermore, TCMDC-135051 showed multi-stage effects against *P. falciparum* 3D7 parasites with high potency, arresting growth, and inhibiting parasite progression. Therefore, TCMDC-135051 was considered more suitable for use to investigate the druggability of *PfCLK3* kinase because it is highly selective and has efficacious biological activity against 3D7 parasites, two important characteristics necessary of tool compounds (Hughes *et al.*, 2011). Hence, TCMDC-135051 was investigated as a tool compound for further study.

Chapter 4 Determining the mechanism of action of TCMDC-135051

4.1 Introduction

In Chapter 3, I showed that TCMDC-138736 and TCMDC-135051 are potent inhibitors of *Pf*CLK3 recombinant kinase and has activity on parasite viability at multiple stages of asexual development, as well as on sexual forms as shown by Alam and colleagues (Alam *et al.*, 2018). However, the mode of action (ATP-competitive or non-ATP competitive) of these inhibitors is not known. The displayed high selectivity for *Pf*CLK3 suggest that the inhibitors are non-ATP competitive, because ATP-competitive inhibitors are more likely to be less selective due to the similarity of the conserved ATP-binding site shared between most kinases (Liang *et al.*, 2012).

Lack of selectivity in kinase inhibitors is a leading cause of failure of ATP-competitive therapeutic inhibitors in pre-clinical or clinical evaluations as this results in higher toxicity (off-target effects) with undesirable side effects and/or low efficacy (Wilson *et al.*, 2016). An additional problem associated with ATP competitive inhibitors is the development of drug resistance due to mutations which could occur within the conserved ATP-binding site (Kirkland and McInnes, 2009).

Not surprisingly therefore, recent kinase drug discovery research approaches are focused on identifying non-ATP competitive inhibitors because they increase target selectivity compared to ATP competitive inhibitors (Xu *et al.*, 2015, Liang *et al.*, 2012). The advantage of non-ATP competitive inhibitors are that they inhibit target kinases by binding to a site outside the catalytic domain to render the kinase non-functional and do not compete with intracellular ATP for the ATP binding site (Garuti *et al.*, 2010). Though this is largely the case, there are few selective ATP

competitive kinase inhibitors that have met specific requirements for binding to the ATP pocket of some kinases with specific sequence structure. For example, selective ATP-competitive inhibitors have been identified for *Toxoplasma gondii* CDPK1 (*TgCDPK1*) and *Cryptosporidium parvum* CDPK1 (*CpCDPK1*), reportedly because of their small gatekeeper residues that only allow enough binding space for pyrazolo-pyrimidine inhibitors containing bulky groups to occupy the ATP-binding pockets (Lourido *et al.*, 2013, Zhang *et al.*, 2012).

This chapter aimed to investigate the mechanism of action of TCMDC-138736 and TCMDC-135051 to determine whether or not they are ATP competitive inhibitors; ATP concentration or affinity for ATP directly affects the potency of ATP-competitive inhibitors (Rudolf *et al.*, 2014). This was investigated first by measuring the steady state Michaelis-Menten constant in the presence of various concentrations of the inhibitors to determine changes in the K_m for ATP and second, by assessing the IC_{50} of the inhibitors in the presence of increasing ATP concentrations as previously described (Haupt *et al.*, 2015). A change in the K_m for ATP at increasing concentrations of inhibitor and a change in IC_{50} in the presence of increased ATP concentration would suggest ATP competitive mechanism of action. If increased ATP and inhibitor concentrations have no significant effect on inhibitor potency (unchanged IC_{50} value and K_m for ATP), the inhibitors are said to be acting through non-ATP competitive mechanism (Wilson *et al.*, 2016). Data in this chapter suggest that TCMDC-135051 is a non-ATP competitive inhibitor because the presence of increasing concentrations of ATP has no effect on its potency whereas TCMDC-138736 inhibitory data in the presence of increasing ATP concentration suggests ATP-competitive mode of inhibition.

4.2 Results

4.2.1 High ATP concentration affects the inhibition potency of TCMDC-135051 and TCMDC-138736 differently

The inhibitors TCMDC-138736 and TCMDC-135051 both show potency to, and selectivity towards, *Pf*CLK3 over other protein kinases and also inhibit asexual parasite growth through an unknown mechanism of action. To investigate the mechanism of action of TCMDC-138736 and TCMDC-135051, γ -32P-ATP kinase inhibition assay of *Pf*CLK3 was setup using 2 μ M of TCMDC-135051 at 50 and 200 μ M ATP to test the effects of increased ATP concentration on the inhibition efficacy of TCMDC-135051. The results from this assay showed that increasing the concentration of ATP by four fold (from 50 to 200 μ M) had no effect on the inhibition efficacy of TCMDC-135051 towards *Pf*CLK3, suggesting TCMDC-135051 is an ATP independent inhibitor (Figure 4.1A and B).

This was investigated further using the TR-FRET inhibition assay setup using ATP at the K_m for ATP concentration and 50X the K_m for ATP concentration to have an indication of the effect of ATP concentration on the inhibition potency of TCMDC-135051 and TCMDC-138736. The data showed that ATP concentration has no effect on the inhibition potency of TCMDC-135051; the IC_{50} values obtained for ATP concentrations at the K_m for ATP and 50X K_m for APT were 40.86 nM ($pIC_{50}=7.39\pm 0.071$) and 65.15 nM ($pIC_{50}=7.19\pm 0.061$) respectively. This showed no significant change in the inhibition curves generated comparing the two ATP concentrations (Figure 4.1C). In contrast, a significant shift to the right was noticeable with TCMDC-138736 between the two ATP concentrations as seen in Figure 4.1D with IC_{50} values of 278.6 nM ($pIC_{50}=6.56\pm 0.077$) and 1326 nM ($pIC_{50}=5.88\pm 0.15$) for K_m for ATP and 50X K_m for ATP respectively and more than half log fold

shift in pIC_{50} value. This analysis suggests that TCMDC-135051 inhibition is ATP-independent whereas TCMDC-138736 is ATP-dependent. In the next section, a more detailed ATP-competitive assay was setup to confirm these results.

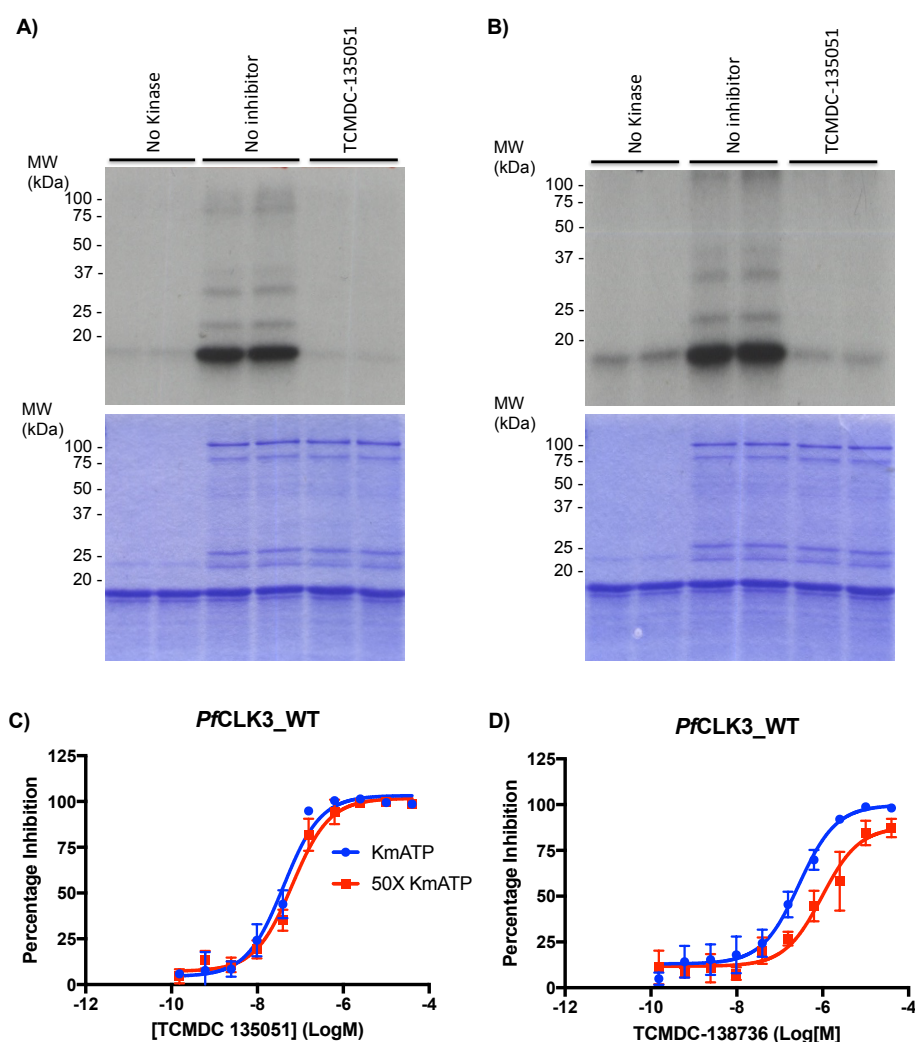


Figure 4.1: Effect of ATP concentration on the potency of TCMDC-135051 and TCMDC-138736 against *PfCLK3* using γ -32P-ATP and TR-FRET kinase assay. A) Kinase inhibition assay of *PfCLK3* using 50 μM ATP in the presence of 2 μM inhibitor. B) Kinase inhibition assay with 200 μM ATP and 2 μM inhibitor. The bottom panels are Coomassie stained gels as loading control and the top is the autoradiography images detecting phosphorylation. C) *PfCLK3* TR-FRET kinase inhibition assay of TCMDC-135051 using ATP concentrations at the K_m for ATP and 50X the K_m for ATP. D) *PfCLK3* TR-FRET kinase inhibition assay of TCMDC-138736 using ATP concentrations at the K_m for ATP and 50X the K_m for ATP using 50 nM MBP as substrate and a range of inhibitor concentrations. Data presented is an average of three independent experiments performed in triplicates and the error bars are \pm S.E.M.

4.2.2 Determining the mechanism of action of TCMDC-138736 and TCMDC-135051

The mode of action of TCMDC-138736 and TCMDC-135051 was investigated to determine the effect of ATP concentration on the potency of both inhibitors against *Pf*CLK3. A fixed concentration of recombinant protein (50 nM) with a range of ATP concentrations on either side of the K_m for ATP (Table 4-1) and different concentrations of inhibitor on either side of the IC_{50} (Table 4-2) were used in a TR-FRET inhibition assay. Using steady-state analysis, the data from the individual drug concentrations were fitted to a Michaelis-Menten equation to obtain the K_m for ATP for each condition and inhibitor (Figure 4.2A and C). The values for each ATP concentrations were analysed and plotted as a function of drug concentration (Figure 4.2B and D) to obtain the inhibition curves and IC_{50} values. The analysis revealed that increased concentrations of TCMDC-138736 resulted in higher K_m for ATP values (Table 4-2) and a change in the K_m for ATP curves (Figure 4.2A). Also, increasing ATP concentrations affected the potency of TCMDC-138736 and changed both the inhibition curves and the IC_{50} values obtained (Figure 4.2B and Table 4-1). Higher ATP concentration shifted the IC_{50} value from 35.62 (± 0.14) nM with 1 μ M ATP to 472.9 (± 0.13) nM with 200 μ M ATP concentration. In contrast, increased concentrations of TCMDC-135051 did not change the K_m for ATP (Figure 4.2C) nor did increasing the concentration of ATP significantly affect the inhibition potency of TCMDC-135051; hence, the obtained IC_{50} values have not changed in the presence of different ATP concentrations suggesting that TCMDC-235051 is acting through a non-ATP competitive mechanism (Table 4-1).

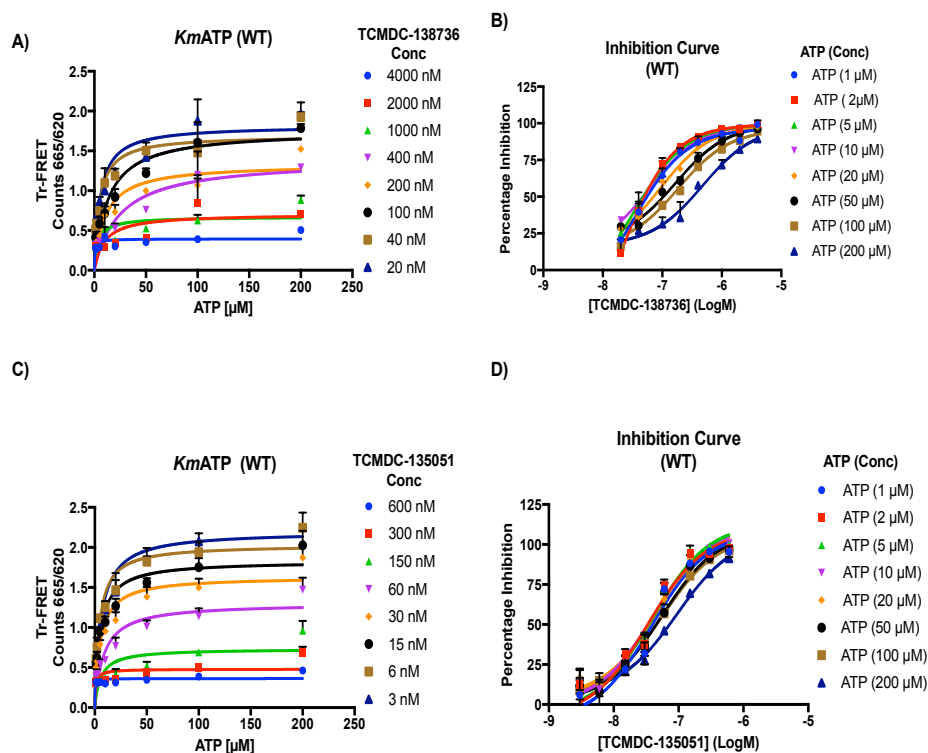


Figure 4.2: Biochemical analysis of *PfCLK3* kinase inhibition by TCMD-135051 and TCMD-138736 using TR-FRET assay. A and C) The K_m for ATP curves represent data fitted to Michaelis-Menten equation using nonlinear regression analysis for data obtained using constant amount of substrate and protein (*PfCLK3*) and various concentrations of ATP and inhibitors (TCMD-138736 and TCMD-135051 respectively). B and D) *PfCLK3* kinase inhibition assays were performed using TR-FRET assay described in methods section with various concentrations of ATP and inhibitor (TCMD-138736 and or TCMD-135051 respectively). The curves were generated by analysing the values of individual samples and plotted as function of inhibitor concentration; the acquired IC_{50} values are shown in **Table 4-1**. Data presented here is the average of three independent experiments done in triplicates with mean S.E.M.

Table 4-1: IC₅₀ values obtained from inhibition of *Pf*CLK3 by TCMDC-138736 and TCMDC-135051 in the presence of various ATP concentrations at constant protein and substrate concentration. Data is the average of three independent experiments in triplicates ±S.E.M.

ATP [μM]	TCMDC-138736	TCMDC-135051
	IC ₅₀ [nM] (±S.E.M)	IC ₅₀ [nM] (±S.E.M.)
1	35.62 (0.14)	38.4 (0.12)
2	18.29 (0.16)	33.63 (0.16)
5	34.34 (0.14)	39.11 (0.12)
10	61.42 (0.06)	41.8 (0.08)
20	91.23 (0.06)	49.56 (0.08)
50	166.4 (0.12)	54.77 (0.10)
100	185.4 (0.10)	55.83 (0.03)
200	472.9 (0.13)	94.5 (0.06)

Table 4-2: The Km for ATP values obtained in the presence of varying concentrations of TCMDC-138736 and TCMDC-135051 at constant protein and substrate concentration. Data is the average of three independent experiments in triplicates ±S.E.M.

TCMDC-138736 [nM]	Km ATP (±S.E.M)	TCMDC-135051 [nM]	Km ATP (±S.E.M)
20	5.6 (1.38)	3	6.06 (1.45)
40	5.15 (1.17)	6	4.29 (0.08)
100	13.03 (3.32)	15	5.08 (1.03)
200	10.44 (2.74)	30	5.4 (1.26)
400	24.51 (8.72)	60	8.56 (2.41)
1000	3.89 (1.77)	150	5.65 (2.39)
2000	9.57 (5.88)	300	1.06 (0.50)
4000	0.66 (0.35)	600	0.24 (0.15)

4.3 Discussion

This chapter focused on testing the mechanism of action of the inhibitors TCMDC-138736 and TCMDC-135051 to ensure the identified inhibitors are independent of ATP for target inhibition. This is important because of the high concentration of intracellular ATP (1-10 mM) (Huang *et al.*, 2010, Wilson *et al.*, 2016, Yaginuma *et al.*, 2014), which directly affects inhibitor potency. Additionally, ATP-competitive inhibitors are less selective compared to non-ATP competitive inhibitors because they bind the highly conserved ATP binding sites (Liang *et al.*, 2012) and generally result in undesirable off-target effects as mentioned earlier. Hence, recent research has focused on identifying non-ATP competitive kinase inhibitors in multiple therapeutic targets, such as non-small-cell lung cancer (Wang *et al.*, 2014).

The mechanism of action of TCMDC-138736 and TCMDC-135051 was investigated using gel-based and TR-FRET inhibition assays. The data showed that high ATP concentration had no effect on the potency of TCMDC-135051 to inhibit *PfCLK3* activity. Further characterisation using steady-state analysis revealed that the potency of TCMDC-135051 remained unchanged in the presence of varying concentrations of ATP. Similarly, the measured K_m for ATP in the presence of high concentrations of the inhibitor remained the same with no significant shift. These observations are typical behaviours suggestive of non-ATP competitive mode of inhibition (Rudolf *et al.*, 2014, Wilson *et al.*, 2016).

In contrast, the initial analysis of TCMDC-138736 revealed behaviour consistent with ATP-dependent mode of inhibition when two concentrations of ATP (K_m for ATP, 10 μ M, and 50X K_m for ATP 500 μ M, concentrations) were compared. The use of such assays for initial analysis of inhibitors has been used by others (Basnet *et al.*, 2015) and is useful to give an indication of the expected behaviour before using a bigger and more detailed

analysis. The steady state assay confirmed that increasing ATP concentration caused a significant shift in the IC_{50} and reduces the potency of TCMDC-138736. Additionally, increased concentration of TCMDC-138736 reduces kinase affinity for ATP as demonstrated by the increased K_m for ATP observed. Taken together, this data suggest TCMDC-138736 has an ATP-competitive mechanism of inhibition, a mechanism described previously (Basnet *et al.*, 2015, Gumireddy *et al.*, 2005).

Non-ATP competitive inhibitors can be allosteric modulators or substrate competitive inhibitors. Two highly potent benzothiazinone compounds (BTO), named BTO-5h and BTO-5s are glycogen synthase kinase 3 β (GSK-3 β) non-ATP competitive kinase inhibitors acting via allosteric modulation and substrate competition respectively (Zhang *et al.*, 2014a). Allosteric modulators, are supposedly more selective because their action is outside the catalytic domain and they do not compete with cellular ATP for binding (Gao *et al.*, 2017). Cyclin dependent kinases undergo substrate recruitment and recognition through interactions within the cyclin groove bringing protein segments in close proximity for phosphorylation to occur, blocking of this recruitment promote specific inhibition of the CDKs (Kirkland and McInnes, 2009). This alternative non-ATP competitive selective inhibition is an example of substrate competitive mode of inhibition and the improved selectivity is due to the fact that each kinase set requires a particular substrate.

The selectivity demonstrated in chapter 3 and the non-ATP competitive mode of inhibition observed here suggest that TCMDC-135051 is inhibiting target *Pf*CLK3 employing both substrate competitive and allosteric modulation mode of inhibition in what is referred to as bi-topic mode of inhibition. Further analysis of this hypothesis is discussed in chapter 5. To conclude, the data presented here shows that TCMDC-135051, meets the

criteria suggestive of non-ATP-competitive inhibitor (Basnet *et al.*, 2015, Wang *et al.*, 2014, Wilson *et al.*, 2016). The multistage and multispecies activity demonstrated by TCMDC-135051 tool compound makes it a suitable template for further characterisation as a novel and effective anti-malarial inhibitor.

Chapter 5 Target Validation

5.1 Introduction

The inhibition experiments described in chapter 3 showed that TCMDC-135051 has a higher potency and selectivity towards *PfCLK3* kinase, inhibiting its phosphorylation activity in *in vitro* kinase assays. Additionally, parasite growth was thwarted by TCMDC-135051 irrespective of the stage (ring, trophozoites or schizonts) it was added to the culture as shown in section chapter 3. However, kinase inhibitors have the potential to inhibit other protein kinases through off-target effects (Uitdehaag *et al.*, 2012), as reported in several kinase inhibitor drug discovery programs causing undesirable side effects hindering progress (Beeharry *et al.*, 2014, Schenone *et al.*, 2013). Therefore, it is important to validate that TCMDC-135051 is killing parasites by inhibiting the *PfCLK3* and not through an off-target effect, to confirm that TCMDC-135051 tool compound is an appropriate therapeutic agent selectively acting on the intended target (Jester *et al.*, 2012).

To garner evidence that TCMDC-135051 is selectively acting on *PfCLK3* to inhibit parasite growth, a mutant *PfCLK3* parasite resistant to inhibition by TCMDC-135051 is needed. This mutant parasite is expected to be resistant to inhibition by TCMDC-135051 and the potency of TCMDC-135051 should be significantly reduced with a shift in the death curve. The TCMDC-135051 resistant *PfCLK1* gene was chosen for its similarity to the *PfCLK3* as template and mutations generated by amino acid substitutions to get a resistant variant kinase with sufficient activity compared to the wild type. This chemo-genetic strategy has been used previously to generate mutant *PfPKG* resistant to the *PfPKG* inhibitor to explore functions of the gene (McRobert *et al.*, 2008a). The generated mutants would be evaluated for sensitivity to TCMDC-135051 and the most resistant transfected in to *P.*

falciparum parasites. To deliver on this approach, mutations (L440M, V443I, G449P, G449P, G449F and G450+) were generated around the *Pf*CLK3 gatekeeper region (F444) in subdomain IV, a region conserved across *Plasmodium* CLK3 kinases as shown in Figure 5.1, B and C using mutagenesis techniques. These were tested for kinase activity mutants retaining sufficient kinase activity were assessed for sensitivity to TCMDC-135051. The mutant most insensitive to the inhibitor was selected for transfection into parasites to replace the wild type *Pf*CLK3 kinase. With this approach, *Pf*CLK3_G449P was generated and found to reduce TCMDC-135051 efficacy significantly in the kinase inhibition assays described earlier. In parasites, the potency of TCMDC-135051 was also significantly reduced confirming TCMDC-135051 selectivity towards *Pf*CLK3.

An alternative strategy, a forward chemo genetic approach, was used to generate parasites resistant to TCMDC-135051 by exposing *P. falciparum* Dd2 parasites to constant drug pressure increased at sub-lethal concentrations over a 2 months period. The genomes of these clones were sequenced and compared to the parent genome to determine any effects on the target gene (Flannery *et al.*, 2013). One variant showed H259P mutation in the *Pf*CLK3 gene, which increased kinase activity by ~3.5 fold and reduced the potency of TCMDC-135051. Two additional variants: one on *Pf*CLK3 (P196R) and another on USP39 gene were detected. This further validates that *Pf*CLK3 is the target for TCMDC-135051 and this strategy has been used to confirm targets in several malaria drug discovery approaches (Dong *et al.*, 2011, Istvan *et al.*, 2011, McNamara *et al.*, 2013, Rottmann *et al.*, 2010).

Here, the confirmation that TCMDC-135051 kill *Plasmodium* parasites by inhibiting *Pf*CLK3 activity is described using data from mutant parasites with *Pf*CLK3_G449P and *Pf*CLK3_H259P genes

resistant to TCMDC-135051. Additionally, the data presented here show that TCMDC-135051 is non-ATP competitive and has a bi-topic mode of binding; one to an allosteric site and another as substrate competition. Together, this shows that *Pf*CLK3 is a drugable target of anti-*Plasmodium* drug development and TCMDC-135051 serves as a good template for a therapeutics tool compound.

5.2 Results

5.2.1 Generation of *PfCLK3* variant gene resistant to TCMDC-135051

PfCLK1 and *PfCLK3* have up to 30% sequence similarity, yet *PfCLK1* is insensitive to TCMDC-135051 inhibition. To validate that TCMDC-135051 action is *PfCLK3* specific in parasites, an inhibitor resistant *PfCLK3* is needed. Using *PfCLK1* kinase as template, a *PfCLK3* *PfCLK1*-like mutant resistant to TCMDC-135051 was generated. Using site directed mutagenesis PCR technique, a series of mutations on *PfCLK3* (G449F, G449M, G449P, G450+, L440M and V443I) were generated by substituting amino acid residues in subdomain IV of *PfCLK3* to the corresponding residues in *PfCLK1* and their kinase activities determined. The results showed that inserting a glycine after the glycine at position 449 in *PfCLK3* (*PfCLK3*_G450+) resulted in total loss of kinase activity (Figure 5.2A and B). Both *PfCLK3*_L440M and *PfCLK3*_V443I retained sufficient kinase activity. *PfCLK3*_L440M had its activity reduced to 70.96% compared to wild type, a significant difference with p value of 0.0158 (Figure 5.2A and B) whereas the *PfCLK3*_V443I mutant show no loss of kinase activity, 97.81% activity compared to wild type (Figure 5.2A and B). Additionally, glycine (G) at position 449 in *PfCLK3* was substituted with a proline (P) a bulkier amino acid as in *PfCLK1*, and then to methionine (M) and phenylalanine (F). Compared to wild type, *PfCLK3*_G449P retained up to 76.41% of kinase activity whereas *PfCLK3*_G449M retained only about 10% of kinase activity (*p* values of 0.0038) and *PfCLK3*_G449F shows complete loss of kinase activity (>98% activity lost) with and 0.0028 as seen in Figure 5.2C and D. This data shows that the mutants (*PfCLK3*_L440M, *PfCLK3*_G449M, *PfCLK3*_G449P and *PfCLK3*-V443I) have retained sufficient kinase activity. These would be tested for inhibition by the inhibitors to determine sensitivity before the transfection to *Plasmodium* parasites.

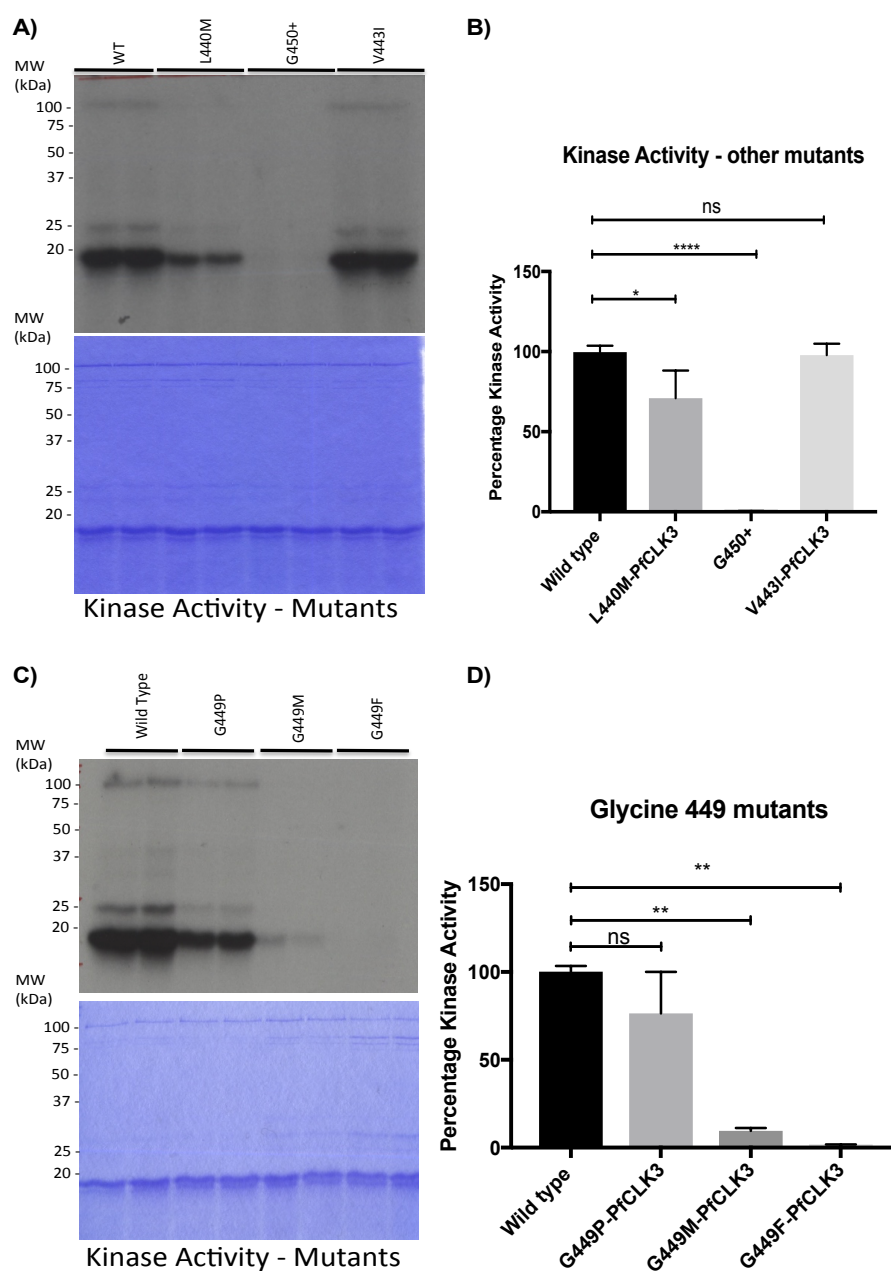


Figure 5.2: Kinase activity of generated *PfCLK3* mutants using γ -32P-ATP kinase assay and MBP as exogenous substrate. A and C, Kinase activities determined using 0.5 μ g of recombinant protein, 2 μ M of MBP substrate and 0.1 MBq of γ -32P-ATP. The top and bottom panels are the autoradiography activity film and the bottom panels are the Coomassie loading controls respectively. B and D, Graphs of ImageJ quantified kinase activity of the mutants normalised to the wild type at 100%. The data analysed with one-way ANOVA and plotted with Prism Graph Pad and the data represents average of 3 independent experiments in duplicates. Gel images are a single representation of three independent experiments.

5.2.1.1 Evaluation of the sensitivity of the *PfCLK3* variants to inhibition by TCMDC-135051 and TCMDC-138736

The mutants that retained sufficient kinase activity (*PfCLK3_L440M*, *PfCLK3_G449M*, *PfCLK3_G449P* and *PfCLK3-V443I*) were evaluated for potential to confer resistance to TCMDC-135051 and TCMDC-138736 inhibition using 2 μ M inhibitor, 0.5 μ g of protein in the presence of 0.1 MBq of γ -³²P-ATP. The results showed that *PfCLK3_L440M* is inhibited by TCMDC-138736 by 46%, which is not significant whereas TCMDC-135051 inhibited its kinase activity significantly to 20% with a *p* value of 0.012 (Figure 5.3A). *PfCLK3_V443I* is inhibited by TCMDC-138736 reducing its kinase activity by 63.5% with a *p* value of 0.0005 whereas TCMDC-135051 completely abolished kinase activity significantly compared to the untreated control with *p*<0.0001 (Figure 5.3B), and these are comparable to wild type *PfCLK3* inhibition. *PfCLK3_G449M* showed sensitivity to both inhibitors, TCMDC-138736 inhibiting its kinase activity by at least 40%, and TCMDC-135051 significantly inhibiting its activity by about 70% with a *p* value of 0.0239 compared to the untreated control (Figure 5.3C). The mutant conferring highest level of resistance was *PfCLK3_G449P*; it remarkably retained 100% of kinase activity when treated with either of the inhibitors (Figure 5.3D). Thus, G449P is the most-important mutation conferring resistance to both TCMDC-138736 and TCMDC-135051. This mutation was characterised further and its *K_m* for ATP and *IC*₅₀ were determined prior to generation of mutant parasite with *PfCLK3_G449P* variant in 3D7 *P. falciparum* parasite lines.

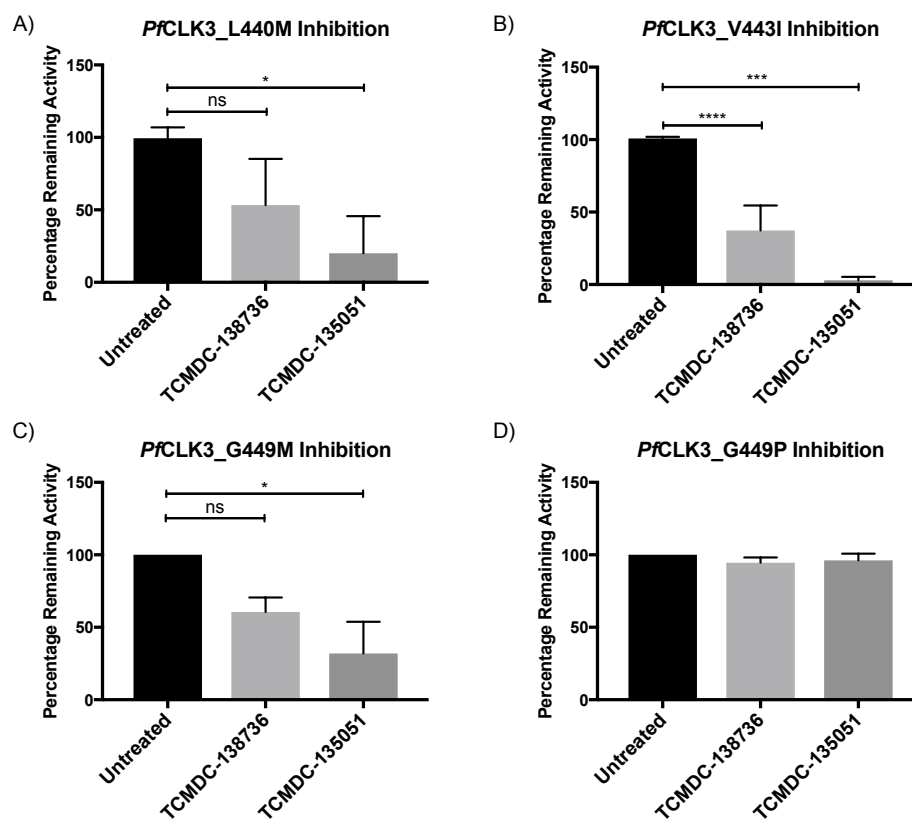


Figure 5.3: Kinase inhibition assay of recombinant *PfCLK3* mutants with TCMDC-138736 and TCDMC-135051 using 0.5 μ g protein, 2 μ M inhibitor, and 50 μ M cold ATP in the presence of 0.1 MBq of γ -³²P-ATP. Reaction was incubated at 37⁰C for 1 hour and stopped by adding equal volume of 2X Laemmli-loading buffer. Inhibition of recombinant mutant kinases: A) *PfCLK3*-L440M, B) *PfCLK3*_V443I C) *PfCLK3*_G449M and D) *PfCLK3*_G449P graphs. Data presented is the average of 3 independent experiments done in triplicate quantified with ImageJ. Graph Pad prism was use to plot the data with the standard error of the mean (S.E.M).

5.2.1.2 Determining the K_m for ATP for the mutant *PfCLK3_G449P* using the TR-FRET assay

The TR-FRET kinase assay was used to confirm the activity of G449P variant. The results indicate that the TR-FRET kinase activity levels are similar to what was previously obtained using γ -³²P-ATP kinase assay described in section 5.2.1; *PfCLK3_G449P* maintaining about 76% of kinase activity, slightly lower than wild type (Figure 5.4A). However, a K_m for ATP of 72.27 (± 11.45) was obtained, which is significant (p value of 0.0011) compared to the K_m for ATP of the wild type (Figure 5.4B).

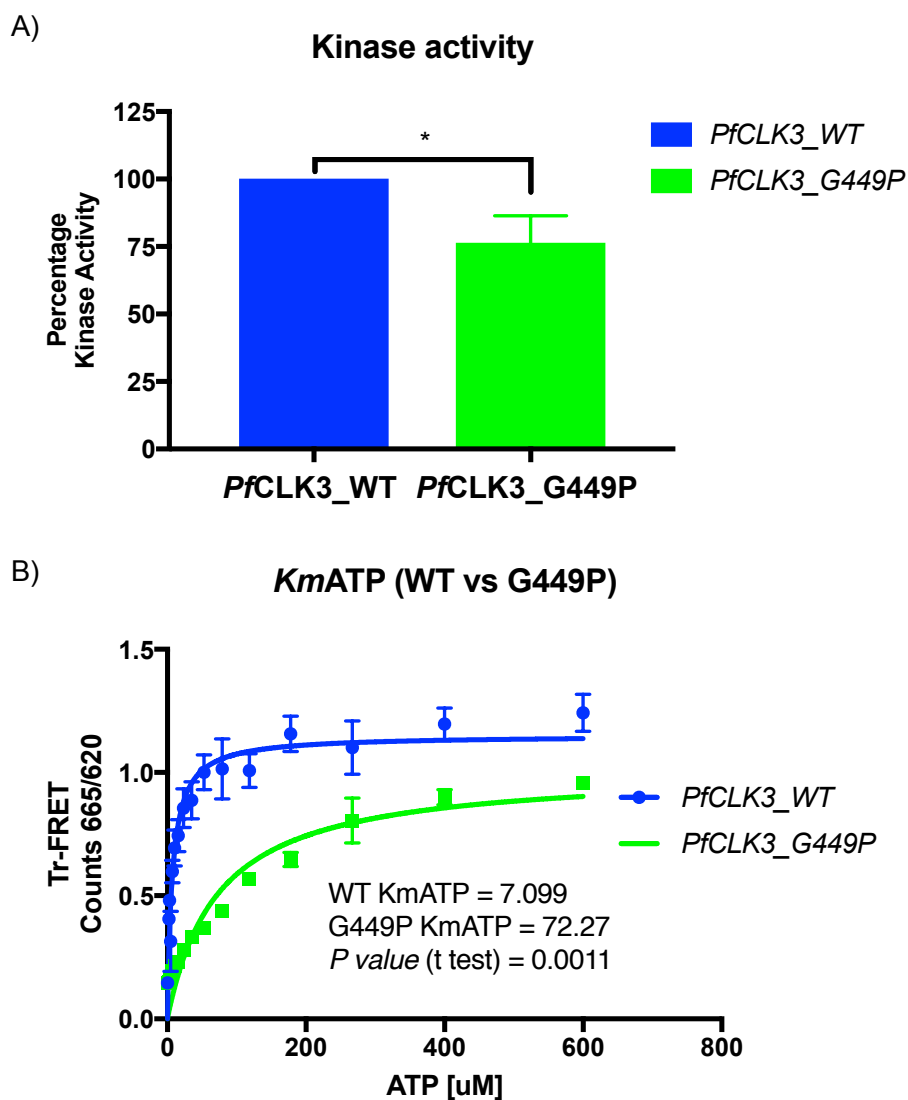


Figure 5.4: Comparison of kinase activity and K_m for ATP for *PfCLK3_WT* and *PfCLK3_G449P* using 50 nM each protein and 100 nM MBP peptide as substrate with the TR-FRET kinase assay described in the methods section. A) Kinase activity for *PfCLK3_WT* compared to *PfCLK3_G449P*. *PfCLK3_WT* data normalised to 100% and *PfCLK3_G449P* expressed as a percentage of the wild type kinase. B) K_m for ATP determined for the both *PfCLK3_WT* and *PfCLK3_G449P* using 50 nM protein and 100 nM MBP substrate in the presence of cold ATP with a starting concentration of 600 μ M diluted 2:3 fold down to 0 μ M. Data presented is the average of three independent experiments run in triplicates plotted using Graph Pad prism and shown S.E.M.

5.2.1.3 Substitution of glycine to proline generating *PfCLK3_G449P* confers TCMDC-135051 insensitivity to recombinant *PfCLK3*

Using 10 and 70 μM ATP concentrations for *PfCLK3_WT* and *PfCLK3_G449P* respectively, 0.5 μg protein and 2 μM MBP as substrate, a γ - ^{32}P -ATP kinase inhibition assay was setup using 2 μM of TCMDC-135051. The results as previously determined in section 5.2.1.1 confirmed this mutant as highly insensitive to TCMDC-135051 compared to *PfCLK3_WT* (Figure 5.5). As shown, *PfCLK3*-mediated MBP phosphorylation by the wild type kinase is completely inhibited in the presence of TCMDC-135051 whereas no inhibition was observed with the *PfCLK3_G449P* mutant, further confirming the insensitivity of the G449P variant to inhibition by TCMDC-135051.

Following the observed insensitivity of *PfCLK3_G449P* to inhibition by TCMDC-135051 using the γ - ^{32}P -ATP inhibition assay, its IC_{50} was determined using TR-FRET assay in the presence of 50 nM of recombinant protein, MBP-peptide substrate, and ATP concentration at the respective K_m for ATP as determined earlier. As shown in Figure 5.6A there is a clear shift in the inhibition curve which shows an increase in the IC_{50} value from 43.78 nM ($\text{pIC}_{50}=7.36\pm 0.12$) in wild type *PfCLK3* to 21.92 μM ($\text{pIC}_{50}=4.66\pm 0.16$) in *PfCLK3_G449P* (representing ~ 500 fold shift in IC_{50}) with ~ 3 log fold shift in pIC_{50} , a change statistically significant with a $p < 0.05$. *PfCLK3_G449P* and *PfCLK1* inhibitions were compared using *PfCLK3_WT* as control.

Figure 5.6B showed the curves overlaying on each other (*PfCLK1* and *PfCLK3_G449P*) demonstrating the accuracy of the targeted mutation. This high level of resistance is a further confirmation of TCMDC-135051 selectivity for wild type *PfCLK3* and suggests that when transfected to the parasite's genome there would be no inhibition if the inhibitor were acting via *PfCLK3* kinase.

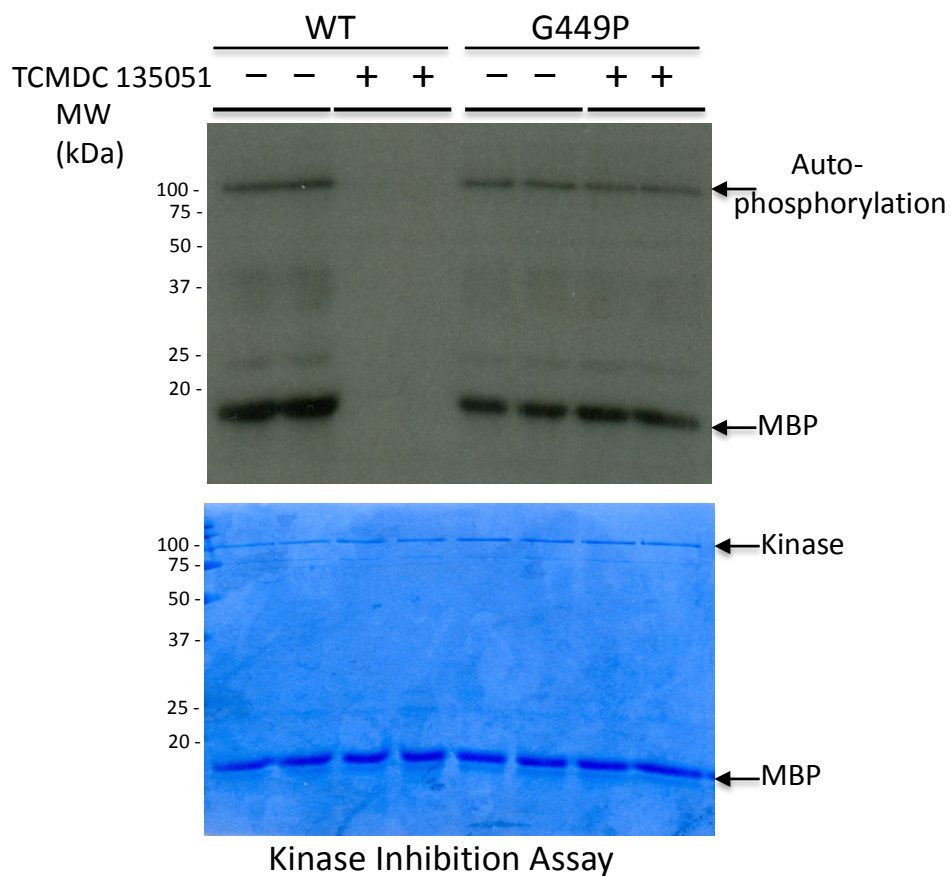


Figure 5.5: γ - 32 P-ATP Kinase inhibition assay comparing inhibition of *Pf*CLK3_H259P and G449P in the presence of 1 μ g protein, 2 μ M MBP substrate and plus or minus 2 μ M inhibitor in the presence of 0.1 Mbq of γ 32 P-ATP. A single representative experiment is shown, comparable data was obtained on 5 further occasions.

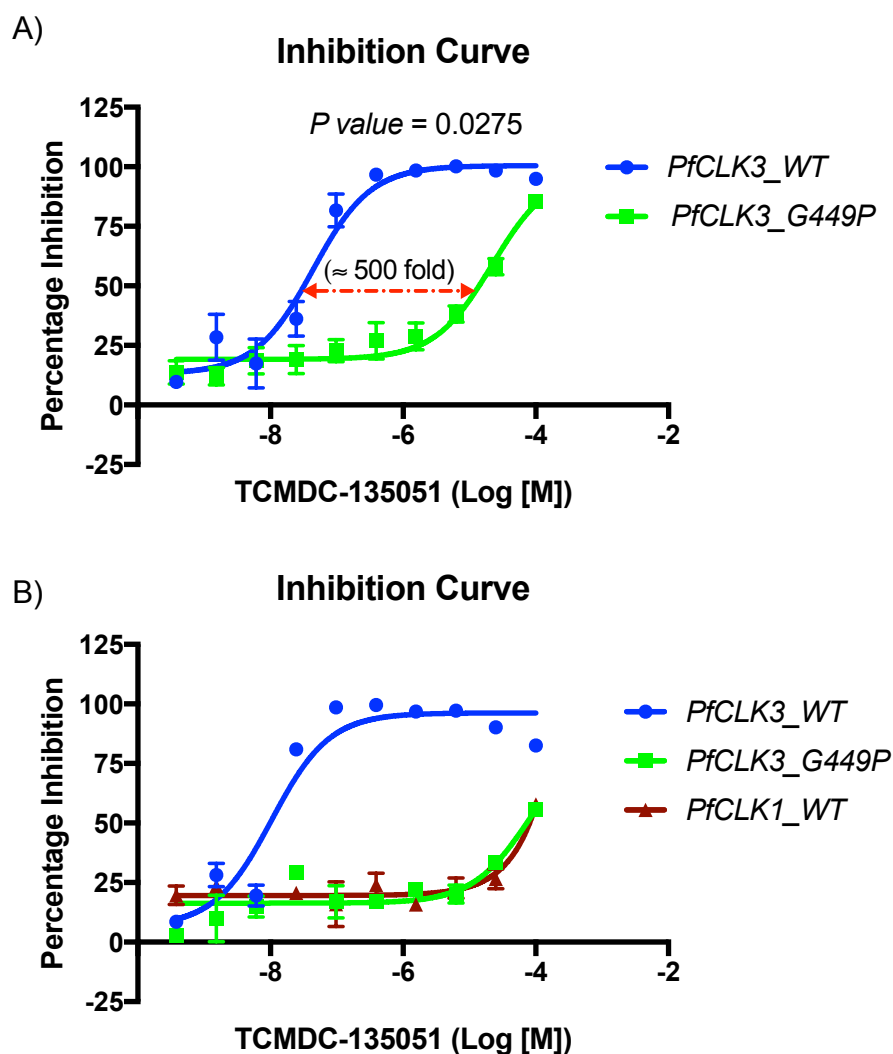


Figure 5.6: Comparison of the inhibition curves of TCMDC-135051 against *PfCLK3_WT* and *PfCLK3_G449P*. A) Inhibition curves of *PfCLK3_WT* and *PfCLK3_G449P* protein kinases. B) Inhibition curves of *PfCLK3_G449P* compared to *PfCLK1_WT*, using *PfCLK3_WT* as control in response to TCMDC-135051. Data presented is the average of three independent experiments run in triplicates. Graphs are drawn with Graph Pad Prism and presented as S.E.M.

5.2.1.4 Growth inhibition curves of TCMDC-135051 against wild type 3D7 parasites and *PfCLK3_G449P* mutant parasites

Single cross over homologous recombination was used to insert the *PfCLK3_G449P* construct sequence in the parasite genome replacing the wild type *PfCLK3*. After clonal selection, two independent clones (G449P-A3 and G449P-A8) were generated, both expressing the mutant *PfCLK3_G449P* in place of the wild type *PfCLK3* gene. These were used to validate *PfCLK3* as a target for TCMDC-135051. The mutants would also help identify any on- and off-target effects of the inhibitor in addition to confirming target selectivity.

Using highly synchronised *P. falciparum* ring stage parasites expressing the *PfCLK3_G449P* variants (A3 and A8), growth inhibitory assays were setup to investigate the potency of TCMDC-135051 and compared to wild type 3D7 parasites as controls. The assay was setup with a starting parasitaemia of 0.5% and 2% haematocrit grown for ~50 hours before the experiment was terminated and read. The results showed that the wild type parasites, as previously determined are sensitive to TCMDC-135051, with an EC_{50} of 443 nM ($pIC_{50}=6.35\pm 0.038$) (Figure 5.7). In contrast, the mutants showed reduced potency by TCMDC-135051 to inhibit mutant parasite growth; *PfCLK3-G449P* (variant A3) showed an EC_{50} value of 13.9 μ M ($pIC_{50}=4.86\pm 0.0128$) and variant A8 had an EC_{50} of 11.59 μ M ($pEC_{50}=4.94\pm 0.013$) significantly shifting the death curve to the right ($p<0.05$) as shown in Figure 5.7. The presented data revealed that compared to wild type parasites, G449P confers resistance to TCMDC-135051 inhibition with a notable ~1.5 log fold shift in both clones, further proving that parasites are killed by TCMDC-135051 via inhibition of *PfCLK3*.

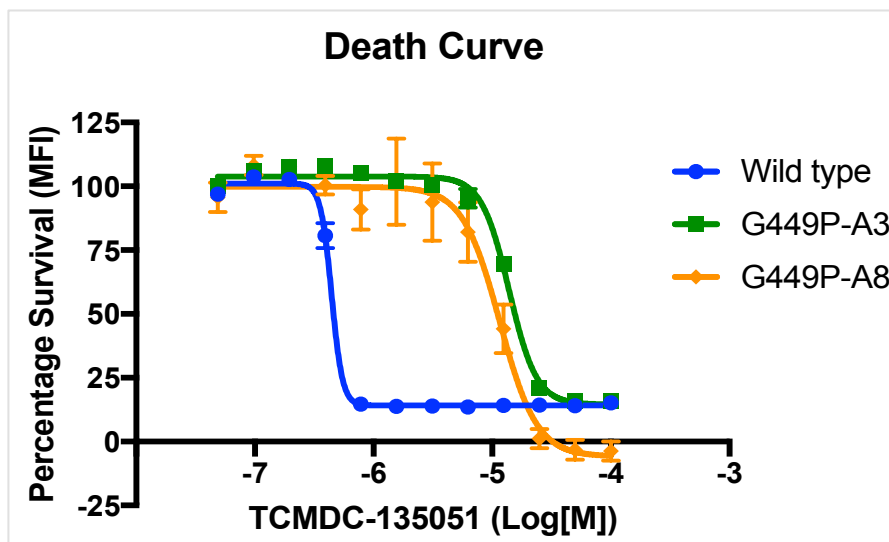


Figure 5.7: Parasite death curve: Wild type 3D7 and *PfCLK3_G449P* parasite death curves. The death curves were setup starting with ring stage parasites at parasitaemia of 0.5% in the presence of previously prepared drug plate. Data presented is the mean of three independent experiments run in triplicates plotted as S.E.M using Graph Pad Prism.

5.2.2 Continuous parasite exposure to TCMDC-135051 results in *PfCLK3* gene mutations causing resistance

To further confirm that TCMDC-135051 was killing parasites by acting on *PfCLK3* as its target and to determine the selectivity of the inhibitor, parasites were challenged with TCMDC-135051, exposing the inhibitor to the biological environment in *in vitro* cultures. This gave the opportunity to detect any off-target effects of TCMDC-135051 on parasites and also show selectivity by revealing any phenotypic change in *P. falciparum* Dd2 parasites continuously exposed to TCMDC-135051. This was done in collaboration with Elizabeth Winzler's lab at the University of California, San Diego. The drug challenge was done over a 2 months period starting with low drug concentration (80 nM) in the culture media at time point zero and increasing this towards 200 nM over this period. Following drug exposure, genomic DNA was prepared from these parasites and sequenced to determine the molecular basis of the resistance. Compared to wild type, two non-synonymous mutations were detected on the *PfCLK3* gene (P196R and H259) and one mutation on USP39 gene (Figure 5.8A and B, schematic representation of the treatment and the position of the mutations). The mutations on the *PfCLK3* gene confirms the inhibitor is acting on this kinase believed to be involve in pre-mRNA splicing. The third mutation on USP39, a member of the U4.U6/U5 tri-snRNP is also involved in splicing.

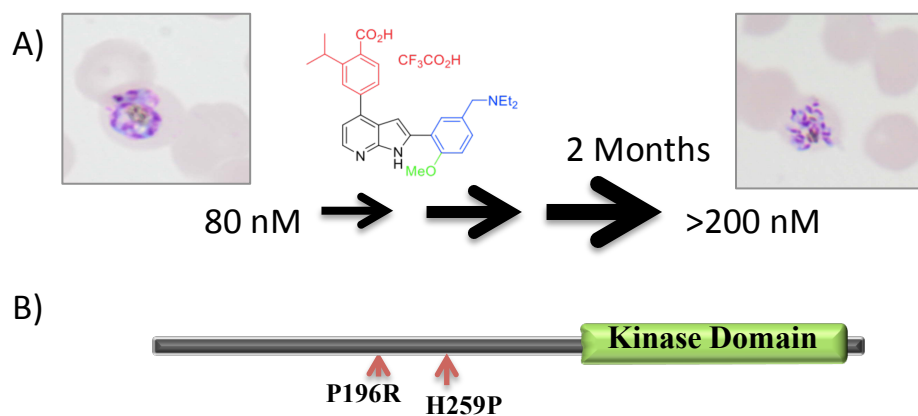


Figure 5.8: Effect of long-term parasite (Dd2) exposure to TCMDC-135051 (schematic representation). A) Dd2 Parasites exposed to increasing concentrations of TCMDC-135051 kinase inhibitor and monitored for two months. B) Schematic representation of the positions of the point mutations on the PfCLK3 protein outside the kinase domain.

5.2.2.1 *Pf*CLK3_H259P mutation increases kinase activity significantly

Recombinant *Pf*CLK3 proteins with P196R and H259P mutations were generated by site directed mutagenesis to investigate the effect of these variants on kinase function and response to TCMDC-135051. The kinase activities of these mutants were profiled, first using the γ -32P-ATP kinase assay for visualisation and a quantitative TR-FRET assay (Figure 5.9A and B respectively). Both assays showed that *Pf*CLK3_P196R did not change the kinase activity much compared to wild type. Notably, a ~3.5 fold increase in kinase activity was detected with *Pf*CLK3_H259P, a significant increase in activity with $p < 0.0001$ compared to wild type (one-way ANOVA analysis).

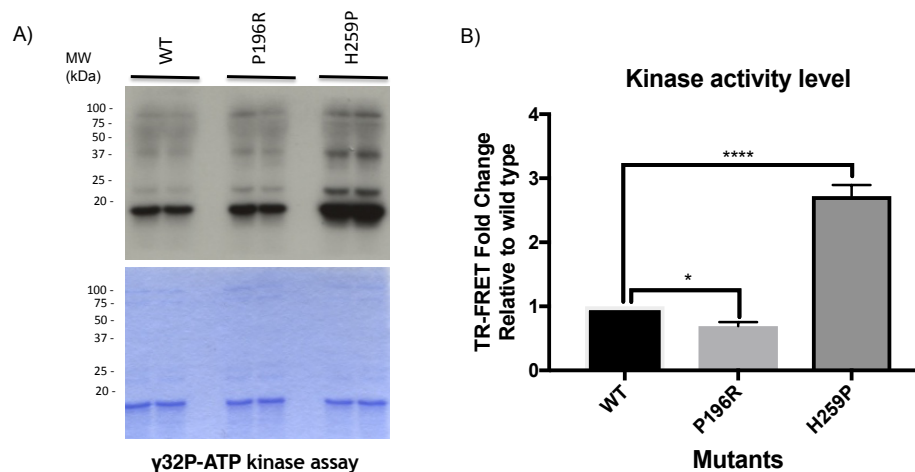


Figure 5.9: Kinase assays to determine the level of activity of the mutants (P196R and H259P) compared to wild type PfCLK3. A) γ 32P-ATP kinase activity assay of the mutants *PfCLK3*_P196R and *PfCLK3*_H259P compared to wild type *PfCLK3* kinase using equal amount of kinase (0.5 μ g) as starting material and 2 μ M MBP substrate. This data is a single representation of three independent experiments. B) TR-FRET Kinase assay using 50 nM kinase in the presence of 50 nM MBP peptide substrate and non-limiting amounts of cold ATP.

5.2.2.2 *PfCLK3_H259P* mutation does not change affinity for ATP or inhibition by TCMDC-135051 using ATP at the K_m for ATP concentration

The effects of the mutants were investigated by evaluating the K_m for ATP for *PfCLK3_H259P* and *PfCLK3_P196R*. Compared to wild type *PfCLK3*, both mutants showed similar K_m for ATP: the K_m for ATP for *PfCLK3_WT*, *PfCLK3_P196R*, and *PfCLK3_H259P* are 6.17 (± 0.61), 5.88 (± 0.67), and 10.32 (± 0.88) respectively (Figure 5.10). The recorded increase in kinase activity showed no effect in the affinity for ATP. The obtained K_m for ATP values were rounded to 10 μM and this was used as the optimum ATP concentration in the inhibition assays of these mutants to determine the potency of TCMDC-135051. The obtained IC_{50} values are in low nanomolar concentrations of 31.42 nM ($\text{pIC}_{50}=7.5\pm 0.094$), 54.16 nM ($\text{pIC}_{50}=7.27\pm 0.117$) and 46.07 nM ($\text{pIC}_{50}=7.34\pm 0.068$) for *PfCLK3_WT*, *PfCLK3_P196R*, and *PfCLK3_H259P* respectively with no difference in pIC_{50} values (Figure 5.10B). These data showed that setting the ATP concentrations at K_m for ATP has no effect on the potency of TCMDC-135051 to inhibit these mutants.

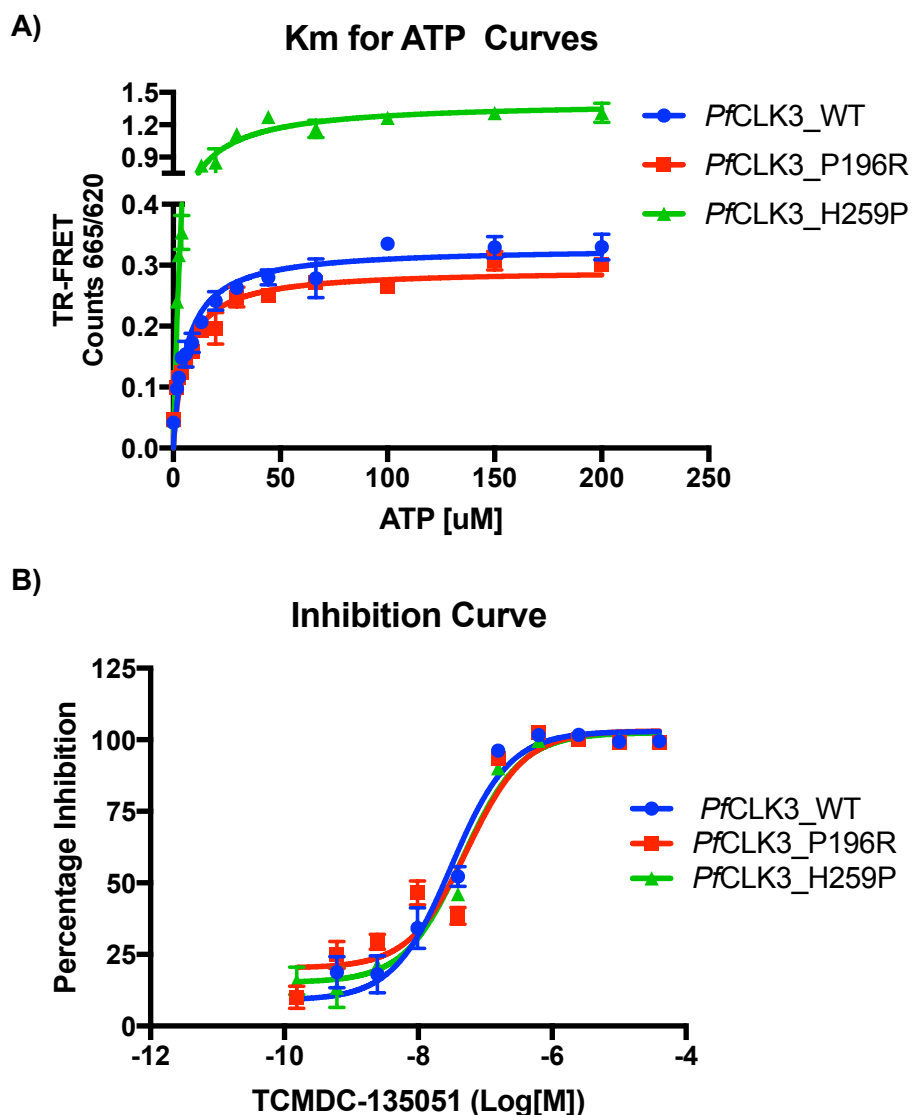
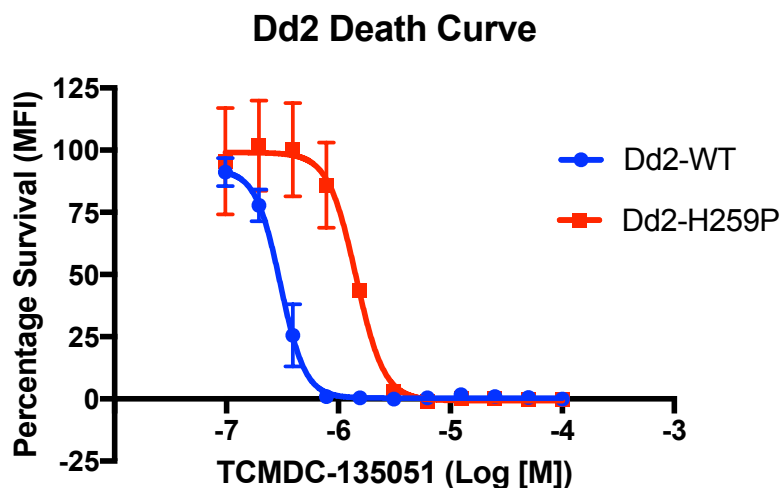


Figure 5.10: TR-FRET kinase assay for Km for ATP determination and inhibition with TCMDC-135051 for *PfCLK3_WT*, *PfCLK3_P196R*, and *PfCLK3_H259P* kinases. A) Km for ATP curves determined using 50 nM of each kinase and 50 nM of MBP substrate with a serially diluted ATP starting from 200 μM ATP. B) Inhibition curves determined using the generated Km for ATP (10 μM), 50 nM MBP substrate and serial dilution of inhibitor (TCMDC-135051) with a starting concentration 100 μM . Data presented is average of three independent experiments in triplicates analysed using Graph Pad prism with S.E.M.

5.2.2.3 The effects of *PfCLK3_H259P* on *P falciparum* parasites response to TCMDC-135051

To confirm that the observed drug resistance was a direct result due to the detected mutations (H259P), the wild type gene was replaced with the mutant variant (H259P) generating transgenic parasites. Following full integration and stable expression of the mutant the transgenic parasites were evaluated for inhibition by TCMDC-135051 and compared to the parent Dd2 as control.

Highly synchronised parasites at ring stage from the mutant Dd2 (expressing the H259P) were tested for inhibition by TCMDC-135051 using the parasite growth inhibition and wild type Dd2 *P. falciparum* parasites as control. The data showed that wild type Dd2 had an EC_{50} of 303.0 nM ($pEC_{50}=6.52\pm0.026$) and H259P has an EC_{50} of 1437 nM ($pEC_{50}=5.8\pm0.049$). This is a shift in the EC_{50} by about five folds with at least ~1 log fold shift in pEC_{50} as shown in Figure 5.11. This is a further confirmation that the expression of *PfCLK3_H259P* in parasites reduces their sensitivity to TCMDC135051 inhibition, and that TCMDC-135051 kills parasites via inhibition of *PfCLK3* activity.



	EC50[nM]	pEC50
Dd2-WT	303.0	6.519
Dd2-H259P	1437.0	5.843

Figure 5.11: Dd2 *PfCLK3*_WT and mutant (Dd2 *PfCLK3*_H259P) sensitivity to TCMDC-1345051 measured using the growth inhibition drug assay. The Dd2_H259P mutant parasite was tested for inhibition by TCMDC-135051 using wild type parasites as control. The experiment was setup with 0.5% parasitaemia ring stage parasites at 4% haematocrit. Data presented is the average of three independent experiments run in triplicates. Graph Pad was used to analyse the data and generate the curve with S.E.M.

5.2.2.4 H259P mutation influences *Pf*CLK3 response to TCMDC-135051 at high ATP concentration

The mutant *Pf*CLK3_H259P increases kinase activity by ~3 folds whereas P196R has no effect on kinase activity (Figure 5.9 and B). Here I investigate the effect of high ATP concentration (50X K_m for ATP) on the potency of TCMDC-135051 to inhibit H259P; if the mutation causes any changed dependent on protein-ATP relationship, this would be revealed.

Testing the mutant P196R, no significant change in the potency of TCMDC-135051 was detected. The IC_{50} of this mutant at the K_m for ATP was 54.16 nM ($pIC_{50}=7.27\pm0.12$) whereas at 50X the K_m for ATP, the IC_{50} was 109.7 nM ($pIC_{50}=6.96\pm0.058$), indicating no significant shift in the IC_{50} value (Figure 5.2A). In contrast, the results for H259P showed that with ATP concentration at the K_m for ATP, the IC_{50} was 49.52 nM ($pIC_{50}=7.31\pm0.06$) whereas at 50X K_m for ATP the IC_{50} value was 378.6 nM ($pIC_{50}=6.42\pm0.07$), representing ~1 log fold shift as shown Figure 5.12B. The shift in inhibition curve showed reduced potency of TCMDC-135051 at high ATP concentration and suggests ATP-competitive mode of inhibition. Interestingly, this mutation is outside the kinase catalytic domain suggesting that TCMDC-135051 is either acting outside the kinase domain or it has two binding sites (bitopic) – the inhibitor interacting with the kinase catalytic domain and at a site outside the catalytic domain otherwise at an allosteric site.

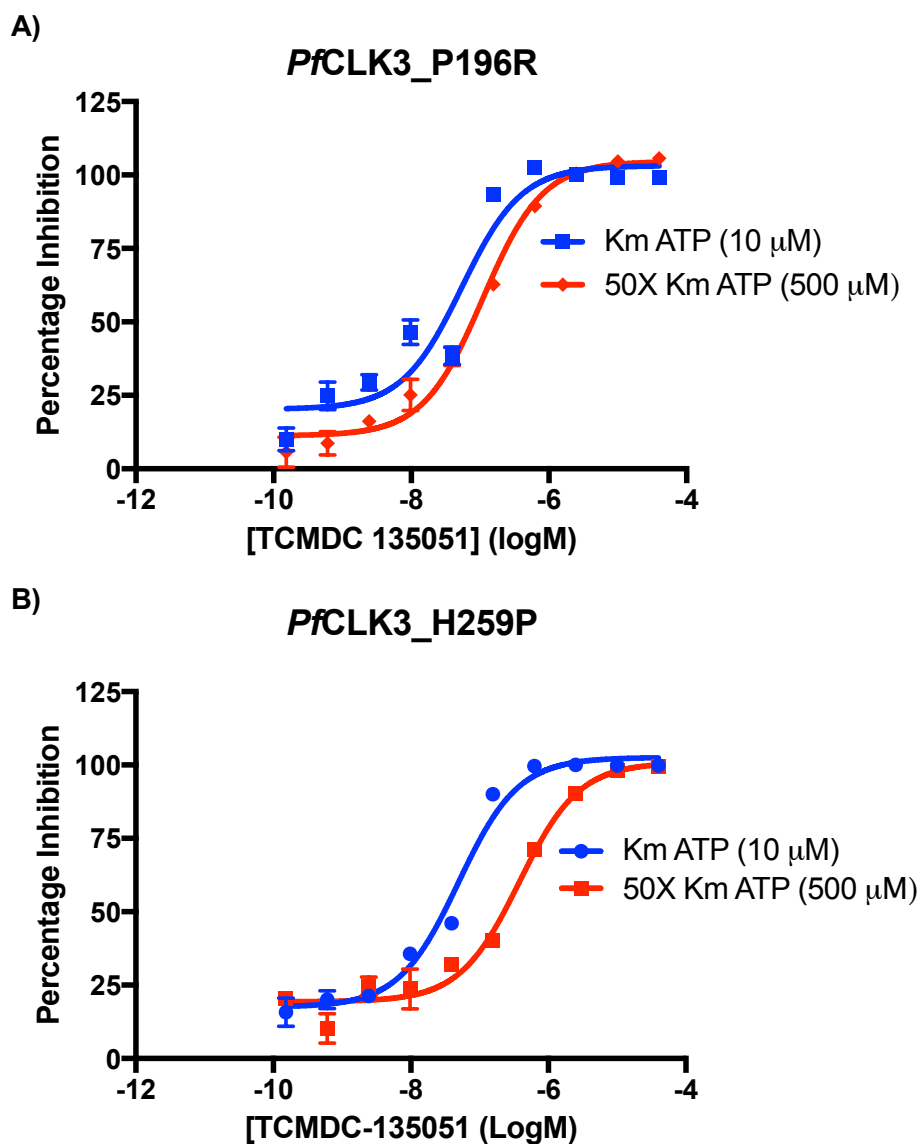


Figure 5.12: Effect of increased ATP concentration on the potency of TCMDC-135051 to inhibit P196R and *Pf*CLK3_H259P. A) Increased ATP concentration did not shift the inhibition curve of P196R significantly. B) Increased ATP concentration reduces the potency of TCMDC-135051 shifting the inhibition curve with ~8 fold increased IC_{50} . Data presented is the average of three independent experiments in triplicates (\pm S.E.M).

5.2.2.5 The effect of *Pf*CLK3_H259P mutation on the mode of action of TCMDC-135051 on *Pf*CLK3 kinase

Section 5.2.2.4 showed that high ATP concentration reduces TCMDC-135051 potency to inhibit *Pf*CLK3_H259P. Here a detailed investigation to determine the mode of inhibition of TCMDC-135051 towards *Pf*CLK3_H259P is investigated using varying concentrations of inhibitor and ATP.

In the presence of increasing concentrations of inhibitors, the obtained K_m for ATP values and curves as shown in Figure 5.13A changed proportionally. The data from inhibition assays fitted as a function of inhibitor and the IC_{50} values determined are shown in Table 5-1. This showed that inhibition of *Pf*CLK3_H259P by TCMDC-135051 is hugely influenced by ATP concentration; at low ATP concentration (1 μ M), the IC_{50} was 29.74 (\pm 0.21) nM and at ATP concentrations of 50, 100, and 200 μ M, the IC_{50} values changed to 81.91 (\pm 0.17), 145.7 (\pm 0.19)- and 290.3 (\pm 0.26) nM respectively (Figure 5.13B and Table 5-1). These inhibition data show that H259P changed the inhibition profile of TCDMC-135051 from mainly non-ATP competitive mode of inhibition in the wild type to ATP-competitive mode of inhibition.

Additionally, in the presence of increased concentrations of inhibitor, the K_m for ATP values also changed significantly. Low inhibitor concentrations such as 3, 6, and 15 nM, gave K_m for ATP values of 11.68 (\pm 2.11), 10.36 (\pm 1.53), and 17.5 (\pm 2.04) respectively. Higher inhibitor concentrations such as 150, 300, and 600 nM gave K_m for ATP values of 141.3 (\pm 31.58), 137.4 (\pm 48.95), and 77.47 (\pm 30.42) respectively, clearly suggesting competition for binding between ATP and the inhibitor.

The demonstrated changes in the K_m for ATP and the obtained IC_{50} values (Figure 5.13 and Table 5-1) indicate that *Pf*CLK3-H259P inhibition by TCMDC-135051 is suggestive of ATP-

competitive mode of inhibition. This change in mode of action of TCMDC-135051 with the variant H259P indicates that the substitution of histidine at 259 to proline might be directly responsible and that TCMDC-135051 has an allosteric effect.

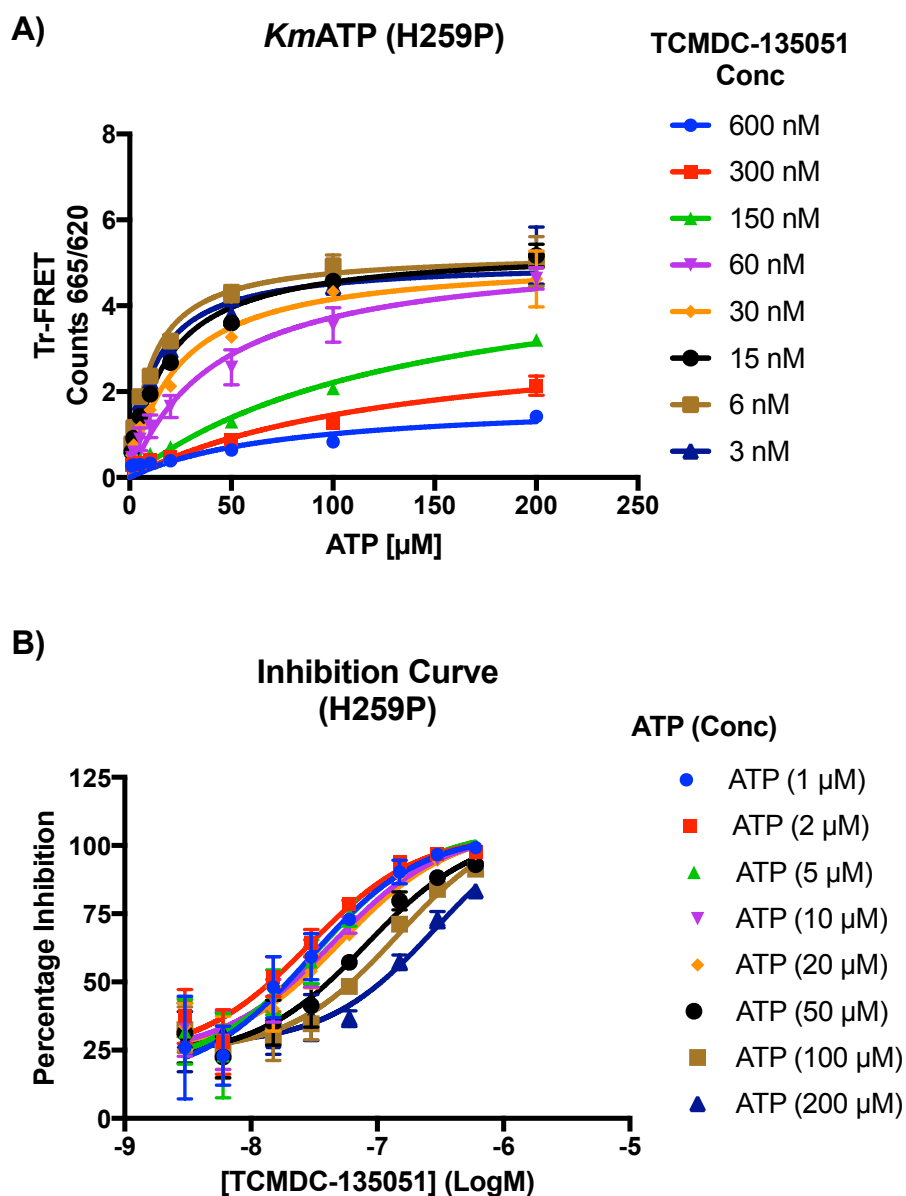


Figure 5.13: Biochemical analysis of *Pf*CLK3_H259P kinase inhibition by TCMDC-135051 using TR-FRET assay described in methods. A) The K_m for ATP curves represent data fitted to Michaelis-Menten equation using the nonlinear regression analysis for data obtained using constant amount of substrate and protein (*Pf*CLK3_H259P) and various amounts of ATP and inhibitors (TCMDC-135051). B) *Pf*CLK3_H259P kinase inhibition assays were performed using TR-FRET assay described in methods section with various concentrations of ATP and inhibitor (TCMDC135051). The curves were generated by analysing the values of individual samples and plotted as function of inhibitor concentration and the acquired IC_{50} values are shown in square brackets. Data presented here is the average of three independent experiments done in triplicates \pm S.E.M.

Table 5-1: The IC₅₀ values obtained from inhibition of *Pf*CLK3_H259P with TCMDC-135051 in the presence of various concentrations of ATP at constant protein and substrate concentration (left panel). The Km for ATP values obtained in the presence of varying concentrations TCMDC-135051 at constant protein and substrate concentration with *Pf*CLK3_H259P (right panel). Data is the average of three independent experiments in triplicates ±S.E.M.

ATP [μM]	TCMDC-135051 IC50 [nM] (±s.e.m)	TCMDC-135051 [nM]	Km ATP (±S.E.M.)
1	29.74 (0.21)	3	11.68 (2.11)
2	28.71 (0.17)	6	10.36 (1.53)
5	34.53 (0.19)	15	17.5 (2.04)
10	44.89 (0.17)	30	23.04 (4.16)
20	52.43 (0.15)	60	43.44 (10.84)
50	81.91 (0.17)	150	141.3 (31.58)
100	145.7 (0.19)	300	137.4 (48.95)
200	290.3 (0.26)	600	77.47 (30.42)

5.2.3 ATP-competitive mechanism of inhibition of *PfCLK3_KD* recombinant kinase by TCMDC-135051

The shift in the potency of TCMDC-135051 on the mutant *PfCLK3_H259P* and the changed mechanism of action, from non-ATP competitive behaviour in wild type *PfCLK3* to ATP-competitive behaviour in *PfCLK3_H259P* mutant suggests that TCMDC-135051 potentially has two binding sites on the kinase in what could be described as bi-topic - binding at two sites: one around the catalytic domain and the other outside the catalytic domain (Figure 5.14). To confirm that the mechanism of inhibition seen is associated with the binding of TCMDC-135051 to an allosteric site on the N-terminal domain of *PfCLK3*, and also at a site within the kinase domain, the kinase was truncated at position 353 from the N-terminal end to produce what is referred the *353-kinase domain c-terminal* (353-KDct). With this construct, the mode of action of TCMDC-135051 is expected to have ATP competitive behaviour because the allosteric binding site is lost. The 353-KDct was tested for inhibition by TCMDC-135051 at low and high ATP concentrations to investigate if this would reveal any effect on inhibitor potency and mode of inhibition.

The K_m for ATP of the kinase domain (353-KDct) was investigated and compared to wild type control. The K_m for ATP for 353-KDct was 61.06 (± 8.74) μM , an increased of ~ 10 folds compared to full-length *PfCLK3* K_m for ATP is 6.65 (± 0.77) as shown in (Figure 5.15A). Interestingly there was an increase in activity with a V_{max} of 0.77 for *PfCLK3_353-KDct* compared to 0.55 for *PfCLK3_FL*.

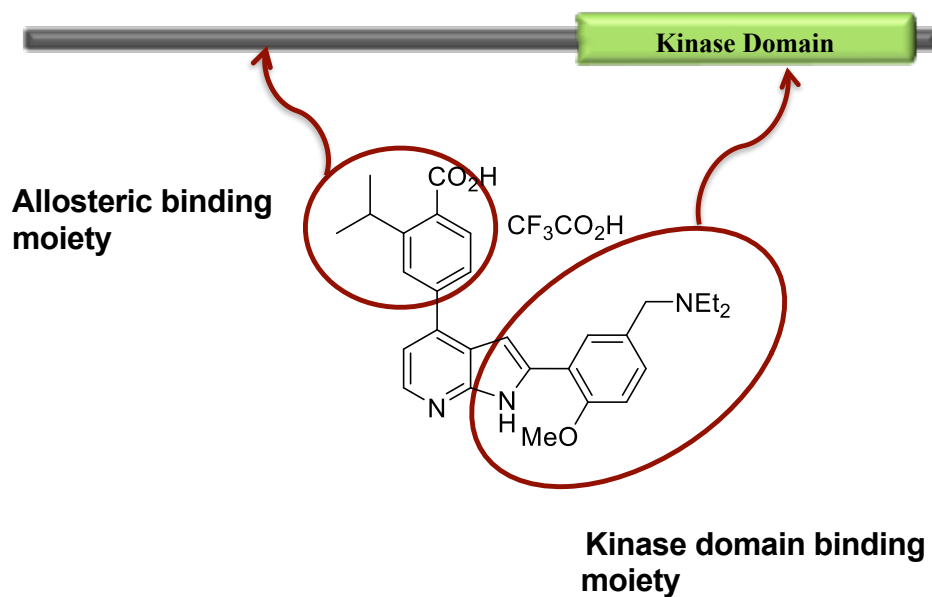


Figure 5.14: Putative binding moieties of the inhibitor TCMDC-135051 to the full length *PfCLK3* kinase. Two putative parts of the compound thought to be binding at different parts of the kinase are identified as allosteric binding moiety and kinase domain binding moiety.

The inhibitory effect of TCMDC-135051 against 353-KDct was evaluated at two ATP concentrations - the K_m for ATP and 50X K_m for ATP using the full-length *PfCLK3* as control. The potency of TCMDC-135051 as reported earlier, did not change with the full length (*PfCLK3_FL*) kinase comparing ATP concentration at the K_m for ATP and 50X K_m for ATP with IC_{50} values of 49.99 (± 0.11) nM and 57.2 (± 0.08) nM respectively as shown in Figure 5.15B. In contrast, using K_m for ATP, and 50X K_m for ATP concentrations, the determined IC_{50} for 353-KDct were 76.17 nM ($pIC_{50}=7.12\pm 0.11$) and 924.2 nM ($pIC_{50}=6.03\pm 0.11$) respectively with curves depicted in Figure 5.15B. This shows a shift in the IC_{50} by at least ~12 fold and a 1-log fold change in pIC_{50} comparing K_m for ATP ($pIC_{50}=7.12$) and 50X K_m for ATP ($pIC_{50}=6.03$). This demonstrates the importance of the N-terminal part of the kinase in the binding of TCMDC-135051 and the inhibition of *PfCLK3* activity. The shift of the inhibition curve in the presence of high ATP concentration suggests that APT concentration influences TCMDC-135051 binding to the kinase domain.

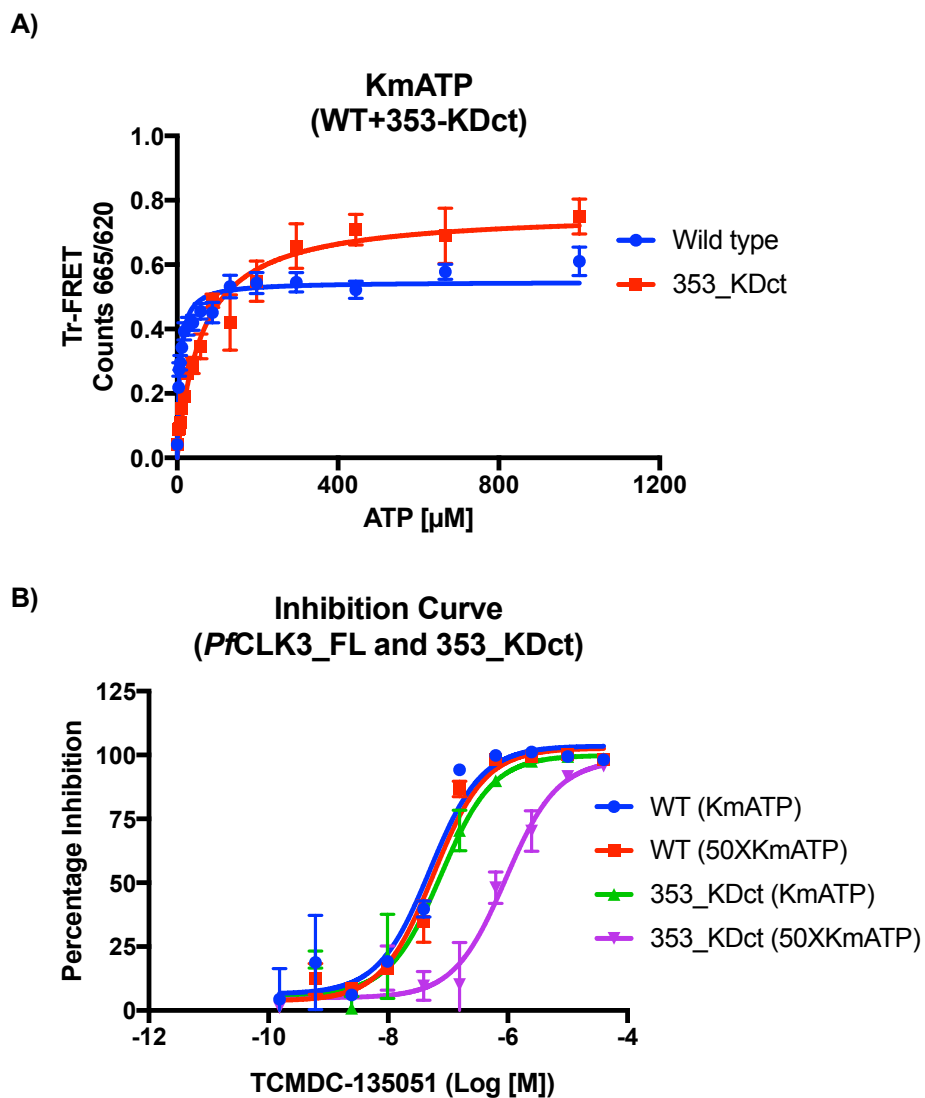


Figure 5.15: TR-FRET Kinase assays for the kinase domain (353-KDct) compared to the wild type *Pf*CLK3 kinase. A) The K_m for ATP for *Pf*CLK3_353-KDct compared to *Pf*CLK3_WT. B) The inhibition curve of *Pf*CLK3_FL and *Pf*CLK3_353-KDct at low ATP concentration (K_m for ATP, 10 and 60 μ M respectively) and high ATP concentration (50X K_m for ATP). Data represent the average of three independent experiments \pm S.E.M.

5.3 Discussion

In this chapter, forward and reverse chemical genetic approach screening was used to generate two mutations, G449P and H259P of *PfCLK3*. These mutants were used to confirm that TCMDC-135051 is selective towards *PfCLK3* and parasites were killed by inhibition of *PfCLK3* rather than through off-target effects; which are a major challenge in identifying target specific protein kinase inhibitors (Alam *et al.*, 2015). Detailed analysis of G449P and H259P recombinant proteins was carried out compared to wild type *PfCLK3*. The mutants were transfected into parasites generating *PfCLK3_G449P* and *PfCLK3_H259P* parasite variants replacing wild *PfCLK3*. These mutants, compared to wild type parasites were evaluated and the selectivity of the TCMDC-135051 determined.

Recombinant *PfCLK3_G449P* protein was tested for inhibition using both the gel-based radioactive assay and the TR-FRET assay and data from both assays showed that *PfCLK3_G449P* is insensitive to TCMDC-135051. In addition, the variant parasites with the *PfCLK3_G449P* mutation demonstrate resistance to the effects of TCMDC-135051 compared to wild type parasite. This confirmed that TCMDC-135051 is killing *Plasmodium* parasites by inhibiting *PfCLK3*, as any off-target effects would have result in inevitable parasite death (Hallyburton *et al.*, 2017b). A mutation similar to *PfCLK3_G449P* at the gatekeeper of PKG in *P. berghei* (PKG^{T619Q}) was shown to significantly reduce the inhibition of ookinetes and confirmed the selectivity of the inhibitor used in that study (Brochet *et al.*, 2014b). Therefore, taken together, this inhibitor demonstrates selectively towards *PfCLK3* similar to target specific mutations used earlier to confirm target selectivity by determining off-target effects of inhibitors in other kinases (Alam *et al.*, 2015, Zaganas and Plaitakis, 2002).

Contrastingly, exposing *P. falciparum* parasites to TCMDC-135051, the impact of TCMDC-135051 on parasites through phenotypic screening in a biological context gave the opportunity of discovering off-target effects (Schenone *et al.*, 2013). Continued drug exposure resulted in two *PfCLK3* mutations (P196R and H259P) outside the kinase domain, confirming TCMDC-135051 selectivity towards *PfCLK3*. Others have reported this approach of target validation as a useful strategy in target based drug discovery approaches (McNamara *et al.*, 2013, Wu *et al.*, 2015). Noteworthy, emergence of compound-resistant laboratory parasites does not indicate a bad target and should not hinder drug development since monotherapy is not an acceptable option in the current drug development strategies (Istvan *et al.*, 2011). Further characterizing the *PfCLK3* mutations showed that *PfCLK3_H259P* increases kinase activity by at least 3 folds; this increased activity influenced the observed shift in the death curve to the right and the increased EC_{50} (Cacace *et al.*, 2017) further confirming target selectivity. Interestingly, *PfCLK3_H259P* changed the mode of action of the inhibitor from non-ATP competitive to ATP-competitive mode of inhibition. This is also directly associated with TCMDC-135051 selectivity towards *PfCLK3* since ATP-competitive inhibition affects inhibitor potency and selectivity because of the conserved ATP binding site and high concentration of cellular ATP (Wilson *et al.*, 2016). From this evidence, it can be logically assumed that TCMDC-135051 is an allosteric modulator because P196R and H259P mutations are outside the kinase domain of the *PfCLK3*. Allosteric modulators are highly selective inhibitors as demonstrated by one the analogues of benzothiazinones (BTOs), towards GSK 3 β , 20g, with no potency against over thirty other kinases tested to confirm its selective action towards GSK 3 β (Gao *et al.*, 2017).

In conclusion, abundant evidence is presented in this chapter demonstrating the selectivity of TCMDC-135051 towards *PfCLK3*. The mutant, *PfCLK3_G449P*, showed stronger resistance compared to *PfCLK3_H259P* and is within the kinase domain where substrates are bound. This suggests that TCMDC-135051 might be a substrate competitive inhibitor in addition to the demonstrated allosterism. However, both mutants have sufficient insensitivity to allow further characterisation of the inhibitor and target. Hence, cellular functions of *PfCLK3* can be investigated further using either of these mutants and the tool compound TCMDC-1435051 as template for drug discovery.

Chapter 6 Inhibition of other *Plasmodium* species by TCMDC-135051

6.1 Introduction

The sequences of CLK3 kinases are conserved across *Plasmodium* species; hence no difference in response to inhibitors is anticipated between the different species, similar to predictions for other apicomplexan genes such as the CPDKs (Keyloun *et al.*, 2014). Important conserved regions include the glycine rich loop (GxGxxG) in domain I, which in *Plasmodium* CLKs is GKGVFS, the presence of only two glycine residues have been reported earlier for some kinases (Kobe and Kemp, 2010). Other conserved domains are DLKPDN, the highly conserved aspartate-phenylalanine-glycine (DFG) as DLG in *Plasmodium* and APE regions in domains VII and VIII respectively as shown in Figure 6.1. The similarity in these important kinase domains is suggestive that TCMDC-135051 would have similar potency across most *Plasmodium* species, because they are important for ATP, substrate binding, and phosphorylation (Roskoski, 2015).

The evidence that *P. vivax*, *P. ovale*, together with other *Plasmodium* species such as *P. knowlesi* are causing significant morbidity and mortality mainly outside SSA (Anstey *et al.*, 2009, Dinko *et al.*, 2013, Nyunt *et al.*, 2017, van Schalkwyk *et al.*, 2017, White and Imwong, 2012), and the emergence of drug resistant *P. vivax* parasites to drugs which were initially designed against *P. falciparum* (Lu *et al.*, 2011, Nyunt *et al.*, 2017, Tjitra *et al.*, 2008) makes it important to consider these species in new antimalarial drug design, and also to ensure the tool compound meets the criteria set for new anti-*Plasmodium* therapeutic agents (Burrows *et al.*, 2017, The mal, 2011).

6.2 Results

6.2.1 Expression of full length *P. vivax* CLK3 (*PvCLK3*) and *PbCLK3*, and kinase domain of *PvCLK1* and *PbCLK1*

Full-length *PvCLK3* and *PbCLK3* kinases and the kinase domains of *PvCLK1* and *PbCLK1* were His-tagged and expressed in inducible bacterial expression systems and purified using Ni-NTA affinity chromatography. These kinases were used in γ -³²P-ATP *in vitro* kinase assay to determine their activity using casein and MBP as substrates. Here, the data show that like the already described *PfCLK* kinases, both the *P. vivax* CLK1 and 3 and *PbCLK1* and 3 kinases purified as recombinant bacterially expressed kinases were enzymatically active. As shown in Figure 6.2A-C, *PvCLK3*, and *PbCLK3* like the previously described *PfCLK3*, shows better phosphorylation of MBP than casein. Similarly, *PvCLK1* and *PbCLK1* also showed better MBP phosphorylation like *PfCLK1* kinase (Figure 6.3A-C). Hence, for the kinase inhibition experiment to determine the efficacy of the inhibitors TCMDC-138736 and TCMDC-135051 towards *PvCLK3* and *PbCLK3*, MBP was used as substrate in *in vitro* γ -³²P-ATP kinase inhibition assay.

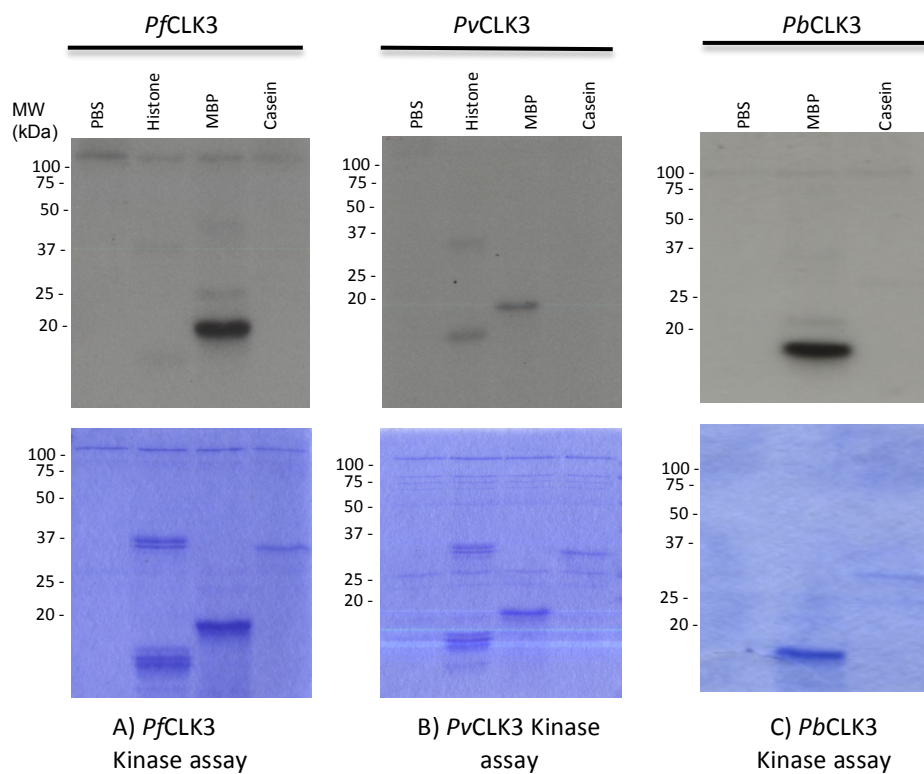


Figure 6.2: *Plasmodium* CLK3 kinases mediated phosphorylation of exogenous substrates using the γ -³²P-ATP kinase assay in the presence of 0.1 MBq of radiolabelled ATP, 0.5 μ g protein and 50 μ M ATP. Coomassie blue staining of radiolabelled gels was used as control (bottom panel) and autoradiography film used to detect phosphorylated radiolabelled substrates. A) *Pf*CLK3 mediated phosphorylation of exogenous substrate and kinase auto-phosphorylation. B) *Pv*CLK3 kinase mediated phosphorylation of exogenous substrates. C) *Pb*CLK3 kinase mediated phosphorylation of exogenous substrates.

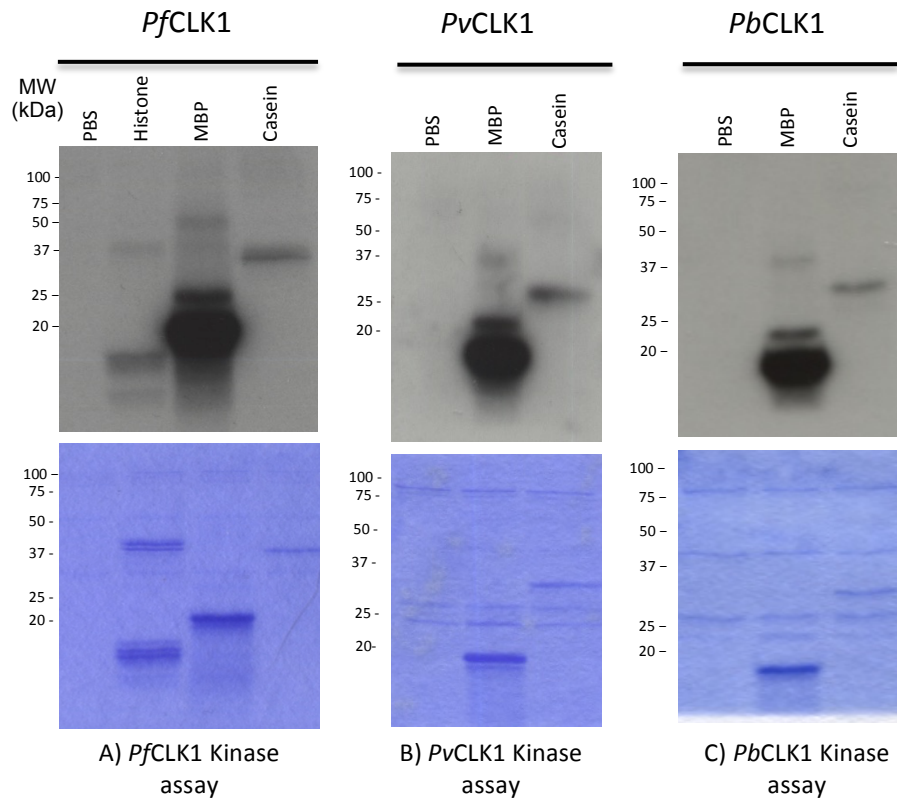


Figure 6.3: Kinase phosphorylation assay of exogenous substrates using the γ -³²P-ATP assay for *Pv*CLK1 and *Pb*CLK1. A) *Pf*CLK1 phosphorylation of substrate Histone, MBP and Casein, used as control for *Pv*CLK1 and *Pb*CLK1 kinase activities. B) *Pv*CLK1 kinase activity for phosphorylation of MBP and Casein. C) *Pb*CLK1 kinase activity for phosphorylation of MBP and casein. Data presented is the representative of three independent experiments.

6.2.2 TCMDC-138736 and TCMDC-135051 inhibits kinase mediated MBP phosphorylation in all *Plasmodium* CLK3 kinases

Recombinant *Pv*CLK3 and *Pb*CLK3 kinases were incubated with the inhibitors in a kinase inhibition reaction for 30 minutes at 37°C in the presence of 2 µM of the inhibitors, TCMDC-138736 and TCMDC-135051, using MBP as substrate to investigate if these inhibitors would be efficacious against these *Plasmodium* CLK3 kinases. A reduction in the phosphorylation intensity detected by autoradiography shows inhibitory effect on kinase mediated MBP phosphorylation.

The results demonstrate that both *Pv*CLK3 and *Pb*CLK3, like *Pf*CLK3, are inhibited by TCMDC-138736 and TCMDC-135051. TCMDC-18736 has a significant inhibitory efficacy on *Pv*CLK3 as shown on the autoradiography film in Figure 6.4A. Quantitatively, kinase activity was significantly reduced by both inhibitors: to about 47% and greater than 91% by TCMDC-138736 and TCMDC-135051 inhibitors respectively with a $p < 0.05$ using one-way ANOVA (Figure 6.4C). Similarly, *Pb*CLK3 was also inhibited significantly - TCMDC-138736 reducing kinase mediated MBP phosphorylation activity to a maximum of 44.85% and TCMDC-135051 reducing kinase activity to less than 10% compared to the untreated control with $p < 0.05$ (Figure 6.4B and D). The inhibition is comparable to those of *Pf*CLK3 described earlier demonstrating the efficacy of these inhibitors against multiple species of *Plasmodium* CLK3. The inhibitory potency of these inhibitors was tested using the TR-FRET assay to determine the IC_{50} for the inhibitors (TCMDC-135051 and TCMDC-138736). Additionally, the corresponding *Pf*CLK3 mutants (P196R and H259P) were generated in *Pv*CLK3 (P210R and H273P) and *Pb*CLK3 (H276P) recombinant protein and tested for inhibition by TR-FRET assay.

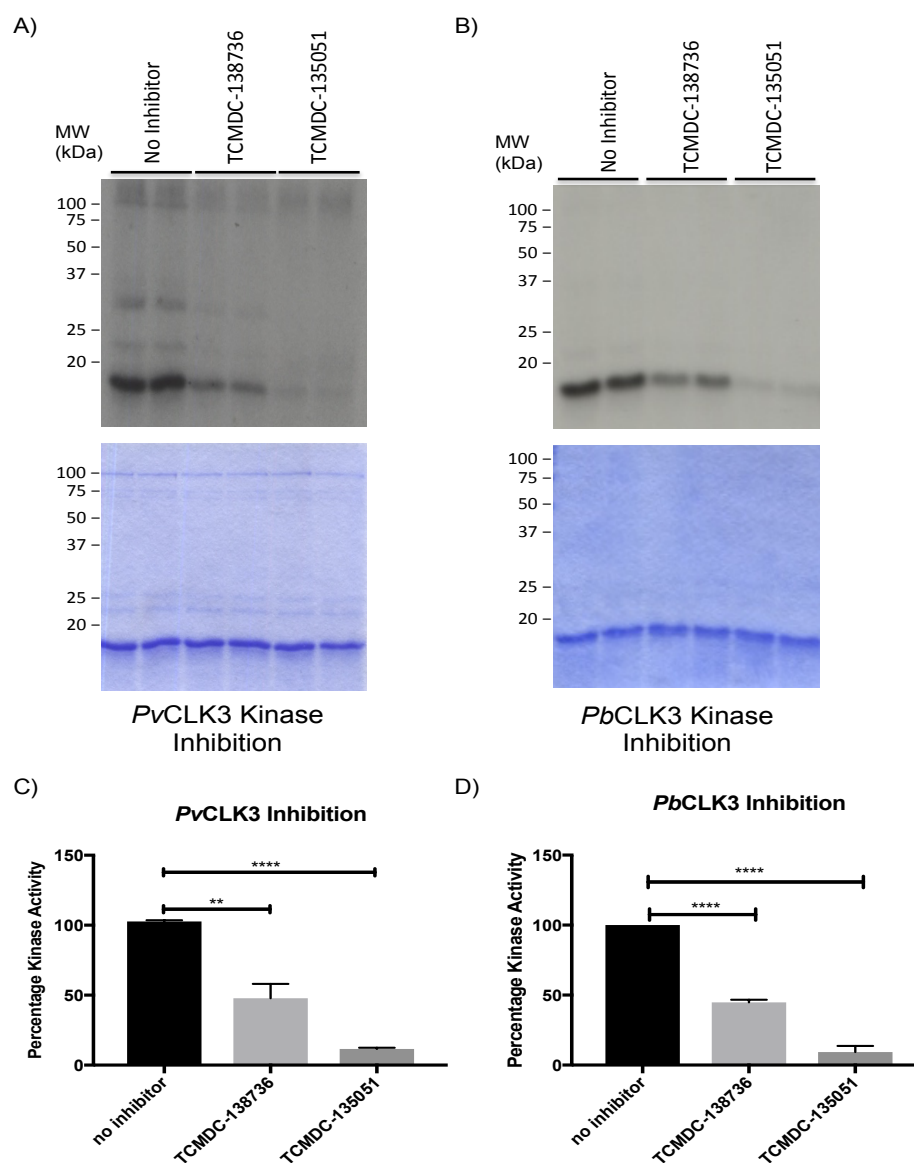


Figure 6.4: Inhibitory effects of TCMDC-138736 and TCMDC-135051 on kinase mediated MBP-phosphorylation by *Pv*CLK3 and *Pb*CLK3 using γ -³²P-ATP kinase assay. A) *Pv*CLK3 inhibition, B) *Pb*CLK3 inhibition, C) Quantification of the inhibition of *Pv*CLK3 kinase activity by TCMDC-138736 and TCMDC-135051 relative uninhibited control, D) Quantification of the inhibition of *Pv*CLK3 kinase activity by TCMDC-138736 and TCMDC-135051 relative uninhibited control. Top panel is the detected radiolabelled MBP phosphorylation and the bottom panel is Coomassie stained gel as loading control. Data is a representation of 3 independent individual experiments run in duplicate.

6.2.3 TCMDC-138736 and TCMDC-135051 have no effect on *Plasmodium* CLK1s kinase mediated substrate phosphorylation

The sequence similarity of *Pv*CLK1 and *Pb*CLK1 to *Pf*CLK1 suggest that these kinases would not be inhibited by TCMDC-138736 or TCMDC-135051. To investigate this hypothesis, γ -³²P-ATP inhibition assay was used to determine the inhibitory effects of these inhibitors on *Pv*CLK1 and *Pb*CLK1 kinases. The inhibition assays revealed that in the presence of either of the inhibitors, kinase mediated MBP phosphorylation was unaffected and equal phosphorylation levels were detected in both the experimental and control samples, confirming that like *Pf*CLK1, none of the *Plasmodium* CLK1 kinases tested were inhibited (Figure 6.5,A-C).

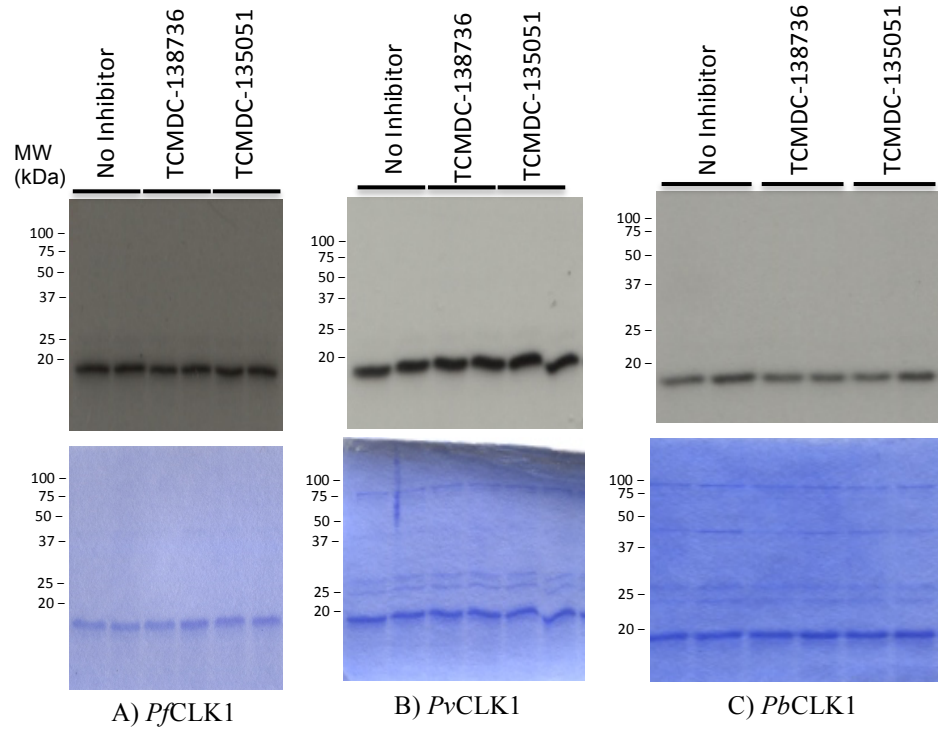


Figure 6.5: Effects of kinase inhibitors (TCMDC-138736 and TCMDC-135051) on MBP phosphorylation by *Pf*CLK1, *Pv*CLK1, and *Pb*CLK1. A) *Pf*CLK1 inhibition by TCMDC-138736 and TCMDC-135051. B) *Pv*CLK1 inhibition by TCMDC-138736 and TCMDC-135051 and C) *Pb*CLK1 inhibition by TCMDC-138736 and TCMDC-135051. Presented figures are a representation of three independent experiments.

6.2.4 Time course for optimum TR-FRET assay conditions for *P. vivax* and *P. berghei* kinases

To set up a kinase inhibition assay using the TR-FRET, the assay conditions were first re-optimised for *Pv*CLKs and *Pb*CLKs to confirm that the conditions (assay run time, substrate and protein concentrations) used for *P. falciparum* were optimum for these kinases. A range of protein concentrations and incubation times were tested and the data is presented as detailed below.

The data showed that *Pv*CLK1, a highly active kinase phosphorylates its substrate CREP-tide even at low nanomolar concentrations. There was linearity of phosphorylation using 5 nM protein at different time points (Figure 6.6A). When the activity was tested for time linearity, two time points, 60 and 75 minutes dominated the other times for linearity (Figure 6.6B). Subsequent *Pv*CLK1 experiments were run using 5 nM protein concentrations and 60 minutes incubation time. Similarly, *Pv*CLK3 was also tested for linearity with time and concentration. Protein concentrations of 50, 75, and 100 nM all show linearity with time, 50 nM showed a lower phosphorylation but with sufficient window (Figure 6.6C). The 60 and 75 minutes tested showed equal phosphorylation levels and linearity (Figure 6.6D). When *Pb*CLK3 was tested for assay linearity at different protein concentration and incubation times, the results showed that like other CLK3 kinases (*Pf*CLK3 and *Pv*CLK3), 50 nM protein incubated for 60 minutes (Figure 6.6E and F) gives an optimum reaction. This data set showed that 5 and 50 nM protein for *Pv*CLK1 and *Pv*CLK3 kinases respectively were optimum for use in a kinase assay when incubated for 60 minutes at 37°C.

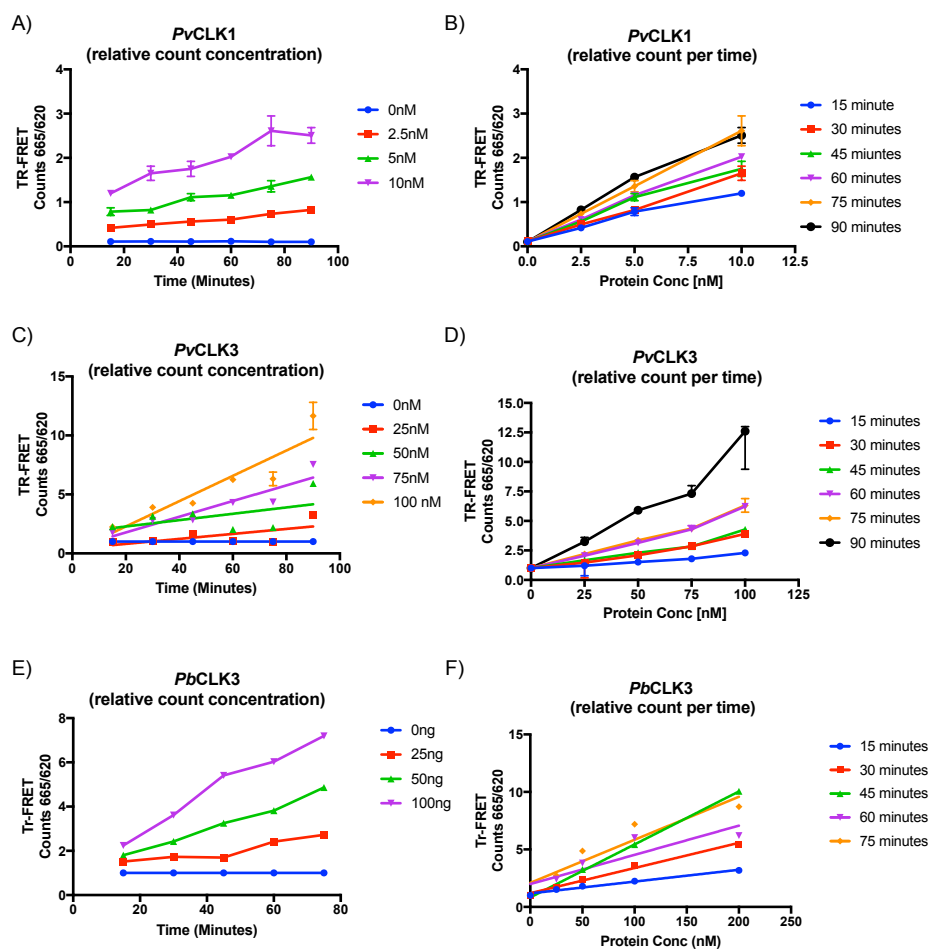


Figure 6.6: Time course experiment to determine the optimum time and protein concentration to use for TR-FRET assays condition for *PvCLK1*, *PvCLK3*, and *PbCLK3*. A) TR-FRET assay with various protein concentrations run at different times; 5 nM protein showed sufficient kinase activity and linearity across the tested time points. B) Kinase phosphorylation activity determined across different protein concentrations against time; 60 and 75 minutes have better linearity for *PvCLK1*. C) TR-FRET assay with various concentrations of protein run at different times showing that 50 nM protein concentration is sufficient linear kinase activity across the time points. D) Kinase phosphorylation activity determine across different protein concentrations, with 60- and 75 minutes demonstrating linearity of activity. E) TR-FRET assay with various concentrations of protein run at different times for *PbCLK3*. Protein concentration of 50 nM shows sufficient kinase activity linear across the time points. Other concentrations are not linear and compared to this concentration. F) Kinase phosphorylation activity determined across different protein concentrations incubated for different times. There is linearity across the different time points with all showing linear activity levels. Sixty minutes incubation shows a steady increase in kinase activity.

6.2.5 The Michaelis-Menten constant (K_m for ATP) for *P. vivax* and *P. berghei* CLKs were determined using TR-FRET.

The established TR-FRET assay conditions were used to determine the K_m for ATP for *P. vivax* (*PvCLK1* and *PvCLK3*) and *P. berghei* (*PbCLK1* and *PbCLK3*). The determined K_m for ATPs was used to investigate the IC_{50} and inhibitor potencies.

The K_m for ATP for *PvCLK1* was determined using 5 nM proteins and 25 nM CREptide and the results showed a K_m for ATP value of 33.14 (± 7.128) (Figure 6.7A). The K_m for ATP for *PvCLK3* wild type and mutants (P210R and H273P) and *PbCLK3* wild type and H276P mutant were also evaluated using 50 nM protein and MBP-peptide substrate. The obtained K_m for ATP values were: 2.387 (± 0.3268), 2.684 (± 0.3086) and 3.497 (± 0.3268) for *PvCLK3*-WT, *PvCLK3*-P210R and *PvCLK3*-H273P respectively (Figure 6.7B). The determined K_m for ATP for *PbCLK3*-WT and *PbCLK3*-H276P were 11.08 (± 1.188) 11.17 (± 0.9088) respectively (Figure 6.7C). For easier handling in experiments, the values for K_m for ATP for *PvCLK1* and *PvCLK3* were rounded to 30 μ M and 5 μ M respectively and those of *PbCLK3* wild type and mutant were rounded up to 10 μ M.

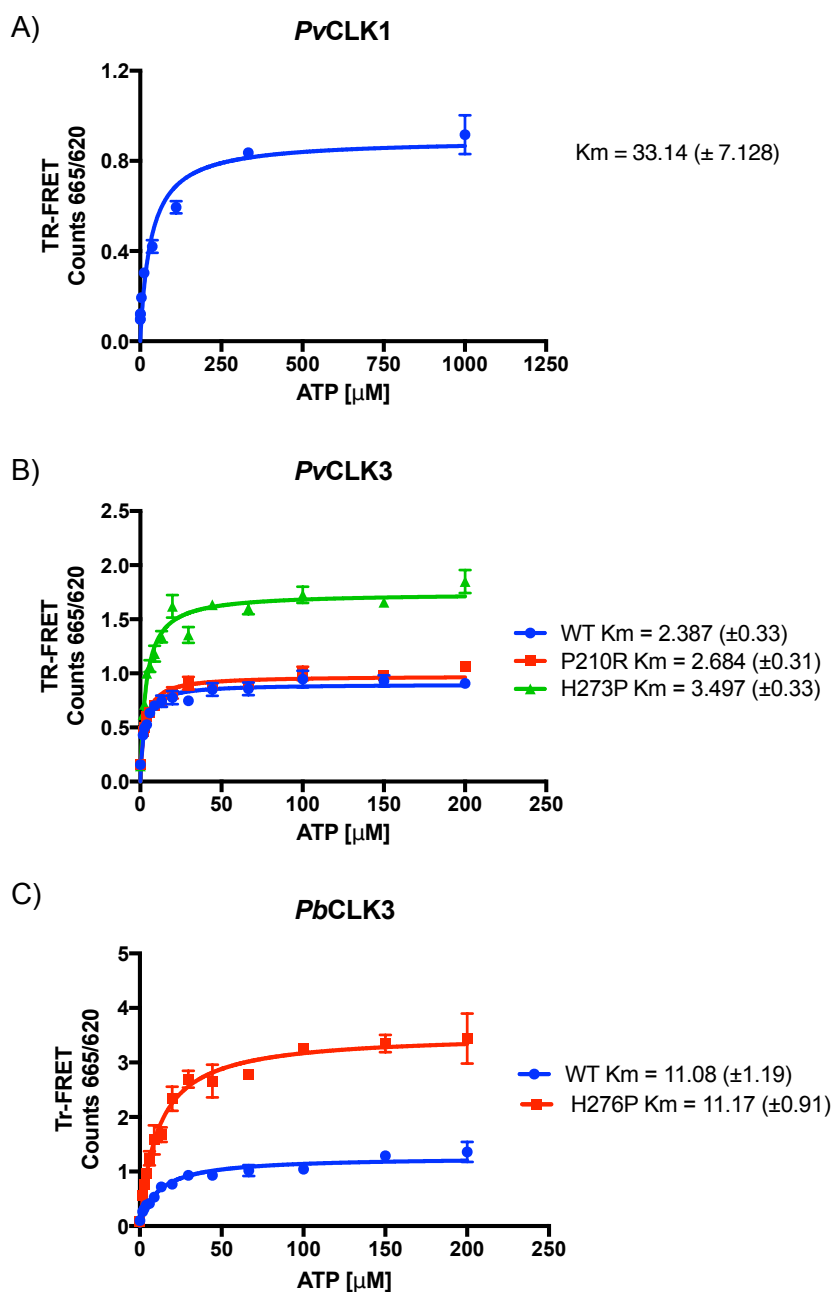


Figure 6.7: TR-FRET assay to determine the K_m for APT for other *Plasmodium* species recombinant kinases. A) *PvCLK1*, B) *PvCLK3* wild type and mutants P210R and H276P and *PbCLK3* wild type and mutant H276P. Data is the average of three independent experiments in triplicates \pm S.E.M.

6.2.6 TCMDC-135051 is a potent inhibitor against *Pv*CLK3 and *Pb*CLK3

The γ -³²P-ATP assay showed that both TCMDC-138736 and TCMDC-135051 efficaciously inhibit the activity of *Pv*CLK3 and *Pb*CLK3. Here, the investigation of potency was narrowed to the non-ATP competitive inhibitor, TCMDC-135051, against these kinases using the TR-FRET assay with ATP concentration at the respective K_m for ATP for each kinase.

Incubation of *Pv*CLK3 and *Pb*CLK3 with TCMDC-135051 resulted in inhibition of kinase activity and generated IC_{50} values in the low nanomolar ranges. TCMDC-135051 shows a strong potency against *Pv*CLK3 with an IC_{50} value of 13.53 nM ($pIC_{50}=7.87\pm 0.09947$) (Figure 6.8A). Similarly, it inhibits *Pb*CLK3 recombinant kinase with an IC_{50} value of 34.01 nM ($pIC_{50}=7.47\pm 0.12$) as shown in Figure 6.8B. As expected, these inhibition results are comparable to the IC_{50} values for *Pf*CLK3, indicating that TCMDC-135051 is potent against multiple species of *Plasmodium* parasite CLK3 kinases.

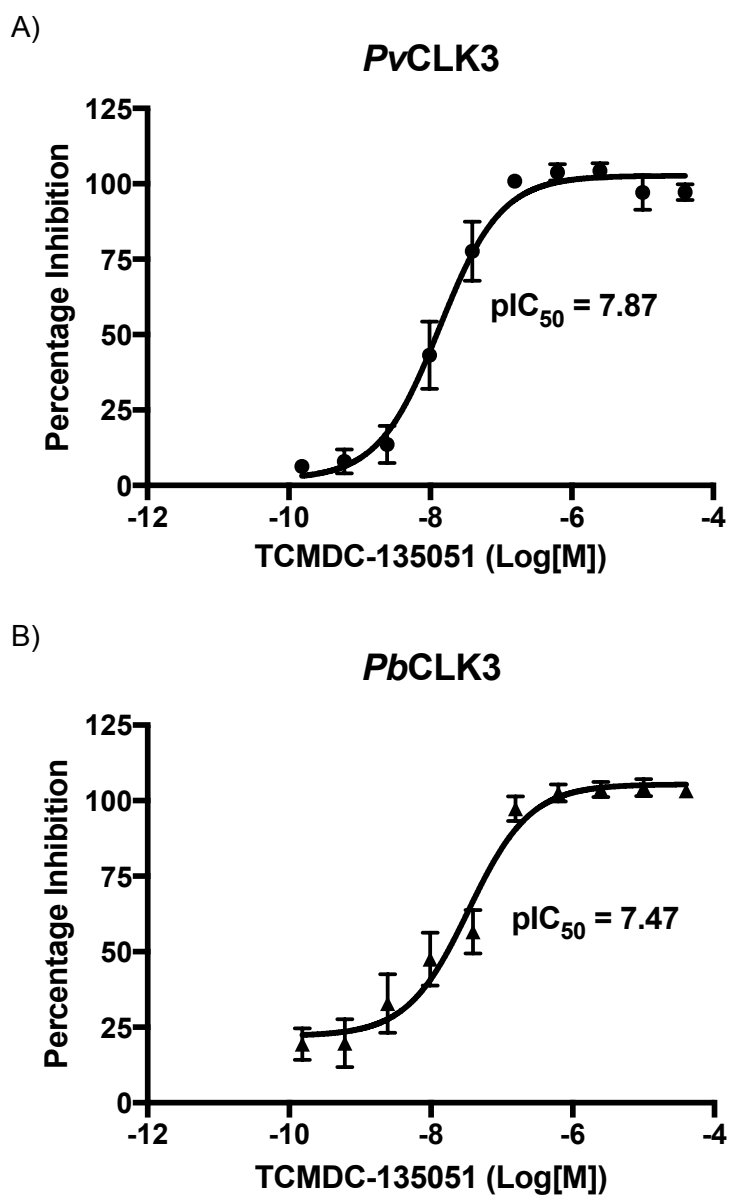


Figure 6.8: Inhibition of *Pv*CLK3 and *Pb*CLK3 with TCMDC-135051 using TR-FRET kinase inhibition assay with 50 nM MBP-peptide substrate and ATP concentrations at the respective K_m for ATP. A) *Pv*CLK3 inhibition curve generated B) *Pb*CLK3 inhibition curve.

6.2.7 The effect of *Pv*CLK3_H273P and *Pb*CLK3_H276P on kinase activity and potency of TCMDC-135051

The mutant *Pf*CLK3_H259P significantly influenced the mode of action of TCMDC-135051, changing it from a non-ATP competitive mode of action, to an ATP-competitive mode of inhibition. Because of the similarity in conserved kinase domain regions and inhibition of these *Plasmodium* CLKs by TCMDC-135051, the corresponding mutations to *Pf*CLK3_H259P were generated in *Pv*CLK3 and *Pb*CLK3 using site-directed mutagenesis producing *Pv*CLK3_P210R for *Pf*CLK3_P196R, *Pv*CLK3_H273P and *Pb*CLK3_H276P for *Pf*CLK3_H259P. It was proposed that these mutants would behave in a way similar to their corresponding *Pf*CLK3 in an activity and inhibition assay.

Using the γ -32P-ATP kinase assay followed by TR-FRET assay to compare their activity levels relative to wild type kinase, it was revealed that the mutant *Pv*CLK3_P210R, corresponding to P196R in *Pf*CLK3, showed similar kinase activity relative to wild type whereas *Pv*CLK3_H273P showed a significant increase in kinase activity compared to wild type (Figure 6.9A). The quantitative TR-FRET assay shows that the increase in kinase activity of *Pv*CLK3_H273P relative to wild type is significant with a *p* value of 0.0001 (Figure 6.9C). Similarly, the kinase activity of *Pb*CLK3_H276P also showed a significant increase of detected MBP phosphorylation compared to wild type using the γ -32P-ATP (Figure 6.9B). The TR-FRET assay shows a three-fold increase in kinase activity (Figure 6.9D), a significant increase with a *p* value of 0.0002 using unpaired two-tailed t-test compared to wild type. Our results thus indicate similarity in response to TCMDC-135051 between the *Plasmodium* kinases tested. Equally, the mutations at corresponding positions demonstrate similar effects to kinase activity and would potentially respond to inhibition by TCMDC-135051 kinase inhibitor in a similar way compared to *Pf*CLK3.

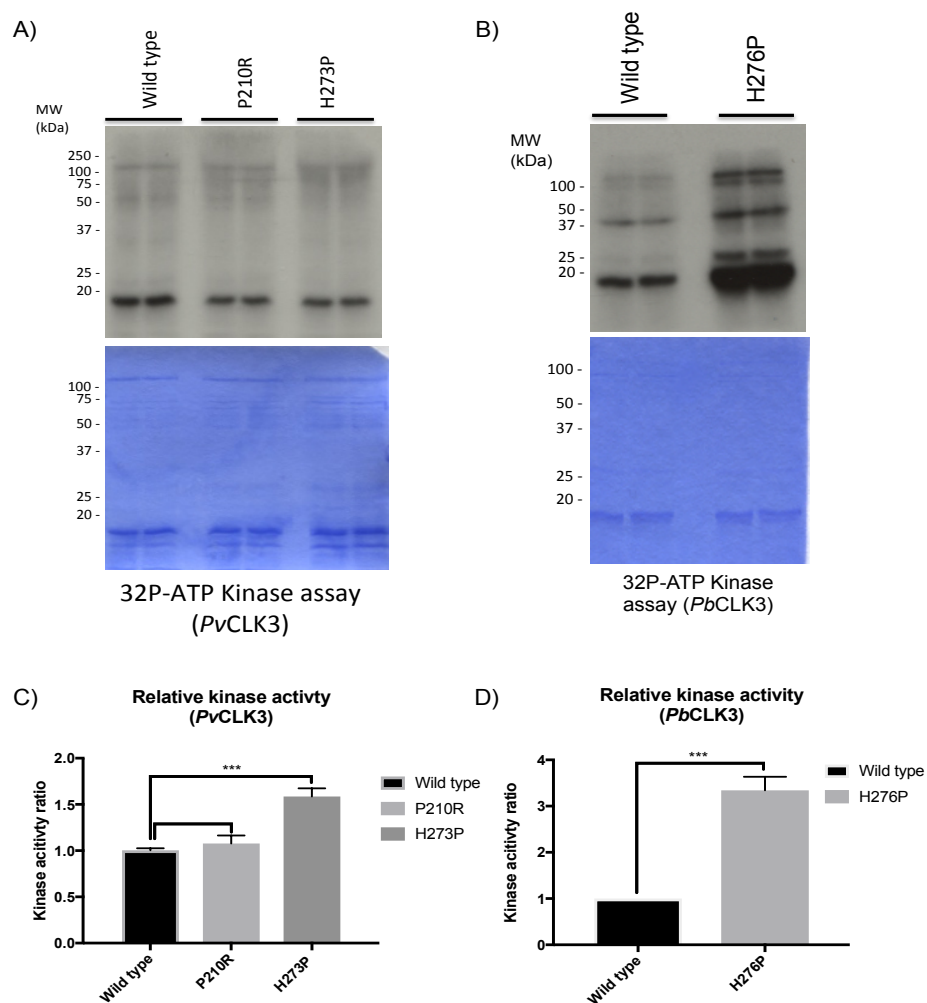


Figure 6.9: Comparison of kinase activities of wild type *PvCLK3* and *PbCLK3* to the mutants P210R, H273P, and H276P. A) γ -32P-ATP kinase assay comparing kinase activities of wild type *PvCLK3* to P210R and H273P. B) γ -32P-ATP kinase assay comparing kinase activities of wild type *PbCLK3* to H276P. C) TR-FRET kinase assay comparing the activity of P210R and H273P mutants against wild type *PvCLK3*. D) TR-FRET kinase assay comparing the activity levels of H276P mutant to wild type *PvCLK3* kinase. Data presented is a representation of three independent experiments (A and B), and the average of three independent experiments done in triplicates with errors as the S.E.M (C and D).

6.2.8 The effects of *Pv*CLK3_H273P and *Pb*CLK3_H276P to the inhibitory activity of TCMDC-135051

The similarity in kinase activity between *Pv*CLK3_H273P and *Pb*CLK3_H276P compared to *Pf*CLK3_H259P suggest that these mutations would respond to TCMDC-135051 comparably. For confirmation, TR-FRET kinase inhibition assays were set up using ATP concentration at the K_m for ATP and at 50X K_m for ATP concentration to evaluate the response of these mutants compared to the parent kinase.

Wild type *Pv*CLK3 inhibition showed an IC_{50} of 13.54 nM ($pIC_{50}=7.87\pm 0.10$) and 69.82 nM ($pIC_{50}=7.16\pm 0.10$) at the K_m for ATP and 50X K_m for ATP respectively, with a negligible shift in the inhibition curve (Figure 6.10A), thus, indicating high ATP concentration did not change the potency of TCMDC-135051. In contrast, exposure of *Pv*CLK3_H273P variant to TCMDC-135051 at the K_m for ATP and at 50X K_m for ATP concentrations, showed IC_{50} values of 16.97 nM ($pIC_{50}=7.7\pm 0.11$) and 336.8 nM ($pIC_{50}=6.47\pm 0.071$) respectively (Figure 6.10B); representing a ~ 1.5 log fold shift demonstrating ATP influence on the mutant.

Inhibition data for *Pb*CLK3 showed negligible change in the IC_{50} values in the presence of ATP at the K_m for ATP and 50X K_m for ATP concentrations with IC_{50} values of 34.01 nM ($pIC_{50}=7.47\pm 0.12$) and IC_{50} of 82.57 nM ($pIC_{50}=7.08\pm 0.11$) respectively as shown in Figure 6.11A. The mutant *Pb*CLK3_H276P, however showed an IC_{50} value of 29.02 nM ($pIC_{50}=7.77\pm 0.081$) at the K_m for ATP and 315.9 nM ($pIC_{50}=6.35\pm 0.13$) at 50X K_m for ATP concentration, representing a shift ~ 1.42 log fold shift in the pIC_{50} (Figure 6.11B). Taken together, the data presented here suggest that TCMDC-135051 inhibits these CLK3 kinases in a non-ATP competitive mode of action similar to *Pf*CLK3 inhibition.

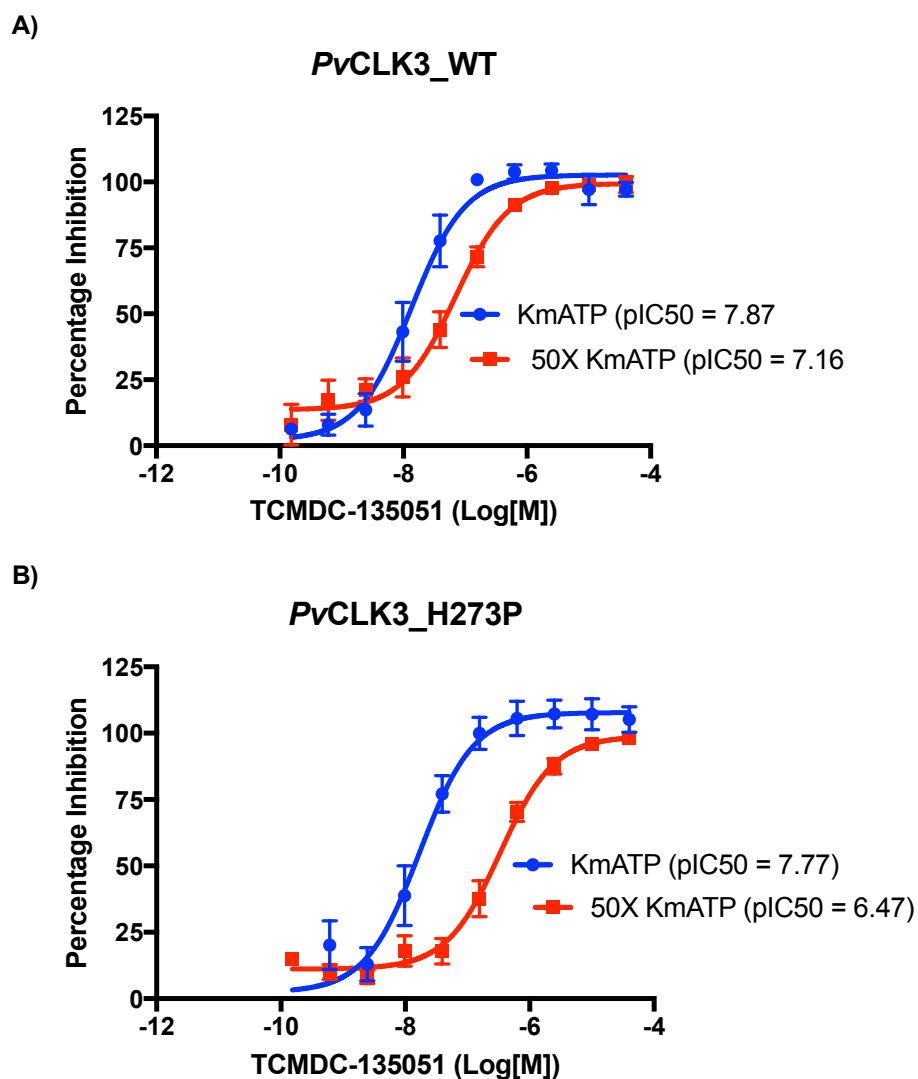


Figure 6.10: Comparison of inhibitory effects of TCMDC-135051 on *Pv*CLK3_H273P and *Pb*CLK3_H276P in the presence of low (K_m for ATP) and high (50X K_m for ATP) using TR-FRET assay. A shift in the IC₅₀ value by a log fold change indicates ATP-competitive behaviour whereas a smaller shift demonstrates an ATP-independent inhibition. A) Kinase inhibition of wild type *Pv*CLK3 with TCMDC-135051 at, K_m for ATP and 50X K_m for ATP concentrations. There is a slight shift in the curve to right but not significant with a small change in the pIC₅₀ values obtained. B) Kinase inhibition of *Pv*CLK3_H273P with TCMDC-135051 at, K_m for ATP and 50X K_m for ATP concentrations. There is a huge shift in the curve to right significant in the presence of high ATP concentration (50X K_m for ATP) enough to cause a change in the pIC₅₀ values obtained from 7.77 to 6.47.

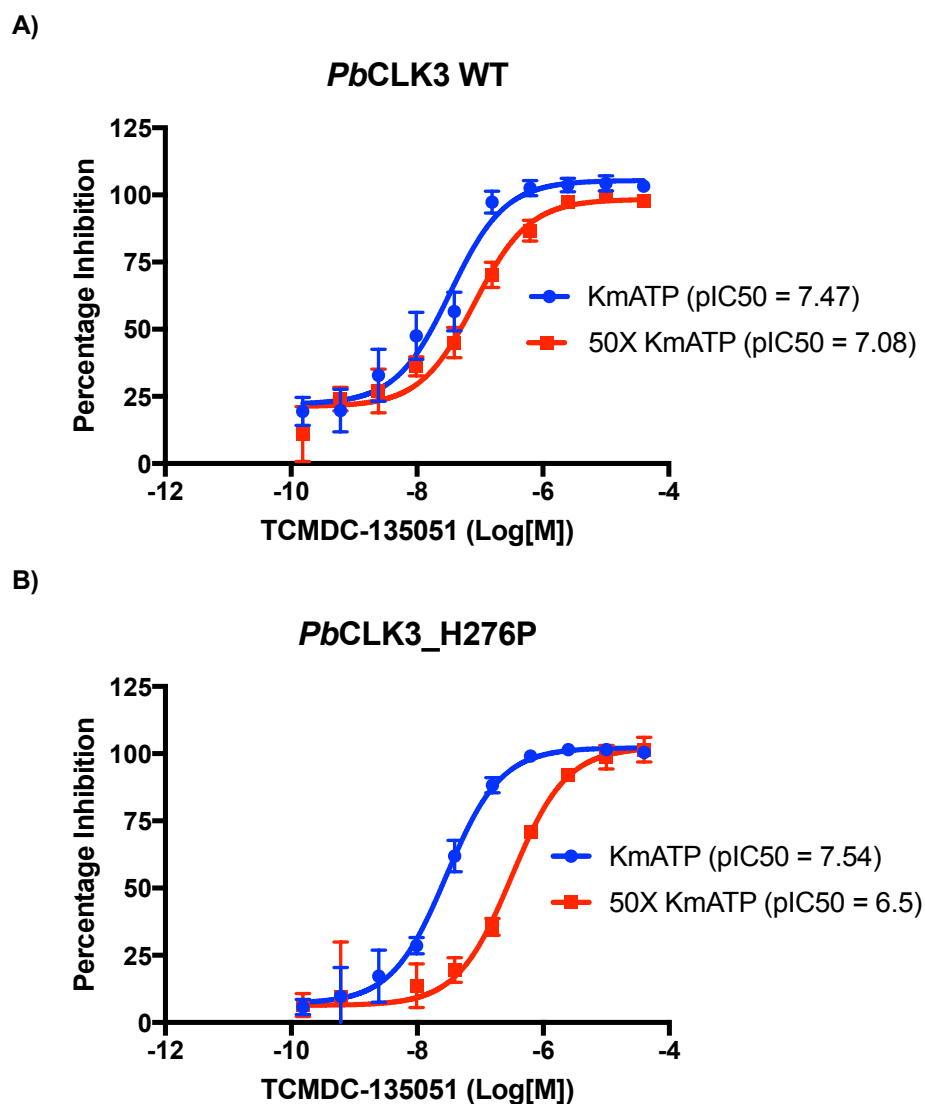


Figure 6.11: A) Kinase inhibition of wild type *Pb*CLK3 with TCMDC-135051 at *K_m* for ATP and 50X *K_m* for ATP concentrations. There is a slight shift in the curve to right but not significant with a small change in the pIC₅₀ values obtained. B) Kinase inhibition of *Pv*CLK3_H273P with TCMDC-135051 at *K_m* for ATP and 50X *K_m* for ATP concentrations. There is a huge shift in the curve to right significant in the presence of high ATP concentration (50X *K_m* for ATP) enough to cause a change in the pIC₅₀ values obtained from 7.54 to 6.5. This data is the average of three independent experiments in triplicates and graphs are drawn using GraphPad prism and errors are the S.E.M.

6.2.9 TCMDC-135051 potently inhibits *P. knowlesi* at low nanomolar concentration in vitro

P. knowlesi parasite CLK3 (*Pk*CLK3) kinase sequence is highly homologous to the *Pf*CLK3 sequence. For this reason, the inhibitory effects of the *Pf*CLK3 kinase inhibitor known to inhibit wild type 3D7 parasites at low nanomolar concentrations were also investigated for inhibition of *P. knowlesi* growth and to determine its potency. For this investigation, conditions similar to those used for *P. falciparum* were used: 0.5% parasitaemia, 4% haematocrit synchronised ring stage parasites. These were exposed to the inhibitor until re-invasion was observed in the untreated well. The inhibition data from this experiment showed that *P. knowlesi* is sensitive to the *Pf*CLK3 inhibitor (TCMDC-135051) in a dose dependent manner. The inhibitor has a distinct potency to this parasite line similar to *P. falciparum* with an EC₅₀ of 279.4 nM (pEC₅₀=6.55±0.043) (Figure 6.12). This potency is comparable to the obtained EC₅₀ values for *P. falciparum* parasites.

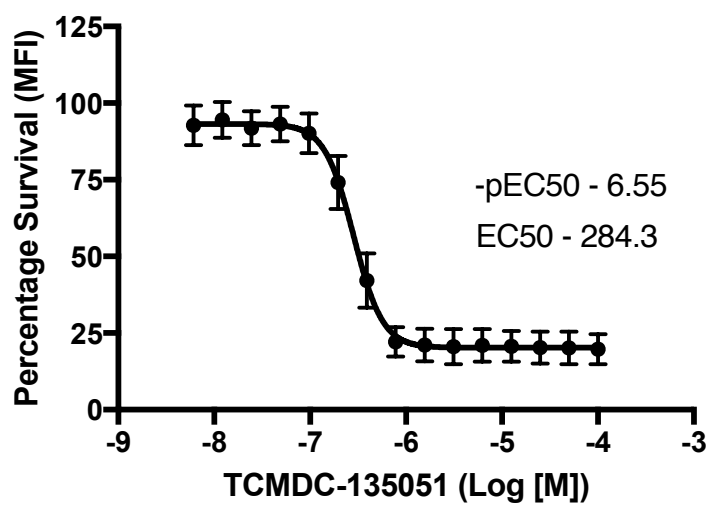
***P. knowlesi* Death curve**

Figure 6.12: Death Curve of *P. knowlesi*. Growth inhibition of curve of *P. knowlesi* parasites with the PfCLK3 kinase inhibitor setup with ring stage parasites at 0.5% parasitaemia and 4% haematocrit incubated for at least 48 hours. The data is the average of three independent experiments run in triplicates \pm S.E.M and analysed using Graph Pad prims non-linear regression analysis.

6.3 Discussion

It is shown here that TCMDC-135051 is a potent *Plasmodium* CLK3 kinase inhibitor across multiple *Plasmodium* species (*Pf*CLK3, *Pv*CLK3, *Pb*CLK3 and *P. knowlesi*). *Plasmodium* CLK3 is an ideal target because it phosphorylates important proteins involved in RNA splicing (Kern *et al.*, 2014). Additionally, a fully optimised TCMDC-135051 would be a good antimalarial tool compound, because inhibitors that target enzymes involved in the biosynthesis of critical biological steps have potent antimalarial activity both *in vitro* and *in vivo* (Garg *et al.*, 2015). The expression of this kinase in both asexual parasite and sexual stages (Agarwal *et al.*, 2011, Kern *et al.*, 2014), suggests that *Pf*CLK3 is a significant target with potential to cure symptomatic malaria and prevent onward disease transmission from person to person through the mosquito vector.

In addition to sequence similarity, all the tested CLK3 kinases phosphorylate MBP at the expected molecular weight (Kern *et al.*, 2014) and both are equally inhibited by TCMDC-138736 and TCMDC-135051. The *Plasmodium* CLK1 kinases however demonstrate no sensitivity to the inhibitors using γ -32P-ATP kinase inhibition assay, proving the selectivity of the inhibitors for CLK3 only. Using the TR-FRET assay, K_m for ATP and the inhibition potency of TCMDC-135051 were evaluated using *Pf*CLK3 as control. The K_m for ATP values obtained for these *Plasmodium* species were similar to those of *Pf*CLK3 and *Pf*CLK1. The inhibition assays showed equipotent inhibition of the *Plasmodium* kinases by TCMDC-135051 in the TR-FRET inhibition assay. In *in vitro* drug assay, *P. knowlesi* asexual parasites were equally inhibited by TCMDC-135051 with EC_{50} values equivalent to *P. falciparum*. In a separate investigation we showed that TCMDC-135051 demonstrate similar potency against *P. berghei* asexual parasites (Alam *et al.*, 2018). Together, this

data shows that TCMDC-135051 potently inhibit multiple species of *Plasmodium* by inhibiting CLK3 activity, an indication that it meets the requirement for multispecies action (Burrows *et al.*, 2017). A similar multi species action inhibitor with submicromolar potency has been reported in a study investigating the inhibition of FK506 binding protein as a therapeutic target for malaria treatment (Harikishore *et al.*, 2013), proving that our finding is overwhelmingly practical.

To further investigate the similarity in sensitivity to TCMDC-135051 action against these *Plasmodium* CLK3 kinases mutations similar to the *Pf*CLK3_H259P were generated for *Pv*CLK3 and *Pb*CLK3 (H273P and H276P respectively) and their response to TCMDC-1345051 investigated. These mutations showed increased kinase activity and changed the mode of inhibition of TCMDC-135051 to a mechanism suggestive of ATP-competitive mode of inhibition, similar to *Pf*CLK3; a property increasing the selectivity of TCMDC-135051 across these (Roskoski, 2015).

In conclusion, TCMDC-135051 demonstrates a potent multi-stage action against of *P. falciparum* parasites. Additionally, TCMDC-135051 can inhibit the activity of *Plasmodium* CLK3 kinases at submicromolar concentration from multiple species of *Plasmodium*. The equipotent activity of this inhibitor against the tested *Plasmodium* CLK3 kinases and the cross species action, together with the multistage effect on *P. falciparum* satisfy the criteria for next generation anti-malarial (Burrows *et al.*, 2017). Together, the data presented here shows that TCMDC-135051 is a suitable therapeutic compound with ability to treat malaria infection and prevent malaria transmission.

Chapter 7 TCMDC-135051 is potent against clinical *P. falciparum* malaria

7.1 Introduction:

The potency of TCMDC-135051 against multiple *Plasmodial* CLK3 kinases and asexual laboratory isolates suggest that it would potentially inhibit clinical isolates in *in vitro* cultures. However, *P. falciparum* clinical isolates usually show evidence of genetic variability of drug resistance markers (Theron *et al.*, 2010), which are hypothesised to reduce sensitivity to standard and novel antimalarial drugs (Cui *et al.*, 2012). It is therefore important to characterise the response of field isolates to TCMDC-135051 and to determine its speed of action (fast acting or moderate/slow acting) compared to standard antimalarial drugs such as ATR, which have a rapid action against all *Plasmodium* asexual erythrocytic stages (Rottmann *et al.*, 2010). The parasite reduction rate (PRR) assay previously described (Linares *et al.*, 2015), was used to carry out this investigation. This is the ratio between initial parasitaemia at the onset of drug treatment and that after completion of one asexual parasite life-cycle and is a direct measure of the speed-of-action of antimalarial compounds on parasite viability (Sanz *et al.*, 2012).

Here, clinical field isolates from the Gambia, an endemic malaria population with a significant level of drug pressure, were assessed to determine the speed of action of TCMDC-135051 compared to standard antimalarial: dihydroartemisinin (DHA) (fast-acting), mefloquine (MFQ) (moderate-acting) and pyrimethamine (PYR) (slow-acting). These isolates were collected from Gambisara, a large village in the upper river region of the Gambia in a previous study (Dieye *et al.*, 2016). Malaria transmission in this area is moderate, and like the rest of the Gambia and other tropical zones, seasonal (Dieye *et al.*, 2016, Mwesigwa *et al.*, 2015). These samples were monoclonal infections and resistance

genotypes were confirmed by sequencing and Table 7-1 shows the prevalence of drug resistance markers in these isolates.

The data presented in this chapter shows the potency of TCMDC-135051 against clinical isolates. It has an artemisinin-like, fast-killing kinetics and distinguished itself from other non-fast acting drugs. Finally, the presence of drug resistance genotype to other antimalarial drugs has no influence on the potency of TCMDC-135051 on these isolates.

Table 7-1: Drug resistance genotypes: Prevalence of drug resistant markers on the selected samples determined using Sanger sequencing techniques. Highlighted in red are confirmed mutations in the tested target genes.

Sample ID	Chloroquine resistant gene (K76T)	Multidrug resistant gene (PfMDR1)			DHFR				DHPS				Artemisinin resistance (K13)		
	K76T	N86Y	Y184F	N1042D	N51I	C59R	S108N	I164L	K540E	A581G	A613S	S436F	A437G	C580Y	I543T
GB0006	X	X	X	N	X	X	N	L	K	A	A	S	A	C	I
GB0004	K	N	Y	N	N	R	N	L	K	A	A	S	A	C	I
GB0026	K	N	X	N	N	R	N	L	K	A	A	S	A	C	I
GB0002	T	N	X	N	I	C	N	L	K	A	A	S	A	C	I
GB0021	K	N	F	N	X	X	N	L	K	A	A	S	A	C	I
GB0048	X	N	F	N	I	C	N	L	K	A	A	S	A	C	I
GB0052	K	N	F	N	I	C	N	L	K	A	A	S	A	C	I
GB0071	X	N	Y	N	N	C	N	L	K	A	A	S	A	C	I
GB0087	T	N	Y	N	I	C	N	L	K	A	A	S	A	C	I
GB0020	T	Y	Y	N	I	C	N	L	K	A	A	S	A	C	I

7.2 Results:

7.2.1 Determining the EC₅₀ of laboratory Isolates

The EC₅₀ values for artemisinin, pyrimethamine, mefloquine, and TCMDC-135051 were determined using wild type *P. falciparum* 3D7 and Dd2 laboratory isolates using standard drug assay methods described in chapter 2. The data obtained showed that the EC₅₀ value for dihydroartemisinin (DHA) with Dd2 is 6.2 (± 0.29) nM; pyrimethamine showed an EC₅₀ of 16.68 (± 0.017) nM with 3D7 parasites, mefloquine showed an EC₅₀ of 32.57 (± 0.035) nM with Dd2; and finally TCMDC-135051 showed an EC₅₀ of 180.2 (± 0.031) nM with Dd2 parasites as shown in the death curves in Figure 7.1. To investigate the potency of TCMDC-135051 against clinical isolate, the parasite reduction rate was setup-using drugs at the concentrations around the established EC₅₀ values: at the EC₅₀, 5X EC₅₀, 10X EC₅₀, and 100X EC₅₀ for each drug. TCMDC-135051 was compared to DHA, MEF, and PYR to determine its speed of action.

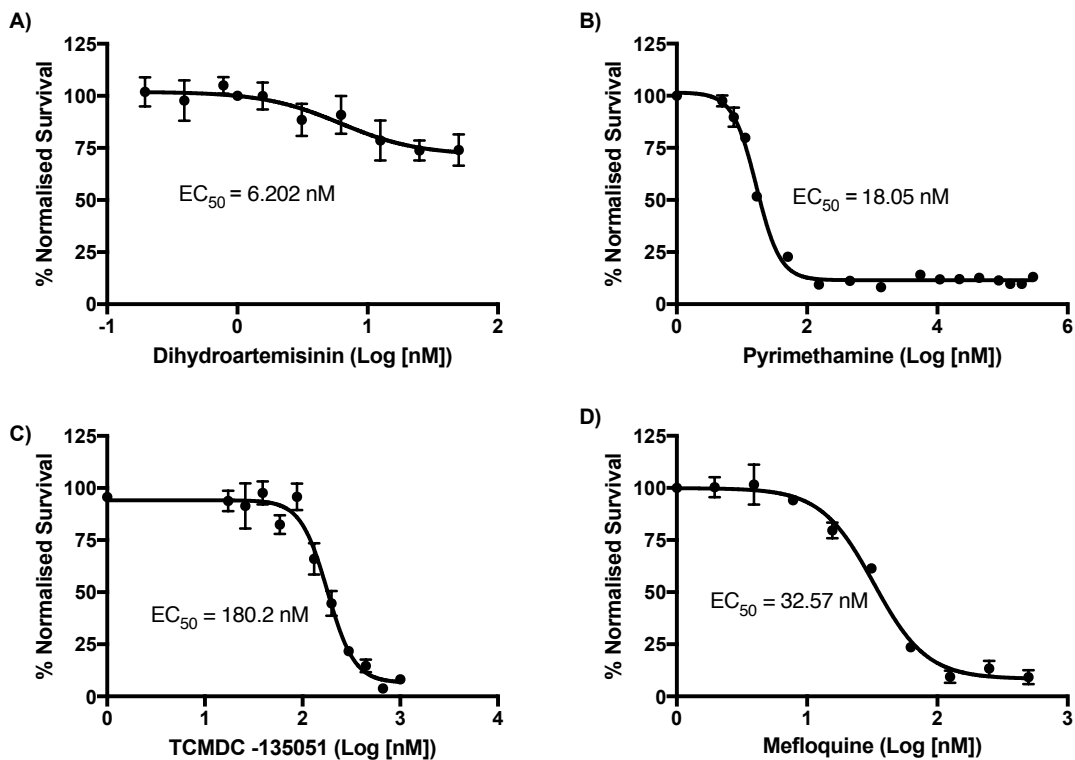


Figure 7.1: *In vitro* parasite (3D7 laboratory isolate) death curve. Each plot shows the death curve of the tested drug and the EC_{50} values derived. A) Dihydroartemisinin (DHA) B) Pyrimethamine (PYR), C) TCMDC_135051 and d) Mefloquine (MFQ). GraphPad Prism was used to analyse the data and plot the graphs using normalised percentage plotted against the logarithm of drug concentration curve fitted using nonlinear regression. Data represent the mean \pm S.E.M. of three independent experiments run in triplicates.

7.2.2 Assay Dynamic Range

The assay dynamic range was estimated by culturing serially diluted synchronised ring stage parasites at 0.5% parasitaemia in the presence of DDAO-SE stained erythrocytes at 2% haematocrit. Parasite infectivity of DDAO-SE stained erythrocytes were quantified after 50 hours of culture to allow reinfection of newly formed rings. These allowed detection of parasitaemia as low as 0.01% in the DDAO-SE stained erythrocytes by flow cytometry with accuracy (R value = 0.9989) (Figure 7.2B). DDAO-SE stained erythrocytes were quantified because infected non-stained erythrocytes could either be new infection or old infections of autologous cells, whereas all infections of DDAO-SE stained erythrocytes result from parasites that survived and remained viable after drug exposure. Quantification of parasitized DDOA-SE stained-erythrocytes correlates to the initial parasitaemia and DDOA-SE stained erythrocytes present in the total culture volume. Thus, this assay differentiated between parasitaemia in samples and treatment time points based on counted parasitaemia (Table 7-2 and Figure 7.2A-B), giving a significant difference between the starting parasitaemia and the final parasitaemia after 48-hours ($p < 0.0001$).

7.2.3 Data analysis and validation

Following treatment, parasite viability was quantified by determining infections of DDAO-SE stained erythrocytes since infection of unstained erythrocytes could either be an old or new infection. Any infections of DDAO-SE stained erythrocytes were new infections that result from viable parasites surviving drug treatment. To determine parasite viability and compare difference in drug treatments and time points, parasitaemia of DDAO-SE infected erythrocytes following treatment were calculated as a percentage of untreated DDAO-SE stained control erythrocytes expressed as a percentage using the formulae below:

$$\text{Parasite viability} = \frac{\text{New infections in treated wells}}{\text{New infections in control}} \times 100$$

Table 7-2: Cell population distribution as acquired by FACS. Distribution of acquired total erythrocyte count in four populations. The ratio of iRBC_DDAO-SE to iRBC is proportional to RBC_DDAO-SE to RBC, showing the robustness of the technique.

	Count	% of total
Total	99,216	100%
iRBC	355	0.36%
iRBC_DDAO-SE	515	0.52%
RBC	34,486	34.76%
RBC_DDAO-SE	63,860	64.36%

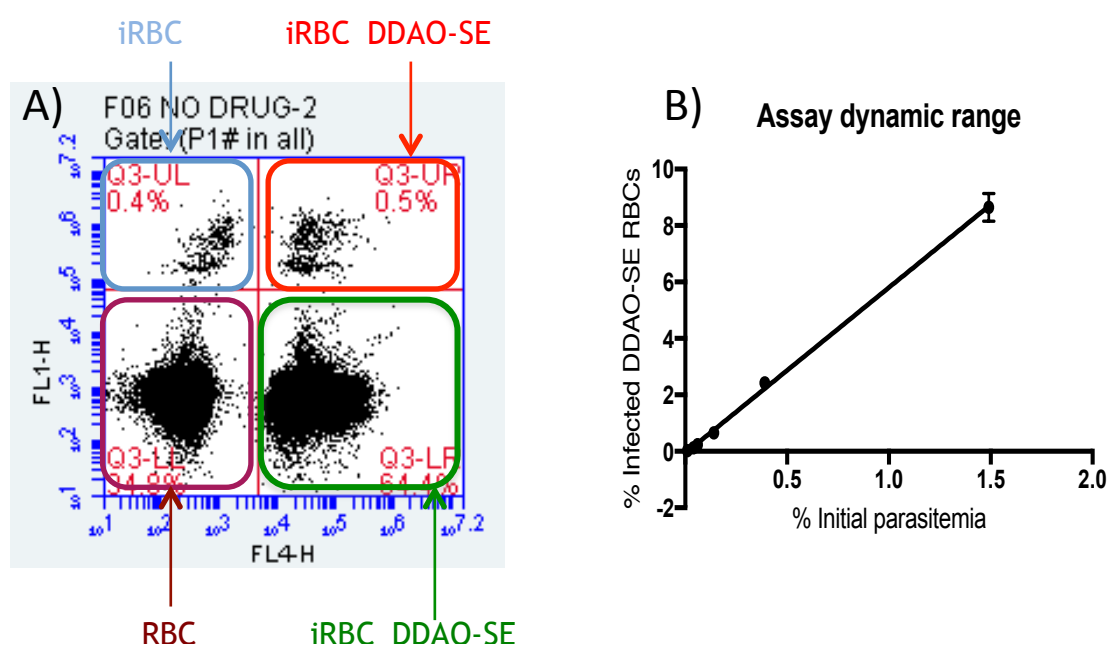


Figure 7.2: Analysis of DDAO-SE infected erythrocytes stained with Sybr Green I by fluorescence cell sorting (FACS). A) Sybr Green I nucleic acid staining of parasites grown in the presence of DDAO-SE labeled erythrocytes allows detection of four distinct population: iRBC – Infected erythrocytes positive for Sybr Green I staining and not DDAO-SE stain (blue panel, top left quadrant); autologous cells. iRBC_DDAO-SE – Infected Sybr Green I and DDAO-SE stained erythrocytes (red panel, top right quadrant); infected donor erythrocytes. RBC – Sybr Green I and DDAO-SE negative erythrocytes (brown panel, bottom left quadrant); non-infected autologous erythrocytes. RBC_DDAO-SE – Sybr Green I negative DDAO-SE positive erythrocytes (green panel, bottom right quadrant); donor erythrocytes not infected with parasites. B) Acquired data following 48 hours plotted against serially diluted starting parasitaemia.

7.2.4 The parasite reduction rate (PRR)

7.2.4.1 Dihydroartemisinin (DHA)

All samples, except GB0026, treated with 1X EC₅₀ DHA showed a reduction of parasitaemia to less than 30, 15 and 10% after 24, 48 and 72 hours, respectively (Figure 7.3A), indicating that DHA reduces parasite survival significantly with treatment at the EC₅₀ concentration. GB0026, an isolate with triple *PfDHFR* resistant mutant alleles, parasitaemia were 75, 60 and 50% at 24, 48, and 72 hours. At higher concentrations (5X, 10X, and 100X EC₅₀), however, all isolates show similar parasitaemia across all time points with parasitaemia levels reduced to less than 15% after 24 hours, between 4-10% after 48 hours and less than 5% at 72 hours of drug treatment as shown in Figure 7.3B-D, indicating near complete parasite clearance after treatment. This rapid parasite clearance rate is a characteristic of artemisinin and all its derivatives against *P. falciparum* malaria. However, the highest DHA concentration used (100X EC₅₀ – 600 nM) in this experiments, was lower than the concentration generally used in the ring stage survival assay (RSA) experiments to monitor artemisinin resistance (Witkowski *et al.*, 2013).

Dihydroartemisinin (DHA)

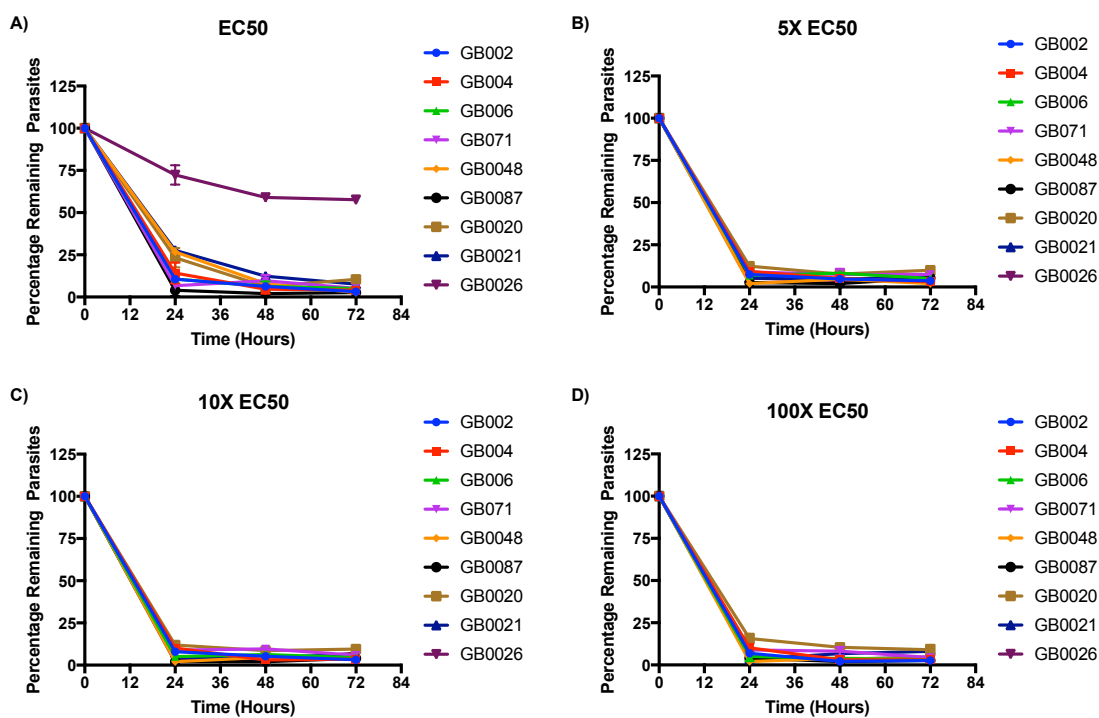


Figure 7.3: Parasite reduction rate of clinical isolates treated with dihydroartemisinin, at 1X, 5X, 10X, and 100X the EC_{50} concentrations of wild type 3D7 for 24, 48 and 72 hours. Percentage infection of donor RBCs (DDAO-SE stained erythrocytes) was determined by flow cytometry (Accuri). Data represent the mean experiments done in triplicates and the error bars represent S.E.M. Graph Pad prism was used to draw the graphs.

7.2.4.2 Pyrimethamine

Pyrimethamine treatment shows a susceptibility and diverse response clearly dependent on the *PfDHFR* drug resistance genotype of isolates. All isolates treated at the EC_{50} drug concentration (18 nM), showed a reduction in parasitaemia by at least 70% except three isolates (GB0020, GB002 and GB0026), with triple mutations on the *PfDHFR* gene and other drug resistant markers. GB0020 and GB0021 have the *PfDHFR* triple mutations N51I, S108N and I164L and the *PfCRT* variant allele K76T and GB0026 has the *PfDHFR* triple mutation C59R, S108N and I164L. For these isolates, 24 hours treatment reduces parasitaemia by 44.76, 63.8, and 35.71% respectively. However, 48 hours of treatment further reduced the parasitaemia of GB0020 and GB0021 to 27.13 and 21.9% respectively and has no effect on the parasitaemia of GB0026 compared to 24 hours treatment (Figure 7.4A). The parasitaemia after 72 hours treatment were 26.67, 15.7, and 118.57% for GB0020, GB0021, and GB0026 respectively. However, GB004, which has similar mutations, has a reduction of roughly 70% across all time points (Figure 7.4). Increasing drug concentrations to 5 and 10X the EC_{50} , however, did not significantly influence parasite reduction rates on the resistant isolates. Treatment of GB0026 with 5 and 10X EC_{50} concentrations showed no effects on parasites and parasitaemia reached 150 and 120% respectively after 72 hours of treatment. The isolate with double mutant (S108N and S164L) GB0071, is highly susceptible to treatment with PYR across all concentrations and time points; within 24 hours of treatment, its parasitaemia was reduced by >85% at the EC_{50} concentration and close to 100% reduction with all other concentrations and time points (Figure 7.4A-D). An isolate with similar double mutant alleles with an unconfirmed C59R mutant allele maintain parasitaemia of more than 50% at 100X EC_{50} for 72 hours of drug exposure. This data set shows that isolates with resistant genotypes demonstrated phenotypic resistance to PYR and delayed parasite reduction.

Pyrimethamine

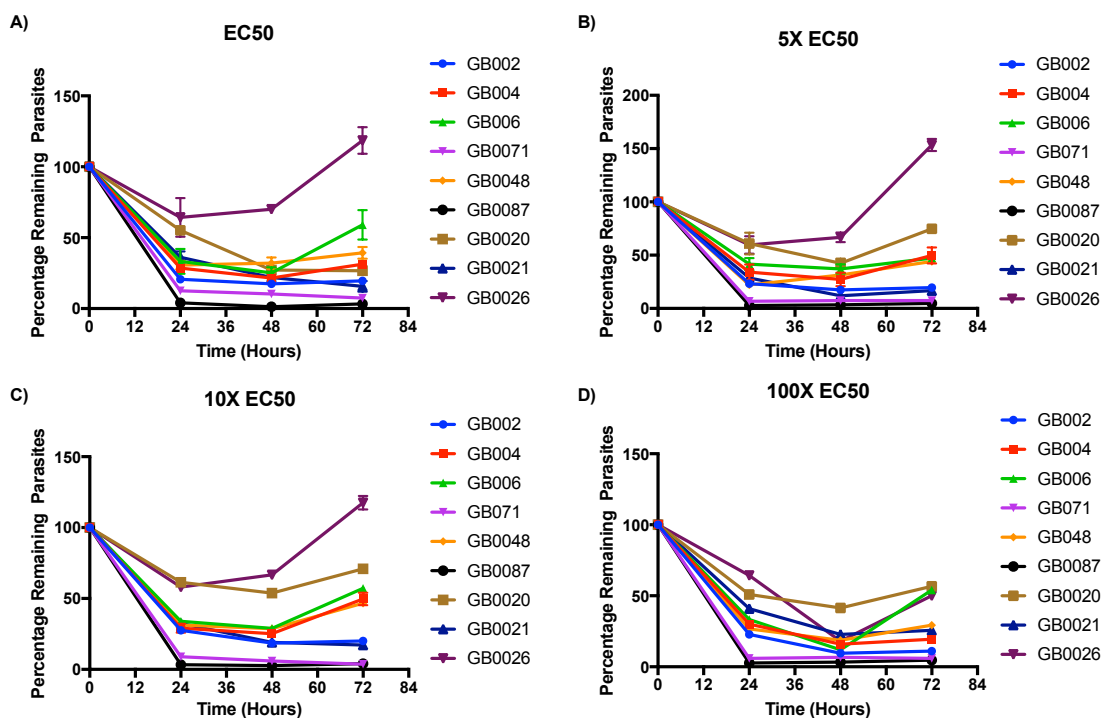


Figure 7.4: Parasite reduction rate of clinical isolates treated with pyrimethamine, at 1X, 5X, 10X and 100X the EC₅₀ concentrations of wild type 3D7 for 24, 48 and 72 hours. Percentage infection of donor RBCs (DDAO-SE stained erythrocytes) was determined by flow cytometry (Accuri). Data represent the mean experiments done in triplicates and the error bars represent S.E.M. Graph Pad prism was used to draw the graphs.

7.2.4.3 Mefloquine

Mefloquine treatment reduced parasitaemia across all drug concentrations efficaciously. At the EC_{50} concentration, all isolates treated for 24 hours showed reduced parasitaemia to between 15% and 2% except GB0021 and GB0026 with average parasitaemia of 29.0% and 76.2% respectively. Forty-eight hours of drug exposure reduces parasitaemia to between 11.9% for GB0071 and 1.33% for GB0087 except for GB0026, which had a parasitaemia of 21.4%. Drug treatment for 72 hours reduces parasitaemia to less than 10% across all isolates tested as shown in figure 7.5A. This response did not correlate with the prevalence of drug resistance markers. GB0087 bears resistant markers to *PfCRT*, K76T, and the *PfDHFR* triple mutation (N51I, S108N and I164L) but demonstrate complete susceptibility to mefloquine with 2% parasitaemia after 24 hours of treatment whereas GB0026 with *PfDHFR* triple mutation (C59R, 108N and 164L) showed significant parasitaemia following treatment. At higher drug concentrations (5, 10 and 100X EC_{50}) however, response to drug exposure is similar across all time points and isolates.

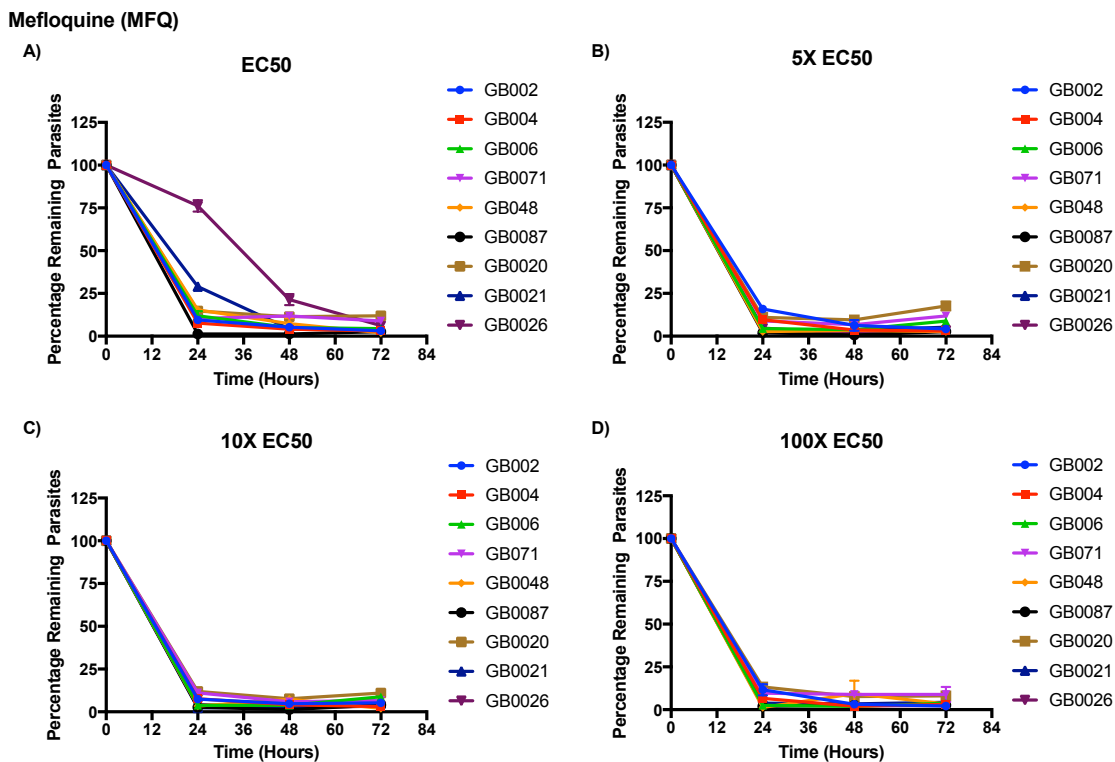


Figure 7.5: Parasite reduction rate of clinical isolates treated with mefloquine 1X, 5X, 10X and 100X EC_{50} concentrations of wild type 3D7 for 24, 48 and 72 hours. Percentage infection of donor RBCs (DDAO-SE stained erythrocytes) was determined by flow cytometry (Accuri). Data represent the mean experiments done in triplicates and the error bars represent S.E.M. Graph Pad prism was used to draw the graphs.

7.2.4.4 TCMDC-135051

TCMDC-135051 treated parasites demonstrated total susceptibility even at the low concentration (1X EC₅₀). Parasites exposed to EC₅₀ drug concentration were reduced by more than 50% within 24 hours. Like DHA, longer treatment time with this inhibitor showed further reduction in parasitaemia from between about 70% reduction for GB006 to almost complete parasite clearance for GB0087 within 48 hours treatment. At 72 hours of treatment, the lowest reduction observed was 75% for GB006 and reduction of more than 96% with GB0048 observed (Figure 7.6A). GB0026 however survived treatment with greater than 55% parasitaemia within the first 24 hours but did not survive greater than 10% with longer drug exposures (Figure 7.6A). Treatment with higher drug concentration (5X EC₅₀) shows greater reductions, with most isolates reduced by more than 70% within 24 hours. This concentration reduces parasite survival further by greater than 85% at 48 hours and 72 hours (Figure 7.6B). Ten and 100X EC₅₀ concentrations gives approximately complete parasite clearance irrespective of treatment length and isolate drug resistant genetic background (Figure 7.6C-D). These results suggest that inhibition of parasite growth targeting *PfCLK3* kinase with this inhibitor is not influenced by the presence of drug resistance genotypes. Similar to DHA and MFQ, this kinase inhibitor has a fast acting activity demonstrated by its rapid killing action on parasites at concentrations greater than its EC₅₀.

TCMDC-135051 (Compound 151)

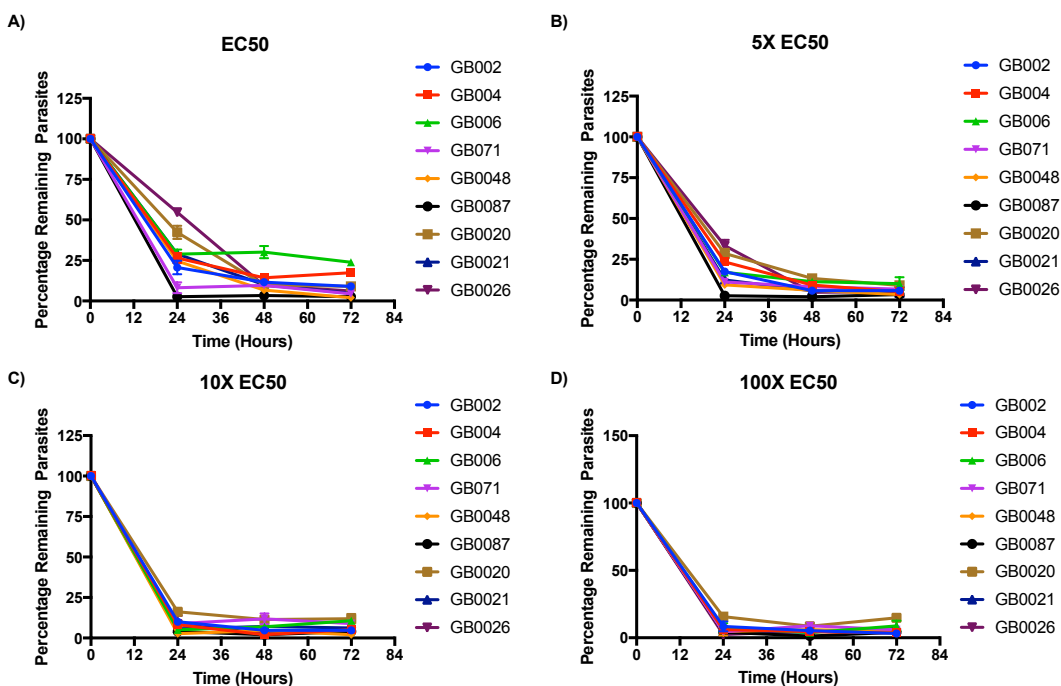


Figure 7.6: Parasite reduction rate of clinical isolates treated with TCMDC-135051, at 1X, 5X, 10X, and 100X the EC₅₀ concentrations of wild type 3D7 for 24, 48 and 72 hours. Percentage infection of donor RBCs (DDAO-SE stained erythrocytes) was determined by flow cytometry (Accuri). Data represent the mean experiments done in triplicates and the error bars represent S.E.M. Graph Pad prism was used to draw the graphs.

7.3 Discussion

The previous chapters showed that TCMDC-135051 is a potent multi-species anti-*Plasmodium* tool compound efficacious at submicromolar concentrations and efficacious against multiple stages of *P. falciparum* parasites. However, to replenish fast-acting artemisinin, it is important that it can mimic the rapid parasite killing action of artemisinin (Linares *et al.*, 2015). Using clinical isolates from the Gambia, a malaria endemic zone with low transmission dynamics (Mwesigwa *et al.*, 2015), TCMDC-135051 was evaluated to determine its speed of action compared to other antimalarial agents using the viability fast assay (Linares *et al.*, 2015).

Parasite growth in the PRR assay was monitored by staining parasite DNA in infected erythrocytes using Sybr Green I as a fluorescent DNA-binding dye and DDAO-SE was used to stain erythrocytes for detection by flow cytometry as previously described (Theron *et al.*, 2010); double stained erythrocytes represent new infections of donor erythrocytes from viable parasites that survived drug treatment. Increased presence of Sybr Green I fluorescence in stained erythrocytes indicates higher parasitaemia and parasites survival after drug treatment (Flannery *et al.*, 2013). As expected, DHA cleared parasites rapidly even at lowest concentration similar to an earlier report testing DHA parasite clearance time (Amambua-Ngwa *et al.*, 2017). Noteworthy, the highest concentration of DHA used for these experiments (100X EC₅₀, 600 nM) were lower than the 700 nM generally used in ring survival assays (RSA) (Kite *et al.*, 2016). Interestingly, the presence of *Pfmdr1* genotype had no effect on DHA efficacy, although it has been reported to influence parasite susceptibility to DHA (Cui *et al.*, 2012). In contrast, the presence of DHFR resistant markers showed a direct impact on phenotypic drug response, with parasites carrying the DHFR variant alleles being resistant to PYR treatment. This corroborate earlier reports that presence of DHFR triple mutations reduce susceptibility to PYR by greater than 1000 fold (Tahita *et al.*, 2015).

Data from the clinical samples showed that TCMDC-135051 potently inhibit the growth of these clinical isolates *in vitro* cultures within 24 hours of exposure at

low concentration (EC_{50}), reducing parasite survival by at least 50%. Longer treatment times (48 and 72 hours) showed further reductions in parasitaemia to less than 10%. Treatment with higher concentrations of TCMDC-135051 showed significant reduction in parasitaemia both in short (24 hours) and longer exposure times. This demonstrates fast killing action of TCMDC-135051 at sufficient drug concentration equivalent to concentrations used in assessing parasite clearance rate (700 nM) in RSA with DHA, about 100X EC_{50} (Kite *et al.*, 2016). Similar to DHA, removal of drug pressure did not reduce the potency of TCMDC-135051, signifying that the action of TCMDC-135051 is irreversible, a finding similar to an earlier report in a study investigating the utilisation of isoleucine by *P. falciparum* (Istvan *et al.*, 2011). Unlike other drugs, the prevalence of drug resistance markers, reported to influence the potency of new antimalarial agents (Veiga *et al.*, 2016) have no effect on the potency of TCMDC-135051. Hence, the data presented here shows that TCMDC-135051 has potency and speed of killed similar to DHA.

In conclusion, TCMDC-135051 has a fast acting antimalarial activity against clinical isolates like artemisinin and mefloquine at equivalent concentrations, a property not affected by prevalence of drug resistant genotypes. This demonstrates the efficacy of TCMDC-135051 in inhibiting clinical isolates of *Plasmodium* parasites with background resistance. Finally, the action of TCMDC-135051 is irreversible because washing off the drugs did not result in loss of potency in the treated isolates.

Chapter 8 Inhibition of *Pf*CLK3 shows direct effect on splicing

8.1 Introduction

The complex life-cycle of *Plasmodium* malaria is achieved from its small genome (containing ~5700 genes), which through post-translational regulation of alternative splicing (AS) of pre-mRNA produce functionally different protein isoforms from the same pre-mRNA transcripts to expand its protein repertoire for this complex life-cycle (Araki *et al.*, 2015, Eshar *et al.*, 2012). Additionally, AS is one of the mechanism used by malaria to “evade strategies devised to curb it”, and almost all *Plasmodium* genes undergo this process (Dixit *et al.*, 2010).

Pre-mRNA splicing is mediated by the spliceosome, which contained serine/arginine (SR) rich proteins regulated by the phosphorylation of their arginine/serine (RS) rich domains (Dixit *et al.*, 2010) by SR protein kinases (SRPKs) and CDC-like kinases (CLKs) (Araki *et al.*, 2015). *Pf*CLKs phosphorylate *Plasmodium* SR proteins (Agarwal *et al.*, 2011, Kern *et al.*, 2014). The phosphorylation of the RS rich domain of SR splicing factor 1 (SRSF1) by SRPK1 is important for its assembly into nuclear speckles which enhances its interactions with nuclear import receptors, transportin SR, and entry into the nucleus to occupy the nuclear speckles (Ghosh and Adams, 2011). Importantly, the CLK family of protein kinases controlled nuclear distribution of SRSF1 and other SR proteins (Ghosh and Adams, 2011).

The effect of inhibiting *Pf*CLK3 phosphorylation activity on splicing was investigated by comparing *Pf*CLK3_WT and *Pf*CLK3_G449P variant *P. falciparum* 3D7 parasites. This is important because it is reported that approximately 54% of parasite genes contain introns and about 30% contain at least two introns (Eshar *et al.*, 2012). In addition, evidence from my data and others (Kern *et al.*, 2014) showed that inhibition of CLKs result in parasite growth arrest and death. Furthermore, the CLKs have been reported as non-redundant kinases demonstrating that multiple kinases are involve in SR protein

phosphorylation within a cell (Kern *et al.*, 2014, Solyakov *et al.*, 2011). This suggests that inhibition of members of this kinase family would result in incomplete splicing.

The data presented in this chapter show that inhibition of *Pf*CLK3 by TCMDC-135051 result in incomplete splicing of pre-mRNA isoforms as shown in the treated wild type parasites compared to untreated controls. In contrast, TCMDC-135051 resistant variant, *Pf*CLK3_G449P, showed no difference between treated and untreated samples, both completed splicing successfully. This confirms that the *Pf*CLK3 kinase is involve in RNA splicing and/or is an important component of the spliceosome complex making it a good anti-*Plasmodium* therapeutic target.

8.2 Experimental Procedure

To study the effects of *Pf*CLK3 inhibition on splicing, highly synchronised wild type and mutant *Pf*CLK3_G449P asexual 3D7 *P. falciparum* parasites at trophozoite stage were challenged with 1 μ M of TCMDC-135051 for 2 hours. Drug pressure was removed by washing and samples from the treated (+) and untreated (-) parasites were prepared for ribonucleic acid (RNA) isolation and complementary DNA (cDNA) synthesised.

A selection of genes were identified (Table 8-1) and primers designed to amplify the flanking regions of introns on these genes: that is the forward primers were selected from the exon on the 3' side of the intron and the reverse primers selected from the other exon on the 5' side of the intron as shown in Figure 8.1. If inhibition of *Pf*CLK3 has an effect on splicing, untreated wild type parasites would completely splice out the intron and the treated wild type parasites should defect in splicing and produce an un-spliced mRNA. However, in the resistant mutant parasite line, both the treated and untreated parasites are expected to successfully splice out introns.

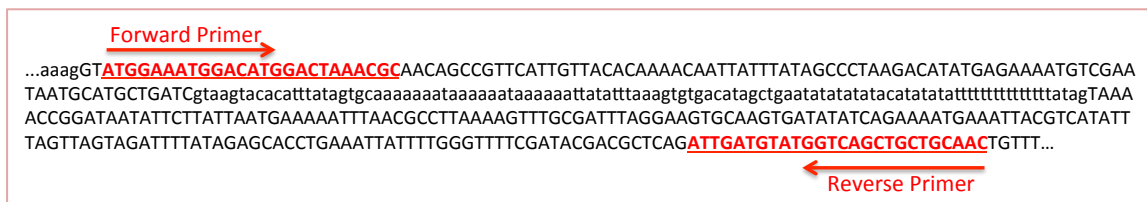


Figure 8.1: Primer design strategy for evaluation of splicing after drug treatment. This region of the selected gene (PF3D7_1114700) has an intron insert size of 106 bp represented by lower case letters. On either side of this selection is a forward primer on the 5' site of the intron and reverse primer on the 3' end of the intron highlighted in red. The product size with the intron is 398, when the intron is spliced out it will be 292 bp.

Table 8-1: Selected genes with introns. The full size of the selected regions within the gene with introns flanked on both sides by the forward and reverse primers on the exons (product size with intron) and the product without the introns as shown is the same gene with the same selected primers but processed and the introns removed.

Gene ID (PlasmODB)	Forward primer	Reverse primer	Product size	Product size
			with intron (bp)	without intron (bp)
PF3D7_1114700	ATGGAATGGACATGGACTAAACGC	GTTGCAGCAGCTGACCATACATCAAT	398	292
PF3D7_0321400	TGTTGAAGGGATGGACATTTCA	TGCTCACTAATAATCGTGCATTGT	288	199
PF3D7_0409700	TCCTAGTCACATGGAAGAATG	AAACACCCTGACTTGTGACAT	183	138
PF3D7_0607600	CGCGAGGTAATTTGAGGCT	ACGTTATTCGGGATGGACGA	452	225
PF3D7_0805000	ATGAGAAAAGCACAGGGACA	TGCACCTTGTAGTATTAAGCC	442	191
PF3D7_1438700	AGACACCCGCTTAAGAGAAGA	ATGCAGCTCTAGCGTCAGTA	273	106
PF3D7_1343700	GCTGCCACATTGTCAGATTCTT	CGGAGTGACCAAATCTGGGA	139	139

8.3 Results:

Following drug exposure, untreated (vehicle only) and treated samples were collected, RNA isolated and cDNA generated. Using standard endpoint RT-PCR, the selected genes were amplified. Figure 8.2A shows the controls for wild type and mutant parasites following drug challenge. The gene PF3D7_1114700 has an intron within the selected region with a length of 398 base pairs (bp) and PF3D7_1343700 with a length of 139 bp without an intron. Treatment of wild type parasites showed inhibition of splicing resulting in a band size of 398 bp; compared to untreated wild type, where the intron is spliced out resulting in a band size reduced to 292 bp, which was the expected size without the intron. In contrast, the resistant parasites (*PfCLK3_G449P*) showed complete splicing both with the treated and the untreated samples showing a band of 292 bp corresponding to the expected size of the spliced form of the RNA. PF3D7_1343700 is an intron-less gene and no difference was observed between treated and untreated wild type parasites and the mutant. Together, this data indicate that *PfCLK3* plays a direct role in splicing and suggest that parasite death following treatment with TCMDC-135051 is due to the inhibition of the splicing machinery (Figure 8.2).

To further investigate the effect of *PfCLK3* inhibition on splicing, other genes with introns were evaluated. First, PF3D7_0321400 gene was evaluated and wild type treated and untreated samples compared to the mutant treated and untreated samples. In wild type parasites, untreated and treated samples result in PCR product sizes of 199 and 288 bp respectively as expected. This indicates that in the untreated sample splicing was successfully completed and in the treated sample splicing was inhibited. The mutant parasite showed no difference between the treated and untreated samples; both were processed completely and had the introns completely spliced out. All the genes tested show

comparable splicing patterns (Figure 8.2B and C). Noteworthy, the presence of incomplete splicing observed within some genes in the G449P variant suggest that TCMDC-135051 has minor potency against the mutant hence the minute levels of inhibition observed.

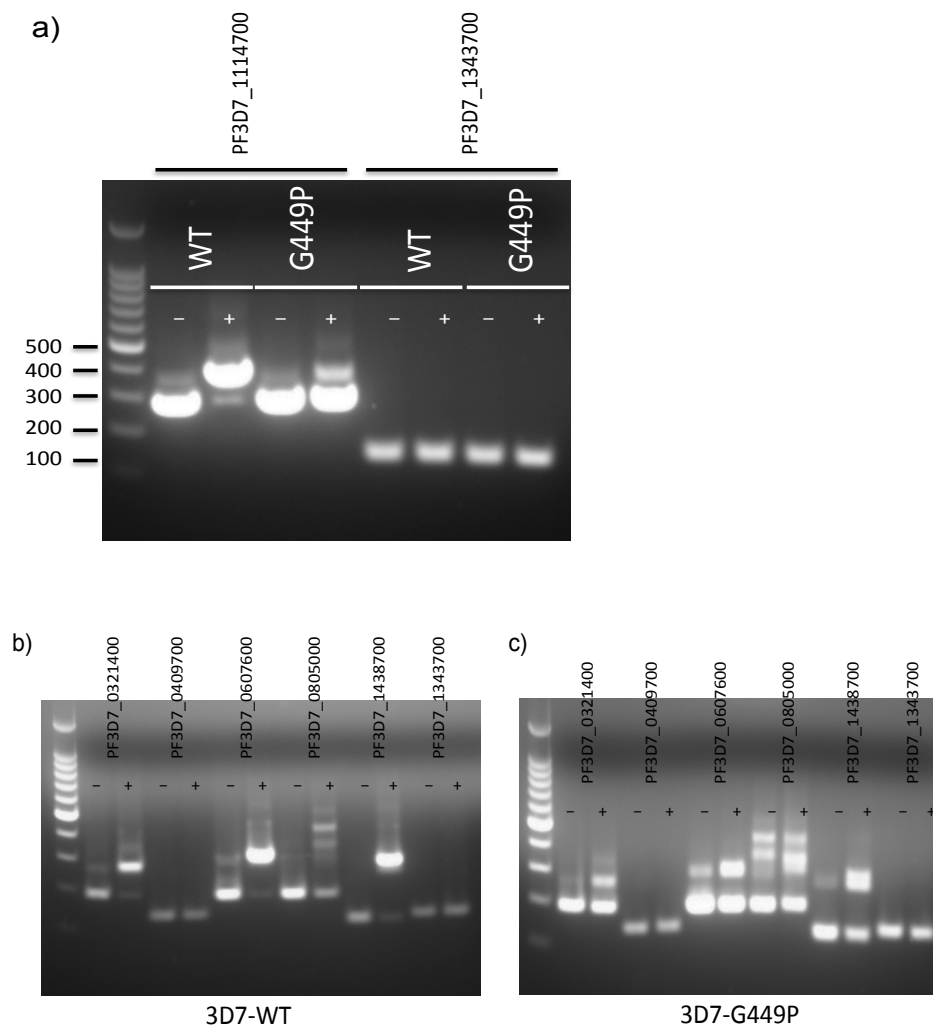


Figure 8.2: Effect of inhibition of *PfCLK3* in parasites on splicing machinery. Parasites were treated (+) with 1 μ M of TCMDC-135051 for 2 hours. Drug pressure was removed and RNA isolated using the Qiagen kit according to the manufacturers instructions and the target genes amplified. In a), the *PfCLK3* (PF3D7_1114700) gene with introns was selected and amplified from both treated and untreated samples. The untreated sample (-) shows a band at the expected molecular weight following the splicing of the intron but the treated sample shows the continuous presence of the intron, thus giving a higher PCR band product. Treatment of the resistant parasite variant, *PfCLK3*_G449P, showed no effect on splicing as demonstrated by the complete splicing in both the treated and the untreated samples. The intron less gene (PF3D7_1343700), show no difference between the two samples. In b), wild type parasite and c) the resistant parasite line this is further confirm. Comparing the effect the inhibitor, it is clearly visible that splicing is inhibited in the wild type and not in the resistant line as seen with several genes with introns.

8.4 Discussion

To explore the direct effect of *Pf*CLK3 inhibition on splicing, inhibition of 3D7 wild type *Pf*CLK3 parasites sensitive to TCMDC-135051 and the mutant parasite (*Pf*CLK3_G449P) resistant to TCMDC-135051 were performed. RNA transcripts of a selection of genes with introns were amplified using endpoint RT-PCR from cDNA preparations with primer pairs specific to flanking exon regions of selected genes. The RT-PCR data from these samples (wild type treated, wild type untreated, and mutant treated and mutant untreated) were analysed using agarose gel electrophoresis and compared. This allows direct visualisation and comparison of splice isoform abundance based on size disparity between differentially spliced transcripts as described in a similar investigation (Harvey and Cheng, 2016).

In the experiments exploring the effects of *Pf*CLK3 inhibition on splicing, evidence showed that in untreated controls, pre-mRNA transcripts were fully spliced out resulting in smaller product sizes due to the removal of introns and joining of exons. However, the treated parasite samples show lack of splicing in pre-mRNA transcripts in parasites sensitive to TCMDC-35051 action, indicating deregulation of splicing activity. Therefore, inhibition of *Pf*CLK3 could result in incomplete spliced variants, leading to down regulation of genes important for transition between the multiple stages of parasite growth. The un-spliced transcript variants seen with the treated wild type samples likely confirmed abnormal regulation of the splicing machinery, which in mammals is recognized to caused several diseases like cancer. A cancer study has shown variations resulting from deregulation activities of splicing factors generating splicing variants; and androgen receptor variants (AR-Vs) including ARv567es and V7 are reportedly generated as a result of mis-splicing that is caused or permitted by genomic alterations (Uo *et al.*, 2016). An indirect

effect of CLK inhibition is the depletion of S6K gene transcript due to the alteration of the splicing specific transcription factors that control levels of S6K (Araki *et al.*, 2015). Additionally, inhibition of *PfCLK3* could result to incomplete phosphorylation (hypo-phosphorylation) of SR proteins.

In contrast to wild type, *PfCLK3_G449P* parasites show complete splicing both in the treated and untreated samples. However, some events of incomplete splicing were observed in some genes from the mutant parasite, which are thought to be due to the sensitivity of *PfCLK3-G449P* to TCMDC-135051, which could result in altered phosphorylation of *PfCLK3*. Altered distribution of phosphorylated and hypo-phosphorylated SR proteins causes hypo-phosphorylated SR proteins to remain in the nucleus affecting AS in pre-mRNA (Saitoh *et al.*, 2012).

Although the importance of AS cannot be overemphasised, we recognise the fact that not all AS events result in functional significance. Premature stop codons (PTCs) could result from AS events and these PTCs target non-sense-mediated decay (NMD) pathways, control of which is important in posttranslational regulation mechanisms to remove non-functional transcripts for gene expression control (Yang *et al.*, 2018).

In conclusion, the high number of genes with at least one intron in the *Plasmodium* genome makes AS an important factor in parasite growth and replication. *PfCLK3*, been an important member of the spliceosome for complete AS to occur by phosphorylating SR proteins is a good therapeutic target for malaria. As presented here, the inhibition of this kinase by TCMDC-135051, a specific inhibitor has a direct effect of AS. Additionally, dysregulation of AS is a cause of many human diseases (Araki *et al.*, 2015), and is therefore expected to result in parasite death if significant pathways are inhibited. Inhibition of *PfCLK3* kinase activity

resulted in dysregulation as shown in our results and the eventual net effect is parasite death. This intriguing finding therefore demonstrates the importance of *Pf*CLK3 as a useful therapeutic target but also shows that the tool compound TCMDC-135051 is a valuable for malaria drug development.

Chapter 9 Discussion

9.1 General Discussion

Drug resistance has significantly hindered progress to control malaria globally, resulting in the continued prevalence of infections, causing significant morbidity and mortality among children under 5 years, pregnant women and non-immune travellers (WHO, 2017b). Resistance to the major antimalarial drugs with promising success to control malaria (such as chloroquine and artemisinin) has been a major hurdle to malaria control and are usually due to mutations in target gene(s) rendering these drugs non-functional (Ashley *et al.*, 2014, Awasthi and Das, 2013, Bareng *et al.*, 2018, Dondorp *et al.*, 2009, Ecker *et al.*, 2012, Patel *et al.*, 2017, Tahita *et al.*, 2015, Tun *et al.*, 2015, Veiga *et al.*, 2016). Unfortunately, the predominant mutation (C580Y in the K13 gene) identified to be responsible for resistance to the front-line antimalarial drug, ART, used in combination therapy is spreading rapidly (WHO, 2018). Mono-therapy, misuse, and use of sub-therapeutic drugs, leads to development of drug resistance, threatening the hopes of malaria elimination and making the successes gained unsustainable (Hanboonkunupakarn and White, 2016). These factors and the lack of a replacement drug for the current front-line antimalarial, make the research for a new and effective antimalarial potent against multiple stages across different *Plasmodium* species an urgent priority (Burrows *et al.*, 2017).

Here I present my contribution to validating *PfCLK3* as an antimalarial therapeutic target selectively inhibited by the tool compound TCMDC-135051. This selective kinase inhibitor was identified from a screen of compounds from a library of small molecules with antiparasitocidal activity and selected for its specificity and selectivity towards *PfCLK3*. As mentioned earlier,

this inhibitor has nanomolar potency for *PfCLK3* inhibition *in vitro* but showed no efficacy inhibiting other protein kinases including the closely related human CLK2 and *PfCLK1*. On asexual *P. falciparum* malaria parasites, this inhibitor has submicromolar parasitocidal activity against ring stages of 3D7 parasites. Furthermore, *PfCLK3* inhibition killed multiple stages of asexual *P. falciparum* parasites (trophozoites–schizonts maturation), thus reducing parasitaemia rapidly. Importantly, using the parasite reduction rate, I found that TCMDC-135051 killed both *P. falciparum* laboratory strains and field isolate parasites as rapidly as ART. Although the tested field isolates contained confirmed drug resistant genotypes, which are suggested to influence clinical isolates' response to new antimalarial drugs (Cui *et al.*, 2012), the potency of TCMDC-135051 was not affected by the presence of the drug resistant genotypes. This demonstrates that TCMDC-135051 has fulfilled significant requirements for new antimalarial (Burrows *et al.*, 2017).

Current antimalarial drug development guidelines require new tool compounds to have potency against multiple *Plasmodium* species (Burrows *et al.*, 2017, The mal, 2011). Against different *Plasmodium* species, TCMDC-135051 acted potently inhibiting the growth of *P. knowlesi* in *in vivo* cultures at submicromolar concentrations and inhibited *PvCLK3* and *PbCLK3* kinases at low nanomolar concentrations *in vitro*. The inhibition of asexual *P. knowlesi* parasites, *PbCLK3*, and *PvCLK3* implies the potency of TCMDC-135051 against *Plasmodium* malaria species, such as *P. vivax*, which reportedly have no specific drugs, but more worryingly are developing resistance to the current antimalarial drugs used for its control (Nyunt *et al.*, 2017). Therefore, in the broader context, targeting *Plasmodium* CLK3 with TCMDC-135051 is useful in controlling malaria in the SEA region where *P. vivax* is the major cause of morbidity and mortality associated to malaria and *P. knowlesi* human infections are reported.

Additionally, colleagues in the Tobin lab showed the potency of TCMDC-135051 against the development and multiplication of blood stage asexual *P. berghei* and gametocytes as well as sporozoites (Alam *et al.*, 2018). This demonstrated transmission-blocking potency of TCMDC-135051 in addition to its multistage and across species potency. Further investigations of transmission blocking potential by testing mosquito infectivity of TCMDC-135051 treated gametocytes is currently on going in collaboration with Dr Lisa Ranford-Cartwright. Also, in collaboration with Prof Andrew Waters lab (Director of the Wellcome Centre for Integrative Parasitology, Glasgow), mouse infection experiments; progression of infection in mice inoculated with *P. berghei* and treated with vehicle or various concentrations of TCMDC-135051 and monitored by determining parasitaemia in blood samples are mirroring to the mosquito infectivity experiments. Excitingly, preliminary data from both experiments show transmission blocking and *in vivo* efficacy of TCDMC-135051 respectively, further indicating *PfCLK3* as a good anti-*Plasmodium* therapeutic target for symptomatic treatment and transmission blocking in malaria.

The combined attributes for TCMDC-135051 are the required characteristics listed for new anti-*Plasmodium* tool compounds to give a radical cure: blocking transmission of gametocytes to mosquitoes, blocking transmission by the vectors by inhibiting sporozoite development, potency against hyponozoites, activity against liver infections and finally ability to clear symptomatic infections in malaria patients (Burrows *et al.*, 2017). However, this single molecule does not meet all the requirements of a radical cure and its use as mono-therapy would result in the rapid emergence of resistance. Consequently, to increase efficacy and reduce chances of drug resistance development, malaria therapeutics are given in combination with multiple targets (Andrews *et al.*, 2018). Because small molecules potent against

both *PfCLK3* and *PfCLK1* were identified (unpublished), optimisations of these molecules would determine if dual *PfCLK1* and *PfCLK3* inhibitors have a lower inclination toward development of parasite resistance to the inhibitor with higher efficacy. Additionally, it would be interesting to investigate if *PfCLK1* is an alternative target in malaria because it is equally important and plays a role in RNA processing (Kern *et al.*, 2014).

Although TCMDC-135051 inhibited asexual parasites potently at submicromolar concentrations, experiments were designed to determine the on-target parasitocidal activity of TCMDC-135051. This was done first using chemical genetic approaches with 3D7 parasites engineered to express the mutant *PfCLK3* gene (*PfCLK3_G449P*) that was insensitive to TCMDC-135051 inhibition. The susceptibility of the mutant parasites to inhibition by TCMDC-135051 was significantly decreased, consistent with an on-target activity against TCMDC-135051. Secondly, adaptive resistance experiments revealed two of the three laboratory generated resistant lines contained mutations in the *PfCLK3* gene and another mutation in an RNA processing protein (*PfUSP-39*) following whole genome sequencing. This is consistent with on-target activity of TCMDC-135051 towards *PfCLK3* and a role of *PfCLK3* in RNA processing because *USP-39* proteins are important components of the spliceosome complex (An *et al.*, 2015).

The generation of these mutants were straightforward following strict single crossover homologous recombination techniques as previously described (Balabaskaran-Nina and Desai, 2018), and mutations genetically validated. The adaptive resistant mutations were detected from whole genome sequencing following an average of 2 months of continuous drug exposure of Dd2 parasites to TCMDC-135051 starting from low to high TCMDC-135051 concentrations. Importantly, neither of these mutations

had an adverse effect on parasite multiplication rates compared to wild type.

Further characterising TCMDC-135051, it was discovered that the wild type *PfCLK3* demonstrated a response suggestive of non-ATP competitive mode of inhibition. This was because inhibitor potency remained insensitive to changes in ATP concentration, a response consistent with an allosteric mode of inhibition (Wenthur *et al.*, 2014). Non-ATP competitive inhibitors have improved selectivity and potency towards their target because they bind outside the ATP binding site and block kinase activity (Roskoski, 2015) – hence the demonstrated high selectivity towards *PfCLK3*. Allosteric inhibitors are generally highly selective because they exploit binding sites and regulatory mechanisms unique to a particular kinase either within or outside the kinase domain (Fabbro, 2015). However, both the mutant variant H259P and the kinase domain 353_KDct showed mechanisms consistent with ATP competitive mode of action. These changes suggest that in addition to acting to an allosteric site, TCMDC-135051 also acts on an orthosteric-binding site, giving the characteristic “bitopic” mode of action (Bradley *et al.*, 2018, Holzgrabe and Decker, 2017).

To confirm this bitopic mode of inhibition by TCMDC-135051, colleagues in the Tobin lab tested inhibitors from chemically distinct series (such as TCMDC-123697) and these showed classical ATP-competitive inhibitors both in the wild type and mutant *PfCLK3* kinase (unpublished data). Bitopic mode of inhibition offers two useful consequences: first, it increase the affinity of the inhibitor for *PfCLK3* and secondly, since off-target effects are likely via the interaction of TCMDC-135051 with the ATP binding sites of other kinases, the high cellular levels of ATP would act to reduce off-target effects. More importantly, the bitopic mode of binding of TCMDC-135051 to *PfCLK3* would mean the

inhibitor maintains activity against *Pf*CLK3 at cellular levels of ATP. Thus, the selectively inhibiting *Pf*CLK3 in parasites in the presence of supposedly high ATP concentrations, is consistent with the high affinity of orthosteric inhibitors and the selectivity of allosteric binding sites (Kamal and Jockers, 2009). This suggested bitopic mode of inhibition could be confirmed by generating co-crystal structure of *Pf*CLK3 in complex with TCMDC-135051 and possibly other molecules in the series. This would show if TCMDC-135051 act in a bitopic manner and also if these bitopic binding mode inhibitors are able to inhibit *Pf*CLK3 in the presence of high ATP concentrations at cellular level and whether this contributes to inhibitor selectivity. It can be argued from this evidence that, the bitopic mode of inhibition of TCMDC-135051 and the conserved CLK3 sequences across *Plasmodium* species improved the selectivity and potency of the inhibitor across a wide range of *Plasmodium* species. Thus increasing the significance of both the therapeutic target and the kinase inhibitor.

However, one of the caveats of measuring IC_{50} values in determining kinase inhibitor potency and selectivity is that IC_{50} values are dependent on enzyme and substrate concentrations (Acker and Auld, 2014, Strelow, 2017) and the determined IC_{50} value of a molecule is the concentration of drug that inhibits 50% of the kinase activity (Cer *et al.*, 2009, Haupt *et al.*, 2015). This indicates that even highly potent inhibitors can only inhibit 50% of the kinase used in the *in vitro* kinase reaction to determine their IC_{50} values – thus suggesting that IC_{50} measurements are not the best indicators of inhibitor potency especially if the concentration of kinase used in the assay is high. Unfortunately, the lowest concentration of enzyme used that gave a reliable measure of IC_{50} with recombinant *Pf*CLK3 in these experiments was 50 nM. Thus, the measured IC_{50} cannot be less than 50% of the concentration of kinase used. Hence, the determined IC_{50} values might in fact be lower for these potentially highly potent inhibitors if a smaller

concentration of kinase was used in the inhibition assays. A more reliable measure to determine inhibitor potency have been identified as measuring the K_i value, an intrinsic, thermo-dynamic quantity independent of the substrate but dependent on the interactions of enzyme and inhibitor (Cer *et al.*, 2009). The relationship between K_i and IC_{50} values determined when the concentration of substrate is equal to the K_m , the mechanism of inhibition is: non-competitive inhibition, $K_i = IC_{50}$; competitive and uncompetitive inhibition, $K_i = IC_{50}/2$; mixed inhibition K_i values range from IC_{50} to $IC_{50}/2$ (Cer *et al.*, 2009). This means that any factor that has an effect on IC_{50} would directly affect the K_i and hence the determined mechanism. Hence, the mechanism of inhibition determined for the inhibitors TCMDC-135051 and TCMDC-138736 in Chapter 4 could only be handle with caution because of these limitations.

In conclusion, the work reported in this Thesis has shown novel data validating *PfCLK3* as a suitable antimalarial therapeutic target. This gene is expressed at all stages of parasite development and conserved across different *Plasmodium* species. The *Plasmodium* CLK3 gene is therefore a useful therapeutic target for symptomatic treatment and transmission blocking of malaria.

9.2 Future work

9.2.1 Conditional knockout

To fully address the protein functionality of PfCLK3 kinase, it is important to have a parasite in which the *PfCLK3* gene can be conditionally knocked out to evaluate its function. Conditional knockout, the move from functional inhibition to destruction of protein is useful in addition to enabling the targeting of proteins that seemed undruggable (Berndt *et al.*, 2017) to evaluating the functions of a gene without the use of an external factor like an inhibitor which in some cases result in off-target effects.

9.2.2 Inhibition of asexual parasites in animal malaria challenge

The data clearly shows that inhibiting *PfCLK3* blocks the development of asexual parasites and interrupt parasite life cycle in *in vitro* cultures. This interruption may not be reflective of the potency of the inhibitor when used in humans; hence the need to confirmed this. Controlled human malaria infection (CHMI) is an effective mechanism to evaluate the efficacy of test drugs. However, because uses of CHMI are complicated and requires stringent ethical procedures (Njue *et al.*, 2018), this option is not easily available. However, mouse models and the mouse malaria species *P. berghei* are used as alternatives in *in vivo* animal model drug assays. These experiments are done by establishing an infection in animal models and then treating them with the inhibitor using two controls; an untreated control, a treated control with standard antimalarial and treatment with the test *PfCLK3* inhibitor. The 3 data sets are compared and a successful treatment with the test drug would give results similar to the control-drug treated mice.

9.2.3 Transmission blocking

Inhibition of *PbCLK3* kinase as reported here and the inhibition of *P. berghei* sporozoites and asexual parasites with an EC_{50} at submicromolar concentration as reported by Alam and colleagues together with the inhibition of stage II gametocytes suggest transmission blocking activity possibility of this therapeutic target (Alam *et al.*, 2018). However, the data presented by both these studies is not a sufficient proof of transmission-blocking capacity of this kinase inhibitor and therefore a detailed analysis of this is needed to confirm this hypothesis. A proof of concept experiment can be done using laboratory reared mosquitoes and animal models through a feeding assay. Using the mosquitoes, stage V gametocytes are feed to the mosquitoes through a membrane-feeding assay and the number of oocysts formed counted compared to untreated control. Furthermore, the infectivity of these oocysts could be confirmed by allowing the infective mosquitoes to feed on animal models and the number of infected animals counted.

9.2.4 Bigger Clinical study

Although TCMDC-135051 is not an approved drug and might still need further optimisation before any clinical trails, testing its efficacy against asexual clinical isolates would give an indication of its potency. A small sample size was used to get a pilot data of this efficacy and great efficacy is demonstrated with a fast acting activity against clinical isolates. However, for a more reliable data, a properly designed study with the desired criteria such as parasitaemia at recruitment and so on can be designed and executed. Also, any samples from such a study can be sequenced to determine the polymorphism of *Plasmodium* CLK3 gene and how that would affect parasite sensitivity to inhibition.

9.2.5 Crystal Structure

Although a bitopic mode of inhibition is suggested for the *Pf*CLK3 kinase inhibitor, it would be great if this is confirmed through co-crystal structure of the kinase with the inhibitor. A crystal structure of full length *Pf*CLK3 kinase generated in complex with TCMDC-135051 would give a clear picture of the binding mode of the inhibitor by revealing the Structure Activity Relationship (SAR). Additionally, a co-crystal structure of the inhibitor with the mutant *Pf*CLK3_H259P and the kinase domain only *Pf*CLK3 variant would further reveal in more details the actual binding mechanism of the inhibitor, and whether or not it binds to an allosteric site and the ATP-binding site or only at the allosteric site will be defined. Once revealed that the inhibitor binds to an allosteric site, this can then be confirmed by generating mutations around the binding site to confirm binding in the form of a target validation approach, an approach similar to one used in GPCR (G-protein coupled receptors) research that confirmed the binding of GSK1034702 to the allosteric site instead of the orthosteric site (Bradley *et al.*, 2018).

Reference:

- ACKER, M. G. & AULD, D. S. 2014. Considerations for the design and reporting of enzyme assays in high-throughput screening applications. *Perspectives in Science*, 1, 56-73.
- AGARWAL, S., KERN, S., HALBERT, J., PRZYBORSKI, J. M., BAUMEISTER, S., DANDEKAR, T., DOERIG, C. & PRADEL, G. 2011. Two nucleus-localized CDK-like kinases with crucial roles for malaria parasite erythrocytic replication are involved in phosphorylation of splicing factor. *J Cell Biochem*, 112, 1295-310.
- AHMED, M. A. & COX-SINGH, J. 2015. Plasmodium knowlesi – an emerging pathogen. *ISBT Sci Ser*, 10, 134-140.
- ALAM, M., SANCHEZ-AZQUETA, A., JANHA, O., FLANNERY, E., MAHINDRA, A., MAPESA, K., BRANCUCCI, N., ANTONOVA-KOCH, Y., CROUCH, K., SIMWELA, N. V., AKINWALE, J., MITCHESON, D., SOLYAKOV, L., DUDEK, K., JONES, C., ZAPATERO, C., DOERIG, C., NWAKANMA, D. C., VAZQUEZ, M.-J., COLMENAREJO, G., LAFUENTE, M.-J., LEON, M. L., WATERS, A. P., JAMIESON, A. G., ALVARO, L. E. F., MARTI, M., WINZELER, E. A., GAMO, F. J. & TOBIN, A. 2018. Validation of the protein kinase PfCLK3 as a multi-stage cross species malarial drug target. *bioRxiv*.
- ALAM, M. M., SOLYAKOV, L., BOTTRILL, A. R., FLUECK, C., SIDDIQUI, F. A., SINGH, S., MISTRY, S., VISKADURAKI, M., LEE, K., HOPP, C. S., CHITNIS, C. E., DOERIG, C., MOON, R. W., GREEN, J. L., HOLDER, A. A., BAKER, D. A. & TOBIN, A. B. 2015. Phosphoproteomics reveals malaria parasite Protein Kinase G as a signalling hub regulating egress and invasion. *Nat Commun*, 6, 7285.
- ALY, A. S., VAUGHAN, A. M. & KAPPE, S. H. 2009. Malaria parasite development in the mosquito and infection of the mammalian host. *Annu Rev Microbiol*, 63, 195-221.
- AMAMBUA-NGWA, A., OKEBE, J., MBYE, H., CEESAY, S., EL-FATOURI, F., JOOF, F., NYANG, H., JANHA, R., AFFARA, M., AHMAD, A., KOLLY, O., NWAKANMA, D. & D'ALESSANDRO, U. 2017. Sustained Ex Vivo Susceptibility of Plasmodium falciparum to Artemisinin Derivatives but Increasing Tolerance to Artemisinin Combination Therapy Partner Quinolines in The Gambia. *Antimicrobial Agents and Chemotherapy*, 61, e00759-17.
- AN, Y., YANG, S., GUO, K., MA, B. & WANG, Y. 2015. Reduced USP39 expression inhibits malignant proliferation of medullary thyroid carcinoma in vitro. *World J Surg Oncol*, 13, 255.
- ANDRADE, L. F., NAHUM, L. A., AVELAR, L. G., SILVA, L. L., ZERLOTINI, A., RUIZ, J. C. & OLIVEIRA, G. 2011. Eukaryotic protein kinases (ePKs) of the helminth parasite Schistosoma mansoni. *BMC Genomics*, 12, 215.
- ANDREWS, K. A., WESCHE, D., MCCARTHY, J., MOHRLE, J. J., TARNING, J., PHILLIPS, L., KERN, S. & GRASELA, T. 2018. Model-Informed Drug Development for Malaria Therapeutics. *Annu Rev Pharmacol Toxicol*, 58, 567-582.
- ANKO, M. L. 2014. Regulation of gene expression programmes by serine-arginine rich splicing factors. *Semin Cell Dev Biol*, 32, 11-21.
- ANSTEY, N. M., RUSSELL, B., YEO, T. W. & PRICE, R. N. 2009. The pathophysiology of vivax malaria. *Trends Parasitol*, 25, 220-7.

- ARAKI, S., DAIRIKI, R., NAKAYAMA, Y., MURAI, A., MIYASHITA, R., IWATANI, M., NOMURA, T. & NAKANISHI, O. 2015. Inhibitors of CLK Protein Kinases Suppress Cell Growth and Induce Apoptosis by Modulating Pre-mRNA Splicing. *PLoS One*, 10, e0116929.
- ARDITO, F., GIULIANI, M., PERRONE, D., TROIANO, G. & MUZIO, L. L. 2017. The crucial role of protein phosphorylation in cell signaling and its use as targeted therapy (Review). *International Journal of Molecular Medicine*, 40, 271-280.
- ARENCIBIA, J. M., PASTOR-FLORES, D., BAUER, A. F., SCHULZE, J. O. & BIONDI, R. M. 2013. AGC protein kinases: from structural mechanism of regulation to allosteric drug development for the treatment of human diseases. *Biochim Biophys Acta*, 1834, 1302-21.
- ASHLEY, E. A., DHORDA, M., FAIRHURST, R. M., AMARATUNGA, C., LIM, P., SUON, S., SRENG, S., ANDERSON, J. M., MAO, S., SAM, B., SOPHA, C., CHUOR, C. M., NGUON, C., SOVANNAROTH, S., PUKRITTAYAKAMEE, S., JITTAMALA, P., CHOTIVANICH, K., CHUTASMIT, K., SUCHATSOONTHORN, C., RUNCHAROEN, R., HIEN, T. T., THUY-NHIEN, N. T., THANH, N. V., PHU, N. H., HTUT, Y., HAN, K. T., AYE, K. H., MOKUOLU, O. A., OLAOSEBIKAN, R. R., FOLARANMI, O. O., MAYXAY, M., KHANTHAVONG, M., HONGVANTHONG, B., NEWTON, P. N., ONYAMBOKO, M. A., FANELLO, C. I., TSHEFU, A. K., MISHRA, N., VALECHA, N., PHYO, A. P., NOSTEN, F., YI, P., TRIPURA, R., BORRMANN, S., BASHRAHEIL, M., PESHU, J., FAIZ, M. A., GHOSE, A., HOSSAIN, M. A., SAMAD, R., RAHMAN, M. R., HASAN, M. M., ISLAM, A., MIOTTO, O., AMATO, R., MACINNIS, B., STALKER, J., KWIATKOWSKI, D. P., BOZDECH, Z., JEEYAPANT, A., CHEAH, P. Y., SAKULTHAEW, T., CHALK, J., INTHARABUT, B., SILAMUT, K., LEE, S. J., VIHOKHERN, B., KUNASOL, C., IMWONG, M., TARNING, J., TAYLOR, W. J., YEUNG, S., WOODROW, C. J., FLEGG, J. A., DAS, D., SMITH, J., VENKATESAN, M., PLOWE, C. V., STEPNIIEWSKA, K., GUERIN, P. J., DONDORP, A. M., DAY, N. P., WHITE, N. J. & TRACKING RESISTANCE TO ARTEMISININ, C. 2014. Spread of artemisinin resistance in *Plasmodium falciparum* malaria. *N Engl J Med*, 371, 411-23.
- AWASTHI, G. & DAS, A. 2013. Genetics of chloroquine-resistant malaria: a haplotypic view. *Memórias do Instituto Oswaldo Cruz*, 108, 947-961.
- BACHMANN, A., PETTER, M., TILLY, A.-K., BILLER, L., ULICZKA, K. A., DUFFY, M. F., TANNICH, E. & BRUCHHAUS, I. 2012. Temporal Expression and Localization Patterns of Variant Surface Antigens in Clinical *Plasmodium falciparum* Isolates during Erythrocyte Schizogony. *PLOS ONE*, 7, e49540.
- BAIRD, J. K. 2004. Chloroquine Resistance in *Plasmodium vivax*. *Antimicrobial Agents and Chemotherapy*, 48, 4075.
- BAKER, D. A. 2010. Malaria gametocytogenesis. *Molecular and Biochemical Parasitology*, 172, 57-65.
- BALABASKARAN-NINA, P. & DESAI, S. A. 2018. Diverse target gene modifications in *Plasmodium falciparum* using Bxb1 integrase and an intronic attB. *Parasites & vectors*, 11, 548-548.
- BANSAL, A., MOLINA-CRUZ, A., BRZOSTOWSKI, J., LIU, P., LUO, Y., GUNALAN, K., LI, Y., RIBEIRO, J. M. C. & MILLER, L. H. 2018. PfCDPK1 is critical for malaria parasite gametogenesis and mosquito infection. *Proc Natl Acad Sci U S A*, 115, 774-779.

- BANSAL, A., SINGH, S., MORE, K. R., HANS, D., NANGALIA, K., YOGAVEL, M., SHARMA, A. & CHITNIS, C. E. 2013. Characterization of Plasmodium falciparum calcium-dependent protein kinase 1 (PfCDPK1) and its role in microneme secretion during erythrocyte invasion. *J Biol Chem*, 288, 1590-602.
- BARAGAÑA, B., HALLYBURTON, I., LEE, M. C. S., NORCROSS, N. R., GRIMALDI, R., OTTO, T. D., PROTO, W. R., BLAGBOROUGH, A. M., MEISTER, S., WIRJANATA, G., RUECKER, A., UPTON, L. M., ABRAHAM, T. S., ALMEIDA, M. J., PRADHAN, A., PORZELLE, A., MARTÍNEZ, M. S., BOLSCHER, J. M., WOODLAND, A., NORVAL, S., ZUCCOTTO, F., THOMAS, J., SIMEONS, F., STOJANOVSKI, L., OSUNA-CABELLO, M., BROCK, P. M., CHURCHER, T. S., SALA, K. A., ZAKUTANSKY, S. E., JIMÉNEZ-DÍAZ, M. B., SANZ, L. M., RILEY, J., BASAK, R., CAMPBELL, M., AVERY, V. M., SAUERWEIN, R. W., DECHERING, K. J., NOVIYANTI, R., CAMPO, B., FREARSON, J. A., ANGULO-BARTUREN, I., FERRER-BAZAGA, S., GAMO, F. J., WYATT, P. G., LEROY, D., SIEGL, P., DELVES, M. J., KYLE, D. E., WITTLIN, S., MARFURT, J., PRICE, R. N., SINDEN, R. E., WINZELER, E., CHARMAN, S. A., BEBREVSKA, L., GRAY, D. W., CAMPBELL, S., FAIRLAMB, A. H., WILLIS, P., RAYNER, J. C., FIDOCK, D. A., READ, K. D. & GILBERT, I. H. 2015. A novel multiple-stage antimalarial agent that inhibits protein synthesis. *Nature*, 522, 315-320.
- BARENG, A. P., ESPINO, F. E., CHAIJAROENKUL, W. & NA-BANGCHANG, K. 2018. Molecular monitoring of dihydrofolatereductase (dhfr) and dihydropteroatesynthetase (dhps) associated with sulfadoxine-pyrimethamine resistance in Plasmodium vivax isolates of Palawan, Philippines. *Acta Trop*, 180, 81-87.
- BASNET, S. K. C., DIAB, S., SCHMID, R., YU, M., YANG, Y., GILLAM, T. A., TEO, T., LI, P., PEAT, T., ALBRECHT, H. & WANG, S. 2015. Identification of a Highly Conserved Allosteric Binding Site on Mnk1 and Mnk2. *Molecular Pharmacology*, 88, 935.
- BEEHARRY, N., BANINA, E., HITTLE, J., SKOBELEVA, N., KHAZAK, V., DEACON, S., ANDRAKE, M., EGLESTON, B. L., PETERSON, J. R., ASTSATUROV, I. & YEN, T. J. 2014. Re-purposing clinical kinase inhibitors to enhance chemosensitivity by overriding checkpoints. *Cell Cycle*, 13, 2172-2191.
- BELLANCA, S., SUMMERS, R. L., MEYRATH, M., DAVE, A., NASH, M. N., DITTMER, M., SANCHEZ, C. P., STEIN, W. D., MARTIN, R. E. & LANZER, M. 2014. Multiple drugs compete for transport via the Plasmodium falciparum chloroquine resistance transporter at distinct but interdependent sites. *J Biol Chem*, 289, 36336-51.
- BENNINK, S., KIESOW, M. J. & PRADEL, G. 2016. The development of malaria parasites in the mosquito midgut. *Cell Microbiol*, 18, 905-18.
- BERNDT, N., KARIM, R. M. & SCHONBRUNN, E. 2017. Advances of small molecule targeting of kinases. *Curr Opin Chem Biol*, 39, 126-132.
- BHARATI, K. & GANGULY, N. K. 2013. Tackling the malaria problem in the South-East Asia Region: Need for a change in policy? *The Indian Journal of Medical Research*, 137, 36-47.
- BHATT, S., WEISS, D. J., CAMERON, E., BISANZIO, D., MAPPIN, B., DALRYMPLE, U., BATTLE, K. E., MOYES, C. L., HENRY, A., ECKHOFF, P. A., WENGER, E. A., BRIËT, O., PENNY, M. A., SMITH, T. A., BENNETT, A., YUKICH, J., EISELE, T. P., GRIFFIN, J. T., FERGUS, C. A., LYNCH, M., LINDGREN, F., COHEN, J. M., MURRAY, C. L. J., SMITH, D. L., HAY, S. I., CIBULSKIS, R. E.

- & GETHING, P. W. 2015. The effect of malaria control on *Plasmodium falciparum* in Africa between 2000 and 2015. *Nature*, 526, 207.
- BIJKER, E. M., BORRMANN, S., KAPPE, S. H., MORDMÜLLER, B., SACK, B. K. & KHAN, S. M. 2015. Novel approaches to whole sporozoite vaccination against malaria. *Vaccine*, 33, 7462-7468.
- BLANC, J., GENEY, R. & MENET, C. 2013. Type II Kinase Inhibitors: An Opportunity in Cancer for Rational Design. *Anti-Cancer Agents in Medicinal Chemistry*, 13, 731-747.
- BLASCO, B., LEROY, D. & FIDOCK, D. A. 2017. Antimalarial drug resistance: linking *Plasmodium falciparum* parasite biology to the clinic. *Nature Medicine*, 23, 917.
- BOESLER, C., RIGO, N., ANOKHINA, M. M., TAUCHERT, M. J., AGAFONOV, D. E., KASTNER, B., URLAUB, H., FICNER, R., WILL, C. L. & LUHRMANN, R. 2016. A spliceosome intermediate with loosely associated tri-snRNP accumulates in the absence of Prp28 ATPase activity. *Nat Commun*, 7, 11997.
- BOUDHAR, A., NG, X. W., LOH, C. Y., CHIA, W. N., TAN, Z. M., NOSTEN, F., DYMOCK, B. W. & TAN, K. S. 2016. Overcoming Chloroquine Resistance in Malaria: Design, Synthesis, and Structure-Activity Relationships of Novel Hybrid Compounds. *Antimicrob Agents Chemother*, 60, 3076-89.
- BOUSEMA, T. & DRAKELEY, C. 2011. Epidemiology and infectivity of *Plasmodium falciparum* and *Plasmodium vivax* gametocytes in relation to malaria control and elimination. *Clin Microbiol Rev*, 24, 377-410.
- BRADLEY, S. J., MOLLOY, C., BUNDGAARD, C., MOGG, A. J., THOMPSON, K. J., DWOMOH, L., SANGER, H. E., CRABTREE, M. D., BROOKE, S. M., SEXTON, P. M., FELDER, C. C., CHRISTOPOULOS, A., BROAD, L. M., TOBIN, A. B. & LANGMEAD, C. J. 2018. Bitopic Binding Mode of an M(1) Muscarinic Acetylcholine Receptor Agonist Associated with Adverse Clinical Trial Outcomes. *Molecular Pharmacology*, 93, 645-656.
- BRANCUCCI, N. M. B., GERDT, J. P., WANG, C., DE NIZ, M., PHILIP, N., ADAPA, S. R., ZHANG, M., HITZ, E., NIEDERWIESER, I., BOLTRYK, S. D., LAFFITTE, M. C., CLARK, M. A., GRURING, C., RAVEL, D., BLANCKE SOARES, A., DEMAS, A., BOPP, S., RUBIO-RUIZ, B., CONEJO-GARCIA, A., WIRTH, D. F., GENDASZEWSKA-DARMACH, E., DURASINGH, M. T., ADAMS, J. H., VOSS, T. S., WATERS, A. P., JIANG, R. H. Y., CLARDY, J. & MARTI, M. 2017. Lysophosphatidylcholine Regulates Sexual Stage Differentiation in the Human Malaria Parasite *Plasmodium falciparum*. *Cell*, 171, 1532-1544 e15.
- BRAUN, V., REMPIS, E., SCHNACK, A., DECKER, S., RUBAIHAYO, J., TUMWESIGYE, N. M., THEURING, S., HARMS, G., BUSINGYE, P. & MOCKENHAUPT, F. P. 2015. Lack of effect of intermittent preventive treatment for malaria in pregnancy and intense drug resistance in western Uganda. *Malaria Journal*, 14, 372.
- BROCHET, M. & BILLKER, O. 2016. Calcium signalling in malaria parasites. *Mol Microbiol*, 100, 397-408.
- BROCHET, M., COLLINS, M. O., SMITH, T. K., THOMPSON, E., SEBASTIAN, S., VOLKMANN, K., SCHWACH, F., CHAPPELL, L., GOMES, A. R., BERRIMAN, M., RAYNER, J. C., BAKER, D. A., CHOUDHARY, J. & BILLKER, O. 2014a. Phosphoinositide Metabolism Links cGMP-Dependent Protein Kinase G to Essential Ca²⁺ Signals at Key Decision Points in the Life Cycle of Malaria Parasites. *PLOS Biology*, 12, e1001806.

- BROCHET, M., COLLINS, M. O., SMITH, T. K., THOMPSON, E., SEBASTIAN, S., VOLKMANN, K., SCHWACH, F., CHAPPELL, L., GOMES, A. R., BERRIMAN, M., RAYNER, J. C., BAKER, D. A., CHOUDHARY, J. & BILLKER, O. 2014b. Phosphoinositide metabolism links cGMP-dependent protein kinase G to essential Ca(2)(+) signals at key decision points in the life cycle of malaria parasites. *PLoS Biol*, 12, e1001806.
- BULLOCK, A. N., DAS, S., DEBRECZENI, J. E., RELLOS, P., FEDOROV, O., NIESEN, F. H., GUO, K., PAPAGRIGORIOU, E., AMOS, A. L., CHO, S., TURK, B. E., GHOSH, G. & KNAPP, S. 2009. Kinase domain insertions define distinct roles of CLK kinases in SR protein phosphorylation. *Structure*, 17, 352-62.
- BURROWS, J. N., DUPARC, S., GUTTERIDGE, W. E., HOOFT VAN HUIJSDUIJNEN, R., KASZUBSKA, W., MACINTYRE, F., MAZZURI, S., MÖHRLE, J. J. & WELLS, T. N. C. 2017. New developments in anti-malarial target candidate and product profiles. *Malaria Journal*, 16, 26.
- CACACE, E., KRITIKOS, G. & TYPAS, A. 2017. Chemical genetics in drug discovery. *Current Opinion in Systems Biology*, 4, 35-42.
- CARTER, L. M., POLLITT, L. C., WILSON, L. G. & REECE, S. E. 2016. Ecological influences on the behaviour and fertility of malaria parasites. *Malaria Journal*, 15, 220.
- CEESAY, S. J., CASALS-PASCUAL, C., ERSKINE, J., ANYA, S. E., DUAH, N. O., FULFORD, A. J., SESAY, S. S., ABUBAKAR, I., DUNYO, S., SEY, O., PALMER, A., FOFANA, M., CORRAH, T., BOJANG, K. A., WHITTLE, H. C., GREENWOOD, B. M. & CONWAY, D. J. 2008. Changes in malaria indices between 1999 and 2007 in The Gambia: a retrospective analysis. *Lancet*, 372, 1545-54.
- CER, R. Z., MUDUNURI, U., STEPHENS, R. & LEBEDA, F. J. 2009. IC50-to-Ki: a web-based tool for converting IC50 to Ki values for inhibitors of enzyme activity and ligand binding. *Nucleic acids research*, 37, W441-W445.
- CHINAPPI, M., VIA, A., MARCATILI, P. & TRAMONTANO, A. 2010. On the Mechanism of Chloroquine Resistance in Plasmodium falciparum. *PLOS ONE*, 5, e14064.
- CLASER, C., MALLERET, B., GUN, S. Y., WONG, A. Y. W., CHANG, Z. W., TEO, P., SEE, P. C. E., HOWLAND, S. W., GINHOUX, F. & RÉNIA, L. 2011. CD8+ T Cells and IFN- γ Mediate the Time-Dependent Accumulation of Infected Red Blood Cells in Deep Organs during Experimental Cerebral Malaria. *PLOS ONE*, 6, e18720.
- COELHO, C. H., DORITCHAMOU, J. Y. A., ZAIDI, I. & DUFFY, P. E. 2017. Advances in malaria vaccine development: report from the 2017 malaria vaccine symposium. *NPJ Vaccines*, 2, 34.
- COLEMAN, S., DADZIE, S. K., SEYOUM, A., YIHDEGO, Y., MUMBA, P., DENGELA, D., RICKS, P., GEORGE, K., FORNADEL, C., SZUMLAS, D., PSYCHAS, P., WILLIAMS, J., APPAWU, M. A. & BOAKYE, D. A. 2017. A reduction in malaria transmission intensity in Northern Ghana after 7 years of indoor residual spraying. *Malaria Journal*, 16, 324.
- COLLINS, C. R., HACKETT, F., ATID, J., TAN, M. S. Y. & BLACKMAN, M. J. 2017. The Plasmodium falciparum pseudoprotease SERA5 regulates the kinetics and efficiency of malaria parasite egress from host erythrocytes. *PLOS Pathogens*, 13, e1006453.
- COSTA, G., GILDENHARD, M., ELDERING, M., LINDQUIST, R. L., HAUSER, A. E., SAUERWEIN, R., GOOSMANN, C., BRINKMANN, V., CARRILLO-

- BUSTAMANTE, P. & LEVASHINA, E. A. 2018. Non-competitive resource exploitation within mosquito shapes within-host malaria infectivity and virulence. *Nature Communications*, 9, 3474.
- COWMAN, A. F., HEALER, J., MARAPANA, D. & MARSH, K. 2016. Malaria: Biology and Disease. *Cell*, 167, 610-624.
- CROMPTON, P. D., MOEBIUS, J., PORTUGAL, S., WAISBERG, M., HART, G., GARVER, L. S., MILLER, L. H., BARILLAS-MURY, C. & PIERCE, S. K. 2014. Malaria immunity in man and mosquito: insights into unsolved mysteries of a deadly infectious disease. *Annu Rev Immunol*, 32, 157-87.
- CROSNIER, C., BUSTAMANTE, L. Y., BARTHOLDSON, S. J., BEI, A. K., THERON, M., UCHIKAWA, M., MBOUP, S., NDIR, O., KWIATKOWSKI, D. P., DURAISINGH, M. T., RAYNER, J. C. & WRIGHT, G. J. 2011. BASIGIN is a receptor essential for erythrocyte invasion by *Plasmodium falciparum*. *Nature*, 480, 534-537.
- CUI, L. & SU, X.-Z. 2009. Discovery, mechanisms of action and combination therapy of artemisinin. *Expert review of anti-infective therapy*, 7, 999-1013.
- CUI, L., WANG, Z., MIAO, J., MIAO, M., CHANDRA, R., JIANG, H., SU, X. Z. & CUI, L. 2012. Mechanisms of in vitro resistance to dihydroartemisinin in *Plasmodium falciparum*. *Mol Microbiol*, 86, 111-28.
- D'ALESSANDRO, U., HILL, J., TARNING, J., PELL, C., WEBSTER, J., GUTMAN, J. & SEVENE, E. 2018. Treatment of uncomplicated and severe malaria during pregnancy. *Lancet Infect Dis*, 18, e133-e146.
- DAR, A. C. & SHOKAT, K. M. 2011. The evolution of protein kinase inhibitors from antagonists to agonists of cellular signaling. *Annu Rev Biochem*, 80, 769-95.
- DAVIS, M. I., HUNT, J. P., HERRGARD, S., CICERI, P., WODICKA, L. M., PALLARES, G., HOCKER, M., TREIBER, D. K. & ZARRINKAR, P. P. 2011. Comprehensive analysis of kinase inhibitor selectivity. *Nat Biotechnol*, 29, 1046-51.
- DE LAVAL, F., SIMON, F., BOGREAU, H., RAPP, C., WURTZ, N., OLIVER, M., DEMAISON, X., DIA, A., DE PINA, J. J., MERENS, A. & MIGLIANI, R. 2014. Emergence of *Plasmodium ovale* malaria among the French Armed Forces in the Republic of Ivory Coast: 20 years of clinical and biological experience. *Clin Infect Dis*, 58, e122-8.
- DE OLIVEIRA, P. S. L., FERRAZ, F. A. N., PENA, D. A., PRAMIO, D. T., MORAIS, F. A. & SCHECHTMAN, D. 2016. Revisiting protein kinase–substrate interactions: Toward therapeutic development. *Science Signaling*, 9, re3.
- DELVES, M., PLOUFFE, D., SCHEURER, C., MEISTER, S., WITTLIN, S., WINZELER, E. A., SINDEN, R. E. & LEROY, D. 2012. The activities of current antimalarial drugs on the life cycle stages of *Plasmodium*: a comparative study with human and rodent parasites. *PLoS Med*, 9, e1001169.
- DESAI, M., HILL, J., FERNANDES, S., WALKER, P., PELL, C., GUTMAN, J., KAYENTAO, K., GONZALEZ, R., WEBSTER, J., GREENWOOD, B., COT, M. & TER KUILE, F. O. 2018. Prevention of malaria in pregnancy. *The Lancet Infectious Diseases*, 18, e119-e132.
- DIEYE, B., AFFARA, M., SANGARE, L., JOOF, F., NDIAYE, Y. D., GOMIS, J. F., NDIAYE, M., MBAYE, A., DIAKITE, M., SY, N., MBENGUE, B., DEME, A. B., DANIELS, R., AHOUIDI, A. D., DIEYE, T., ABDULLAHI, A., DOUMBIA,

- S., NDIAYE, J. L., DIARRA, A., ISMAELA, A., COULIBALY, M., WELTY, C., NGWA, A. A., SHAFFER, J., D'ALESSANDRO, U., VOLKMAN, S. K., WIRTH, D. F., KROGSTAD, D. J., KOITA, O., NWAKANMA, D. & NDIAYE, D. 2016. West Africa International Centers of Excellence for Malaria Research: Drug Resistance Patterns to Artemether-Lumefantrine in Senegal, Mali, and The Gambia. *Am J Trop Med Hyg*, 95, 1054-1060.
- DINKO, B., OGUIKE, M. C., LARBI, J. A., BOUSEMA, T. & SUTHERLAND, C. J. 2013. Persistent detection of *Plasmodium falciparum*, *P. malariae*, *P. ovale curtisi* and *P. ovale wallikeri* after ACT treatment of asymptomatic Ghanaian school-children. *International Journal for Parasitology: Drugs and Drug Resistance*, 3, 45-50.
- DIXIT, A., SINGH, P. K., SHARMA, G. P., MALHOTRA, P. & SHARMA, P. 2010. PfsRPK1, a novel splicing-related kinase from *Plasmodium falciparum*. *J Biol Chem*, 285, 38315-23.
- DIXIT, A., YI, L., GOWTHAMAN, R., TORKAMANI, A., SCHORK, N. J. & VERKHIVKER, G. M. 2009. r. *PLOS ONE*, 4, e7485.
- DOERIG, C. 2004. Protein kinases as targets for anti-parasitic chemotherapy. *Biochim Biophys Acta*, 1697, 155-68.
- DOERIG, C., BILLKER, O., HAYSTEAD, T., SHARMA, P., TOBIN, A. B. & WATERS, N. C. 2008. Protein kinases of malaria parasites: an update. *Trends Parasitol*, 24, 570-7.
- DOERIG, C., RAYNER, J. C., SCHERF, A. & TOBIN, A. B. 2015. Post-translational protein modifications in malaria parasites. *Nat Rev Microbiol*, 13, 160-72.
- DOMINGUEZ, D., TSAI, Y. H., WEATHERITT, R., WANG, Y., BLENCOWE, B. J. & WANG, Z. 2016. An extensive program of periodic alternative splicing linked to cell cycle progression. *Elife*, 5.
- DONDORP, A. M., NOSTEN, F., YI, P., DAS, D., AUNG PHAE PHYO, A. P., TARNING, J., LWIN, K. M., ARIEY, F., HANPITHAKPONG, W., LEE, S. J., RINGWALD, P., SILAMUT, K., IMWONG, M., CHOTIVANICH, K., LIM, P., HERDMAN, T., S.S., A., YEUNG, S., SINGHASIVANON, P., DAY, N. P. J., LINDEGARDH, N., SOCHEAT, D. A. & WHITE, N. J. 2009. Artemisinin Resistance in *Plasmodium falciparum* Malaria. *The new england journal of medicine*, 361, 455-467.
- DONG, C. K., URGAONKAR, S., CORTESE, J. F., GAMO, F.-J., GARCIA-BUSTOS, J. F., LAFUENTE, M. J., PATEL, V., ROSS, L., COLEMAN, B. I., DERBYSHIRE, E. R., CLISH, C. B., SERRANO, A. E., CROMWELL, M., BARKER, R. H., JR., DVORIN, J. D., DURASINGH, M. T., WIRTH, D. F., CLARDY, J. & MAZITSCHKE, R. 2011. Identification and validation of tetracyclic benzothiazepines as *Plasmodium falciparum* cytochrome bc1 inhibitors. *Chemistry & biology*, 18, 1602-1610.
- DOOLAN, D. L., DOBANO, C. & BAIRD, J. K. 2009. Acquired immunity to malaria. *Clin Microbiol Rev*, 22, 13-36, Table of Contents.
- DOUGLAS, A. D., WILLIAMS, A. R., ILLINGWORTH, J. J., KAMUYU, G., BISWAS, S., GOODMAN, A. L., WYLLIE, D. H., CROSNIER, C., MIURA, K., WRIGHT, G. J., LONG, C. A., OSIER, F. H., MARSH, K., TURNER, A. V., HILL, A. V. & DRAPER, S. J. 2011. The blood-stage malaria antigen PfrH5 is susceptible to vaccine-inducible cross-strain neutralizing antibody. *Nat Commun*, 2, 601.
- DRANCHAK, P., MACARTHUR, R., GUHA, R., ZUERCHER, W. J., DREWRY, D. H., AULD, D. S. & INGLESE, J. 2013. Profile of the GSK published protein

- kinase inhibitor set across ATP-dependent and-independent luciferases: implications for reporter-gene assays. *PLoS One*, 8, e57888.
- DRAPER, S. J., SACK, B. K., KING, C. R., NIELSEN, C. M., RAYNER, J. C., HIGGINS, M. K., LONG, C. A. & SEDER, R. A. 2018. Malaria Vaccines: Recent Advances and New Horizons. *Cell Host & Microbe*, 24, 43-56.
- ECKER, A., LEHANE, A. M., CLAIN, J. & FIDOCK, D. A. 2012. PfCRT and its role in antimalarial drug resistance. *Trends in parasitology*, 28, 504-514.
- EKSI, S., MORAHAN, B. J., HAILE, Y., FURUYA, T., JIANG, H., ALI, O., XU, H., KIATTIBUTR, K., SURU, A., CZESNY, B., ADEYEMO, A., MYERS, T. G., SATTABONGKOT, J., SU, X. Z. & WILLIAMSON, K. C. 2012. Plasmodium falciparum gametocyte development 1 (Pfgdv1) and gametocytogenesis early gene identification and commitment to sexual development. *PLoS Pathog*, 8, e1002964.
- EMAMI, S. N., RANFORD-CARTWRIGHT, L. C. & FERGUSON, H. M. 2017. The transmission potential of malaria-infected mosquitoes (*An.gambiae*-Keele, *An.arabiensis*-Ifakara) is altered by the vertebrate blood type they consume during parasite development. *Scientific Reports*, 7, 40520.
- ESHAR, S., ALLEMAND, E., SEBAG, A., GLASER, F., MUCHARDT, C., MANDEL-GUTFREUND, Y., KARNI, R. & DZIKOWSKI, R. 2012. A novel Plasmodium falciparum SR protein is an alternative splicing factor required for the parasites' proliferation in human erythrocytes. *Nucleic Acids Res*, 40, 9903-16.
- FABBRO, D. 2015. 25 Years of Small Molecular Weight Kinase Inhibitors: Potentials and Limitations. *Molecular Pharmacology*, 87, 766.
- FANG, H., KLAGES, N., BAECHLER, B., HILLNER, E., YU, L., PARDO, M., CHOUDHARY, J. & BROCHET, M. 2017. Multiple short windows of calcium-dependent protein kinase 4 activity coordinate distinct cell cycle events during Plasmodium gametogenesis. *eLife*, 6, e26524.
- FARID, R., DIXON, M. W., TILLEY, L. & MCCARTHY, J. S. 2017. Initiation of gametocytogenesis at very low parasite density in Plasmodium falciparum infection. *The Journal of Infectious Diseases*, 215, 1167-1174.
- FASANO, M., CORTE, C. M. D., CALIFANO, R., CAPUANO, A., TROIANI, T., MARTINELLI, E., CIARDIELLO, F. & MORGILLO, F. 2014. Type III or allosteric kinase inhibitors for the treatment of non-small cell lung cancer. *Expert Opinion on Investigational Drugs*, 23, 809-821.
- FEDOROV, O., HUBER, K., EISENREICH, A., FILIPPAKOPOULOS, P., KING, O., BULLOCK, A. N., SZKLARCZYK, D., JENSEN, L. J., FABBRO, D., TRAPPE, J., RAUCH, U., BRACHER, F. & KNAPP, S. 2011. Specific CLK inhibitors from a novel chemotype for regulation of alternative splicing. *Chem Biol*, 18, 67-76.
- FICA, S. M., TUTTLE, N., NOVAK, T., LI, N. S., LU, J., KOODATHINGAL, P., DAI, Q., STALEY, J. P. & PICCIRILLI, J. A. 2013. RNA catalyses nuclear pre-mRNA splicing. *Nature*, 503, 229-34.
- FLANNERY, E. L., CHATTERJEE, A. K. & WINZELER, E. A. 2013. Antimalarial drug discovery - approaches and progress towards new medicines. *Nat Rev Microbiol*, 11, 849-62.
- FORNACE, K. M., HERMAN, L. S., ABIDIN, T. R., CHUA, T. H., DAIM, S., LORENZO, P. J., GRIGNARD, L., NUIN, N. A., YING, L. T., GRIGG, M. J., WILLIAM, T., ESPINO, F., COX, J., TETTEH, K. K. A. & DRAKELEY, C. J. 2018. Exposure and infection to Plasmodium knowlesi in case study communities in

- Northern Sabah, Malaysia and Palawan, The Philippines. *PLOS Neglected Tropical Diseases*, 12, e0006432.
- FRANCIS, S. H., BUSCH, J. L., CORBIN, J. D. & SIBLEY, D. 2010. cGMP-dependent protein kinases and cGMP phosphodiesterases in nitric oxide and cGMP action. *Pharmacol Rev*, 62, 525-63.
- FROSCH, A. E., LAUFER, M. K., MATHANGA, D. P., TAKALA-HARRISON, S., SKARBINSKI, J., CLAASSEN, C. W., DZINJALAMALA, F. K. & PLOWE, C. V. 2014. Return of widespread chloroquine-sensitive *Plasmodium falciparum* to Malawi. *J Infect Dis*, 210, 1110-4.
- FUEHRER, H. P. & NOEDL, H. 2014. Recent advances in detection of *Plasmodium ovale*: implications of separation into the two species *Plasmodium ovale wallikeri* and *Plasmodium ovale curtisi*. *J Clin Microbiol*, 52, 387-91.
- GAMO, F. J., SANZ, L. M., VIDAL, J., DE COZAR, C., ALVAREZ, E., LAVANDERA, J. L., VANDERWALL, D. E., GREEN, D. V., KUMAR, V., HASAN, S., BROWN, J. R., PEISHOFF, C. E., CARDON, L. R. & GARCIA-BUSTOS, J. F. 2010. Thousands of chemical starting points for antimalarial lead identification. *Nature*, 465, 305-10.
- GAO, Y., YE, D.-Y., ZHOU, W.-C. & CHU, Y. 2017. The discovery of novel benzothiazinones as highly selective non-ATP competitive glycogen synthase kinase 3 β inhibitors for the treatment of ovarian cancer. *European Journal of Medicinal Chemistry*, 135, 370-381.
- GARG, A., LUKK, T., KUMAR, V., CHOI, J.-Y., AUGAGNEUR, Y., VOELKER, D. R., NAIR, S. & MAMOUN, C. B. 2015. Structure, Function and Inhibition of the Phosphoethanolamine Methyltransferases of the Human Malaria Parasites *Plasmodium vivax* and *Plasmodium knowlesi*. *Scientific Reports*, 5, 9064.
- GARUTI, L., ROBERTI, M. & BOTTEGONI, G. 2010. Non-ATP competitive protein kinase inhibitors. *Curr Med Chem*, 17, 2804-21.
- GERALD, N., MAHAJAN, B. & KUMAR, S. 2011. Mitosis in the human malaria parasite *Plasmodium falciparum*. *Eukaryot Cell*, 10, 474-82.
- GETHING, P. W., ELYAZAR, I. R. F., MOYES, C. L., SMITH, D. L., BATTLE, K. E., GUERRA, C. A., PATIL, A. P., TATEM, A. J., HOWES, R. E., MYERS, M. F., GEORGE, D. B., HORBY, P., WERTHEIM, H. F. L., PRICE, R. N., MÜELLER, I., BAIRD, J. K. & HAY, S. I. 2012. A Long Neglected World Malaria Map: *Plasmodium vivax* Endemicity in 2010. *PLOS Neglected Tropical Diseases*, 6, e1814.
- GHOSH, G. & ADAMS, J. A. 2011. Phosphorylation mechanism and structure of serine-arginine protein kinases. *Febs j*, 278, 587-97.
- GIERSING, B. K., MODJARRAD, K., KASLOW, D. C., OKWO-BELE, J.-M. & MOORTHY, V. S. 2016. The 2016 Vaccine Development Pipeline: A special issue from the World Health Organization Product Development for Vaccine Advisory Committee (PDVAC). *Vaccine*, 34, 2863-2864.
- GREENWOOD, B., DICKO, A., SAGARA, I., ZONGO, I., TINTO, H., CAIRNS, M., KUEPFER, I., MILLIGAN, P., OUEDRAOGO, J.-B., DOUMBO, O. & CHANDRAMOHAN, D. 2017. Seasonal vaccination against malaria: a potential use for an imperfect malaria vaccine. *Malaria Journal*, 16, 182.
- GREENWOOD, B. M., FIDOCK, D. A., KYLE, D. E., KAPPE, S. H. I., ALONSO, P. L., COLLINS, F. H. & DUFFY, P. E. 2008. Malaria: progress, perils, and

- prospects for eradication. *The Journal of Clinical Investigation*, 118, 1266-1276.
- GUERRA, C. A., HOWES, R. E., PATIL, A. P., GETHING, P. W., VAN BOECKEL, T. P., TEMPERLEY, W. H., KABARIA, C. W., TATEM, A. J., MANH, B. H., ELYAZAR, I. R. F., BAIRD, J. K., SNOW, R. W. & HAY, S. I. 2010. The International Limits and Population at Risk of Plasmodium vivax Transmission in 2009. *PLOS Neglected Tropical Diseases*, 4, e774.
- GUMIREDDY, K., BAKER, S. J., COSENZA, S. C., JOHN, P., KANG, A. D., ROBELL, K. A., REDDY, M. V. R. & REDDY, E. P. 2005. A non-ATP-competitive inhibitor of BCR-ABL overrides imatinib resistance. *Proceedings of the National Academy of Sciences of the United States of America*, 102, 1992.
- GUNALAN, K., NIANGALY, A., THERA, M. A., DOUMBO, O. K. & MILLER, L. H. 2018. Plasmodium vivax Infections of Duffy-Negative Erythrocytes: Historically Undetected or a Recent Adaptation? *Trends in Parasitology*, 34, 420-429.
- GURAL, N., MANCIO-SILVA, L., MILLER, A. B., GALSTIAN, A., BUTTY, V. L., LEVINE, S. S., PATRAPUVICH, R., DESAI, S. P., MIKOLAJCZAK, S. A., KAPPE, S. H. I., FLEMING, H. E., MARCH, S., SATTABONGKOT, J. & BHATIA, S. N. 2018. In Vitro Culture, Drug Sensitivity, and Transcriptome of Plasmodium Vivax Hypnozoites. *Cell Host Microbe*, 23, 395-406 e4.
- HALE, V. L., WATERMEYER, J. M., HACKETT, F., VIZCAY-BARRENA, G., VAN OOIJ, C., THOMAS, J. A., SPINK, M. C., HARKIOLAKI, M., DUKE, E., FLECK, R. A., BLACKMAN, M. J. & SAIBIL, H. R. 2017. Parasitophorous vacuole egress precedes its rupture and rapid host erythrocyte cytoskeleton collapse in Plasmodium falciparum. *Proceedings of the National Academy of Sciences*.
- HALLYBURTON, I., GRIMALDI, R., WOODLAND, A., BARAGAÑA, B., LUKSCH, T., SPINKS, D., JAMES, D., LEROY, D., WATERSON, D., FAIRLAMB, A. H., WYATT, P. G., GILBERT, I. H. & FREARSON, J. A. 2017a. Screening a protein kinase inhibitor library against Plasmodium falciparum. *Malaria Journal*, 16, 446.
- HALLYBURTON, I., GRIMALDI, R., WOODLAND, A., BARAGAÑA, B., LUKSCH, T., SPINKS, D., JAMES, D., LEROY, D., WATERSON, D., FAIRLAMB, A. H., WYATT, P. G., GILBERT, I. H. & FREARSON, J. A. 2017b. Screening a protein kinase inhibitor library against Plasmodium falciparum. *Malaria Journal*, 16, 446.
- HANBOONKUNUPAKARN, B. & WHITE, N. J. 2016. The threat of antimalarial drug resistance. *Tropical Diseases, Travel Medicine and Vaccines*, 2, 10.
- HANKS, S. K. 2003. Genomic analysis of the eukaryotic protein kinase superfamily- a perspective. *Genome Biology*, 4.
- HANKS, S. K. A. & HUNTER, T. 1995. Protein kinases 6. The eukaryotic protein kinase superfamily- kinase (catalytic) domain structure and classification. 9.
- HARIKISHORE, A., NIANG, M., RAJAN, S., PREISER, P. R. & YOON, H. S. 2013. Small molecule Plasmodium FKBP35 inhibitor as a potential antimalaria agent. *Scientific Reports*, 3, 2501.
- HARVEY, S. E. & CHENG, C. 2016. Methods for Characterization of Alternative RNA Splicing. *Methods Mol Biol*, 1402, 229-241.

- HAUBRICH, B. A. & SWINNEY, D. C. 2016. Enzyme Activity Assays for Protein Kinases: Strategies to Identify Active Substrates. *Curr Drug Discov Technol*, 13, 2-15.
- HAUPT, L. J., KAZMI, F., OGILVIE, B. W., BUCKLEY, D. B., SMITH, B. D., LEATHERMAN, S., PARIS, B., PARKINSON, O. & PARKINSON, A. 2015. The Reliability of Estimating K_i Values for Direct, Reversible Inhibition of Cytochrome P450 Enzymes from Corresponding IC_{50} Values: A Retrospective Analysis of 343 Experiments. *Drug Metab Dispos*, 43, 1744-50.
- HEINBERG, A. & KIRKMAN, L. 2015. The molecular basis of antifolate resistance in *Plasmodium falciparum*: looking beyond point mutations. *Ann N Y Acad Sci*, 1342, 10-8.
- HODDER, A. N., MALBY, R. L., CLARKE, O. B., FAIRLIE, W. D., COLMAN, P. M., CRABB, B. S. & SMITH, B. J. 2009. Structural insights into the protease-like antigen *Plasmodium falciparum* SERA5 and its noncanonical active-site serine. *J Mol Biol*, 392, 154-65.
- HOLZGRABE, U. & DECKER, M. 2017. Bitopic muscarinic agonists and antagonists and uses thereof: a patent evaluation of US20160136145A1. *Expert Opinion on Therapeutic Patents*, 27, 121-125.
- HOWLAND, S. W., CLASER, C., POH, C. M., GUN, S. Y. & RENIA, L. 2015. Pathogenic CD8+ T cells in experimental cerebral malaria. *Semin Immunopathol*, 37, 221-31.
- HSU, K. C., SUNG, T. Y., LIN, C. T., CHIU, Y. Y., HSU, J. T., HUNG, H. C., SUN, C. M., BARVE, I., CHEN, W. L., HUANG, W. C., HUANG, C. T., CHEN, C. H. & YANG, J. M. 2015. Anchor-based classification and type-C inhibitors for tyrosine kinases. *Sci Rep*, 5, 10938.
- HUANG, H., ZHANG, X., LI, S., LIU, N., LIAN, W., MCDOWELL, E., ZHOU, P., ZHAO, C., GUO, H., ZHANG, C., YANG, C., WEN, G., DONG, X., LU, L., MA, N., DONG, W., DOU, Q. P., WANG, X. & LIU, J. 2010. Physiological levels of ATP negatively regulate proteasome function. *Cell Research*, 20, 1372.
- HUGGINS, D. J., SHERMAN, W. & TIDOR, B. 2012. Rational approaches to improving selectivity in drug design. *J Med Chem*, 55, 1424-44.
- HUGHES, J. P., REES, S., KALINDJIAN, S. B. & PHILPOTT, K. L. 2011. Principles of early drug discovery. *British Journal of Pharmacology*, 162, 1239-1249.
- INVERGO, B. M., BROCHET, M., YU, L., CHOUDHARY, J., BELTRAO, P. & BILLKER, O. 2017. Sub-minute Phosphoregulation of Cell Cycle Systems during *Plasmodium* Gamete Formation. *Cell Reports*, 21, 2017-2029.
- ISMAIL, H. M., BARTON, V., PHANCHANA, M., CHAROENSUTTHIVARAKUL, S., WONG, M. H. L., HEMINGWAY, J., BIAGINI, G. A., O'NEILL, P. M. & WARD, S. A. 2016. Artemisinin activity-based probes identify multiple molecular targets within the asexual stage of the malaria parasites *Plasmodium falciparum* 3D7. *Proceedings of the National Academy of Sciences of the United States of America*, 113, 2080-2085.
- ISTVAN, E. S., DHARIA, N. V., BOPP, S. E., GLUZMAN, I., WINZELER, E. A. & GOLDBERG, D. E. 2011. Validation of isoleucine utilization targets in *Plasmodium falciparum*. *Proceedings of the National Academy of Sciences of the United States of America*, 108, 1627-1632.
- IYER, G. R., SINGH, S., KAUR, I., AGARWAL, S., SIDDIQUI, M. A., BANSAL, A., KUMAR, G., SAINI, E., PAUL, G., MOHMMED, A., CHITNIS, C. E. & MALHOTRA, P. 2018. Calcium-dependent phosphorylation of

- Plasmodium falciparum serine repeat antigen 5 triggers merozoite egress. *J Biol Chem*, 293, 9736-9746.
- JAIN P., KARTHIKEYAN C., MOORTHY N.S.H.N., WAIKER D.K., AND, J. A. K. & P., T. 2014. Human CDC2-Like Kinase 1 (CLK1)- A Novel Target for Alzheimer's Disease.pdf. *Current Drug Targets*, 15, 12.
- JAYABALASINGHAM, B., BANO, N. & COPPENS, I. 2010. Metamorphosis of the malaria parasite in the liver is associated with organelle clearance. *Cell research*, 20, 1043-1059.
- JESTER, B. W., GAJ, A., SHOMIN, C. D., COX, K. J. & GHOSH, I. 2012. Testing the Promiscuity of Commercial Kinase Inhibitors Against the AGC Kinase Group Using a Split-luciferase Screen. *Journal of Medicinal Chemistry*, 55, 1526-1537.
- JOHNSON, L. N., LOWE, E. D., NOBLE, M. E. M. A. & D.J., O. 1998. The structural basis for substrate recognition and control by protein kinases. *Federation of European Biochemical Societies.*, 430.
- JOSLING, G. A. & LLINÁS, M. 2015. Sexual development in Plasmodium parasites: knowing when it's time to commit. *Nature Reviews Microbiology*, 13, 573.
- KAFSACK, B. F. C., ROVIRA-GRAELLS, N., CLARK, T. G., BANCELLS, C., CROWLEY, V. M., CAMPINO, S. G., WILLIAMS, A. E., DROUGHT, L. G., KWIATKOWSKI, D. P., BAKER, D. A., CORTÉS, A. & LLINÁS, M. 2014. A transcriptional switch underlies commitment to sexual development in human malaria parasites. *Nature*, 507, 248-252.
- KAMAL, M. & JOCKERS, R. 2009. Bitopic ligands: all-in-one orthosteric and allosteric. *F1000 biology reports*, 1, 77-77.
- KAMAU, E., CAMPINO, S., AMENGA-ETEGO, L., DRURY, E., ISHENGOMA, D., JOHNSON, K., MUMBA, D., KEKRE, M., YAVO, W., MEAD, D., BOUYOU-AKOTET, M., APINJOH, T., GOLASSA, L., RANDRIANARIVELOJOSIA, M., ANDAGALU, B., MAIGA-ASCOFARE, O., AMAMBUA-NGWA, A., TINDANA, P., GHANSAH, A., MACINNIS, B., KWIATKOWSKI, D. & DJIMDE, A. A. 2015. K13-propeller polymorphisms in Plasmodium falciparum parasites from sub-Saharan Africa. *J Infect Dis*, 211, 1352-5.
- KANO, F. S., DE SOUZA, A. M., DE MENEZES TORRES, L., COSTA, M. A., SOUZA-SILVA, F. A., SANCHEZ, B. A. M., FONTES, C. J. F., SOARES, I. S., DE BRITO, C. F. A., CARVALHO, L. H. & SOUSA, T. N. 2018. Susceptibility to Plasmodium vivax malaria associated with DARC (Duffy antigen) polymorphisms is influenced by the time of exposure to malaria. *Scientific Reports*, 8, 13851.
- KARUNAMOORTHY, K. 2014. Malaria Vaccine: A Future Hope to Curtail the Global Malaria Burden. *International Journal of Preventive Medicine*, 5, 529-538.
- KASLOW, D. C. & BIERNAUX, S. 2015. RTS,S: Toward a first landmark on the Malaria Vaccine Technology Roadmap. *Vaccine*, 33, 7425-7432.
- KELLY-HOPE, L. A. & MCKENZIE, F. E. 2009. The multiplicity of malaria transmission: a review of entomological inoculation rate measurements and methods across sub-Saharan Africa. *Malar J*, 8, 19.
- KERN, S., AGARWAL, S., HUBER, K., GEHRING, A. P., STRODKE, B., WIRTH, C. C., BRUGL, T., ABODO, L. O., DANDEKAR, T., DOERIG, C., FISCHER, R., TOBIN, A. B., ALAM, M. M., BRACHER, F. & PRADEL, G. 2014. Inhibition of the SR protein-phosphorylating CLK kinases of Plasmodium falciparum impairs blood stage replication and malaria transmission. *PLoS One*, 9, e105732.

- KEYLOUN, K. R., REID, M. C., CHOI, R., SONG, Y., FOX, A. M. W., HILLESLAND, H. K., ZHANG, Z., VIDADALA, R., MERRITT, E. A., LAU, A. O. T., MALY, D. J., FAN, E., BARRETT, L. K., VAN VOORHIS, W. C. & OJO, K. K. 2014. The Gatekeeper Residue and Beyond: Homologous Calcium Dependent Protein Kinases as drug development targets for veterinarian Apicomplexa parasites. *Parasitology*, 141, 1499-1509.
- KIARIE, W. C., WANGAI, L., AGOLA, E., KIMANI, F. T. & HUNGU, C. 2015. Chloroquine sensitivity: diminished prevalence of chloroquine-resistant gene marker pfcr-76 13 years after cessation of chloroquine use in Msambweni, Kenya. *Malaria Journal*, 14, 328.
- KIRKLAND, L. O. & MCINNES, C. 2009. Non-ATP competitive protein kinase inhibitors as anti-tumor therapeutics. *Biochemical Pharmacology*, 77, 1561-1571.
- KITE, W. A., MELENDEZ-MUNIZ, V. A., MORAES BARROS, R. R., WELLEMS, T. E. & SA, J. M. 2016. Alternative methods for the Plasmodium falciparum artemisinin ring-stage survival assay with increased simplicity and parasite stage-specificity. *Malar J*, 15, 94.
- KLONIS, N., CRESPO-ORTIZ, M. P., BOTTOVA, I., ABU-BAKAR, N., KENNY, S., ROSENTHAL, P. J. & TILLEY, L. 2011. Artemisinin activity against Plasmodium falciparum requires hemoglobin uptake and digestion. *Proc Natl Acad Sci U S A*, 108, 11405-10.
- KOBE, B. & KEMP, B. E. 2010. Chapter 74 - Principles of Kinase Regulation. In: BRADSHAW, R. A. & DENNIS, E. A. (eds.) *Handbook of Cell Signaling (Second Edition)*. San Diego: Academic Press.
- KORNEV, A. P., HASTE, N. M., TAYLOR, S. S. & EYCK, L. F. 2006. Surface comparison of active and inactive protein kinases identifies a conserved activation mechanism. *Proc Natl Acad Sci U S A*, 103, 17783-8.
- KORNEV, A. P. & TAYLOR, S. S. 2015. Dynamics driven allostery in protein kinases. *Trends in biochemical sciences*, 40, 628-647.
- KORNEV, A. P., TAYLOR, S. S. & TEN EYCK, L. F. 2008. A helix scaffold for the assembly of active protein kinases. *Proc Natl Acad Sci U S A*, 105, 14377-82.
- KOUSSIS, K., WITHERS-MARTINEZ, C., YEOH, S., CHILD, M., HACKETT, F., KNUEPFER, E., JULIANO, L., WOHLBIER, U., BUJARD, H. & BLACKMAN, M. J. 2009. A multifunctional serine protease primes the malaria parasite for red blood cell invasion. *The EMBO Journal*, 28, 725.
- KUEHN, A. & PRADEL, G. 2010. The Coming-Out of Malaria Gametocytes. *Journal of Biomedicine and Biotechnology*, 2010, 1-11.
- KUNG, JENNIFER E. & JURA, N. 2016. Structural Basis for the Non-catalytic Functions of Protein Kinases. *Structure*, 24, 7-24.
- LAMARQUE, M., BESTEIRO, S., PAPOIN, J., ROQUES, M., VULLIEZ-LE NORMAND, B., MORLON-GUYOT, J., DUBREMETZ, J. F., FAUQUENOY, S., TOMAVO, S., FABER, B. W., KOCKEN, C. H., THOMAS, A. W., BOULANGER, M. J., BENTLEY, G. A. & LEBRUN, M. 2011. The RON2-AMA1 interaction is a critical step in moving junction-dependent invasion by apicomplexan parasites. *PLoS Pathog*, 7, e1001276.
- LEE, Y. & RIO, D. C. 2015. Mechanisms and Regulation of Alternative Pre-mRNA Splicing. *Annu Rev Biochem*, 84, 291-323.
- LEROUX, A. E., SCHULZE, J. O. & BIONDI, R. M. 2018. AGC kinases, mechanisms of regulation and innovative drug development. *Seminars in Cancer Biology*, 48, 1-17.

- LIANG, G., LIU, Z., WU, J., CAI, Y. & LI, X. 2012. Anticancer molecules targeting fibroblast growth factor receptors. *Trends Pharmacol Sci*, 33, 531-41.
- LINARES, M., VIERA, S., CRESPO, B., FRANCO, V., GOMEZ-LORENZO, M. G., JIMENEZ-DIAZ, M. B., ANGULO-BARTUREN, I., SANZ, L. M. & GAMO, F. J. 2015. Identifying rapidly parasiticidal anti-malarial drugs using a simple and reliable in vitro parasite viability fast assay. *Malar J*, 14, 441.
- LIU, Y. & GRAY, N. S. 2006. Rational design of inhibitors that bind to inactive kinase conformations. *Nature Chemical Biology*, 2, 358-364.
- LIU, Z., MIAO, J. & CUI, L. 2011. Gametocytogenesis in malaria parasite: commitment, development and regulation. *Future microbiology*, 6, 1351-1369.
- LOURIDO, S., ZHANG, C., LOPEZ, M. S., TANG, K., BARKS, J., WANG, Q., WILDMAN, S. A., SHOKAT, K. M. & SIBLEY, L. D. 2013. Optimizing Small Molecule Inhibitors of Calcium-Dependent Protein Kinase 1 to Prevent Infection by *Toxoplasma gondii*. *Journal of Medicinal Chemistry*, 56, 3068-3077.
- LU, F., LIM, C. S., NAM, D.-H., KIM, K., LIN, K., KIM, T.-S., LEE, H.-W., CHEN, J.-H., WANG, Y., SATTABONGKOT, J. & HAN, E.-T. 2011. Genetic polymorphism in *pvm-dr1* and *pv-cr-t-o* genes in relation to in vitro drug susceptibility of *Plasmodium vivax* isolates from malaria-endemic countries. *Acta Tropica*, 117, 69-75.
- LU, F., ZHANG, M., CULLETON, R. L., XU, S., TANG, J., ZHOU, H., ZHU, G., GU, Y., ZHANG, C., LIU, Y., WANG, W., CAO, Y., LI, J., HE, X., CAO, J. & GAO, Q. 2017. Return of chloroquine sensitivity to Africa? Surveillance of African *Plasmodium falciparum* chloroquine resistance through malaria imported to China. *Parasites & Vectors*, 10, 355.
- MAGHENDJI-NZONDO, S., NZOUGHE, H., LEMAMY, G. J., KOUNA, L. C., PEGHAMOUKANDJA, I., LEKOULOU, F., MBATCHI, B., TOURE-NDOUO, F. & LEKANA-DOUKI, J. B. 2016. Prevalence of malaria, prevention measures, and main clinical features in febrile children admitted to the Franceville Regional Hospital, Gabon. *Parasite*, 23, 32.
- MANNING, G., WHYTE, D. B., MARTINEZ, R., HUNTER, T. & SUDARSANAM, S. 2002. The protein kinase complement of the human genome. *Science*, 298, 1912-34.
- MARGOS, G., BANNISTER, L. H., DLUZEWSKI, A. R., HOPKINS, J., WILLIAMS, I. T. & MITCHELL, G. H. 2004. Correlation of structural development and differential expression of invasion-related molecules in schizonts of *Plasmodium falciparum*. *Parasitology*, 129, 273-87.
- MARKUS, M. B. 2015. Do hypnozoites cause relapse in malaria? *Trends in Parasitology*, 31, 239-245.
- MATHEW, R., HARTMUTH, K., MOHLMANN, S., URLAUB, H., FICNER, R. & LUHRMANN, R. 2008. Phosphorylation of human PRP28 by SRPK2 is required for integration of the U4/U6-U5 tri-snRNP into the spliceosome. *Nat Struct Mol Biol*, 15, 435-43.
- MATONDO, S. I., TEMBA, G. S., KAVISHE, A. A., KAUKI, J. S., KALINGA, A., VAN ZWETSELAAR, M., REYBURN, H. & KAVISHE, R. A. 2014. High levels of sulphadoxine-pyrimethamine resistance *Pfdhfr*-*Pfdhps* quintuple mutations: a cross sectional survey of six regions in Tanzania. *Malar J*, 13, 152.
- MBENGUE, A., BHATTACHARJEE, S., PANDHARKAR, T., LIU, H., ESTIU, G., STAHELIN, R. V., RIZK, S., NJIMOH, D. L., RYAN, Y., CHOTIVANICH, K.,

- NGUON, C., GHORBAL, M., LOPEZ-RUBIO, J.-J., PFRENDER, M., EMRICH, S., MOHANDAS, N., DONDORP, A. M., WIEST, O. & HALDAR, K. 2015. A molecular mechanism of artemisinin resistance in *Plasmodium falciparum* malaria. *Nature*, 520, 683-687.
- MCNAMARA, C. W., LEE, M. C. S., LIM, C. S., LIM, S. H., ROLAND, J., NAGLE, A., SIMON, O., YEUNG, B. K. S., CHATTERJEE, A. K., MCCORMACK, S. L., MANARY, M. J., ZEEMAN, A.-M., DECHERING, K. J., KUMAR, T. R. S., HENRICH, P. P., GAGARING, K., IBANEZ, M., KATO, N., KUHEN, K. L., FISCHLI, C., ROTTMANN, M., PLOUFFE, D. M., BURSULAYA, B., MEISTER, S., RAMEH, L., TRAPPE, J., HAASEN, D., TIMMERMAN, M., SAUERWEIN, R. W., SUWANARUSK, R., RUSSELL, B., RENIA, L., NOSTEN, F., TULLY, D. C., KOCKEN, C. H. M., GLYNNE, R. J., BODENREIDER, C., FIDOCK, D. A., DIAGANA, T. T. & WINZELER, E. A. 2013. Targeting *Plasmodium* PI(4)K to eliminate malaria. *Nature*, 504, 248.
- MCRROBERT, L., TAYLOR, C. J., DENG, W., FIVELMAN, Q. L., CUMMINGS, R. M., POLLEY, S. D., BILLKER, O. & BAKER, D. A. 2008a. Gametogenesis in malaria parasites is mediated by the cGMP-dependent protein kinase. *PLoS Biol*, 6, e139.
- MCRROBERT, L., TAYLOR, C. J., DENG, W., FIVELMAN, Q. L., CUMMINGS, R. M., POLLEY, S. D., BILLKER, O. & BAKER, D. A. 2008b. Gametogenesis in Malaria Parasites Is Mediated by the cGMP-Dependent Protein Kinase. *PLOS Biology*, 6, e139.
- MEKONNEN, S. K., ASEFFA, A., BERHE, N., TEKLEHAYMANOT, T., CLOUSE, R. M., GEBRU, T., MEDHIN, G. & VELAVAN, T. P. 2014. Return of chloroquine-sensitive *Plasmodium falciparum* parasites and emergence of chloroquine-resistant *Plasmodium vivax* in Ethiopia. *Malaria Journal*, 13, 244.
- MERCEREAU-PUJALON, O. & MÉNARD, D. 2010. *Plasmodium vivax* and the Duffy antigen: A paradigm revisited. *Transfusion Clinique et Biologique*, 17, 176-183.
- MIAO, J., CHEN, Z., WANG, Z., SHRESTHA, S., LI, X., LI, R. & CUI, L. 2017. Sex-Specific Biology of the Human Malaria Parasite Revealed from the Proteomes of Mature Male and Female Gametocytes. *Molecular & Cellular Proteomics : MCP*, 16, 537-551.
- MIKOLAJCZAK, SEBASTIAN A., VAUGHAN, ASHLEY M., KANGWANRANGSAN, N., ROOBSOONG, W., FISHBAUGHER, M., YIMAMNUAYCHOK, N., REZAKHANI, N., LAKSHMANAN, V., SINGH, N., KAUSHANSKY, A., CAMARGO, N., BALDWIN, M., LINDNER, SCOTT E., ADAMS, JOHN H., SATTABONGKOT, J. & KAPPE, STEFAN H. I. 2015. *Plasmodium vivax* Liver Stage Development and Hypnozoite Persistence in Human Liver-Chimeric Mice. *Cell Host & Microbe*, 17, 526-535.
- MILLAR, S. B. & COX-SINGH, J. 2015. Human infections with *Plasmodium knowlesi*—zoonotic malaria. *Clinical Microbiology and Infection*, 21, 640-648.
- MILLER, R. H., OBUYA, C. O., WANJA, E. W., OGUTU, B., WAITUMBI, J., LUCKHART, S. & STEWART, V. A. 2015. Characterization of *Plasmodium ovale curtisi* and *P. ovale wallikeri* in Western Kenya Utilizing a Novel Species-specific Real-time PCR Assay. *PLOS Neglected Tropical Diseases*, 9, e0003469.
- MONCUNILL, G., MAYOR, A., JIMÉNEZ, A., NHABOMBA, A., PUYOL, L., MANACA, M. N., BARRIOS, D., CISTERÓ, P., GUINOVART, C., AGUILAR, R., BARDAJÍ, A., PINAZO, M.-J., ANGOV, E., DUTTA, S., CHITNIS, C. E.,

- MUÑOZ, J., GASCÓN, J. & DOBAÑO, C. 2013. Cytokine and Antibody Responses to Plasmodium falciparum in Naïve Individuals during a First Malaria Episode: Effect of Age and Malaria Exposure. *PLOS ONE*, 8, e55756.
- MWANZA, S., JOSHI, S., NAMBOZI, M., CHILESHE, J., MALUNGA, P., KABUYA, J.-B. B., HACHIZOVU, S., MANYANDO, C., MULENGA, M. & LAUFER, M. 2016. The return of chloroquine-susceptible Plasmodium falciparum malaria in Zambia. *Malaria Journal*, 15, 584.
- MWESIGWA, J., OKEBE, J., AFFARA, M., DI TANNA, G. L., NWAKANMA, D., JANHA, O., OPONDO, K., GRIETENS, K. P., ACHAN, J. & D'ALESSANDRO, U. 2015. On-going malaria transmission in The Gambia despite high coverage of control interventions: a nationwide cross-sectional survey. *Malar J*, 14, 314.
- NAHRENDORF, W., SCHOLZEN, A., SAUERWEIN, R. W. & LANGHORNE, J. 2015. Cross-stage immunity for malaria vaccine development. *Vaccine*, 33, 7513-7517.
- NANKABIRWA, J., BROOKER, S. J., CLARKE, S. E., FERNANDO, D., GITONGA, C. W., SCHELLENBERG, D. & GREENWOOD, B. 2014. Malaria in school-age children in Africa: an increasingly important challenge. *Trop Med Int Health*, 19, 1294-309.
- NINOMIYA, K., KATAOKA, N. & HAGIWARA, M. 2011. Stress-responsive maturation of Clk1/4 pre-mRNAs promotes phosphorylation of SR splicing factor. *J Cell Biol*, 195, 27-40.
- NIXON, C. P. 2016. Plasmodium falciparum gametocyte transit through the cutaneous microvasculature: A new target for malaria transmission blocking vaccines? *Human Vaccines & Immunotherapeutics*, 12, 3189-3195.
- NJUE, M., NJUGUNA, P., KAPULU, M. C., SANGA, G., BEJON, P., MARSH, V., MOLYNEUX, S. & KAMUYA, D. 2018. Ethical considerations in Controlled Human Malaria Infection studies in low resource settings: Experiences and perceptions of study participants in a malaria Challenge study in Kenya. *Wellcome Open Res*, 3, 39.
- NKOLI MANDOKO, P., ROUVIER, F., MATENDO KAKINA, L., MOKE MBONGI, D., LATOUR, C., LOSIMBA LIKWELA, J., NGOYI MUMBA, D., BI SHAMAMBA, S. K., TAMFUM MUYEMBE, J. J., MUEPU TSHILOLO, L., PARZY, D. & SINOUE, V. 2018. Prevalence of Plasmodium falciparum parasites resistant to sulfadoxine/pyrimethamine in the Democratic Republic of the Congo: emergence of highly resistant pfdhfr/pfdhps alleles. *J Antimicrob Chemother*.
- NYUNT, M. H., HAN, J. H., WANG, B., AYE, K. M., AYE, K. H., LEE, S. K., HTUT, Y., KYAW, M. P., HAN, K. T. & HAN, E. T. 2017. Clinical and molecular surveillance of drug resistant vivax malaria in Myanmar (2009-2016). *Malar J*, 16, 117.
- O'NEILL, P. M., BARTON, V. E. & WARD, S. A. 2010. The molecular mechanism of action of artemisinin--the debate continues. *Molecules*, 15, 1705-21.
- ORFANO, A. S., NACIF-PIMENTA, R., DUARTE, A. P. M., VILLEGAS, L. M., RODRIGUES, N. B., PINTO, L. C., CAMPOS, K. M. M., PINILLA, Y. T., CHAVES, B., BARBOSA GUERRA, M. G. V., MONTEIRO, W. M., SMITH, R. C., MOLINA-CRUZ, A., LACERDA, M. V. G., SECUNDINO, N. F. C., JACOBS-LORENA, M., BARILLAS-MURY, C. & PIMENTA, P. F. P. 2016. Species-specific escape of Plasmodium sporozoites from oocysts of avian, rodent, and human malarial parasites. *Malaria Journal*, 15, 394.

- ORUGANTY, K. & KANNAN, N. 2012. Design principles underpinning the regulatory diversity of protein kinases. *Philos Trans R Soc Lond B Biol Sci*, 367, 2529-39.
- OTTO, T. D., WILINSKI, D., ASSEFA, S., KEANE, T. M., SARRY, L. R., BOHME, U., LEMIEUX, J., BARRELL, B., PAIN, A., BERRIMAN, M., NEWBOLD, C. & LLINAS, M. 2010. New insights into the blood-stage transcriptome of *Plasmodium falciparum* using RNA-Seq. *Mol Microbiol*, 76, 12-24.
- OUATTARA, A., BARRY, A. E., DUTTA, S., REMARQUE, E. J., BEESON, J. G. & PLOWE, C. V. 2015. Designing malaria vaccines to circumvent antigen variability. *Vaccine*, 33, 7506-7512.
- OWUSU-BOATENG, I. & ANTO, F. 2017. Intermittent preventive treatment of malaria in pregnancy: a cross-sectional survey to assess uptake of the new sulfadoxine–pyrimethamine five dose policy in Ghana. *Malaria Journal*, 16, 323.
- PAPASAIKAS, P., TEJEDOR, J. R., VIGEVANI, L. & VALCARCEL, J. 2015. Functional splicing network reveals extensive regulatory potential of the core spliceosomal machinery. *Mol Cell*, 57, 7-22.
- PARTEY, F. D., CASTBERG, F. C., SARBAH, E. W., SILK, S. E., AWANDARE, G. A., DRAPER, S. J., OPOKU, N., KWEKU, M., OFORI, M. F., HVIID, L. & BARFOD, L. 2018. Kinetics of antibody responses to PfRH5-complex antigens in Ghanaian children with *Plasmodium falciparum* malaria. *PLoS ONE*, 13, e0198371.
- PATEL, P., BHARTI, P. K., BANSAL, D., ALI, N. A., RAMAN, R. K., MOHAPATRA, P. K., SEHGAL, R., MAHANTA, J., SULTAN, A. A. & SINGH, N. 2017. Prevalence of mutations linked to antimalarial resistance in *Plasmodium falciparum* from Chhattisgarh, Central India: A malaria elimination point of view. *Scientific Reports*, 7, 16690.
- POSFAL, D., SYLVESTER, K., REDDY, A., GANLEY, J. G., WIRTH, J., CULLEN, Q. E., DAVE, T., KATO, N., DAVE, S. S. & DERBYSHIRE, E. R. 2018. *Plasmodium* parasite exploits host aquaporin-3 during liver stage malaria infection. *PLoS Pathogens*, 14, e1007057.
- PRADO, M., EICKEL, N., DE NIZ, M., HEITMANN, A., AGOP-NERSESIAN, C., WACKER, R., SCHMUCKLI-MAURER, J., CALDELARI, R., JANSE, C. J., KHAN, S. M., MAY, J., MEYER, C. G. & HEUSSLER, V. T. 2015. Long-term live imaging reveals cytosolic immune responses of host hepatocytes against *Plasmodium* infection and parasite escape mechanisms. *Autophagy*, 11, 1561-1579.
- PRICE, R. N., VON SEIDLEIN, L., VALECHA, N., NOSTEN, F., BAIRD, J. K. & WHITE, N. J. 2014. Global extent of chloroquine-resistant *Plasmodium vivax*: a systematic review and meta-analysis. *The Lancet Infectious Diseases*, 14, 982-991.
- PRUDENCIO, M., RODRIGUEZ, A. & MOTA, M. M. 2006. The silent path to thousands of merozoites: the *Plasmodium* liver stage. *Nat Rev Microbiol*, 4, 849-56.
- RAABE, A., BERRY, L., SOLLELIS, L., CERDAN, R., TAWK, L., VIAL, H. J., BILLKER, O. & WENDELNIK, K. 2011. Genetic and transcriptional analysis of phosphoinositide-specific phospholipase C in *Plasmodium*. *Experimental Parasitology*, 129, 75-80.
- REILING, S. J., KROHNE, G., FRIEDRICH, O., GEARY, T. G. & ROHRBACH, P. 2018. Chloroquine exposure triggers distinct cellular responses in sensitive versus resistant *Plasmodium falciparum* parasites. *Scientific Reports*, 8, 11137.

- RICHIE, T. L., BILLINGSLEY, P. F., SIM, B. K. L., JAMES, E. R., CHAKRAVARTY, S., EPSTEIN, J. E., LYKE, K. E., MORDMÜLLER, B., ALONSO, P., DUFFY, P. E., DOUMBO, O. K., SAUERWEIN, R. W., TANNER, M., ABDULLA, S., KREMSNER, P. G., SEDER, R. A. & HOFFMAN, S. L. 2015. Progress with Plasmodium falciparum sporozoite (PfSPZ)-based malaria vaccines. *Vaccine*, 33, 7452-7461.
- RITCHIE, D. B., SCHELLENBERG, M. J. & MACMILLAN, A. M. 2009. Spliceosome structure: piece by piece. *Biochim Biophys Acta*, 1789, 624-33.
- ROEPE, P. D. 2009. Molecular and physiologic basis of quinoline drug resistance in Plasmodium falciparum malaria. *Future Microbiol*, 4, 441-55.
- RONCALÉS, M., VIDAL, J., TORRES, P. A. A. & HERREROS, E. 2015. In Vitro Culture of Plasmodium falciparum Obtention of Synchronous Asexual Erythrocytic stages. *Open Journal of Epidemiology*, 5, 71-80.
- ROSKOSKI, R., JR. 2015. A historical overview of protein kinases and their targeted small molecule inhibitors. *Pharmacol Res*, 100, 1-23.
- ROTTMANN, M., MCNAMARA, C., YEUNG, B. K. S., LEE, M. C. S., ZOU, B., RUSSELL, B., SEITZ, P., PLOUFFE, D. M., DHARIA, N. V., TAN, J., COHEN, S. B., SPENCER, K. R., GONZÁLEZ-PÁEZ, G. E., LAKSHMINARAYANA, S. B., GOH, A., SUWANARUSK, R., JEGLA, T., SCHMITT, E. K., BECK, H.-P., BRUN, R., NOSTEN, F., RENIA, L., DARTOIS, V., KELLER, T. H., FIDOCK, D. A., WINZELER, E. A. & DIAGANA, T. T. 2010. Spiroindolones, a potent compound class for the treatment of malaria. *Science (New York, N.Y.)*, 329, 1175-1180.
- ROUCHER, C., ROGIER, C., SOKHNA, C., TALL, A. & TRAPE, J.-F. 2014. A 20-Year Longitudinal Study of Plasmodium ovale and Plasmodium malariae Prevalence and Morbidity in a West African Population. *PLOS ONE*, 9, e87169.
- RTS, S. C. T. P. 2015. Efficacy and safety of RTS,S/AS01 malaria vaccine with or without a booster dose in infants and children in Africa: final results of a phase 3, individually randomised, controlled trial. *The Lancet*, 386, 31-45.
- RUDOLF, A. F., SKOVGAARD, T., KNAPP, S., JENSEN, L. J. & BERTHELSEN, J. 2014. A Comparison of Protein Kinases Inhibitor Screening Methods Using Both Enzymatic Activity and Binding Affinity Determination. *PLOS ONE*, 9, e98800.
- SACK, B., KAPPE, S. H. & SATHER, D. N. 2017. Towards functional antibody-based vaccines to prevent pre-erythrocytic malaria infection. *Expert Rev Vaccines*, 16, 403-414.
- SAHEBI, M., HANAFI, M. M., VAN WIJNEN, A. J., AZIZI, P., ABIRI, R., ASHKANI, S. & TAHERI, S. 2016. Towards understanding pre-mRNA splicing mechanisms and the role of SR proteins. *Gene*, 587, 107-19.
- SAITOH, N., SAKAMOTO, C., HAGIWARA, M., AGREDANO-MORENO, L. T., JIMÉNEZ-GARCÍA, L. F. & NAKAO, M. 2012. The distribution of phosphorylated SR proteins and alternative splicing are regulated by RANBP2. *Molecular Biology of the Cell*, 23, 1115-1128.
- SAKO, Y., NINOMIYA, K., OKUNO, Y., TOYOMOTO, M., NISHIDA, A., KOIKE, Y., OHE, K., KII, I., YOSHIDA, S., HASHIMOTO, N., HOSOYA, T., MATSUO, M. & HAGIWARA, M. 2017. Development of an orally available inhibitor of CLK1 for skipping a mutated dystrophin exon in Duchenne muscular dystrophy. *Sci Rep*, 7, 46126.
- SANZ, L. M., CRESPO, B., DE-COZAR, C., DING, X. C., LLERGO, J. L., BURROWS, J. N., GARCIA-BUSTOS, J. F. & GAMO, F. J. 2012. P. falciparum in vitro

- killing rates allow to discriminate between different antimalarial mode-of-action. *PLoS One*, 7, e30949.
- SATOGUINA, J., WALTHER, B., DRAKELEY, C., NWAKANMA, D., ORIERO, E. C., CORREA, S., CORRAN, P., CONWAY, D. J. & WALTHER, M. 2009. Comparison of surveillance methods applied to a situation of low malaria prevalence at rural sites in The Gambia and Guinea Bissau. *Malar J*, 8, 274.
- SCHEEFF, E. D. & BOURNE, P. E. 2005. Structural evolution of the protein kinase-like superfamily. *PLoS Comput Biol*, 1, e49.
- SCHENK, P. W. A. & SNAAR-JAGALSKA, E. B. 1999. Signal perception and transduction- the role of protein kinases . 1449, 1-24.
- SCHENONE, M., DANCİK, V., WAGNER, B. K. & CLEMONS, P. A. 2013. Target identification and mechanism of action in chemical biology and drug discovery. *Nat Chem Biol*, 9, 232-40.
- SCHNEIDER, M., HSIAO, H. H., WILL, C. L., GIET, R., URLAUB, H. & LUHRMANN, R. 2010. Human PRP4 kinase is required for stable tri-snRNP association during spliceosomal B complex formation. *Nat Struct Mol Biol*, 17, 216-21.
- SCHNEIDER, P., LIU, M. G., B.; SUTTIE, P.; , MCHUGH, A. A., E.; , BATINOVIC, D., WILLIAMSON, S. E. H., N.; MCMILLAN, P.; MARION, H.; LEANN, T. & DIXON, M. W. A. D. 2017. Disrupting assembly of the inner membrane complex blocks Plasmodium falciparum sexual stage development. *PLOS Pathogens*, 13, e1006659.
- SCHWARTZ, P. A. & MURRAY, B. W. 2011. Protein kinase biochemistry and drug discovery. *Bioorg Chem*, 39, 192-210.
- SHAW, W. R. & CATTERUCCIA, F. 2018. Vector biology meets disease control: using basic research to fight vector-borne diseases. *Nature Microbiology*.
- SICILIANO, G. & ALANO, P. 2015. Enlightening the malaria parasite life cycle: bioluminescent Plasmodium in fundamental and applied research. *Frontiers in Microbiology*, 6, 391.
- SINDEN, R. E. 2015. The cell biology of malaria infection of mosquito: advances and opportunities. *Cellular Microbiology*, 17, 451-466.
- SINGH, B. & DANESHVAR, C. 2013. Human Infections and Detection of Plasmodium knowlesi. *Clinical Microbiology Reviews*, 26, 165-184.
- SINGH, H., PARAKH, A., BASU, S. & RATH, B. 2011. Plasmodium vivax malaria: is it actually benign? *J Infect Public Health*, 4, 91-5.
- SINGH, R., JAIN, V., SINGH, P. P., BHARTI, P. K., THOMAS, T., BASAK, S. & SINGH, N. 2013. First report of detection and molecular confirmation of Plasmodium ovale from severe malaria cases in central India. *Tropical Medicine & International Health*, 18, 1416-1420.
- SINGH, S., ALAM, M. M., PAL-BHOWMICK, I., BRZOSTOWSKI, J. A. & CHITNIS, C. E. 2010. Distinct External Signals Trigger Sequential Release of Apical Organelles during Erythrocyte Invasion by Malaria Parasites. *PLOS Pathogens*, 6, e1000746.
- SINHA, A., HUGHES, K. R., MODRZYNSKA, K. K., OTTO, T. D., PFANDER, C., DICKENS, N. J., RELIGA, A. A., BUSHELL, E., GRAHAM, A. L., CAMERON, R., KAFSACK, B. F. C., WILLIAMS, A. E., LLINAS, M., BERRIMAN, M., BILLKER, O. & WATERS, A. P. 2014. A cascade of DNA binding proteins for sexual commitment and development in Plasmodium. *Nature*, 507, 253-257.

- SISSOKO, M. S., HEALY, S. A., KATILE, A., OMASWA, F., ZAIDI, I., GABRIEL, E. E., KAMATE, B., SAMAKE, Y., GUINDO, M. A., DOLO, A., NIANGALY, A., NIARÉ, K., ZEGUIME, A., SISSOKO, K., DIALLO, H., THERA, I., DING, K., FAY, M. P., O'CONNELL, E. M., NUTMAN, T. B., WONG-MADDEN, S., MURSHEDKAR, T., RUBEN, A. J., LI, M., ABEBE, Y., MANOJ, A., GUNASEKERA, A., CHAKRAVARTY, S., SIM, B. K. L., BILLINGSLEY, P. F., JAMES, E. R., WALTHER, M., RICHIE, T. L., HOFFMAN, S. L., DOUMBO, O. & DUFFY, P. E. 2017. Safety and efficacy of PfSPZ Vaccine against *Plasmodium falciparum* via direct venous inoculation in healthy malaria-exposed adults in Mali: a randomised, double-blind phase 1 trial. *The Lancet Infectious Diseases*, 17, 498-509.
- SMITH, R. C. & BARILLAS-MURY, C. 2016. Plasmodium Oocysts: Overlooked Targets of Mosquito Immunity. *Trends Parasitol*, 32, 979-990.
- SMITH, R. C., VEGA-RODRÍGUEZ, J. & JACOBS-LORENA, M. 2014. The Plasmodium bottleneck: malaria parasite losses in the mosquito vector. *Memórias do Instituto Oswaldo Cruz*, 109, 644-661.
- SMOLY, I., SHEMESH, N., ZIV-UKELSON, M., BEN-ZVI, A. & YEGER-LOTEM, E. 2017. An Asymmetrically Balanced Organization of Kinases versus Phosphatases across Eukaryotes Determines Their Distinct Impacts. *PLoS Comput Biol*, 13, e1005221.
- SMYTH, L. A. & COLLINS, I. 2009. Measuring and interpreting the selectivity of protein kinase inhibitors. *J Chem Biol*, 2, 131-51.
- SOLYAKOV, L., HALBERT, J., ALAM, M. M., SEMBLAT, J. P., DORIN-SEMBLAT, D., REININGER, L., BOTTRILL, A. R., MISTRY, S., ABDI, A., FENNELL, C., HOLLAND, Z., DEMARTA, C., BOUZA, Y., SICARD, A., NIVEZ, M. P., ESCHENLAUER, S., LAMA, T., THOMAS, D. C., SHARMA, P., AGARWAL, S., KERN, S., PRADEL, G., GRACIOTTI, M., TOBIN, A. B. & DOERIG, C. 2011. Global kinomic and phospho-proteomic analyses of the human malaria parasite *Plasmodium falciparum*. *Nat Commun*, 2, 565.
- SPANGENBERG, T., BURROWS, J. N., KOWALCZYK, P., MCDONALD, S., WELLS, T. N. C. & WILLIS, P. 2013. The Open Access Malaria Box: A Drug Discovery Catalyst for Neglected Diseases. *PLOS ONE*, 8, e62906.
- ST. LAURENT, B., MILLER, B., BURTON, T. A., AMARATUNGA, C., MEN, S., SOVANNAROTH, S., FAY, M. P., MIOTTO, O., GWADZ, R. W., ANDERSON, J. M. & FAIRHURST, R. M. 2015. Artemisinin-resistant *Plasmodium falciparum* clinical isolates can infect diverse mosquito vectors of Southeast Asia and Africa. *Nature Communications*, 6, 8614.
- STRELOW, J. M. 2017. A Perspective on the Kinetics of Covalent and Irreversible Inhibition. *SLAS Discov*, 22, 3-20.
- SUTHERLAND, C. J., TANOMSING, N., NOLDER, D., OGUIKE, M., JENNISON, C., PUKRITTAYAKAMEE, S., DOLECEK, C., HIEN, T. T., DO ROSARIO, V. E., AREZ, A. P., PINTO, J., MICHON, P., ESCALANTE, A. A., NOSTEN, F., BURKE, M., LEE, R., BLAZE, M., OTTO, T. D., BARNWELL, J. W., PAIN, A., WILLIAMS, J., WHITE, N. J., DAY, N. P., SNOUNOU, G., LOCKHART, P. J., CHIODINI, P. L., IMWONG, M. & POLLEY, S. D. 2010. Two nonrecombining sympatric forms of the human malaria parasite *Plasmodium ovale* occur globally. *J Infect Dis*, 201, 1544-50.
- TAHITA, M. C., TINTO, H., ERHART, A., KAZIENGA, A., FITZHENRY, R., VANOVERMEIR, C., ROSANAS-URGELL, A., OUEDRAOGO, J.-B., GUIGUEMDE, R. T., VAN GEERTRUYDEN, J.-P. & D'ALESSANDRO, U. 2015. Prevalence of the dhfr and dhps Mutations among Pregnant Women in Rural Burkina Faso Five Years after the Introduction of

- Intermittent Preventive Treatment with Sulfadoxine-Pyrimethamine. *PLOS ONE*, 10, e0137440.
- TAKALA-HARRISON, S. & LAUFER, M. K. 2015. Antimalarial drug resistance in Africa: key lessons for the future. *Annals of the New York Academy of Sciences*, 1342, 62-67.
- TAKEM, E. N., AFFARA, M., AMAMBUA-NGWA, A., OKEBE, J., CEESAY, S. J., JAWARA, M., ORIERO, E., NWAKANMA, D., PINDER, M., CLIFFORD, C., TAAL, M., SOWE, M., SUSO, P., MENDY, A., MBAYE, A., DRAKELEY, C. & D'ALESSANDRO, U. 2013. Detecting Foci of Malaria Transmission with School Surveys: A Pilot Study in the Gambia. *PLoS One*, 8, e67108.
- TALEVICH, E., MIRZA, A. & KANNAN, N. 2011. Structural and evolutionary divergence of eukaryotic protein kinases in Apicomplexa. *BMC Evol Biol*, 11, 321.
- TALEVICH, E., TOBIN, A. B., KANNAN, N. & DOERIG, C. 2012. An evolutionary perspective on the kinome of malaria parasites. *Philos Trans R Soc Lond B Biol Sci*, 367, 2607-18.
- TAYLOR, S. S.; AND, R.-A. E. & T., H. 1995. How do protein kinases discriminate between serine:threonine and tyrosine? Structural insights from the insulin receptor protein-tyrosine kinase. *The FASEB Journal* 9, 1255 - 1266.
- TAYLOR, S. S., KESHWANI, M. M., STEICHEN, J. M. & KORNEV, A. P. 2012. Evolution of the eukaryotic protein kinases as dynamic molecular switches. *Philos Trans R Soc Lond B Biol Sci*, 367, 2517-28.
- TAYLOR, S. S. & KORNEV, A. P. 2011. Protein kinases: evolution of dynamic regulatory proteins. *Trends Biochem Sci*, 36, 65-77.
- THAM, W. H., HEALER, J. & COWMAN, A. F. 2012. Erythrocyte and reticulocyte binding-like proteins of Plasmodium falciparum. *Trends Parasitol*, 28, 23-30.
- THE MAL, E. R. A. C. G. O. D. 2011. A Research Agenda for Malaria Eradication-Drugs. *PLoS Med*, 8.
- THERON, M., HESKETH, R. L., SUBRAMANIAN, S. & RAYNER, J. C. 2010. An adaptable two-color flow cytometric assay to quantitate the invasion of erythrocytes by Plasmodium falciparum parasites. *Cytometry A*, 77, 1067-74.
- THOMAS, J. A., TAN, M. S. Y., BISSON, C., BORG, A., UMREKAR, T. R., HACKETT, F., HALE, V. L., VIZCAY-BARRENA, G., FLECK, R. A., SNIJDERS, A. P., SAIBIL, H. R. & BLACKMAN, M. J. 2018. A protease cascade regulates release of the human malaria parasite Plasmodium falciparum from host red blood cells. *Nature Microbiology*, 3, 447-455.
- TIBURCIO, M., DIXON, M. W., LOOKER, O., YOUNIS, S. Y., TILLEY, L. & ALANO, P. 2015. Specific expression and export of the Plasmodium falciparum Gametocyte EXported Protein-5 marks the gametocyte ring stage. *Malar J*, 14, 334.
- TILLEY, L., STRAIMER, J., GNADIG, N. F., RALPH, S. A. & FIDOCK, D. A. 2016. Artemisinin Action and Resistance in Plasmodium falciparum. *Trends Parasitol*, 32, 682-696.
- TJITRA, E., ANSTEY, N. M., SUGIARTO, P., WARIKAR, N., KENANGALEM, E., KARYANA, M., LAMPAH, D. A. & PRICE, R. N. 2008. Multidrug-resistant Plasmodium vivax associated with severe and fatal malaria: a prospective study in Papua, Indonesia. *PLoS Med*, 5, e128.
- TONKIN, M. L., ROQUES, M., LAMARQUE, M. H., PUGNIÈRE, M., DOUGUET, D., CRAWFORD, J., LEBRUN, M. & BOULANGER, M. J. 2011. Host Cell

- Invasion by Apicomplexan Parasites: Insights from the Co-Structure of AMA1 with a RON2 Peptide. *Science*, 333, 463.
- TUN, K. M., IMWONG, M., LWIN, K. M., WIN, A. A., HLAING, T. M., HLAING, T., LIN, K., KYAW, M. P., PLEWES, K., FAIZ, M. A., DHORDA, M., CHEAH, P. Y., PUKRITTAYAKAMEE, S., ASHLEY, E. A., ANDERSON, T. J. C., NAIR, S., MCDEW-WHITE, M., FLEGG, J. A., GRIST, E. P. M., GUERIN, P., MAUDE, R. J., SMITHUIS, F., DONDORP, A. M., DAY, N. P. J., NOSTEN, F., WHITE, N. J. & WOODROW, C. J. 2015. Spread of artemisinin-resistant *Plasmodium falciparum* in Myanmar: a cross-sectional survey of the K13 molecular marker. *The Lancet Infectious Diseases*, 15, 415-421.
- TUSTING, L. S., IPPOLITO, M. M., WILLEY, B. A., KLEINSCHMIDT, I., DORSEY, G., GOSLING, R. D. & LINDSAY, S. W. 2015. The evidence for improving housing to reduce malaria: a systematic review and meta-analysis. *Malaria Journal*, 14, 209.
- UITDEHAAG, J. C. M., VERKAAR, F., ALWAN, H., DE MAN, J., BUIJSMAN, R. C. & ZAMAN, G. J. R. 2012. A guide to picking the most selective kinase inhibitor tool compounds for pharmacological validation of drug targets. *British Journal of Pharmacology*, 166, 858-876.
- UO, T., DVINGE, H., SPRENGER, C. C., BRADLEY, R. K., NELSON, P. S. & PLYMATE, S. R. 2016. Systematic and functional characterization of novel androgen receptor variants arising from alternative splicing in the ligand-binding domain. *Oncogene*, 36, 1440.
- VAN SCHALKWYK, D. A., MOON, R. W., BLASCO, B. & SUTHERLAND, C. J. 2017. Comparison of the susceptibility of *Plasmodium knowlesi* and *Plasmodium falciparum* to antimalarial agents. *J Antimicrob Chemother*, 72, 3051-3058.
- VARJOSALO, M., KESKITALO, S., VAN DROGEN, A., NURKKALA, H., VICHALKOVSKI, A., AEBERSOLD, R. & GSTAIGER, M. 2013. The protein interaction landscape of the human CMGC kinase group. *Cell Rep*, 3, 1306-20.
- VAUGHAN, A. M., ALY, A. S. & KAPPE, S. H. 2008. Malaria parasite pre-erythrocytic stage infection: gliding and hiding. *Cell Host Microbe*, 4, 209-18.
- VEIGA, M. I., DHINGRA, S. K., HENRICH, P. P., STRAIMER, J., GNADIG, N., UHLEMANN, A. C., MARTIN, R. E., LEHANE, A. M. & FIDOCK, D. A. 2016. Globally prevalent PfMDR1 mutations modulate *Plasmodium falciparum* susceptibility to artemisinin-based combination therapies. *Nat Commun*, 7, 11553.
- VILLEGAS-MENDEZ, A., STRANGWARD, P., SHAW, T. N., RAJKOVIC, I., TOSEVSKI, V., FORMAN, R., MULLER, W. & COUPER, K. N. 2017. Gamma Interferon Mediates Experimental Cerebral Malaria by Signaling within Both the Hematopoietic and Nonhematopoietic Compartments. *Infection and Immunity*, 85, e01035-16.
- VINAYAK, S., ALAM, M. T., MIXSON-HAYDEN, T., MCCOLLUM, A. M., SEM, R., SHAH, N. K., LIM, P., MUTH, S., ROGERS, W. O., FANDEUR, T., BARNWELL, J. W., ESCALANTE, A. A., WONGSRICHANALAI, C., ARIEY, F., MESHNICK, S. R. & UDHAYAKUMAR, V. 2010. Origin and evolution of sulfadoxine resistant *Plasmodium falciparum*. *PLoS Pathog*, 6, e1000830.
- WAHL, M. C., WILL, C. L. & LUHRMANN, R. 2009. The spliceosome: design principles of a dynamic RNP machine. *Cell*, 136, 701-18.

- WANG, C. W., MWAKALINGA, S. B., SUTHERLAND, C. J., SCHWANK, S., SHARP, S., HERMSEN, C. C., SAUERWEIN, R. W., THEANDER, T. G. & LAVSTSEN, T. 2010a. Identification of a major rif transcript common to gametocytes and sporozoites of *Plasmodium falciparum*. *Malar J*, 9, 147.
- WANG, G. S. & COOPER, T. A. 2007. Splicing in disease: disruption of the splicing code and the decoding machinery. *Nat Rev Genet*, 8, 749-61.
- WANG, J., HUANG, L., LI, J., FAN, Q., LONG, Y., LI, Y. & ZHOU, B. 2010b. Artemisinin directly targets malarial mitochondria through its specific mitochondrial activation. *PLoS One*, 5, e9582.
- WANG, Y., CAI, Y., JI, J., LIU, Z., ZHAO, C., ZHAO, Y., WEI, T., SHEN, X., ZHANG, X., LI, X. & LIANG, G. 2014. Discovery and identification of new non-ATP competitive FGFR1 inhibitors with therapeutic potential on non-small-cell lung cancer. *Cancer Letters*, 344, 82-89.
- WARD, P., EQUINET, L., PACKER, J. & DOERIG, C. 2004. Protein kinases of the human malaria parasite *Plasmodium falciparum*: the kinome of a divergent eukaryote. *BMC Genomics*, 5, 79.
- WEISS, G. E., GILSON, P. R., TAECHALERTPAISARN, T., THAM, W.-H., DE JONG, N. W. M., HARVEY, K. L., FOWKES, F. J. I., BARLOW, P. N., RAYNER, J. C., WRIGHT, G. J., COWMAN, A. F. & CRABB, B. S. 2015. Revealing the Sequence and Resulting Cellular Morphology of Receptor-Ligand Interactions during *Plasmodium falciparum* Invasion of Erythrocytes. *PLOS Pathogens*, 11, e1004670.
- WELLEMS, T. E. & PLOWE, C. V. 2001. Chloroquine-Resistant Malaria. *The Journal of Infectious Diseases* 184, 770-776.
- WENTHUR, C. J., GENTRY, P. R., MATHEWS, T. P. & LINDSLEY, C. W. 2014. Drugs for Allosteric Sites on Receptors. *Annu Rev Pharmacol Toxicol*, 54, 165-84.
- WHITE, N. J. & IMWONG, M. 2012. Chapter Two - Relapse. In: HAY, S. I., PRICE, R. & BAIRD, J. K. (eds.) *Advances in Parasitology*. Academic Press.
- WHO 2011. WHO . Global plan for artemisinin resistance containment (GPARC) World Health Organization (archieved).
- WHO 2015a. Guidelines for the treatment of malaria - 3rd Edition.
- WHO 2015b. Guidelines for the treatment of malaria.pdf.
- WHO 2015c. world malaria report-2014.
- WHO 2017a. Artemisinin and artemisinin-based combination therapy resistance.
- WHO 2017b. World malaria report 2017.
- WHO 2018. Artemisinin resistance and artemisinin-based combination therapy efficacy *Global Malaria Programme*.
- WILLIAM, T., JELIP, J., MENON, J., ANDERIOS, F., MOHAMMAD, R., AWANG MOHAMMAD, T. A., GRIGG, M. J., YEO, T. W., ANSTEY, N. M. & BARBER, B. E. 2014. Changing epidemiology of malaria in Sabah, Malaysia: increasing incidence of *Plasmodium knowlesi*. *Malar J*, 13, 390.
- WILLIAMS, J., NJIE, F., CAIRNS, M., BOJANG, K., COULIBALY, S. O., KAYENTAO, K., ABUBAKAR, I., AKOR, F., MOHAMMED, K., BATIONO, R., DABIRA, E., SOULAMA, A., DJIMDÉ, M., GUIROU, E., AWINE, T., QUAYE, S. L., ORDI, J., DOUMBO, O., HODGSON, A., ODURO, A., MAGNUSSEN, P., TER KUILE, F. O., WOUKEU, A., MILLIGAN, P., TAGBOR, H., GREENWOOD, B. & CHANDRAMOHAN, D. 2016. Non-falciparum malaria infections in pregnant women in West Africa. *Malaria Journal*, 15, 53.

- WILSON, B. A., ALAM, M. S., GUSZCZYNSKI, T., JAKOB, M., SHENOY, S. R., MITCHELL, C. A., GONCHAROVA, E. I., EVANS, J. R., WIPF, P., LIU, G., ASHWELL, J. D. & O'KEEFE, B. R. 2016. Discovery and Characterization of a Biologically Active Non-ATP-Competitive p38 MAP Kinase Inhibitor. *J Biomol Screen*, 21, 277-89.
- WINZELER, E. A. & MANARY, M. J. 2014. Drug resistance genomics of the antimalarial drug artemisinin. *Genome Biology*, 15.
- WITKOWSKI, B., AMARATUNGA, C., KHIM, N., SRENG, S., CHIM, P., KIM, S., LIM, P., MAO, S., SOPHA, C., SAM, B., ANDERSON, J. M., DUONG, S., CHUOR, C. M., TAYLOR, W. R. J., SUON, S., MERCEREAU-PUIJALON, O., FAIRHURST, R. M. & MENARD, D. 2013. Novel phenotypic assays for the detection of artemisinin-resistant *Plasmodium falciparum* malaria in Cambodia: in-vitro and ex-vivo drug-response studies. *The Lancet. Infectious diseases*, 13, 1043-1049.
- WONGSRICHANALAI C., A. M. S. R. 2008. Declining Artesunate-Mefloquine Efficacy against *Falciparum* Malaria on the Cambodia–Thailand Border. *Emerging Infectious Diseases*, 14.
- WRIGHT, K. E., HJERRILD, K. A., BARTLETT, J., DOUGLAS, A. D., JIN, J., BROWN, R. E., ILLINGWORTH, J. J., ASHFIELD, R., CLEMMENSEN, S. B., DE JONGH, W. A., DRAPER, S. J. & HIGGINS, M. K. 2014. Structure of malaria invasion protein RH5 with erythrocyte basigin and blocking antibodies. *Nature*, 515, 427-30.
- WU, T. J., WANG, X., ZHANG, Y., MENG, L., KERRIGAN, J. E., BURLEY, S. K. & ZHENG, X. F. 2015. Identification of a Non-Gatekeeper Hot Spot for Drug-Resistant Mutations in mTOR Kinase. *Cell Rep*, 11, 446-59.
- XING, L., KLUG-MCLEOD, J., RAI, B. & LUNNEY, E. A. 2015. Kinase hinge binding scaffolds and their hydrogen bond patterns. *Bioorganic & Medicinal Chemistry*, 23, 6520-6527.
- XU, C., LI, W., QIU, P., XIA, Y., DU, X., WANG, F., SHEN, L., CHEN, Q., ZHAO, Y., JIN, R., WU, J., LIANG, G. & LI, X. 2015. The therapeutic potential of a novel non-ATP-competitive fibroblast growth factor receptor 1 inhibitor on gastric cancer. *Anticancer Drugs*, 26, 379-87.
- YAGINUMA, H., KAWAI, S., TABATA, K. V., TOMIYAMA, K., KAKIZUKA, A., KOMATSUZAKI, T., NOJI, H. & IMAMURA, H. 2014. Diversity in ATP concentrations in a single bacterial cell population revealed by quantitative single-cell imaging. *Scientific Reports*, 4, 6522.
- YANG, Y., GUO, W., SHEN, X., LI, J., YANG, S., CHEN, S., HE, Z., ZHOU, R. & SHI, S. 2018. Identification and characterization of evolutionarily conserved alternative splicing events in a mangrove genus *Sonneratia*. *Scientific Reports*, 8, 4425.
- YEOH, S., O'DONNELL, R. A., KOUSSIS, K., DLUZEWSKI, A. R., ANSELL, K. H., OSBORNE, S. A., HACKETT, F., WITHERS-MARTINEZ, C., MITCHELL, G. H., BANNISTER, L. H., BRYANS, J. S., KETTLEBOROUGH, C. A. & BLACKMAN, M. J. 2007. Subcellular discharge of a serine protease mediates release of invasive malaria parasites from host erythrocytes. *Cell*, 131, 1072-83.
- ZAGANAS, I. & PLAITAKIS, A. 2002. Single amino acid substitution (G456A) in the vicinity of the GTP binding domain of human housekeeping glutamate dehydrogenase markedly attenuates GTP inhibition and abolishes the cooperative behavior of the enzyme. *J Biol Chem*, 277, 26422-8.

- ZAW, M. T. & LIN, Z. 2017. Two sympatric types of *Plasmodium ovale* and discrimination by molecular methods. *Journal of Microbiology, Immunology and Infection*, 50, 559-564.
- ZHANG, J., YANG, P. L. & GRAY, N. S. 2009. Targeting cancer with small molecule kinase inhibitors. *Nat Rev Cancer*, 9, 28-39.
- ZHANG, L., LI, X. & ZHAO, R. 2013. Structural analyses of the pre-mRNA splicing machinery. *Protein Sci*, 22, 677-92.
- ZHANG, P., LI, S., GAO, Y., LU, W., HUANG, K., YE, D., LI, X. & CHU, Y. 2014a. Novel benzothiazinones (BTOs) as allosteric modulator or substrate competitive inhibitor of glycogen synthase kinase 3 β (GSK-3 β) with cellular activity of promoting glucose uptake. *Bioorganic and Medicinal Chemistry Letters*, 24, 5639-5643.
- ZHANG, Y., YAN, H., WEI, G., HAN, S., HUANG, Y., ZHANG, Q. & PAN, W. 2014b. Distinctive Origin and Spread Route of Pyrimethamine-Resistant *Plasmodium falciparum* in Southern China. *Antimicrobial Agents and Chemotherapy*, 58, 237.
- ZHANG, Z., OJO, K. K., JOHNSON, S. M., LARSON, E. T., HE, P., GEIGER, J. A., CASTELLANOS-GONZALEZ, A., WHITE, A. C., PARSONS, M., MERRITT, E. A., MALY, D. J., VERLINDE, C. L. M. J., VAN VOORHIS, W. C. & FAN, E. 2012. Benzoylbenzimidazole-based selective inhibitors targeting *Cryptosporidium parvum* and *Toxoplasma gondii* calcium-dependent protein kinase-1. *Bioorganic & Medicinal Chemistry Letters*, 22, 5264-5267.
- ZHU, G., XIA, H., ZHOU, H., LI, J., LU, F., LIU, Y., CAO, J., GAO, Q. & SATTABONGKOT, J. 2013. Susceptibility of *Anopheles sinensis* to *Plasmodium vivax* in malarial outbreak areas of central China. *Parasit Vectors*, 6, 176.
- ZUCCOTTO, F., ARDINI, E., CASALE, E. & ANGIOLINI, M. 2010. Through the "gatekeeper door": exploiting the active kinase conformation. *J Med Chem*, 53, 2681-94.